CONTENTS

DISCUSSION

Proc. Paper 16410

INFORMATION RETRIEVAL

The key words, abstract, and reference "cards" for each article in this Journal represent part of the ASCE participation in the EJC information retrieval plan. The retrieval data are placed herein so that each can be cut out, placed on a 3 × 5 card and given an accession number for the user's file. The accession number is then entered on key word cards so that the user can subsequently match key words to choose the articles he wishes. Details of this program were given in an August, 1962 article in CIVIL ENGINEERING, reprints of which are available on request to ASCE headquarters.

---

*Discussion period closed for this paper. Any other discussion received during this discussion period will be published in subsequent Journals.

U.S. CUSTOMARY-SI CONVERSION FACTORS

In accordance with the October, 1970 action of the ASCE Board of Direction, which stated that all publications of the Society should list all measurements in both U.S. Customary and SI (International System) units, the following list contains conversion factors to enable readers to compute the SI unit values of measurements. A complete guide to the SI system and its use has been published by the American Society for Testing and Materials. Copies of this publication (ASTM E-380) can be purchased from ASCE at a price of $3.00 each; orders must be prepaid.

All authors of *Journal* papers are being asked to prepare their papers in this dual-unit format. To provide preliminary assistance to authors, the following list of conversion factors and guides are recommended by the ASCE Committee on Metrication.

To convert	To	Multiply by
inches (in.)	millimeters (mm)	25.4
feet (ft)	meters (m)	0.305
yards (yd)	meters (m)	0.914
miles (miles)	kilometers (km)	1.61
square inches (sq in.)	square millimeters (mm^2)	645
square feet (sq ft)	square meters (m^2)	0.093
square yards (sq yd)	square meters (m^2)	0.836
square miles (sq miles)	square kilometers (km^2)	2.59
acres (acre)	hectares (ha)	0.405
cubic inches (cu in.)	cubic millimeters (mm^3)	16,400
cubic feet (cu ft)	cubic meters (m^3)	0.028
cubic yards (cu yd)	cubic meters (m^3)	0.765
pounds (lb) mass	kilograms (kg)	0.453
tons (ton) mass	kilograms (kg)	907
pound force (lbf)	newtons (N)	4.45
kilogram force (kgf)	newtons (N)	9.81
pounds per square foot (psf)	pascals (Pa)	47.9
pounds per square inch (psi)	kilopascals (kPa)	6.89
U.S. gallons (gal)	liters (L)	3.79
acre-feet (acre-ft)	cubic meters (m^3)	1,233

16419 Earthquake Response of Concrete Dam

ABSTRACT: The displacement and stress responses are presented for Pine Flat Dam to the S69E component of the Taft ground motion only, and to the S69E and vertical components acting simultaneously. For each of these excitations, the response of the dam is analyzed four times corresponding to the following four sets of assumptions: (1) Rigid foundation, hydrodynamic effects excluded; (2) rigid foundation, hydrodynamic effects included; (3) flexible foundation, hydrodynamic effects excluded; and (4) flexible foundation, hydrodynamic effects included. Based on these results, the separate effects of dam-water interaction and dam-foundation rock interaction, and the combined effects of the two sources of interaction, on earthquake response of dams are investigated.

REFERENCE: Chopra, Anil K. (Prof. of Civ. Engrg., Univ. of California, Berkeley, Calif. 94720), and Gupta, Sunil, "Earthquake Response of Concrete Dam," *Journal of the Structural Division,* ASCE, Vol. 107, No. ST8, **Proc. Paper 16419,** August, 1981, pp. 1399-1412

16420 ECONOMIC REVIEW OF EARTHQUAKE DESIGN LEVELS

ABSTRACT: Current Navy criteria specifies that for important buildings a site seismicity study shall be performed and the design earthquake level shall be taken as the site acceleration having an 80 percent chance of not being exceeded in 50 years. Construction cost increases are reviewed for seismic strengthening and expected damage from seismic shaking. Economic analysis techniques were used to study earthquake design levels. Results indicate optimal least cost designs occur at lower design levels than is specified by current criteria.

REFERENCE: Ferritte, John M. (Research Structural Engr., Naval Civ. Engrg. Lab., Naval Construction Battalion Center, Port Hueneme, Calif. 93043), "Economic Review of Earthquake Design Levels," *Journal of the Structural Division,* ASCE, Vol. 107, No. ST8, **Proc. Paper 16420,** August, 1981, pp. 1413-1425

16440 STEEL FRAMES WITH NONLINEAR CONNECTIONS

ABSTRACT: Various simplifying assumptions, commonly used in the design of unbraced multistory steel building frames, are explored. An analysis program was developed to account for the nonlinear flexibility of the girder-column connections as well as for the response to variable load histories. Analyses were performed on three different structures. The results show the importance of including actual connection behavior for realistic prediction of sway and internal forces. The possibility of the occurrence of alternating connection plasticity is also pointed out. The inclusion of linearly-elastic connection flexibilities in the analysis appears to lead to very satisfactory results.

REFERENCE: Moncarz, Piotr D. (Doctoral Candidate, The John A. Blume Earthquake Engrg. Center, Stanford Univ., Stanford, Calif.), and Gerstl, Kurt H., "Steel Frames with Nonlinear Connections," *Journal of the Structural Division,* ASCE, Vol. 107, No. ST8, **Proc. Paper 16440,** August, 1981, pp. 1427-1441

16428 CONTINUUM SOLUTION OF SIMULATED PIPE WHIP PROBLEM

ABSTRACT: The pipe whip problem is a highly nonlinear problem which, except for special conditions, is usually solved numerically. When a dynamic load is applied to the base of a pipe (striker) whose end impacts another pipe (target), it is possible for both the striker and the target to experience plastic deformations during impact. A finite element solution considering the nonlinear impact problem with material nonlinearity has been carried out. At the point when the material becomes plastic, high frequency oscillations can set up in the continuum model. Experimental data indicate that these oscillations quickly disappear due to material damping. The effects of plasticity are considered, as are Rayleigh damping and nonlinear damping in the target material.

16427 SEISMIC EFFECTIVENESS OF TUNED MASS DAMPERS

ABSTRACT: Time history analysis of 1DOF systems with and without a tuned mass damper, subjected to a set of historical earthquakes, shows that the peak response ratio (ratio between the peak responses with and without damper) depends primarily on damping constants and on earthquake duration. The same analysis reveals that response ratio values are widely scattered and that the mean response ratio in underestimated by conventional stationary random vibration calculations. Improvement is obtained by considering response movement and broadening of the response spectral density function caused by the damper. Based on these considerations, a probabilistic model is developed that gives the distribution of peak response of buildings modified by addition of a tuned mass damper in terms of the same distribution for the unmodified structures. For elastic systems tuned mass dampers have small antiseismic effectiveness.

16432 DYNAMICS OF THREE-DIMENSIONAL FRAMES

ABSTRACT: The time-history response of a three-dimensional reinforced concrete frame structure to concurrent earthquake ground motions is analyzed. Yielding is allowed in both beams and columns by a series of yield surface options selected according to the principal structural actions of the component elements. Comparisons between the behavior patterns arising from unidirectional and concurrent earthquake loading indicate that the non-linear response predicted by a full three-dimensional analysis is significantly different from the response based on a planar frame idealization. Concurrent loading causes asymmetric distribution of yield as a result of the interaction of the orthogonal displacement components, and this gives rise to an eccentricity between the mass and the instantaneous center of stiffness at some levels in the building. Nominally symmetric buildings can develop torsional responses in moderate earthquakes.

16441 COLLAPSE OF PLATE GIRDERS UNDER EDGE LOADING

ABSTRACT: A simple analysis is presented for predicting the ultimate load carrying capacity of slender plate girder webs subjected to edge loading, uniformly distributed between vertical web stiffeners, and combined bending. The analysis is based on an assumed failure mechanism which considers the formation of plastic hinges in the flange and yield lines in the web. An alternative mechanism solution is also considered for situations in which failure may be initiated by direct yielding of the web. The analysis is compared with a limited number of existing test results and is found to give satisfactory agreement.

REFERENCE: Roberts, Terence M. (Lect., Dept. of Civ. Engrg., University College, Newport Road, Cardiff, CF2 1TA, Wales), and Chong, Chooi K., "Collapse of Plate Girders under Edge Loading," *Journal of the Structural Division,* ASCE, Vol. 107, No. ST8, **Proc. Paper 16441,** August, 1981, pp. 1503-1509

16423 CODE COMPARISONS OF FACTOR DESIGN FOR WOOD

ABSTRACT: The formulation of an alternate methodology for the design of wood structural members is described. Load and resistance factors are developed to convert existing code requirements into a limits states design format. Comparisons of the resulting factors are obtained by examining existing codes from several European countries as well as the National Design Specification of the United States. Current factors vary significantly. Use of the load and resistance format for design of wood structures is propose, based on further studies using probability-based criteria.

REFERENCE: Goodman, James R. (Prof. of Civ. Engrg., Colorado State Univ., Fort Collins, Colo. 80523), Kovacs, Zsolt, and Bodig, Jozsef, "Code Comparisons of Factor Design for Wood," *Journal of the Structural Division,* ASCE, Vol. 107, No. ST8, **Proc. Paper 16423,** August, 1981, pp. 1511-1527

16451 HISTORY OF STRUCTURAL STABILITY RESEARCH COUNCIL

ABSTRACT: The origin, growth and contributions of the Structural Stability Research Council are examined. Originally named the Column Research Council, the organization has annually provided a forum on structural stability by bringing together researchers from all parts of the world. The Council has initiated research, and it has cooperated with specification writing bodies. Three successive editions of the council's design guide have been published; a fourth is underway. Research contributions include: (1) The recognition and quantification of the residual stress effect on column stability; (2) the definition and application of the strain-hardening modulus in steel; (3) the determination of maximum inelastic column strength; and, (4) through the council's technical memoranda, the establishment of methods and criteria for tests of columns and metals in compression.

REFERENCE: Johnston, Bruce G. (Prof. Emeritus of Struct. Engrg., Univ. of Mich., Ann Arbor, Mich. 48104), "History of Structural Stability Research Council," *Journal of the Structural Division,* ASCE, Vol. 107, No. ST8, **Proc. Paper 16451,** August, 1981, pp. 1529-1550

16426 INELASTIC LATERAL TORSIONAL BUCKLING OF BEAMS

ABSTRACT: A numerical procedure is presented for predicting elastic and inelastic beam buckling loads. The procedure uses a finite difference solution to the differential equations defining lateral torsional buckling. The reduction in beam stiffness in the inelastic range is estimated by using an approximate tangent modulus method. A computer program has been developed using the numerical procedure presented for general elastic and inelastic buckling solutions. Solutions from the program are compared against approximately 123 test buckling results. Inelastic program buckling solutions are compared with and without using the shear center adjustment method. The approximate tangent modulus method and the shear center adjustment method agreed favorably with the test results.

REFERENCE: Hollinger, Bruce A. (Engr., Floyd Browne Associates, Ltd., 181 South Main Street, P.O. Box 587, Marion, Ohio), and Magelsdorf, C. P., "Inelastic Lateral Torsional Buckling of Beams," *Journal of the Structural Division*, ASCE, Vol. 107, No. ST8, **Proc. Paper 16426**, August, 1981, pp. 1551-1567

16453 TORSIONAL COUPLING AND EARTHQUAKE RESPONSE

ABSTRACT: The effects are analyzed of torsional coupling on the earthquake response of simple one-story structures in elastic and inelastic ranges of behavior. The structures considered are symmetrical about one principal axis of resistance, resulting in coupling only between lateral displacement along the perpendicular axis and the torsional displacement. Torsional coupling arising only from eccentricity between centers of mass and elastic resistance is considered. Systems with several resisting elements are idealized by a single element model. Response of such a model to a selected earthquake ground motion are presented for a range of the basic structural parameters. The response quantities presented include maximum lateral and torsional deformations of the system as well as maximum deformations of individual columns. The response in the inelastic range of behavior is effected by torsional coupling to generally a lesser degree than elastic response.

REFERENCE: Kan, Christopher L. (Asst. Research Engr., Dept. of Civ. Engrg., Univ. of California, Berkeley, Calif. 94720), and Chopra, Anil K., "Torsional Coupling and Earthquake Response of Simple Elastic and Inelastic Systems," *Journal of the Structural Division*, ASCE, Vol. 107, No. ST8, **Proc. Paper 16453**, August, 1981, pp. 1569-1588

16459 LATERAL LOAD ANALYSIS OF HIGH-RISE BUILDINGS

ABSTRACT: An approximate method for the design of long, high-rise buildings under horizontal wind loading is described. The method is based on the reduction of the framed structure to one built-in column with equivalent bending and torsional stiffnesses. Discrete actions of the horizontal members on the columns are distributed over the story heights. The floors are treated as rigid in the horizontal plane. The calculation is reduced to the solution of a system of four linear equations; the determination of internal actions only requires some very simple operations. The accuracy of the method is demonstrated by comparison to the displacement method.

REFERENCE: Mortelmans, Fernand K.E.C. (Prof. of Struct. Engrg., Struct. Engrg. Dept., Katholieke Universteit, Leuven, Belgium), De Roeck, Guido P.J.M., and Van Gemert, Dionys A., "Approximate Method for Lateral Load Analysis of High-Rise Buildings," *Journal of the Structural Division*, ASCE, Vol. 107, No. ST8, **Proc. Paper 16459**, August, 1981, pp. 1589-1610

16463 LAP SPLICES IN REINFORCED CONCRETE UNDER IMPACT

KEY WORDS: Bonding strength; Comparative studies; **Concrete (reinforced); Deflection; Failure; Impact; Impact loads; Splices; Static loads;** Strength of materials; **Structural dynamics**

ABSTRACT: The performance of lap splices subjected to impact loading was studied and compared with that of splices under static loading. Nineteen specimens were tested under impact loading, with failure produced in either one impact, in the three to five impacts of incrementally increasing magnitude, or under either unidirectional or reversed cycling of the impact load. Analytical studies were carried out to help evaluate the experimental data. The impact moment capacity of the splices tested was equal to or greater than the static moment capacity. The splice strength achieved under impact could be computed using material strengths adjusted for the strain rate imposed. Under large impact loads (producing high strain rates), the moment capacity of the splice region can greatly exceed the static moment capacity, but failure occurs after only a few load applications. With smaller impacts loads, more cycles of load were carried before failure.

16476 LOGICAL ANALYSIS OF TENTATIVE SEISMIC PROVISIONS

KEY WORDS: **Building codes; Earthquake resistant structures;** Regulation; **Seismic design; Standards;** Structural design

ABSTRACT: A study is described of the format and expression of the Tentative Provisions for the Development of Seismic Regulations for Buildings developed by the Applied Technology Council. The methods of analysis employed provide objective measures of clarity, completeness and consistency, as well as an alternative formal representation with which to examine the correctness of the provisions. The formal representation of the seismic provisions and the findings of the analysis will assist those concerned with the future development of the provisions and their implementation within the various national standards and model codes.

16475 WARPING RESTRAINT IN THREE-DIMENSIONAL FRAMES

KEY WORDS: **Beams;** Displacement; **Elasticity;** Finite elements; Foundations; **Framed structures; Frames;** Internal forces; Strain; Stress; **Three-dimensional; Warpage**

ABSTRACT: The general solution of the restrained warping of beams in three-dimensional frames has been developed. The general beam strain-displacement relations are used in developing a finite element solution to this problem. The solution can account for arbitrary cross-sectional shapes and arbitrary loadings. It also accounts for the coupling between the different internal forces of the beam. The concepts of continuous and restrained warping are introduced as an aid in analyzing general three-dimensional framed structures. The known analytical solutions of simple problems are predicted by the finite element solution. The method is used in a case study of a massive three-dimensional turbine generator pedestal. The warping restraints are found to have a considerable effect on the computed displacements and stresses.

16466 SHEET STEEL WELDING

ABSTRACT: Light, cold formed steel sections have been arc welded without the benefit of a general guiding specification for many years. By the late 1960's the structural use of the fastening was sufficient to create a demand for a more systematic approach. In a series of tests at Cornell University, the behavior of the most common types of arc welds in sheet steel has been studied, and strength prediction equations have been derived. The strength prediction equations can be converted into design equations through the use of appropriate safety factors. Except for the case of the arc spot welds, the correlation between the test results and the computed results is quite satisfactory. In the case of the arc spot welds, the variability of the quality of welds has led to a rather large scatter in the test results.

16465 CONCRETE MASONRY UNDER BIAXIAL STRESSES

ABSTRACT: The available failure hypotheses for masonry under combined stresses are reviewed. The applicability of the failure theories for composite materials to masonry is examined utilizing experimental results of concrete block masonry test. Failure theories for isotropic materials are not applicable to masonry. Also, failure theories for composite materials cannot be directly applied to predict the masonry strength under biaxial stresses. Failure criteria are proposed for masonry under biaxial stresses, taking into consideration its anisotropic nature as a composite material. Two failure criteria are proposed, with each describing a single mode of failure—a shear failure along one of the criterical bed or head joint direction, and a tension failure incorporating the interaction of the block, mortar and grout. The proposed criteria are capable of predicting both the mode of failure and the strength of concrete block masonry under biaxial stresses.

HYDRODYNAMIC AND FOUNDATION INTERACTION EFFECTS IN EARTHQUAKE RESPONSE OF A CONCRETE GRAVITY DAM

By Anil K. Chopra[1] M. ASCE and Sunil Gupta[2]

INTRODUCTION

During the past decade, significant progress has been made in the analysis of the response of concrete gravity dams to earthquake ground motion. A general analytical procedure and computer program—wherein the effects of dam-water-foundation rock interaction and water compressibility are included—are now available for two-dimensional finite element analysis of gravity dam monoliths subjected to horizontal and vertical components of ground motion (3,4).

Response results from an earlier version of this procedure (1), applicable to dams on rigid foundations, provided an improved understanding of the hydrodynamic effects in earthquake response of concrete gravity dams. It was shown that, in general, dam-water interaction and water compressibility have significant influence on the earthquake response of concrete gravity dams (2). In addition to being influenced by dam-water interaction, the dynamic response of a massive, short period structure such as a concrete gravity dam, would be affected by the properties of the foundation rock (6,8). Therefore, the aforementioned procedure (3,4) was developed to simultaneously include the effects of dam-water interaction and dam-foundation rock interaction in response analyses.

Utilizing this analytical procedure the responses of Pine Flat Dam to the S69E component of the Taft ground motion only; and to the S69E and vertical components acting simultaneously are determined. This dam has been the subject of several studies including forced vibration tests (7) and earlier analytical studies of hydrodynamic effects in dam response (2). For each of the excitations, the response of the dam is analyzed four times corresponding to the following four sets of assumptions: (1) Rigid foundation, hydrodynamic effects excluded; (2) rigid foundation rock, hydrodynamic effects included; (3) flexible foundation rock, hydrodynamic effects excluded; and (4) flexible foundation rock, hydro-

dynamic effects included. These results provide insight into the effects of dam-water interaction and dam-foundation rock interaction, considered separately or together, in the earthquake response of dams.

PINE FLAT DAM, GROUND MOTION, CASES ANALYZED AND RESPONSE RESULTS

Pine Flat Dam.—Located on the King's River near Fresno, California, Pine Flat Dam consists of 36 50-ft and one 40-ft wide monoliths. The crest length is 1,840 ft and the height of the tallest monolith is 400 ft.

The tallest, nonoverflow monolith of the dam with water at El. 951.00 is selected for purposes of this study. The two-dimensional finite element idealization
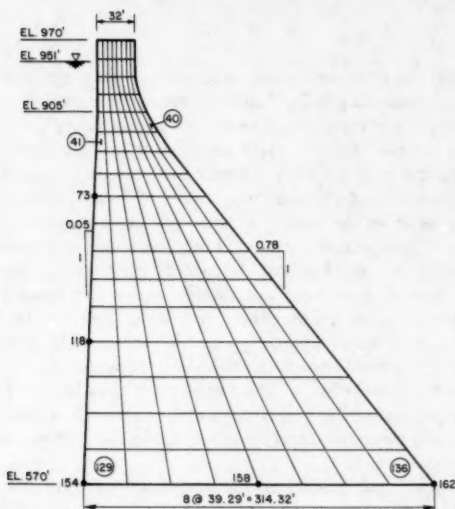
FIG. 1.—Finite Element Idealization of Tallest, Nonoverflow Monolith of Pine Flat Dam (1 ft = 0.305 m)

for this monolith in plane stress is shown in Fig. 1, consisting of 136 quadrilateral elements with 162 nodal points. The nine nodal points at the base of the dam are equally spaced, as required for developing the dynamic stiffness matrix for the foundation (5). This finite element system has 306 degrees-of-freedom analysis of the dam on rigid base. In analyses considering the foundation flexibility and the resulting motion at the dam-foundation interface, the system has 324 degrees of freedom. The mass concrete in the dam is assumed to be a homogeneous, isotropic, elastic solid with the following properties: (1) Young's modulus of elasticity = 3,250,000 psi, unit weight = 155 pcf; and (2) Poisson's ratio = 0.2. The selected elastic modulus, determined by forced vibration tests on the dam (7), is different from that used in earlier analyses (2). The damping factors associated with the modes of vibration of the dam, determined from

the previously mentioned forced vibration tests, were in the range of 2%–3.5% of critical damping. A constant hysteretic damping coefficient of 0.1, which corresponds to a 5% damping factor in all modes of vibration of the dam, has been selected. This is considered appropriate for the much larger motions and stress levels expected during strong earthquake ground shaking.

The foundation rock is idealized as a homogeneous, isotropic, viscoelastic half plane (in plane stress) of constant hysteretic solid with the following properties: (1) Young's modulus of elasticity = 10,000,000 psi, a value which is appropriate for the granites and basalts at the site; (2) Poisson's ratio = 1/3, unit weight = 165 pcf; and (3) the energy loss coefficient for constant hysteretic solid, = 0.05 (3). The P-wave velocity for rock with these properties = 10,266 ft/sec.

The following properties are assumed for water: unit weight = 62.5 pcf, wave velocity = 4,720 ft/sec. For these properties of water and rock, the wave reflection coefficient at the bottom of the reservoir is $\alpha = 0.817$.
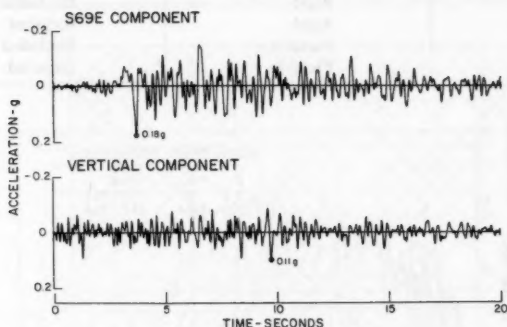
FIG. 2.—Ground Motion at Taft Lincoln School Tunnel; Kern County, California, Earthquake, July 21, 1952

Ground Motion.—The ground motion recorded at the Taft Lincoln School Tunnel during the Kern County, California, earthquake of July 21, 1952, is selected as the excitation for analyses of Pine Flat Dam. The ground motion acting transverse to the axis of the dam and in the vertical direction is defined by the S69E and vertical components of the recorded motion, respectively. These two components of the recorded ground motion and the maximum values of acceleration are shown in Fig. 2.

Cases Analyzed.—Using the computer program based on the analysis procedure presented elsewhere, (3,4), responses of the tallest monolith of Pine Flat Dam to the selected ground motion are analyzed. The dam monolith and the foundation rock are assumed to be in plane stress.

Responses of the dam to the S69E component of the Taft ground motion only and to the S69E and vertical components acting simultaneously are analyzed. For each of these excitations the response of the dam is separately analyzed four times, corresponding to the four sets of assumptions listed in Table 1

for the hydrodynamic effects and the foundation rock.

In order to consider hydrodynamic effects realistically, compressibility of water is included. The displacements and stresses due to the weight of the dam and to hydrostatic pressures are included in all analyses. As mentioned in the development of the analysis procedure (3,4), the rigid body displacement of the dam due to a deformable foundation have been excluded.

All the vibration modes or generalized coordinates, as appropriate, are necessary to obtain accurate results for complex frequency response up to excitation frequencies of approx 25 cps were included in the analysis. The first five natural

TABLE 1.—Assumptions for Foundation Rock and Hydrodynamic Effects

Case (1)	Foundation rock (2)	Hydrodynamic effects (3)
1	Rigid	Excluded
2	Rigid	Included
3	Flexible	Excluded
4	Flexible	Included
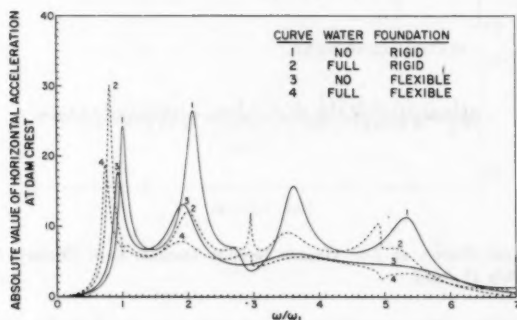
FIG. 3.—Responses of Pine Flat Dam to Harmonic, Horizontal Ground Motion Computed for Four Conditions; Dam with No Water on Rigid Foundation Rock, Dam with Full Reservoir on Rigid Foundation Rock, Dam with No Water on Flexible Foundation Rock, and Dam with Full Reservoir on Flexible Foundation Rock

modes of vibration of the dam were included in the analyses assuming a rigid base. The first 10 generalized coordinates, were included in analyses considering the effects of interaction between the dam and the foundation rock (3).

Response Results.—The complex frequency response functions for the horizontal acceleration at the crest of Pine Flat Dam, with horizontal ground motion as the excitation, for the four sets of assumptions for the hydrodynamic effects and the foundation rock are presented in Fig. 3. From these results, the fundamental resonant period of vibration and the effective damping, determined by the half-power band width method, are listed in Table 2.

These vibration periods are identified on the response spectrum of the S69E component of the Taft ground motion (Fig. 4). The spectrum ordinates at these vibration periods corresponding to damping ratio of 5% can be observed in the same figure.

TABLE 2.—Fundamental Resonant Period of Vibration and Damping Ratio

Case (1)	Foundation rock (2)	Hydrodynamic effects (3)	Fundamental Resonance	
			Vibration period, in seconds (4)	Damping ratio, as a percentage (5)
1	Rigid	Excluded	0.317	5.0
2	Rigid	Included	0.397	3.2
3	Flexible	Excluded	0.341	6.7
4	Flexible	Included	0.429	5.2
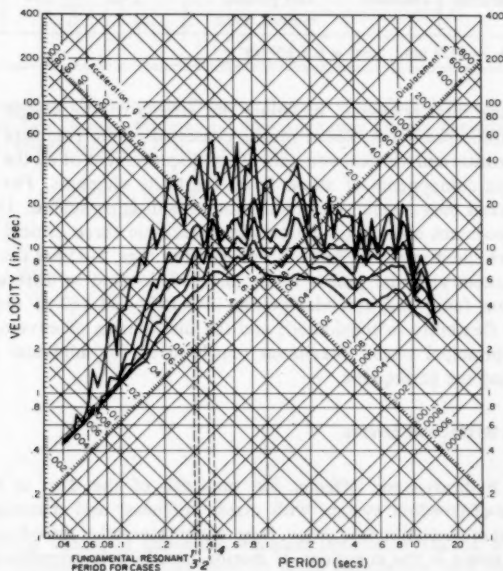
FIG. 4.—Response Spectrum for S69E Component of Taft Ground Motion. Fundamental Vibration Period of Pine Flat Dam Computed for Four Sets of Assumptions (Table 2) for Hydrodynamic Effects and Foundation Rock is as Noted

The response of Pine Flat Dam was determined for the selected ground motions and the aforementioned four sets of assumptions for the hydrodynamic effects and the foundation rock. In each case, the computer results of dynamic analysis

TABLE 3.—Summary of Responses of Pine Flat Dam to Taft Ground Motion

Case (1)	System Properties		Excitation (4)	Maximum horizontal crest displacement, in inches (5)	Maximum Tensile Stresses, in pounds per square inch		
	Foundation rock (2)	Hydrodynamic effects (3)			Upstream face (6)	Downstream face (7)	Heel (8)
1	Rigid	Excluded	S69E component,	1.38	153	208	257
2	Rigid	Included	Taft ground	1.83	223	254	366
3	Flexible	Excluded	motion, 1952	1.46	143	158	150
4	Flexible	Included		2.55	297	355	428
5	Rigid	Excluded	S69E and	1.46	177	225	276
6	Rigid	Included	vertical	1.72	238	233	329
7	Flexible	Excluded	components,	1.57	166	183	170
8	Flexible	Included	Taft ground motion, 1952	2.42	274	347	406

Note: 1 in. = 25.4 mm; 1 psi = 6.9 kN/m^2.

represent the total response, including the effects of the weight of the dam and hydrostatic pressures. These results consisted of the complete time-history of the horizontal and vertical components of displacement of all the nodal points and of three components of stress in all the finite elements. For each of the cases analyzed only a small part of the total result is presented. The maximum crest displacement and maximum tensile stresses in three critical parts of the monolith are summarized in Table 3. Presented in Figs. 5–15 are the time-history of displacement at nodal points 1, 73, and 118, located at different levels on the upstream face, and at nodal points 154, 158, and 162 at the base when foundation flexibility is considered; and the distribution of envelope values of maximum principal stress (maximum tensile stress or minimum compressive stress) during the earthquake.

DAM-WATER INTERACTION EFFECTS

Without hydrodynamic effects, the response of the dam is typical of a multidegree-of-freedom system with mass, stiffness, and damping properties independent of excitation frequency. Dam-water interaction introduces frequency dependent terms in the equations of motion, resulting in complicated response curves, especially in the neighborhood of the resonant frequencies for the impounded water (Fig. 3). A decrease in the fundamental resonant frequency of the dam is apparent from a comparison of the responses with and without hydrodynamic effects.

When the excitation is the S69E component of Taft ground motion, the inclusion of hydrodynamic effects increases the maximum displacement at the crest of the dam from 1.38 ft–1.83 ft (Fig. 5). The maximum tensile stresses in the dam are increased at the upstream face from 153 psi–223 psi, from 208 psi–254

psi at the downstream face, and from 257 psi–366 psi at the heel (Fig. 6). The area enclosed by a particular stress contour increases due to hydrodynamic effects, indicating that stresses exceed the value corresponding to that stress contour over a larger portion of the monolith.
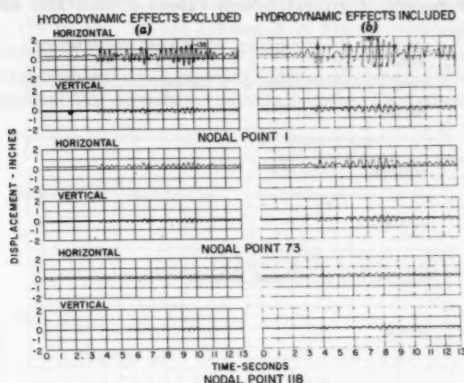
FIG. 5.—Displacement Response of Pine Flat Dam on Rigid Foundation Rock to S69E Component of Taft Ground Motion: (a) Hydrodynamic Effects Excluded; and (b) Hydrodynamic Effects Included (1 in. = 25.4 mm)
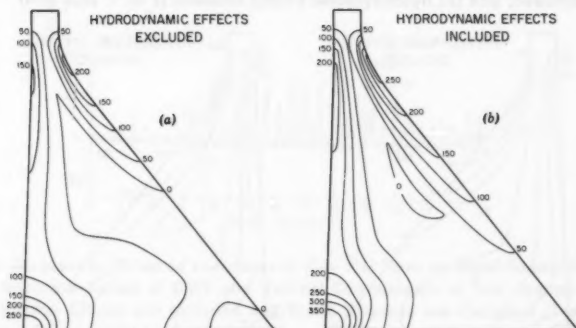
FIG. 6.—Envelope Values of Maximum Principal (Maximum Tensile or Minimum Compressive) Stresses in Pine Flat Dam on Rigid Foundation Rock due to S69E Component of Taft Ground Motion: (a) Hydrodynamic Effects Excluded; and (b) Hydrodynamic Effects Included (1 psi = 6.9 kN/m²)

When hydrodynamic effects are excluded, the response of the dam is only slightly increased by the contribution of the vertical component of ground motion (compare Figs. 5 and 6 with Figs. 7 and 8). But, contrary to the earlier results for Pine Flat Dam (2), the displacements and stresses in the dam with hydrodynamic effects included are slightly decreased by the contributions of the vertical

component of ground motion (again compare Figs. 5 and 6 with Figs. 7 and 8).

Earlier results (2) for the response of Pine Flat Dam subjected to Taft ground motion but assuming a different value of Young's modulus, demonstrated that the vertical component of ground motion causes considerable increase in the
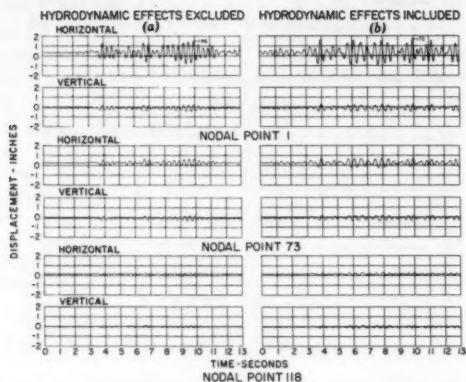
FIG. 7.—Displacement Response of Pine Flat Dam on Rigid Foundation Rock to S69E and Vertical Components, Simultaneously, of Taft Ground Motion: (a) Hydrodynamic Effects Excluded; and (b) Hydrodynamic Effects Included (1 in. = 25.4 mm)
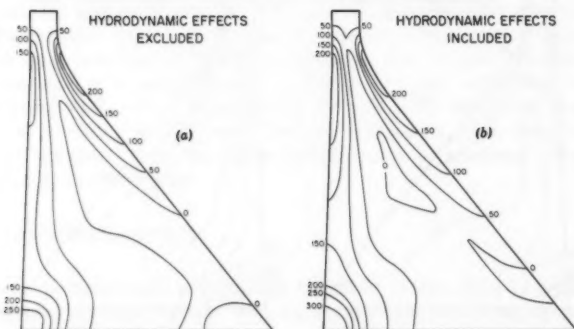
FIG. 8.—Envelope Values of Maximum Principal (Maximum Tensile or Minimum Compressive) Stresses in Pine Flat Dam on Rigid Foundation Rock due to S69E and Vertical Components, Simultaneously, of Taft Ground Motion: (a) Hydrodynamic Effects Excluded; and (b) Hydrodynamic Effects Included (1 psi = 6.9 kN/m²)

response of the dam. The vertical ground motion causes lateral hydrodynamic forces resulting in significant lateral displacements and associated stresses. Because the principal change in the system properties and ground motion from the earlier results to those presented here is in the value of assumed Young's

modulus for the dam (the other change is the damping model); it is surprising that the results presented here are not consistent with the earlier conclusions. In order to resolve what appears to be an anomaly, the earthquake stresses (excluding initial static stresses) due to horizontal and vertical ground motions, separately, and including hydrodynamic effects, for selected finite elements (Nos. 40, 41, 129 in Fig. 1), are presented in Fig. 9. Although considerable stresses are caused by vertical ground motion, they partially cancel the stresses due to horizontal ground motion, resulting in reduced response when both ground motion components are considered simultaneously. The contribution of the
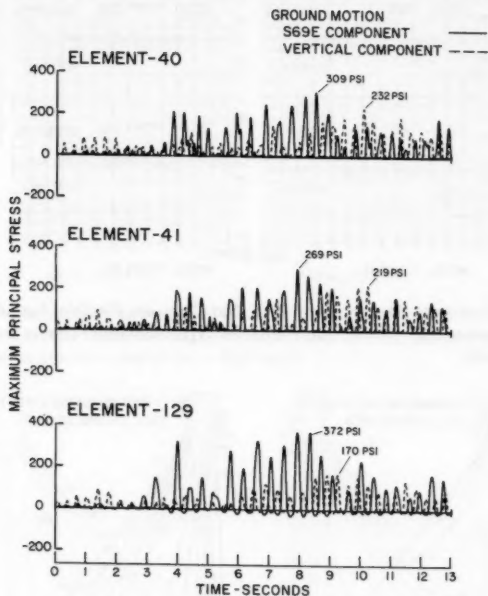
FIG. 9.—Stresses at Selected Locations of Pine Flat Dam on Rigid Foundation Rock due to Separate Action of S69E and Vertical Components of Taft Ground Motion. Hydrodynamic Effects are Included but Static Stresses are Excluded (1 psi = 6.9 kN/m²)

vertical component of ground motion to the total response of a dam, including hydrodynamic effects, therefore depends on the relative phasing of the responses to horizontal and vertical ground motion, which in turn, depends on the phasing of the ground motion components and the vibration properties of the dam.

DAM-FOUNDATION ROCK INTERACTION EFFECTS

The foundation impedances for a half plane are smooth, slowly varying functions of the excitation frequency. However, the hydrodynamic terms are unbounded

at the natural frequencies of water in the reservoir. As a result, the dam-foundation rock interaction influences the response of the dam in a simpler manner than the hydrodynamic effects do (Fig. 3). The fundamental resonant frequency of the dam is decreased and the corresponding damping ratio is increased due
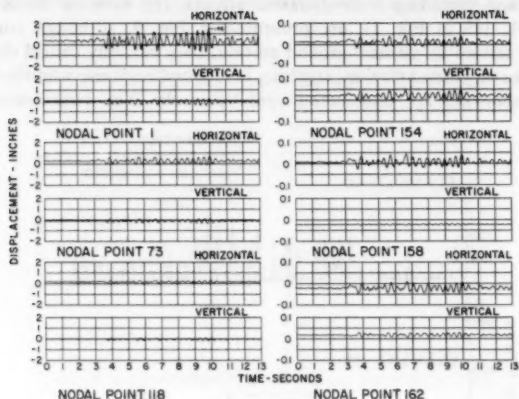
FIG. 10.—Displacement Response of Pine Flat Dam on Flexible Foundation Rock to S69E Component of Taft Ground Motion. Hydrodynamic Effects are Excluded (1 in. = 25.4 mm)
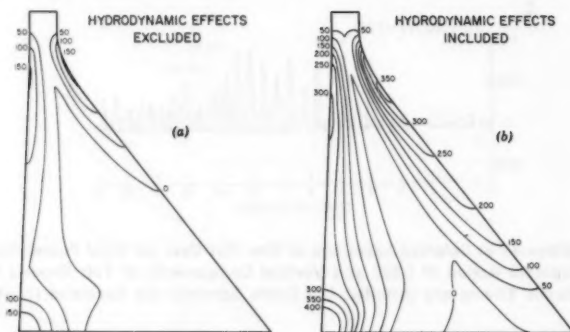
FIG. 11.—Envelope Values of Maximum Principal (Maximum Tensile or Minimum Compressive) Stresses in Pine Flat Dam on Flexible Foundation Rock due to S69E Component of Taft Ground Motion: (a) Hydrodynamic Effects Excluded; and (b) Hydrodynamic Effects Included (1 psi = 6.9 kN/m²)

to dam-foundation rock interaction (Fig. 3). This decrease in frequency is, however, smaller than the frequency reduction due to hydrodynamic effects. The ordinate of the pseudo-acceleration response spectrum for the S69E component of Taft ground motion is essentially unaffected by the increase in vibration

period but would be reduced due to the increased damping (Fig. 4). This leads to increase in displacements (compare Figs. 5a and 10) and reduction in stresses [compare Figs. 6(a) and 11(a)]. The displacements increase due to lengthening of the vibration period [Figs. 5(a) and 10]. Flexibility of the foundation rock
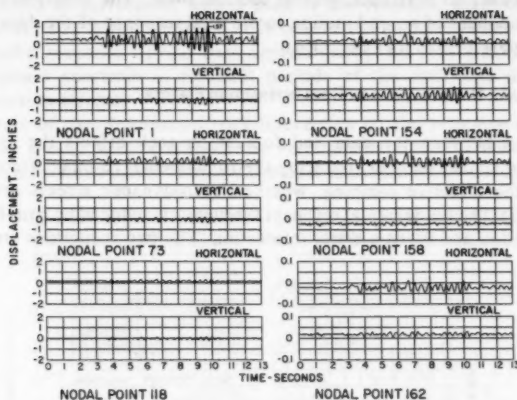
FIG. 12.—Displacement Response of Pine Flat Dam on Flexible Foundation Rock to S69E and Vertical Components, Simultaneously, of Taft Ground Motion. Hydrodynamic Effects are Excluded (1 in. = 25.4 mm)
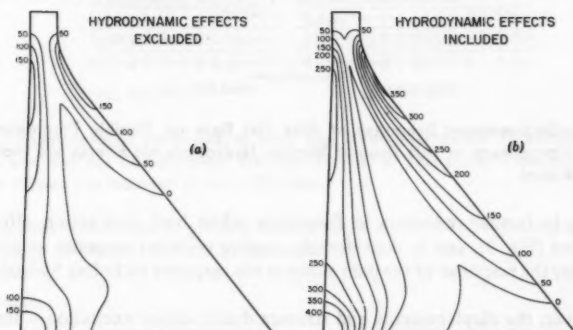
FIG. 13.—Envelope Values of Maximum Principal (Maximum Tensile or Minimum Compressive) Stresses in Pine Flat Dam on Flexible Foundation Rock due to S69E and Vertical Components of Taft Ground Motion: (a) Hydrodynamic Effects Excluded; and (b) Hydrodynamic Effects Included (1 psi = 6.9 kN/m²)

permits motions at the base of the dam (Fig. 10) but these are much smaller than the motions at the crest of the dam. Comparison of Figs. 6(a) and 11(a) indicates that the stresses near the base of the dam are relaxed because of rock flexibility.

The effects of dam-foundation rock interaction on the response of the dam to horizontal and vertical components of ground motion acting simultaneously can be observed by comparing Figs. 7(a) and 12 with Figs. 8(a) and 13(a), respectively. These effects are generally similar to those observed in the foregoing in the responses to horizontal ground motion alone. The contributions of the vertical component of ground motion to the total response of the dam are rather small [compare Figs. 11(a) and 13(a)].

DAM-WATER AND DAM-FOUNDATION ROCK INTERACTION EFFECTS

Interaction between the dam and foundation rock affects the response of the dam in a similar manner, reducing the fundamental resonant frequency and increasing the effective damping, whether hydrodynamic effects are included or not (Fig. 3). The fundamental resonant frequency is reduced by dam-foundation rock interaction and by dam-water interaction. The two reductions are additive,
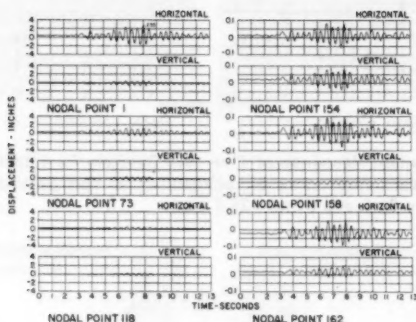
FIG. 14.—Displacement Response of Pine Flat Dam on Flexible Foundation Rock to S69E Component of Taft Ground Motion. Hydrodynamic Effects are Included (1 in. = 25.4 mm)

resulting in further reduction in frequency when both interaction effects are considered (Fig. 3), and in considerably smaller resonant response as compared with either the response of the dam alone or the response including hydrodynamic effects.

However, the displacements and stresses due to either excitation—horizontal ground motion only or horizontal and vertical ground motions simultaneously—are considerably increased due to dam-foundation rock interaction, [compare Figs. 5(b) and 14, 6(b) and 11(b), 7(b) and 15, and 8(b) and 13(b)]. Compared to the response of the dam including only hydrodynamic effects, the stresses in upper parts of the dam are increased due to dam-foundation rock interaction when the excitation is only the horizontal component of ground motion [Figs. 6(b) and 11(b)]; also, when the excitation included the vertical component of ground motion [Figs. 8(b) and 13(b)]. Stresses at the heel of the dam are increased to a much lesser extent because of the stress-relaxation due to foundation flexibility. The area enclosed by a particular stress contour increases due to

dam-foundation rock interaction, indicating that the dam is stressed beyond that contour value over a larger portion. This increase in earthquake response occurs in spite of the decreased response indicated by complex frequency responses, because dam-foundation rock interaction shifts the fundamental resonant period to correspond with a peak of the response spectrum (Fig. 4). Thus, the effects of dam-foundation rock interaction and dam-water interaction on earthquake response of the dam depend partly on the relative ordinates of the response spectrum at resonant periods of the dam with and without these interaction effects.

The effects of dam-foundation rock interaction on the response of the dam are generally similar with or without the vertical component of ground motion. For reasons mentioned under "Dam-Water Interaction Effects," the contributions
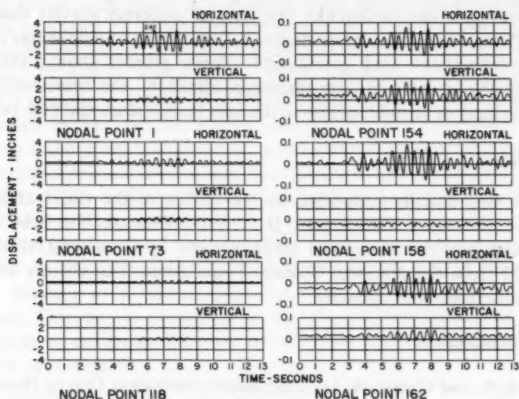
FIG. 15.—Displacement Response of Pine Flat Dam on Flexible Foundation Rock to S69E and Vertical Components, Simultaneously, of Taft Ground Motion. Hydrodynamic Effects are Included (1 in. = 25.4 mm)

of the vertical component of ground motion to the response of the dam, including both sources of interaction, are rather small.

CONCLUSIONS

The displacements and stresses of Pine Flat Dam due to the Taft ground motion are increased significantly because of hydrodynamic effects. Compared to the response of the dam including only hydrodynamic effects, the stresses in the upper parts of the dam are significantly increased due to interaction between the dam and the foundation rock. Stresses at the heel of the dam are increased to a lesser extent because of the stress relaxation due to foundation flexibility. The influence of dam-foundation rock interaction and dam-water interaction on the response of a dam depends in part on the change in the earthquake response spectrum ordinate associated with changes in resonant frequencies and apparent damping due to these interaction effects. As such,

these effects would depend on the resonant frequencies of the dam and the shape of the earthquake response spectrum in a neighborhood of these resonant frequencies. Although considerable stresses in Pine Flat Dam are caused by the vertical component of Taft ground motion, they partially cancel the stresses due to the horizontal component, resulting in reduced response when both ground motion components are considered simultaneously. The contribution of the vertical component of ground motion to the total response of a dam, including hydrodynamic effects, depends on the relative phasing of the responses to horizontal and vertical ground motion, which in turn depends on the phasing of the ground motion components and the vibration properties of the dam.

All the details of observations from the response of Pine Flat Dam to Taft ground motion presented in this paper may not apply to other dams or ground motions. However, the broad conclusions presented should be valid for many cases. In particular, the earthquake response of concrete gravity dams will be generally influenced to a significant degree by the effects of dam-water interaction and of dam-foundation rock interaction. These effects should therefore be considered in the analysis of dam response. Similarly, the contributions of the vertical component of ground motion to the dam response should also be included.

ACKNOWLEDGMENTS

APPENDIX.—REFERENCES

1. Chakrabarti, P., and Chopra, A. K., "Earthquake Analysis of Gravity Dams Including Hydrodynamic Interaction," *International Journal of Earthquake Engineering and Structural Dynamics*, Vol. 2, 1973, pp. 143–160.
2. Chakrabarti, P., and Chopra, A. K., "Hydrodynamic Effects in Earthquake Response of Gravity Dams," *Journal of the Structural Division*, ASCE, Vol. 100, No. ST6, Proc. Paper 10616, June, 1974, pp. 1211–1224.
3. Chopra, A. K., Chakrabarti, P., and Gupta, S., "Earthquake Response of Concrete Gravity Dams Including Hydrodynamic and Foundation Interaction Effects," *Report No. UCB/EERC-80/01*, Earthquake Engineering Research Center, University of California, Berkeley, Calif., 1980, 187 pp.
4. Chopra, A. K., and Chakrabarti, P., "Earthquake Analysis of Concrete Gravity Dams Including Dam-Water-Foundation Rock Interaction," *Earthquake Engineering and Structural Dynamics*, Vol. 9, No. 4, July–Aug., 1981.
5. Dasgupta, G., and Chopra, A. K., "Dynamic Stiffness Matrices for Homogeneous Viscoelastic Half Planes," *Journal of the Engineering Mechanics Division*, ASCE, Vol. 105, No. EM5, Proc. Paper 14888, Oct., 1979, pp. 729–745.
6. Liam Finn, W. D., Varoglu, E., and Cherry, S., "Seismic Water Pressure Against Dams," *Structural and Geotechnical Mechanics*, W. J. Hall, ed., Chapter 21, Prentice-Hall, Inc., New York, N.Y., 1977, pp. 420–442.
7. Rea, D., Liaw, C. Y., and Chopra, A. K., "Mathematical Models for the Dynamic Analysis of Concrete Gravity Dams," *International Journal of Earthquake Engineering and Structural Dynamics*, Vol. 3, No. 3, Jan.–Mar., 1975, pp. 249–258.
8. Vaish, A. K., and Chopra, A. K., "Earthquake Finite Element Analysis of Structure-Foundation Systems," *Journal of the Engineering Mechanics Division*, ASCE, Vol. 100, No. EM6, Proc. Paper 10990, December 1974, pp. 1101–1116.

Economic Review of Earthquake Design Levels

By John M. Ferritto,[1] M. ASCE

Introduction

The seismic design of a structure can be a complex task. There are several alternative design techniques in use which vary from a relatively simple static assignment of shears to a full complete nonlinear dynamic analysis. The total plant replacement value of Navy shore installations in seismic zones 3 and 4 is approx 21 billion dollars. The Naval Facilities Engineering Command (NAVFAC) guidelines specify that for critical buildings a site seismicity study be performed in lieu of the lateral load coefficients. Previous Naval Civil Engineering Laboratory reports (5-9) demonstrated an approach for computing the probability of seismic loading at a site. Current NAVFAC criteria for important structures specifies a 225-yr return time earthquake (80% probability of not being exceeded in 50 yr) as the basis for seismic design. This study will investigate risk-optimized procedures for Navy shore structures to minimize damage and repair costs in relation to initial construction cost. A damage function relating expected damage as a function of the imposed acceleration level can be constructed. This may be combined with a function relating cost of construction as a function of design acceleration level. Total cost may be related to design earthquake return time.

The probability of site acceleration used in this study is based on the total risk to the site from *All* of the faults in the area, and as such represents a rigorous estimation of the actual risk. Less rigorous studies attempt to design for the most significant fault, ignoring all others. This is a simplification perhaps useful for design; however it understates the risk in most situations where there are several faults of almost equal seismic capability.

Building Damage.—There is a correlation between the degree of damage and the intensity of shaking. Whitman et al. (8) give an example of a damage probability matrix for buildings in the 1971 San Fernando earthquake. This gives an overview of structural performance, but does not relate structure design parameters. In a similar way Culver et al. (3), knowing the quality of construction in terms of strength, physical condition integrity, and workmanship estimate drift to yield

and ductility to failure. These set up allowable deflection guides for comparison with results from an analysis. Refs. 4 and 19 give damage as a function of intensity, and an attempt is made to identify both the subsystems of the structure and the damage to each subsystem. Another study by Sauter (17) also gives damage ratios as a function of intensity; see Fig. 1.

In evaluating the total loss to a facility from an earthquake, one must include the physical damage, the injury and loss of life, the damage to contents of the building, and the interruption in the functional use of the facility and its associated cleanup. Ref. 1 presents an analysis of damage levels and suggests desired performance levels. In evaluating the physical damage, the cost of repair
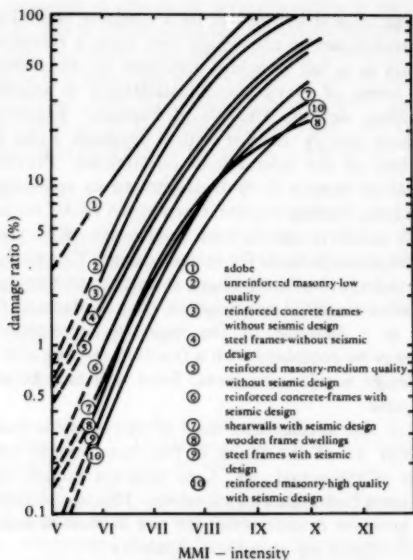
FIG. 1.—Average Damage Ratio Relationships (from Ref. 17)

may exceed the original cost of the structure. Thus, the damage ratio (percent of damage) must reflect the present worth or replacement of the facility.

Physical damage involves both the structural elements and the nonstructural. Nonstructural elements include interior and exterior walls partitions, ceilings, plumbing, glazing, lighting fixtures, stairs, and elevators. These may represent a larger monetary loss than the damage to the structural system. Such is usually the case with steel frame buildings. Damage to the contents and downtime may represent 30% of the total loss.

It is possible to use previous data in the form of Fig. 1 to determine damage as a function of site acceleration. Once the function has been established for each type of construction it is possible to divide the acceleration by some form
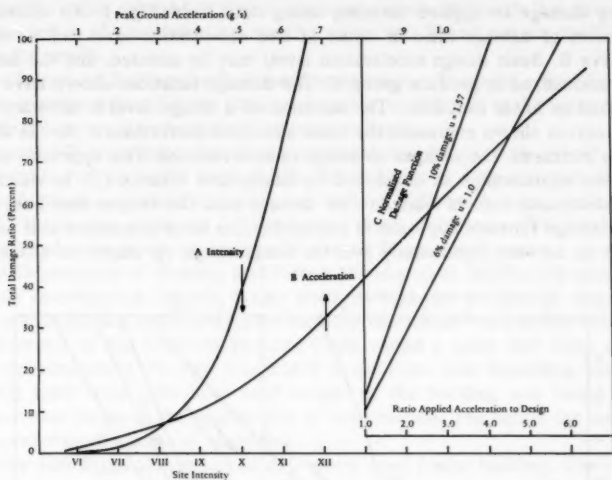
FIG. 2.—Reinforced Masonry with Seismic Design
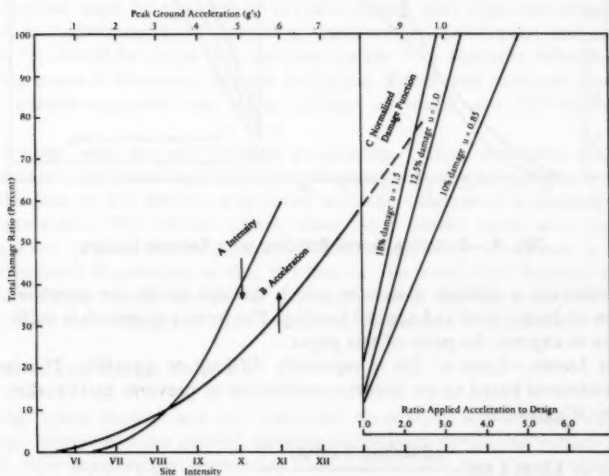
FIG. 3.—Steel Frame Building with Seismic Design

of design level acceleration and thus normalize the acceleration axis (see Figs. 2, 3, and 4). For the types of construction indicated, curve A may be drawn relating damage to applied intensity using data from Fig. 1. An alternative expression of damage ratio in terms of site acceleration level can be made; see curve B. Basic design acceleration levels may be selected, and the damage curve normalized to produce group C. The damage functions shown have been simplified as linear functions. The selection of a design level is arbitrary; any of the curves shown expresses the same structural performance. As the design level is increased, the collapse to design ratio is reduced. This approach results in similar relationships as developed by Blume and Munroe (2), in which the demand-capacity ratio is related to the damage ratio for various ductilities. The linear damage function approach is a simplification since it assumes that natural periods do not vary significantly over the design range. An improved alternative
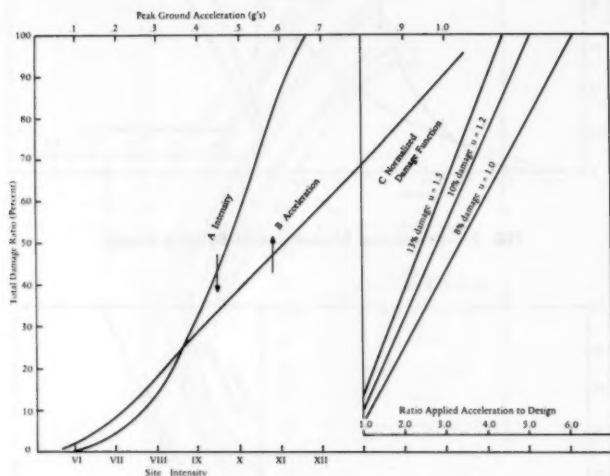
FIG. 4.—Concrete Frame Building with Seismic Design

is to construct a damage matrix in which damage levels are tabulated as a function of design level and applied loading. The former approach is sufficiently accurate to express the point of this paper.

Other Losses.—Loss of life is especially difficult to quantify. The loss of life is estimated based on an historical evaluation of previous earthquakes from work by Wiggins (20)

$$\text{Number of Lives Lost} = \frac{(\text{Building \$ Loss})^{0.813}}{100,000} \quad \ldots \ldots \ldots \ldots \ldots (1)$$

The number of injuries may be estimated as

$$\text{All injured} = 43.0 \times \text{Loss Life}; \quad \text{Seriously Injured} = 2.8 \times \text{Loss Life} \quad \ldots (2)$$

The value of a human life is assumed to be $300,000. The writer realizes that many readers may not approve of quantifying the value of life; further, the specific value selected is always open for debate. Although this parameter was needed in the analysis, its specific value was found not to significantly affect the results.

Cost Increase of Earthquake Resistant Construction.—The basic costs of seismic resistant design is found in the structural system, specifically in the beam girders and the columns. Other costs include the foundation.

Nakano (12) investigated structure costs for elastic design, with seismic design coefficients and allowable stress limits. Whitman, et al. (18) note the increase in cost for typical apartment buildings for various Uniform Building Code design levels. These data appear to be lower than those of Nakano. Whitman's data are believed to be more appropriate for United States construction.

The Department of Housing and Urban Development (HUD) (10) sponsored a study investigating seismic design costs of high-rise residential structures. They concluded that upgrading typical high-rise residential construction to seismic requirements of the Uniform Building Code varied a great deal from city to city. Approximately 0%–30% was added to the basic cost depending upon the existing local code. The total dead weight of the building was found to be an important factor in the general cost of construction. The lighter the building, the lower were the costs of upgrading.

Leslie and Biggs (11) analyzed a 13-story steel frame building. They show a breakdown of costs of structural and nonstructural items. The costs of strengthening nonstructural systems is low. The major factor in strengthening the nonstructural system is providing proper anchoring and bracing. Restraint of equipment must be provided to prevent sliding. Restraints and bracing are needed for ventilating ducts, plumbing, transformers, switchgear, and elevator motors. It should be noted that the dead weight of a structure influences the resulting costs of increasing seismic resistance. Reinforced concrete structures would exhibit increased cost ratios, perhaps as much as a 75% increase in cost.

Disruption costs are very difficult to quantify. Critical structures that must be operated after an earthquake involve secondary interaction with the community. The loss of life directly associated with the collapse of a hospital is the first interaction. The second comes when other deaths occur as a result of the mobility to treat the community. For strategic Navy structures, a degree of redundancy is provided in that the loss of one structure's function can be picked up by a facility not in the earthquake area. For the purposes of this study, secondary disruption costs will not be considered in such cases.

EARTHQUAKE COST DAMAGE ANALYSIS

Using typical damage and cost functions, an analysis was made of expected damage, injury, and the cost of earthquake resistant design for various design levels. Site acceleration probability distributions for San Diego, Memphis, Bremerton, Long Beach, and Port Hueneme were used. For important structures, the Navy has adopted a 50-yr exposure/life period. Typical results are shown in Fig. 5, which is a plot of design acceleration and total cost increase. The total cost includes construction increase and expected damage and injury. A

Total cost shows increase in costs for strengthening and expected damage to a new building without seismic design or loss.
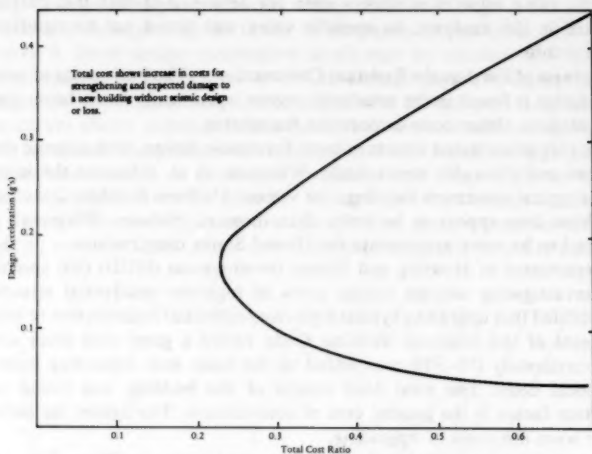
FIG. 5.—Typical Cost as Function of Design Acceleration
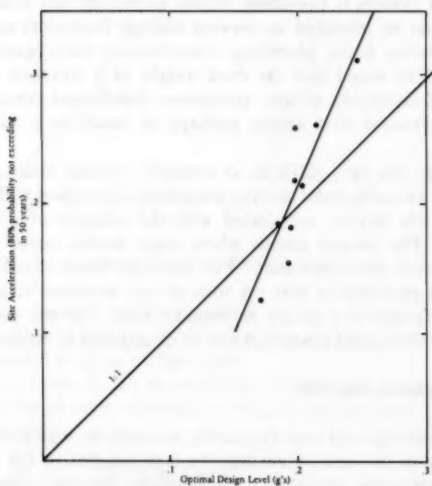
FIG. 6.—Optimal Design Acceleration

(preliminary) minimum cost in this example occurs for a design acceleration of 0.17 g, which has a return period of 357 yr. Numerous analyses were performed using the probability distributions for the aforementioned sites. Results are shown in Figs. 6 and 7. Fig. 6 shows the least cost design acceleration as a function of the 225-yr return time acceleration. The 225-yr (20% chance of exceedance in 50 yr) acceleration characterizes the site seismicity sufficiently accurately for all the sites and the data give a clear trend with minimal scatter, which is significant, considering the variation in locations.

Fig. 6 shows that for a 225-yr acceleration of 0.2 g, the least cost design acceleration would be about 0.19 g. "Design acceleration," in this case, implies a design of a steel building to about yield level (see Fig. 4). The selection of the design level is based on the ratio of collapse to design level and its
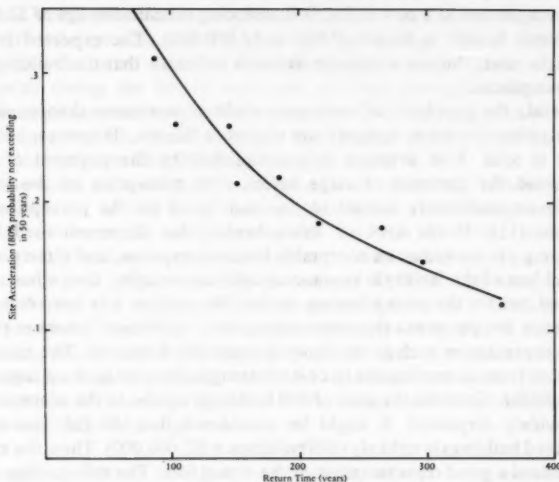
FIG. 7.—Optimal Design Acceleration Return Time

associated ductility and damage, as shown in Fig. 4. These curves are not intended to be generalized for use in design but rather to illustrate a concept.

ANALYSIS OF STUDY RESULTS

First, it is important to point out that the data used in this study is an accumulation of average behavior and has a wide scatter. The intent is to demonstrate a trend, not to give guidance for a specific building.

An examination of Fig. 6 shows that the data trends away from the 1:1 correspondence line. The optimal design is not related to a unique return period. Rather, at low accelerations, it is greater than the 225-yr return time, and at high accelerations it is less. This is in agreement with basic structural engineering experience, that it is difficult and costly to resist high-level shaking. There

is uncertainty in the data; however based on a sensitivity analysis, it is believed the uncertainty will basically shift the curve to the left or the right, but not change its slope. So, the basic premise that a constant return time is not a general optimal design level should remain.

ANALYSIS OF RISK

Two elements in establishing design levels are: (1) The perception of the probability of the catastrophic event; and (2) the net cost of the lives saved and reduced damage given a design level is placed in effect. From an economic viewpoint, an acceptable decision exists whenever the benefits minus the costs is positive. The optimal decision level maximizes the net present value (11).

The probability of the damaging earthquakes occurring is 0.002. A building may be strengthened at a cost of $10,000, reducing seismic damage of $2,000,000. The expected benefit is $4,000 (0.002 × $2,000,000). The expected benefit is less than the cost; thus an economic decision indicates that the building should not be strengthened.

In general, the purchase of insurance violates economic theory, since the insurance policy premium exceeds the expected benefit. However, substantial insurance is sold. Risk aversion is accomplished by the payment of a fixed cost to avoid the potential of large losses. The preception of the loss may be linearly or nonlinearly related to the cost based on the preception of the investigator (11). If the cost of strengthening the aforementioned building ($10,000), e.g., is viewed as an acceptable business expense, and if the possibility of the total loss of the facility is an unacceptable catastrophy, then a businessman may indeed opt for the strengthening option. He realizes it is not economically advantageous but perceives the consequence in a "nonlinear" manner (15).

A large organization such as the Navy is regionally dispersed. The relationship of dollar loss from an earthquake to cost of strengthening for such an organization should be linear. Consider the case of 100 buildings similar to the aforementioned building widely dispersed. It might be considered that the full loss of these 100 separated buildings is unlikely (100 buildings × $2,000,000). Thus, the expected value is indeed a good representation of the actual loss. The risk-pooling concept is applicable to large organizations like the Navy (15).

NAVY ECONOMIC ANALYSIS

Ref. 13 specifies procedures for use in conducting economic analyses of facilities. The objectives of the analyses are: (1) To insure an optimum allocation of scarce resources; (2) to effectively consider alternatives and life-cycle funding implications; and (3) to recognize that money has value over time expressed by an interest rate.

In this problem, the earthquake strengthening is expressed as a current cost increase to protect against a future dollar loss. The real world is complicated by cost increases over time referred to as inflation. This means that to repair or replace the damaged building some time in the future will cost more than it would today. Further, money has a value in time. The work in the previous sections expressed costs of strengthening and damage as a percent of building value to maintain a common reference.

The government has placed a value on money in time. Ref. 13 and DODINST 7041.3 specify the (differential) discount rate as 10%. Ref. 13 states:

> The rationale for adopting the private-sector rate of return as the discount rate for analyzing Government investment proposals turns on the notion that *Government investments are funded with money taken from the private sector* (preponderantly via taxation), *are made in the ultimate behalf of the private sector* (i.e., the individuals comprising it), *and thus bear an implicit rate of return comparable to that of projects undertaken in the private sector.* In this interpretation, 10% measures the opportunity cost of investment capital forgone by the private sector.

The 10% rate is a differential rate considered in addition to inflation. When the present worth of the annual expected damage is considered using a discount rate of 10%, the present worth estimate of the damage would effectively be reduced by a factor of about 5. To restate this, the earthquake could occur at any point during the life of structure; the best estimate is to consider an annual series of expected losses. The present worth of this series can be computed and its value is about one-fifth of the total expected loss. This has a major effect on the optimum design levels; see Figs. 8 and 9.

It is important to note that the discount rate specified for use is actually a differential rate of 10% over the rate of inflation. It is recognized that the future cost of the repair would increase in cost with time. One could use the differential rate and not consider inflation, or one could consider the rate of inflation to project an increased repair cost and discount that using a discount rate of 10% plus the inflation rate. The results for modest inflation rates are approximately the same. The differential cost approach is used in this study.

Comparing the NAVFAC criteria (80% probability of nonexceedance in 50 yr) acceleration with the optimal least cost acceleration the cost per life saved may be estimated (see Fig. 10). For a 50-yr exposure of a building with an initial cost of $1 million, e.g.

1. Acceleration level having 80% probability of not being exceeded in 50 yr: 0.26 g.—cost of seismic strengthening: $338,700; present worth of expected damage: $26,200; and lives lost: 0.0491 people.

2. Least cost design acceleration: 0.12 g.—cost of seismic strengthening: $123,900; present worth of expected damage: $95,100; and lives lost: 0.1711 people.

3. Damage difference (least cost design acceleration − 80% probability of not being exceeded acceleration): $68,900.

4. Cost difference (80% probability of not being exceeded acceleration − least cost design acceleration): $214,800.

5. Lives lost (least cost design acceleration − 80% probability of not being exceeded acceleration): 0.122.

6. Marginal value (cost difference − damage difference)/lives lost: $1,200,000.

A marginal value, $1,200,000, for the current criteria earthquake of 80% probability of not being exceeded in 50 yr is high in comparison with other sectors.
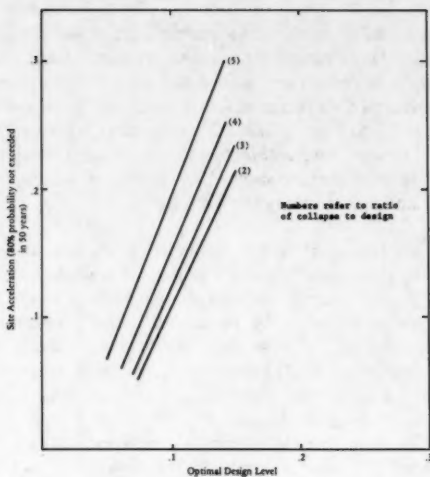
FIG. 8.—Optimal Design Acceleration Discounting Damage
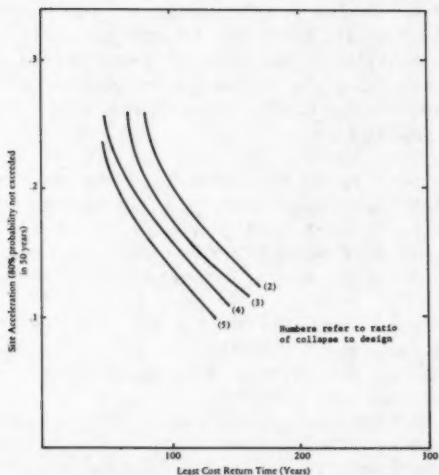
FIG. 9.—Optimum Return Time Discounting Damage
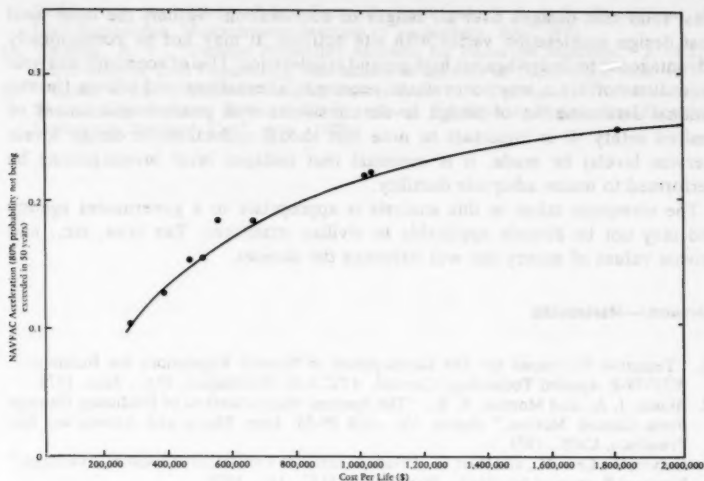
FIG. 10.—Cost per Life

Paté (16) has calculated the marginal value per life which is necessary to have benefits exceed costs for seismic design level in the San Francisco bay area. Her results, although tentative, indicate that to adopt the 1973 Uniform Building Code, a value of life on the order of $6,000,000/life for the enforcement of the seismic provisions in new buildings and $22,000,000/life for the upgrading of old buildings to the same standards. A value of $20,000,000/life is required to adopt the 1976 provisions for new construction. The marginal cost per life saved in other sectors of public safety is much lower. In the transportation sector cost benefit analysis projects are around $300,000. The conclusion of Paté's work is that it is hard to justify the 1973 and 1976 seismic design provisions solely on the interest of life safety.

Organizational theory suggests that an individual within an organization accepts a framework which defines the areas of his responsibilities and correspondingly narrows the scope of his alternative decisions.

Engineers in seismic design are not usually tasked to resolve problems from the viewpoint of investment costs and protection benefits. Engineering regulations from as far back as the Code of Hammurabie have had public safety foremost. The public perceives a requirement for the government to assure safety. Yet according to Paté (16), the value of life in other sectors such as health is markedly lower than imposed for building safety; take, e.g., the $20,000/life value as a result of the program to reduce the risks of heart attack. The perceived action results from the public and the professional engineers risk aversion of large catastrophes.

Conclusion

The specification of a 225-yr return time acceleration does not produce optimal

least total cost designs over all ranges of acceleration. Rather, the least total cost design acceleration varies with site activity. It may not be economically advantageous to design against high ground acceleration. Use of economic analysis procedures offers a way to evaluate economic alternatives and allows for the rational determination of design levels consistent with prudent assessment of desired safety. It is important to note that should reductions in design levels (service levels) be made, it is essential that collapse level investigations be performed to insure adequate ductility.

The viewpoint taken in this analysis is appropriate to a government agency and may not be directly applicable to civilian structures. Tax laws, etc., and private values of money use will influence the choices.

APPENDIX.—REFERENCES

1. "Tentative Provisions for The Development of Seismic Regulations for Buildings," *NSF-78-8*, Applied Technology Council, *ATC 3-06*, Washington, D.C., June, 1978.
2. Blume, J. A., and Monroe, R. E., "The Spectral Matrix Method of Predicting Damage From Ground Motion," *Report No. JAB 99-88*, John Blume and Associates, San Francisco, Calif., 1971.
3. Culver, G., Lew, H., and Hart, G., "Natural Hazards Evaluation of Existing Buildings," National Bureau of Standards, Washington, D.C., Jan., 1975.
4. "A Rational Approach to Damage Mitigation in Existing Structures Exposed to Earthquakes," Earthquake Engineering Systems, San Francisco, Calif.
5. Ferritto, J. M., "A Probabilistic Procedure for Estimating Seismic Loading Based on Historic and Geologic Data," *Technical Report R-867*, Civil Engineering Laboratory, Port Hueneme, Calif., Aug., 1978.
6. Ferritto, J. M., "Revisions to Program RECUR and An Example Case Study," *Technical Memorandum M-51-79-03*, Port Hueneme, Calif., Mar., 1979.
7. Ferritto, J. M., "A Probabilistic Evaluation of Seismic Loading at Naval Submarine Base, Bonger, Bremerton, Washington," *Technical Memorandum M-51-79-01*, Port Hueneme, Calif., Mar., 1979.
8. Ferritto, J. M., "A Probabilistic Evaluation of Seismic Loading at a Typical Los Angeles Site," *Technical Memorandum M-51-79-04*, Port Hueneme, Calif., Aug., 1979.
9. Ferritto, J. M., "Earthquake Loading and Soil-Structure Interaction," *Technical Memorandum M-51-79-12*, Port Hueneme, Calif., July, 1979.
10. "Seismic Design Cost Impact on High-Rise Residential Construction," Housing and Urban Development, Washington, D.C., Sept., 1977.
11. Leslie, S. K., and Biggs, "Optimum Seismic Protection and Building Damage Statistics," *#341*, Massachusetts Institute of Technology, Cambridge, Mass., May, 1972.
12. Nakano, K., et al., "On the Object Postulate for Earthquake Resistant Code," *NBS Special Publication 523: Wind and Seismic Effects*, National Bureau of Standards, Sept., 1978.
13. *NAVFAC P-442 Economic Analysis Handbook*, Department of the Navy, Naval Facilities Engineering Command, Alexandria, Va., June, 1975 (revised Oct., 1975).
14. Olivera, C. S., "Seismic Risk Analysis for a Site and a Metropolitan Area," *EERC 75-3*, University of California, Berkeley, Calif., 1973.
15. Oppenheim, I. J., "Economic Analysis of Earthquake Engineering Investment," *Proceedings*, Second United States National Conference on Earthquake Engineering, Stanford University, Stanford, Calif., Aug., 1979.
16. Paté, M. E., "Acceptance of a Social Cost for Human Safety—A Narrative Approach," *Proceedings*, Second United States National Conference on Earthquake Engineering, Stanford University, Stanford, Calif., Aug., 1979.
17. Sauter, F., "Damage Prediction for Earthquake Insurance," *Proceedings*, Second United States National Earthquake Conference on Earthquake Engineering, Stanford University, Stanford, Calif., Aug., 1979.
18. Whitman, R. V., Hong, S. T., and Reed, J. W., "Damage Statistics for High-Rise

Buildings in the Vicinity of San Fernando Earthquake," *R 73-24*, Department of Civil Engineering, Massachusetts Institute of Technology, Apr., 1973.

19. Whitman, R. V., "Damage Probability Matrices for Prototype Buildings," *R 73-57*, Department of Civil Engineering, Massachusetts Institute of Technology, Oct., 1973.

20. Wiggins, J. H., "Estimated Building Losses from U.S. Earthquakes," *Proceedings*, Second United States National Conference on Earthquake Engineering, Stanford University, Stanford, Calif., Aug., 1979.

STEEL FRAMES WITH NONLINEAR CONNECTIONS [a]

By Piotr D. Moncarz[1] and Kurt H. Gerstle,[2] M. ASCE

INTRODUCTION

Problem and Objective.—To facilitate the design of unbraced multistory steel building frames, the American Institute of Steel Construction Specifications (2), Sec. 1.2, provide for their idealization as either rigid-jointed frames, designated as "Type 1," or for the assumption of a "Type 2" construction which allows gravity loads to be resisted by simple-beam action, while lateral loads are to be carried by moment-resistant girder-column joints. "Type 3," finally, provides for more rigorous analysis, which includes the effect of actual connection flexibility.

Both Types 1 and 2 construction are commonly used and, when followed with discretion and judgment, have resulted in satisfactory structures. However, because Type 1 assumes perfectly-rigid joints, it may underestimate the sway of the bare frame, and might result in overly heavy columns. Buildings designed as Type 2 may have girders which are too heavy, and columns which are too weak, when compared to more exact analysis.

In many locations, climatic conditions limit year-round field welding, and field-bolted frames may therefore be preferred. Bolted connections may be more flexible than fully-welded joints, thus accentuating the need for Type 3 construction. While modern analysis methods allow inclusion of connection flexibility, necessary information regarding connection behavior and suitable computer programs are lacking so that Type 3 construction is rarely used at this time.

Therefore, it appears useful to obtain, by rational analysis which includes the effects of realistic connection behavior, information about the expected response of structures designed according to Type 2 methods under real loads, and to shed light on the validity of the underlying assumptions and the safety and economy of the resulting structures.

With this goal in mind, this paper, in subsequent sections, will briefly examine actual connection behavior, outline a method of analysis which accounts for nonlinear connection behavior and variable load histories, and apply it to a variety of frames to document the consequences of approximations on the prediction of sway, force distribution among girders and columns, deflection stability, and response to load histories.

BACKGROUND

The behavior of riveted girder-column connections and explored by various investigators (11,16,18) beginning in the 1930s. These studies lead in general to curves of applied moment versus joint rotation. Frye and Morris (8) developed equations for moment-rotation relations for a wide range of connections. Interest in earthquake response has led to a number of studies of joint behavior under load cycles (5,17).

Early analyses of flexibly-connected frames (4) could solve only simple situations. With the advent of matrix-computer methods, more general structures were analyzed statically and dynamically (10,13,19), usually with the assumption of linearized connection behavior. Recent studies (8) have also considered the effects of nonlinear connection response under proportionally-increasing loads. The solid foundation provided by these analytical studies has so far not been utilized for systematic investigation of real building systems.

On the practical side, Disque (6,7) has provided justification of Type 2 construction, based on the concept of plastic redistribution of excess moments and eventual shakedown to elastic response. This approach is well-explained in a recent American Iron and Steel Institute (AISI) publication (1). On the other hand, McGuire (14), by example calculations of a simple frame, pointed out some pitfalls of Type 2 construction. A general overview of current thinking is provided by a recent ASCE monograph (3), which stresses, in several places, the importance of a realistic assessment of the effects of connection flexibility.

ANALYTICAL APPROACH

Frame Analysis.—The matrix displacement method (9) is used to determine displacements $\{\Delta\}$ and forces $\{X\}$ under loads causing fixed-end forces $\{X^F\}$

$$\{X\} = [K]\{\Delta\} + \{X^F\} \quad \dots \dots \dots \dots \dots \dots \dots \dots \dots \dots \dots \dots \dots \dots \dots (1)$$

In Eq. 1, $[K]$ = the structure stiffness matrix which can be obtained by
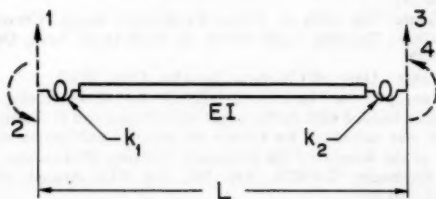
FIG. 1.—Analytical Model of Beam with Flexible Connections

superposition of the element stiffness matrices $[k^i]$. In this nonlinear analysis, these element stiffness matrices, and therefore $[K]$, may vary as function of load and load history, and may have to be modified from load step to load step through an iterative process.

Element Stiffness.—The effects of connection flexibility is modeled by attaching rotational springs of moduli k_1, k_2 to girder ends as shown in Fig. 1. By classical methods (10), the following girder stiffnesses are obtained

$$k_{33} = \frac{-\left(\dfrac{L}{EI} + \dfrac{1}{k_1} + \dfrac{1}{k_2}\right)}{L^2\left[\left(\dfrac{L}{2EI} + \dfrac{1}{k_1}\right)^2 - \left(\dfrac{L}{3EI} + \dfrac{1}{k_1}\right)\left(\dfrac{L}{EI} + \dfrac{1}{k_1} + \dfrac{1}{k_2}\right)\right]} \quad \ldots\ldots\ldots \text{(1a)}$$

$$k_{43} = k_{34} = \frac{\left(\dfrac{L}{2EI} + \dfrac{1}{k_1}\right)}{L\left[\left(\dfrac{L}{2EI} + \dfrac{1}{k_1}\right)^2 - \left(\dfrac{L}{3EI} + \dfrac{1}{k_1}\right)\left(\dfrac{L}{EI} + \dfrac{1}{k_1} + \dfrac{1}{k_2}\right)\right]} \quad \ldots\ldots \text{(1b)}$$

$$k_{44} = \frac{-\left(\dfrac{L}{3EI} + \dfrac{1}{k_1}\right)}{\left(\dfrac{L}{2EI} + \dfrac{1}{k_1}\right)^2 - \left(\dfrac{L}{3EI} + \dfrac{1}{k_1}\right)\left(\dfrac{L}{EI} + \dfrac{1}{k_1} + \dfrac{1}{k_2}\right)} \quad \ldots\ldots\ldots \text{(1c)}$$

The remaining stiffnesses can be found by statics and symmetry.

The fixed-end forces on the member ends due to a uniform downward load, w, are:

$$X_3^F = \frac{wL}{2} \times \frac{\left(\dfrac{L}{2EI} + \dfrac{1}{k_1}\right)\left(\dfrac{L}{3EI} + \dfrac{1}{k_1}\right) - \left(\dfrac{L}{4EI} + \dfrac{1}{k_1}\right)\left(\dfrac{L}{EI} + \dfrac{1}{k_1} + \dfrac{1}{k_2}\right)}{\left(\dfrac{L}{2EI} + \dfrac{1}{k_1}\right)^2 - \left(\dfrac{L}{3EI} + \dfrac{1}{k_1}\right)\left(\dfrac{L}{EI} + \dfrac{1}{k_1} + \dfrac{1}{k_2}\right)} \quad \text{(2a)}$$

$$X_4^F = -\frac{wL^2}{2} \times \frac{\left(\dfrac{L}{2EI} + \dfrac{1}{k_1}\right)^2 - \left(\dfrac{L}{4EI} + \dfrac{1}{k_1}\right)\left(\dfrac{L}{2EI} + \dfrac{1}{k_1}\right)}{\left(\dfrac{L}{2EI} + \dfrac{1}{k_1}\right)^2 - \left(\dfrac{L}{3EI} + \dfrac{1}{k_1}\right)\left(\dfrac{L}{EI} + \dfrac{1}{k_1} + \dfrac{1}{k_2}\right)} \quad \ldots\ldots \text{(2b)}$$

The remaining fixed-end forces can be determined by statics.

Connection Behavior.—Following the cited references, the moment-rotation behavior for the girder-column connections was assumed to have the characteristics shown in Fig. 2. The following information is obtained from connection tests under monotonically-increasing moment: (1) Initial modulus, k_{el}; (2) proportional limit, M_{el}; (3) shape of nonlinear portion of curve; and (4) asymptotic linear strain-hardening envelope.

For prediction of the response under load histories, the following assumptions were made on the basis of experimental curves shown elsewhere (5,17): (1) Elastic unloading with modulus, k_{el}; (2) constancy of elastic range equals 2 M_{el}; and (3) equal positive and negative strength envelopes.
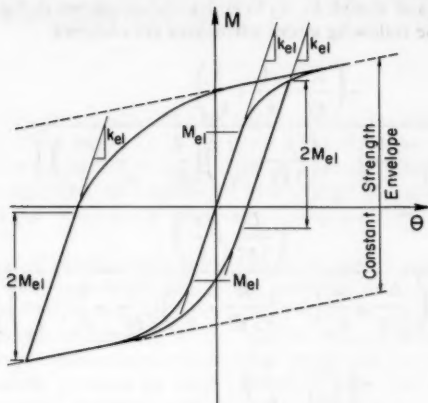
FIG. 2.—Moment-Rotation Hysteresis Loops
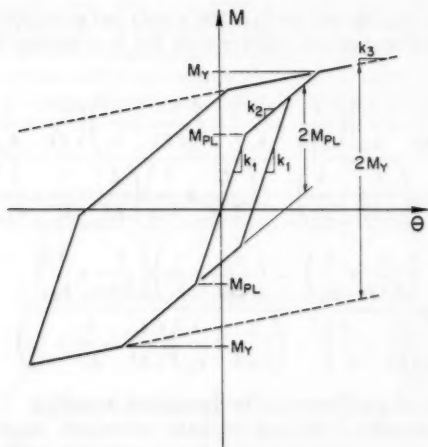
FIG. 3.—Trilinearized Moment-Rotation Hysteresis Loops

For purposes of this analysis, this behavior was trilinearized as shown in Fig. 3. Thus, the complete specification of connection response requires two

moment values, M_{el} and M_y, and three moduli, k_1, k_2, and k_3. In view of the uncertainty of actual connection behavior, this simplification appears permissible.

Computer Implementation.—To accommodate both arbitrary load histories and connection nonlinearity, the solution of Eq. 1 is carried out incrementally and piecewise-linearly. Under increasing loads, each connection is checked for attainment of the critical moments, M_{el} and M_y; the load step is factored to this event, and incremental displacements and forces are calculated. The stiffnesses are modified by substitution of the new moduli, a new solution is carried out, and the incremental results added to previously accumulated values. In addition, during each load increment, each connection rotation has to be checked for increase or decrease, so that appropriate loading or unloading moduli can be inserted.

The computer program with its automated input and its plotting capability for output is presented in details in Ref. 15.

APPLICATIONS

Example 1

Problem Statement.—The two-story, single-bay frame shown in Fig. 4 was designed by Kahl (12) on the basis of Type 2 construction followed by redesign
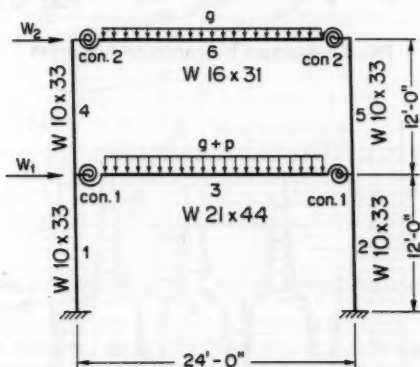
FIG. 4.—Example 1: Structure

based on elastic analysis, which included linear connection flexibility to resist the following service loads: (1) Dead loads $g = 0.07$ kips/sq ft, or 1.86 kips/ft of each girder; (2) live load $p = 0.05$ kips/sq ft on the lower floor only, or 1.20 kips/ft of lower girder; and (3) lateral load of intensity, $w = 0.02$ kips/sq ft of wall, resulting in concentrated floor loads of $W_1 = 5.76$ kips, $W_2 = 2.88$ kips.

The joints were chosen by Kahl from among the top and seat angles tested by Johnston and Hechtman (11); Specimen 25 was selected for the lower beam

connection, and Specimen 23 was selected for the upper beam connection. The experimentally-determined moment-rotation curves are shown in Fig. 5, along with the trilinear approximations and the linearly-elastic moduli used by Kahl.

Line No.	Description	Stiffness			Limit Moments	
		k_1	k_2	k_3	M_{pL}	M_Y
		(kips-in/rad·10³)			(kips-in·10³)	
1	trilinearized lower connection	4.000	0.625	0.319	1.20	1.90
2	linearized lower connection	2.670				
3	trilinearized upper connection	4.000	0.513	0.208	0.66	1.01
4	linearized upper connection	2.000				
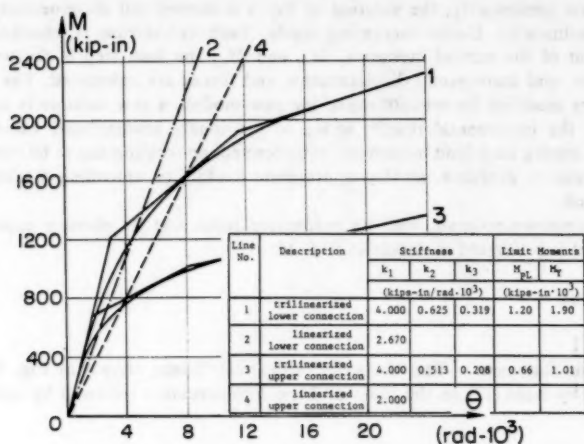
FIG. 5.—Example 1: Connection Properties
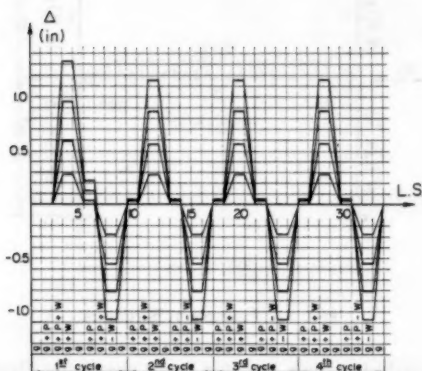
FIG. 6.—Example 1: Sways

The following analysis is intended to check the validity of this design scheme under a severe load history. The following questions have been posed:

1. Do the lateral deflections of the structure stabilize?

2. Do the internal forces exceed the design forces?
3. Is the assumption of linearly-elastic connection behavior adequate?

To this purpose, the loading sequence presented at the bottom of Fig. 6 has been chosen. The gravity loads are of values previously stated; the lateral loads were assumed of four different intensities, $w = 0.01$, 0.02, 0.03, and 0.04 kips/sq ft of wall area.

Results

Deflections.—Fig. 6 shows the sway of the top story during the full load history for several lateral load intensities. The first load application causes the largest deflection, part of which is inelastic as can be deduced by the curved load-deflection curves, and by the residual racking after removal of the lateral load for all but the lowest load level. The constant behavior under subsequent load cycles indicates shakedown of the structure.
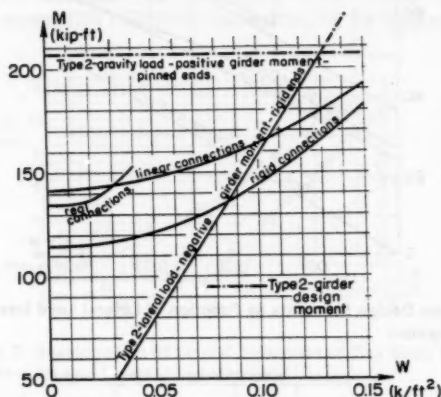
FIG. 7.—Girder Design Moments as Function of Lateral Load Intensity for Different Design Assumptions

The maximum top story sway of 1.33 in. for $w = 0.04$ kips/sq ft may be compared to a corresponding value of 0.84 in. assuming rigid joints, and 1.26 in. assuming the linearly-elastic moduli shown in Fig. 5.

Girder and Column Moments.—The largest critical girder moments obtained during the entire load history are shown plotted versus lateral load intensity in Fig. 7, and those for the leeward lower column top in Fig. 8 according to several types of analysis. Figs. 7 and 8 show that the assumption of linearly-elastic connection behavior yields results close to the "real" behavior. The results of the various approximate methods are as expected (the maximum girder moment varies nonlinearly with load intensity because of variable location of the critical section).

Connection Behavior.—The occurrence of shakedown to linearly-elastic connection behavior as postulated in Ref. 1 can be checked by observing the

moment-rotation histories of the connections. In Ref. 15, these are plotted; they show that after initial inelastic excursions during the first half of the first cycle for the leeward, during the second half of this cycle for the windward connection, all further moments vary along the linear unloading curve. For this structure and loading therefore, the postulate of Ref. 1 is satisfied.

Example 2

Problem Statement.—The eleven-story frame with nonlinear flexible connections shown in Fig. 9 was designed and analyzed by Frye and Morris (8) for
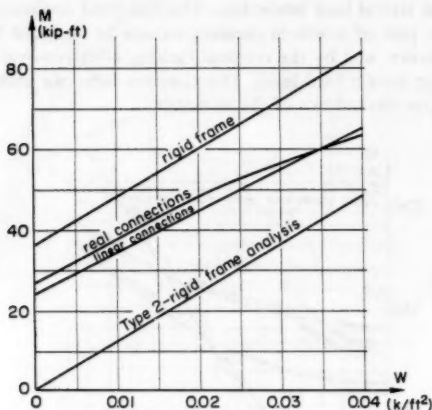
FIG. 8.—Column Design Moments as Function of Lateral Load Intensity for Different Design Assumptions
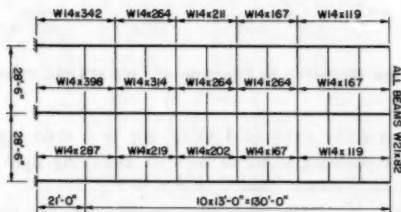
FIG. 9.—Example 2: Structure

proportionally-applied gravity and lateral loads. The structure, which has very conservatively chosen members, was to be reanalyzed to investigate the following two factors:

1. The increase of sway over the calculated by rigid-jointed frame analysis because of connection flexibility.

2. The effect of nonproportional loading; because the superposition principle is invalid for nonlinear structures, the actual load history must be considered. To simulate a more realistic sequence of loading, the gravity load is applied first, followed by the lateral loads, and sways are compared for the two load histories.

No actual connection properties were specified by Frye and Morris (8), so the given sizes of the bolted split-tee connections were used to deduce moment-rotation curves using the formulas in Ref. 8. These curves are then lumped into seven different types, and trilinearized in an appropriate fashion for use in the program. Because of program limitations, the concentrated girder loads of Frye and Morris were replaced by statically-equivalent uniform loads. Connection details and loads can be found in detail in Ref. 15.

Results

Fig. 10 shows the maximum sway as function of the fraction of the applied design load. The assumption of proportional loading on the nonlinear structure,
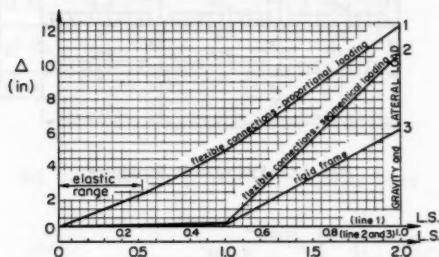
FIG. 10.—Example 2: Development of Lateral Deflection of Top Story for Segmental and Proportional Gravity and Lateral Load Histories

Curve 1, results in an overestimate of the sway over that due to a more realistic load history, in which the wind is acting on the fully-loaded structure. With increasing wind pressure, the different load histories yield closer results. As expected, the assumption of rigid joints results in a considerable underestimate of the sway of the bare frame.

Example 3

Problem Statement.—The design method involving directional moment connections was demonstrated by Disque in Ref. 7, and led to the single-story subassemblage design shown in Fig. 11. Loads are: (1) Dead load $g = 1.5$ kips/ft; (2) life load $p = 1.5$ kips/ft; and (3) total lateral shear $W = 30$ kips. Member sizes and connections as designed to resist the loading by Disque by the proposed method are shown in Fig. 13. The purpose of the present analysis is to investigate the behavior of the structure as designed under a real load history.

Disque assumed a particular distribution of column shears as shown in Fig.

11. To determine these shears more accurately, the subassemblage was replaced by the three-story structure shown in Fig. 12. All results and comparisons refer to its lowest story. The properties of the connection designed by Disque in Ref. 7 and shown in Fig. 13 are predicted differently by various methods. To bracket its probable response, analyses were performed based on Curves 1 and 3 of Fig. 13; the former is the curve predicted by Frye and Morris (8), the latter is the same curve modified to yield the perfectly-plastic strength

FIG. 11.—Disque's Subassemblage (7)

FIG. 12.—Example 3: Structure

FIG. 13.—Example 3: Connection

assumed by Disque (7). Several cycles of the postulated load history are shown in the lower part of Fig. 14.

Results

Sway.—The plot of sway of the lower story during the first four cycles of loading is shown in Fig. 14. The sway of a similar structure with rigid connections is also shown for comparison. The importance of connection strain hardening

is evident by comparing the sways with the perfectly-plastic Connection 3 with those with Connection 1. The lateral sways tend to stabilize; those during Cycles 3 and 4 are almost identical; full shakedown might be expected during the following cycles. However, the curved nature of the plot during application of lateral loads (Steps 4, 8, 12, etc.) indicates nonlinear behavior during each load cycle; this will be documented further while describing connection response.

Internal Forces.—Plots of girder moment variation (15) will not be shown here; similar to the sways, they tend to shake down after a few cycles. Because
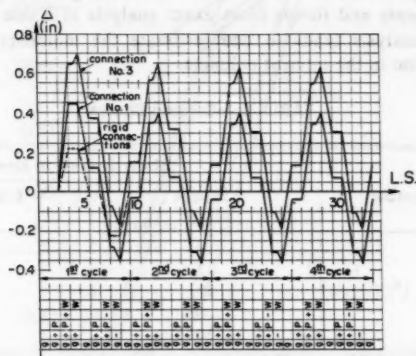
FIG. 14.—Example 3: Relative First Story Sway
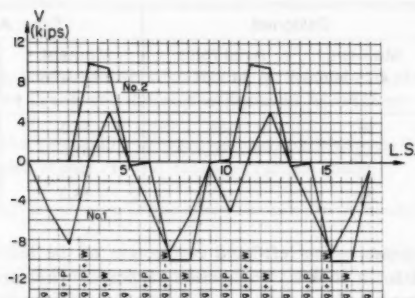
FIG. 15.—Example 3: Shear Force in Windward Columns

the girder sizes were selected according to simple beam moment requirements as is usual in Type 2 construction, all actual girder moments are well on the safe side.

Column moments tend to be more critical, as usually in buildings designed as Type 2. We present results for column shears, defined as in Fig. 11 as a measure of moments at the column top. All results presented here were obtained

for Connection Response 3, which is deemed closest to that envisioned by Disque.

Fig. 15 shows the "exact" shear forces in the two windward columns, Numbers 1 and 2. Disque attributed all column shears to the effect of lateral loads; these are shown in Col. 2 of Table 1. For comparison, exact values were obtained as the difference of shears between Load Steps 2 and 3 of Fig. 15, and shown in Col. 3 of Table 1. It is seen that Disque's approximate shears match the exact values reasonably well.

Column design moments and axial forces according to Disque are compared to critical moments and forces from exact analysis in Table 2. They indicate that Disque's analysis tends to underestimate the moments in the exterior, overestimate them in the interior columns.

TABLE 1.—Column Shears

| Column number (1) | Shear Forces, in kips | |
	Disque (2)	Exact analysis (3)
1	6.	8.17
2	12.	9.94
3	12.	10.20
4	0.	1.39
Total	30.	30.00

TABLE 2.—Critical Column Forces

| Column number (1) | Designed | | Exact Analysis | |
	Moment, in kips-feet (2)	Axial force, in kips (3)	Moment, in kips-feet (4)	Axial force, in kips (5)
1	36.	145.	58.3	157.6
2	72.	290.	61.3	288.7
3	72.	290.	61.3	288.7
4	36.	145.	58.3	157.6

Connection Response.—The left-hand connection of the left-hand first-story girder is selected for a look at connection response. The more conservative connection response No. 3 is used again. Fig. 16 shows the moment and rotation; the numbers are keyed to the load steps of Fig. 14. It is seen that the connection gradually shakes down, i.e., incremental deformations cease. However, the connection enters a state of alternating plasticity, with energy loss during each cycle represented by the area within the hysteresis loop of Fig. 16. Similar behavior could be observed in other connections. It is this behavior which is responsible for the alternating permanent racking of the frame during each half of each load cycle apparent in Fig. 14.

For the connection behavior shown in Fig. 2, such energy-dissipative response will occur under any loading sequence for which the range between extreme

connection moments exceeds the value $2 M_{el}$. If, for instance, only one-half of the live load, p, were to be removed and reapplied, then this range would be within this limit, and all further behavior would indeed proceed elastically. It appears that probabilistic methods might be in order to define such load histories in the light of acceptable probabilities.
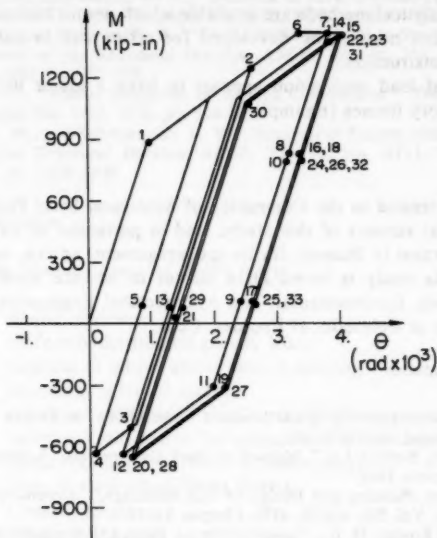
FIG. 16.—Example 3: Moment-Rotation History for Windward Connection of Member 5 for Four Full Load Cycles and Connection Behavior Assumption 3

In any case, the possibility of such alternating plasticity is contrary to the behavior postulated in Ref. 1, and deserves further study.

CONCLUSIONS

On the basis of the examples presented, the following conclusions may be drawn regarding the validity of various design assumptions for unbraced multistory steel frames:

1. The assumption of rigid joints is inadvisable for frames with field-bolted or lightly-welded connections. It will result in an underestimation of the bare-frame sway, and may lead to an inaccurate prediction of critical member forces (Examples 1, 2, and 3).

2. Type 2 construction may result in frames which are uneconomical and of unknown strength. The reduction to purely elastic connection response under load cycles which has been cited as justification may not always take place;

rather, alternating connection plasticity appears a possibility (Example 3). A more exact analysis and redesign should always follow a Type 2 preliminary design.

3. The assumption of linear response of flexible connections seems reasonable and appears to give a good prediction of the actual bare-frame response, although judgment and more testing is required to establish good connection moduli (Example 1). Analytical methods are available which permit inclusion of connection flexibility, but need to be developed for office use to encourage wider use of Type 3 construction.

4. Sequence of load application appears to have a minor influence on the sways of multistory frames (Example 2).

ACKNOWLEDGMENT

APPENDIX I.—REFERENCES

1. "Type 2 Construction with Wind Moment Connections: A Return to Simplicity," American Iron and Steel Institute.
2. "Specifications, Section 1.2," *Manual of Steel Construction*, American Institute of Steel Construction, 1980.
3. "Monograph on Planning and Design of Tall Buildings," *Structural Design of Tall Steel Buildings*, Vol. SB, ASCE, 1979, Chapter SB-7.
4. Batho, C., and Rowan, H. C., "Investigation on Beam and Staunchion Connections," Report of the Steel Structures Committee of the Division of Scientific and Industrial Research, Vols. 1 and 2, 1931–1934.
5. Bertero, V. V., Popov, E. P., and Krawinkler, H., "Beam-Column Subassemblages under Repeated Loading," *Journal of the Structural Division*, ASCE, Vol. 98, No. ST5, Proc. Paper 8915, May, 1972, pp. 1137–1159.
6. Disque, R. O., "Wind Connections with Simple Framing," *AISC Engineering Journal*, July, 1964.
7. Disque, R. O., "Directional Moment Connections: A Proposed Design Method for Unbraced Steel Frames," *AISC Engineering Journal*, First Quarter, 1975.
8. Frye, M. J., and Morris, G. A., "Analysis of Flexibly Connected Steel Frames," *Canadian Journal of Civil Engineering*, Vol. 2, 1975.
9. Gerstle, K. H., *Basic Structural Analysis*, Prentice-Hall, Inc., Englewood Cliffs, N.J., 1974.
10. Goble, G. G., "A Study of the Behavior of Building Frames with Semi-Rigid Joints," a report submitted to the American Institute of Steel Construction and The Ohio Steel Fabricators Association, Case Institute of Technology, 1963.
11. Hechtman, R. A., and Johnson, B. G., "Riveted Semi-Rigid Beam-to-Column Building Connections," *Progress Report Number One*, the American Institute of Steel Construction Publication, Nov., 1947, Appendix B.
12. Kahl, T. L., "Flexibly-Connected Steel Frames," thesis presented to the University of Colorado, at Boulder, Colo., in partial fulfillment of the requirements for the degree of master of science.
13. Lionberger, S. R., and Weaver, W., Jr., "Dynamic Response of Frames with Non-Rigid Connections," *Journal of the Engineering Mechanics Division*, ASCE, Vol. 95, No. EM1, Proc. Paper 6393, Feb., 1969, pp. 95–114.

14. McGuire, W., "The Simple Design-Wind Connection Method," presented at the May, 1977, American Institute of Steel Construction Second Conference on Steel Developments, held at Melbourne, Australia.

15. Moncarz, P. D., "Effects of Non-Linear Connections in Steel Frames," thesis presented to the University of Colorado, at Boulder, Colo., in 1976, in partial fulfillment of the requirements for the degree of master of science.

16. Chesson, E., Jr., and Munse, W. H., "Behavior of Riveted Truss-Type Connections," *Transactions*, ASCE, Vol. 123, Paper No. 2955, 1958, pp. 1087–1126.

17. Popov, E. P., and Pinkney, R. B., "Cyclic Yield Reversal in Steel Building Connections," *Journal of the Structural Division*, ASCE, Vol. 95, No. ST3, Proc. Paper 6441, Mar., 1969, pp. 327–353.

18. Rathbun, J. C., "Elastic Properties of Riveted Connections," *Transactions*, ASCE, Vol. 101, Paper No. 1933, 1936, pp. 524–563.

19. Romstad, K. M., and Subramanian, C. V., "Analysis of Frames with Partial Rigidity," *Journal of the Structural Division*, ASCE, Vol. 96, No. ST11, Proc. Paper 7664, Nov., 1970, pp. 2283–2300.

Appendix II.—Notation

The following symbols are used in this paper:

E = elastic modulus;
g = uniformly-distributed gravity load;
I = moment of inertia about axis of bending;
$[K]$ = structural stiffness matrix;
k_1, k_2 = rotational stiffness of left and right beam end springs;
k_1, k_2, k_3 = rotational stiffnesses for trilinearized connection behavior;
k_{el} = initial rotational stiffness of connection;
k_{ij} = term of element stiffness matrix;
L = element length;
M = bending moment;
M_u = connection proportional limit moment;
M_y = connection yielding moment;
p = uniformly-distributed live load;
V = shear force;
W = concentrated horizontal load;
w = uniformly-distributed horizontal load;
X_i^F = fixed end force;
$\{X\}$ = vector of nodal forces;
$\{X^F\}$ = vector of fixed-end forces;
Δ = deflection;
$\{\Delta\}$ = vector of nodal displacements; and
θ = angle of rotation.

CONTINUUM SOLUTION OF SIMULATED PIPE WHIP PROBLEM [a]

By Mehran Lashkari[1] and Victor I. Weingarten[2]

INTRODUCTION

Extensive piping equipment networks constitute an important part of nuclear power plants. All utility companies involved in the design and operation of nuclear power plants are required by the Nuclear Regulatory Commission (NRC) to consider the safe shut-down of the plant if a major pipe break occurs. Therefore, all essential equipment for the safe shut-down of the plant must be protected against the effects of pipe breaks by installing pipe restraints. The analysis and design of these piping restraints, particularly under the action of dynamic type loadings, is a critical task from the standpoint of safety. In actual construction of such systems snubber restraints are frequently used in appropriate locations in order to limit the transverse displacements of the pipes and their subsequent possible breakdown due to large and uncontrolled deformations. The analysis of the pipe restraint problem is usually performed by computer models. A number of studies have been performed both analytically and experimentally to determine the nature of the problem and also to investigate the system response subject to dynamic and impact type action (1,2,5,6,8). The piping system model that has become more or less standard in such studies, Fig. 1, is formed from a cantilever member whose free end initially rests at a preset distance (gap) from a truss type element. This element selected with a suitable measure of stiffness has the essential task of restraining the displacement response of the pipe. As the pipe impinges upon this element with a gap—henceforth, called "gap element"—depending on the magnitude of the force and also the material properties of both the pipe and the gap element, it responds with a varying degree of complexity.

In the present study using the finite element method, the pipe whip problem

has been analyzed with a consideration of material nonlinearity both in the pipe (striker) and the gap (target) elements. The effect of material damping in the forms of Rayleigh damping coefficients as well as damping due to impact between the striker and the target which may behave in a nonlinear fashion has also been studied. The program SAP7 (8), which is based on the NONSAP program (4), was used to provide solutions to a series of pipe whip problems. Experimental results by Anderson and Masri (2) were then utilized to determine the correlation between the analytical and test values of the system response. Finally, in a parametric study, the effect of several parameters on the response of the system was evaluated and certain conclusions regarding the effectiveness
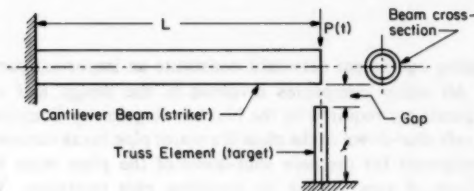
FIG. 1.—Simulated Pipe Whip Problem Model

of these parameters to construct models that most suitably duplicate experimental results were drawn.

COMPUTER PROGRAM SAP7

The SAP7 program is a general purpose nonlinear static and dynamic finite element analysis program (8). The system response using the SAP7 program is calculated by the step-by-step incremental solution of the nonlinear equations of motion with the Wilson Θ or Newmark time integration scheme (3). In the present investigation, the Newmark operator with $\alpha = 1/4$, $\delta = 1/2$ (average constant acceleration method) was used. Both material and geometric nonlinearities can be considered. Details of the solution procedures as well as various nonlinear material representations are given in Reference (8). The program was modified to perform this study. A 3/D linear elastic beam element was incorporated into the program element library. The nonlinear material and deflection option for this element is currently being developed. In addition, a gap element which has exactly the same features as the truss element (8) plus nonlinear damping characteristics was added specifically for the purpose of the pipe whip problem. An out-of-core equation solver and subspace iteration eigenvalue subroutines were added to the program. Pre- and post-processor subprograms were also developed for SAP7.

EXPERIMENTAL STUDIES

An experimental study was recently conducted by Anderson and Masri (2) to determine the effect of both material and geometric nonlinearities on the response of the pipe whip problem. The dynamic system considered for this

study was a cantilever beam with a concentrated mass at the free end. The geometric nonlinearity was introduced by placing a fixed-fixed beam (target) normal to the cantilever beam (striker) and at a specified distance from the concentrated mass. A typical configuration is shown in Fig. 2. This system was then subjected to both sinusoidal and impulsive base accelerations. Because

TABLE 1.—Test Summary

Test number (1)	Maximum acceleration, in gravitational acceleration (2)	Gap, in inches (3)	Striker (4)	Target (5)
27	9.5	1/2	Elastic	Elastic
36	42.0	1/2	Elastic	Plastic
40	57.0	1/2	Plastic	Plastic

Note: 1 in. = 25.4 mm.
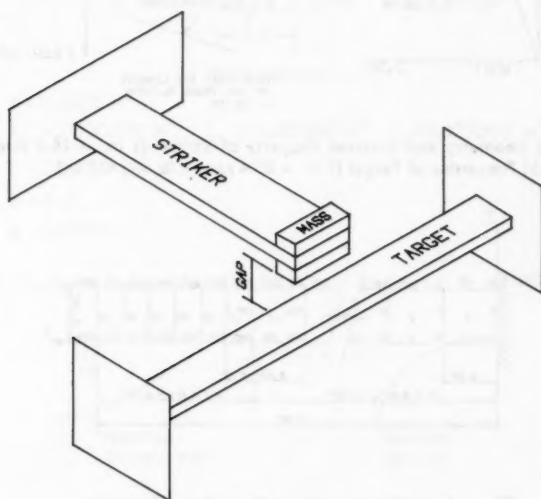
FIG. 2.—Basic Model Configuration

of the high power required to drive a dynamic system in the inelastic range only the impulsive acceleration tests considered material nonlinearity. The sinusoidal tests considered elastic material and geometric nonlinearity.

In the present inquiry, three of the tests performed in Ref. 2 and summarized in Table 1 were selected for an analytical scrutiny by means of the finite element method. The finite element method procedure not only permits the rapid change
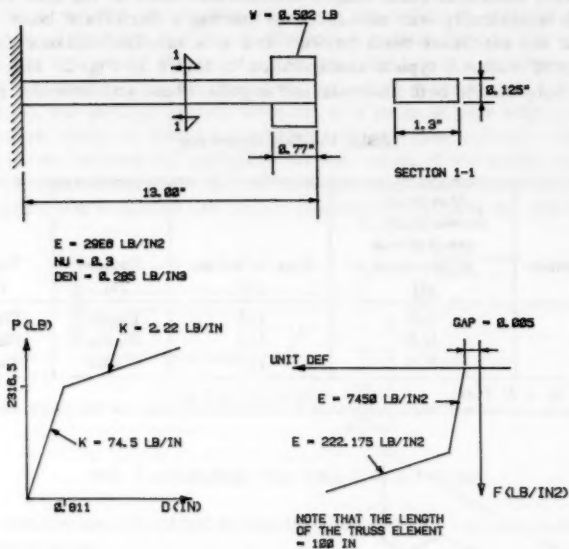
FIG. 3.—(a) Geometry and Material Property of Striker (1 in. = 25.4 mm, 1 lb = 0.453 kg); (b) Properties of Target (1 in. = 25.4 mm, 1 lb = 0.453 kg)
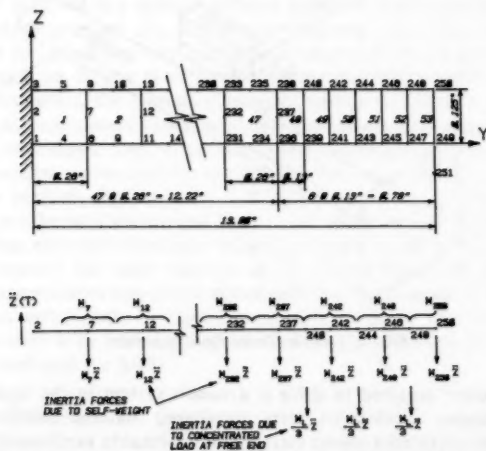
FIG. 4.—Finite Element 2/D Elasticity Model (1 in. = 25.4 mm)

in the value of various parameters and the observance of their corresponding effects, but also is a viable technique which allows the analysis of very complex piping system problems.

FINITE ELEMENT MODELS

The geometry and material properties of the striker-target system is given schematically in Fig. 3. The pipe cantilever beam was modeled using separately
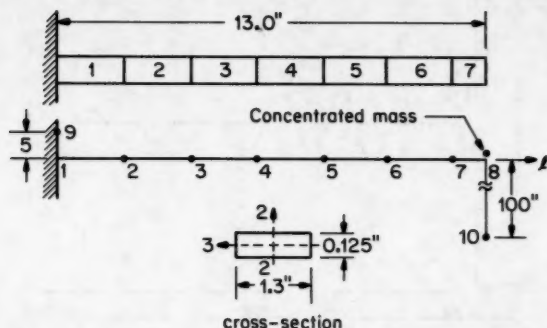
A = 0.1625 in^2

I_{3-3} = 0.0002116 in^4 I_{2-2} = 0.022885 in^4 I_{1-1} = 0.023097 in^4

E = 29 × 10^6 psi

ν = 0.3

ρ = 0.285 lb/in^3

FIG. 5.—Finite Element Beam Model (1 in. = 25.4 mm, 1 lb = 0.453 kg)
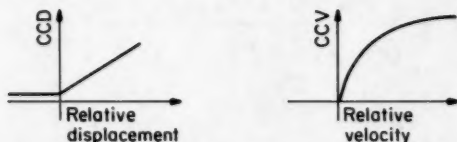
FIG. 6.—Nonlinear Damping Definition

the 8-node isoparametric plane stress element and the three-dimensional beam element. Also, a gap element with nonlinear damping characteristics was developed to implement the damping effect between the striker and the target during the short period of impact. These are described briefly in the following.

2/D Element Model.—Initially, an assemblage of 53 8-node isoparametric plane stress elements shown in Fig. 4 modeled the striker beam. In the numerical evaluation of the element stiffness matrices, 2-point gauss quadrature was used

and the plastic behavior of the pipe during the dynamic response was considered using flow theory of plasticity with Von Mises yield condition. The effect of the initial gap was modeled by providing an interface or gap element (truss element) with a stress-strain relationship which could be linear or nonlinear
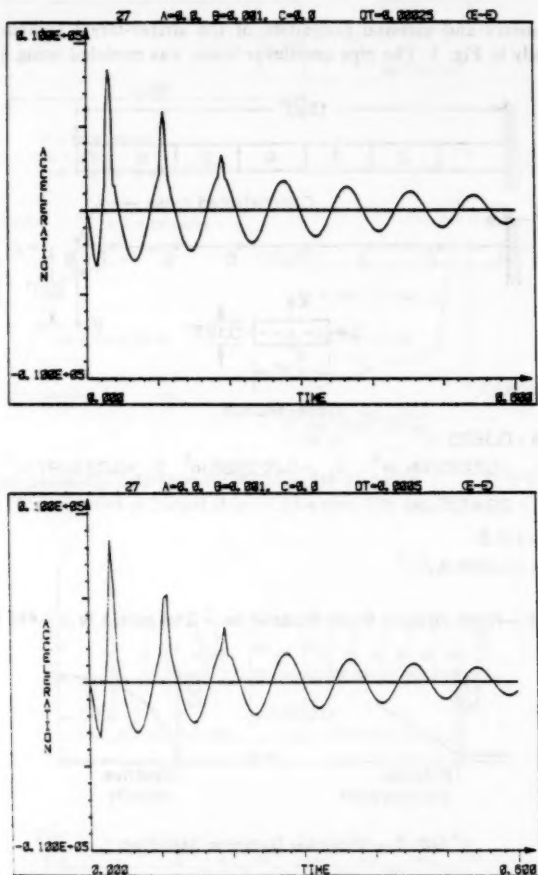
FIG. 7.—Acceleration Response for Different Δt's

reflecting the elastic or the elastic-plastic nature of the target material. For the case under consideration, the mass of the restraint (gap element) was assumed negligible and therefore was not a factor in the finite element modeling. It should be observed that two difficulties were experienced in the use of this

element. First of all, the system response without any damping allowance resulted in a poor correlation between the analytical and the experimental values, mainly due to the presence of some high frequency oscillations. This problem was remedied to some degree by introducing a measure of Rayleigh damping into the striker beam material. Also, in view of the relatively large number of degrees of freedom for this model, the computer runs turned out quite long and costly.

Beam Element Model.—Seven 3/D beam elements were used to model the striker beam, as shown in Fig. 5. Only tests 27 and 36 from Table 1 were
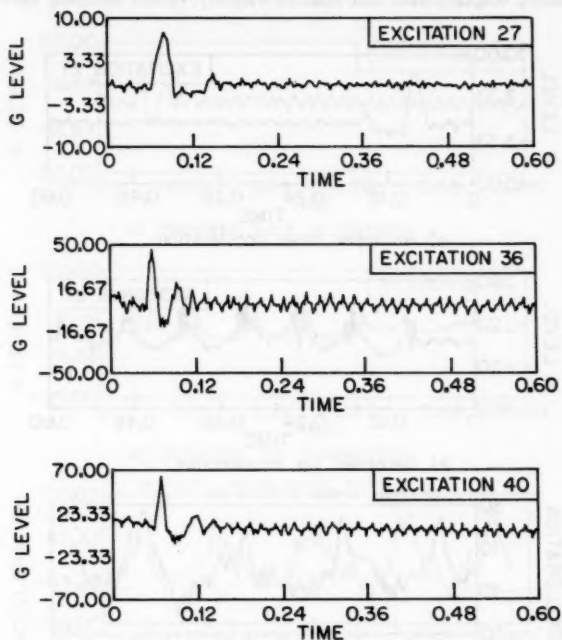
FIG. 8.—Base Accelerations

analyzed using the beam element model. Again, the mass of the gap element was disregarded in the analysis.

A point that deserves notice is associated with the difference observed in the system response when it was modeled with isoparametric continuum elements as opposed to that with beam elements. The high frequency oscillations that occurred in the elasticity solution as a result of elastic waves causing perturbation were not present in the case of beam theory.

Gap Element with Nonlinear Damping.—The gap element is an extension of the truss element with material and geometric nonlinearities in which linear and nonlinear damping properties was also incorporated. These properties are defined by means of relative displacement and relative velocity versus damping

coefficient curves exemplified by those of Fig. 6. The designation of "gap element" is due to the fact that by defining a nonlinear material and a nonlinear damping for the element, special effects such as locked displacement within a specified gap can be obtained. The final damping coefficient utilized by the element at each time step is determined by

$$C_{tot} = C_{dis} \cdot CCD + C_{vel} \cdot CCV \dots\dots\dots\dots\dots\dots\dots\dots\dots\dots (1)$$

in which C_{tot} = the total damping coefficient; C_{dis} and C_{vel} = factors applied to the relative displacement and relative velocity versus damping curves; and
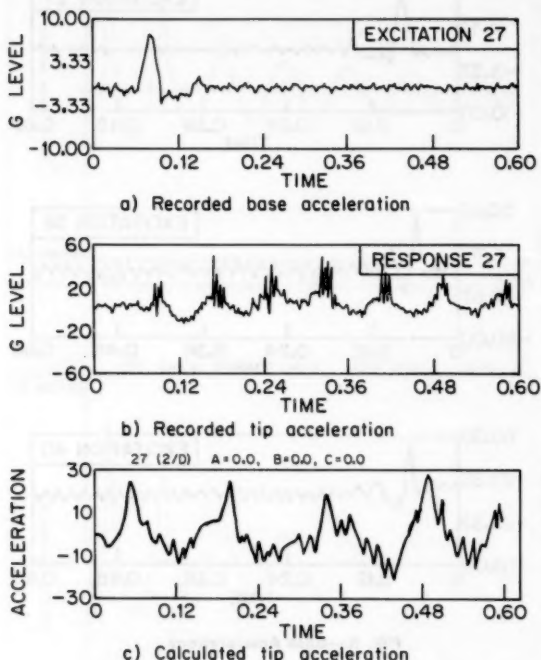
FIG. 9.—Experimental-Analytical Response for Test 27 (2/D Element)

CCD and CCV = the interpolated damping coefficients due to relative displacement and relative velocity of the gap element ends. The total damping coefficient multiplied by the relative axial velocity gives the magnitude of the axial force which, when added to the elastic force, produces the resultant axial force in the gap element. As stated earlier, in the current finite element analysis of the pipe and restraint model, the effect of several parameters, such as: (1) Different time step sizes, Δt; (2) different values of the Rayleigh coefficient factors, α and β, from $C = \alpha M + \beta K$, in which C, M, and K = damping,

mass, and stiffness matrices, respectively; and (3) different values of the nonlinear damping factors are studied.

Analytical and Experimental Comparison

The three test cases selected for consideration in the present work will now be discussed in detail. All three cases were run primarily on the basis of a time step of $\Delta t = 0.00025$, which resulted in system responses of sufficient accuracy. It was observed that when the striker beam was modeled with 2/D

a) Recorded base acceleration

b) Recorded tip acceleration

c) Calculated tip acceleration
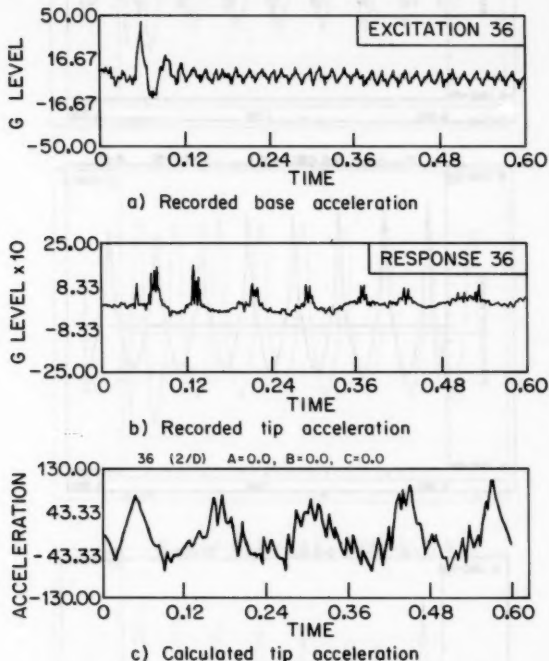
FIG. 10.—Experimental-Analytical Response for Test 36 (2/D Element)

elasticity element, any larger time steps were inducive to unacceptable approximations in the system response. This condition, however, was not as pronounced when the striker was ideolized with beam elements. Time steps as large as $\Delta t = 0.0005$ could be used even though some of the higher mode effects are partially neglected in the process. The use of time steps such as $\Delta t = 0.0005$ and larger seemed particularly appropriate with increasing values of the Rayleigh damping coefficient, β, which results in diminished significance of the higher modes, Fig. 7.
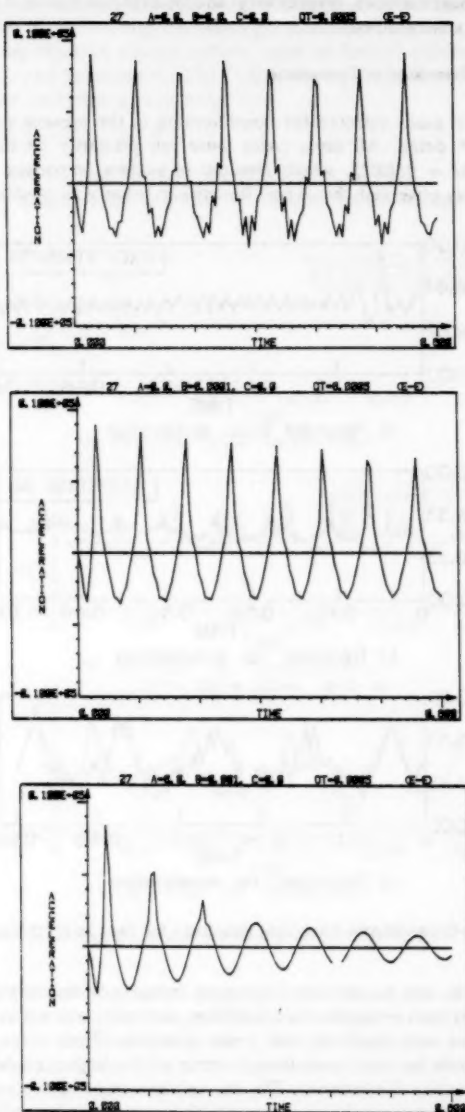
FIG. 11.—Effect of Rayleigh Damping on Acceleration Response (Test 27)
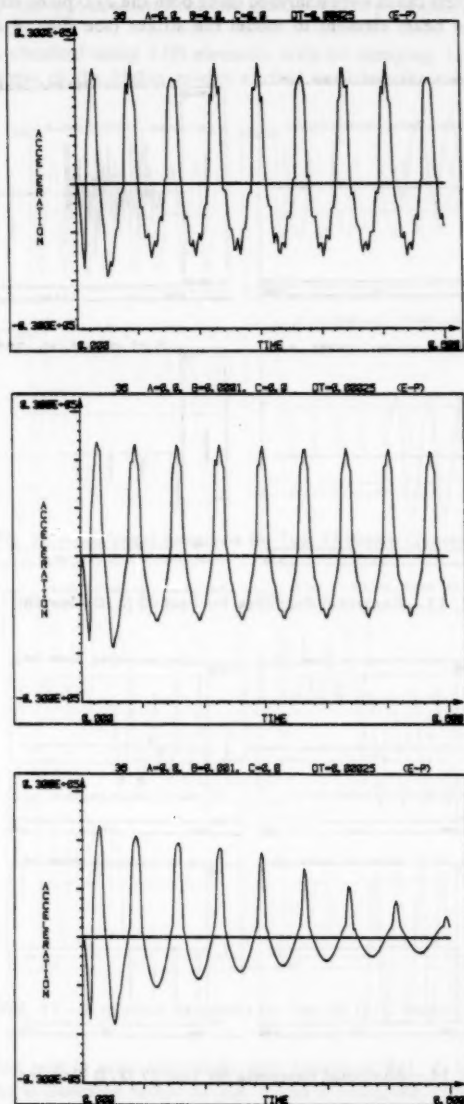
FIG. 12.—Effect of Rayleigh Damping on Acceleration Response (Test 36)

The first two test cases were analyzed using both the 2/D plane stress elasticity element and the beam element to model the striker (see Figs. 4 and 5). They
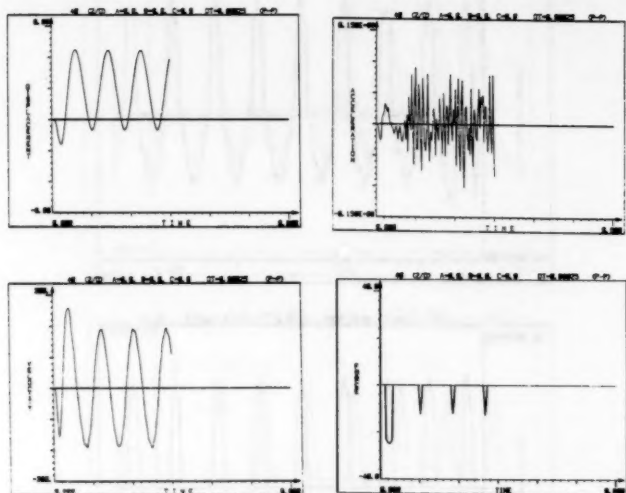
FIG. 13.—Analytical Response for Test 40 (2/D Element)
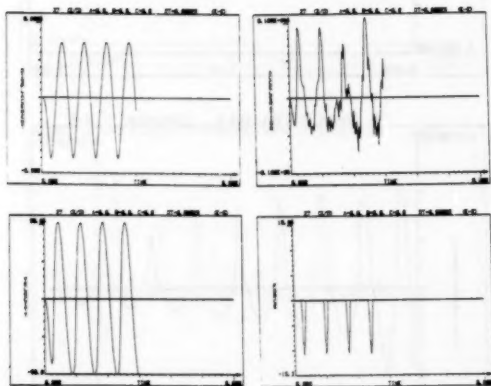
FIG. 14.—Analytical Response for Test 27 (2/D Element)

were subjected in each instance to impulsive base accelerations shown in Fig. 8 with peak values of 9.5G and 42.0G, respectively. Calculations of the tip

displacement, velocity, acceleration, and also the force produced in the restraint element were made.

The results obtained using 2/D elements with no damping, i.e., $\alpha = 0$, and $\beta = 0$, had some of the higher modes excited and thus the calculated striker
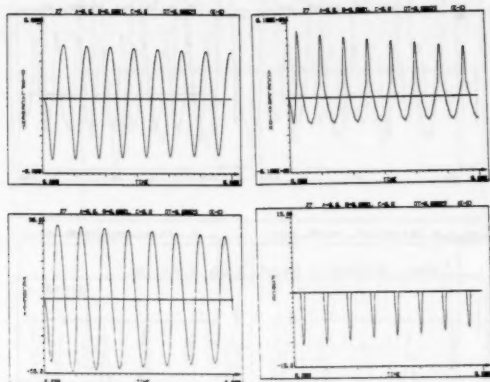
FIG. 15.—Analytical Response for Test 27 (Beam Element)
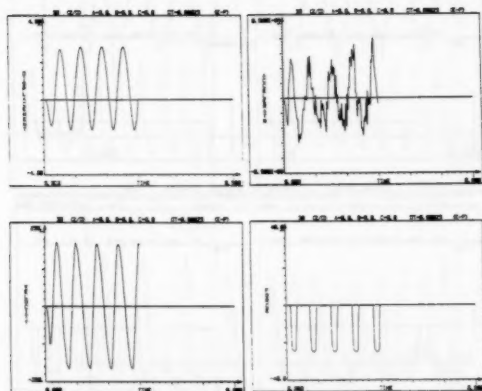
FIG. 16.—Analytical Response for Test 36 (2/D Element)

tip acceleration was in poor agreement with results of Ref. 2, as seen in Figs. 9 and 10. The α damping factor of Eq. 2 has a negligible effect on damping out the higher frequency modes, and therefore was disregarded in the current study. However, with the gradual increase of the β factor, which is basically effective in the higher modes, marked improvement was observed in the response

of the striker tip. The optimum value for the β damping factor appears to be in the range of 0.0001–0.0005. With higher β values, the response begins to damp out rather quickly after the initial impact. This behavior can be observed for both test cases 27 and 36 in the acceleration response of the system, Figs.
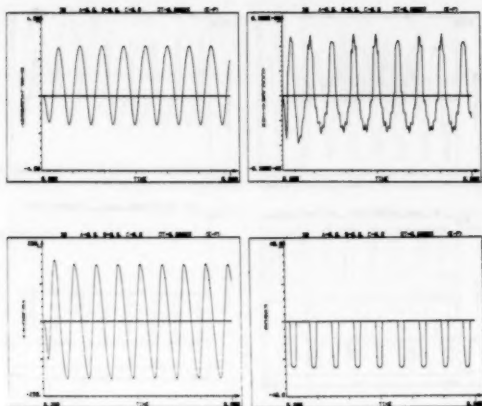
FIG. 17.—Analytical Response for Test 36 (Beam Element)
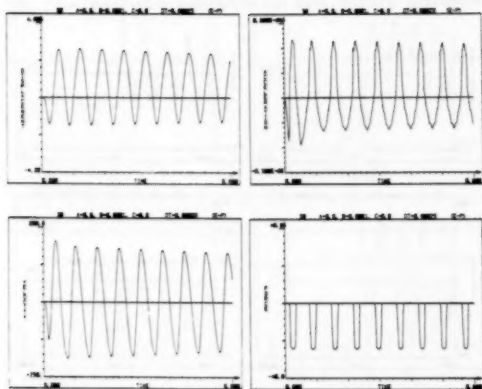
FIG. 18.—Analytical Response for Test 36 (Beam Element)

11 and 12, as β is increased. Results obtained for test case 40, which considered plasticity effects, are indicated in Fig. 13. Due to the high computer cost involved in running the 2/D plane stress elasticity model, computer numerical experiments considering the target damping effects were not carried out for this model but
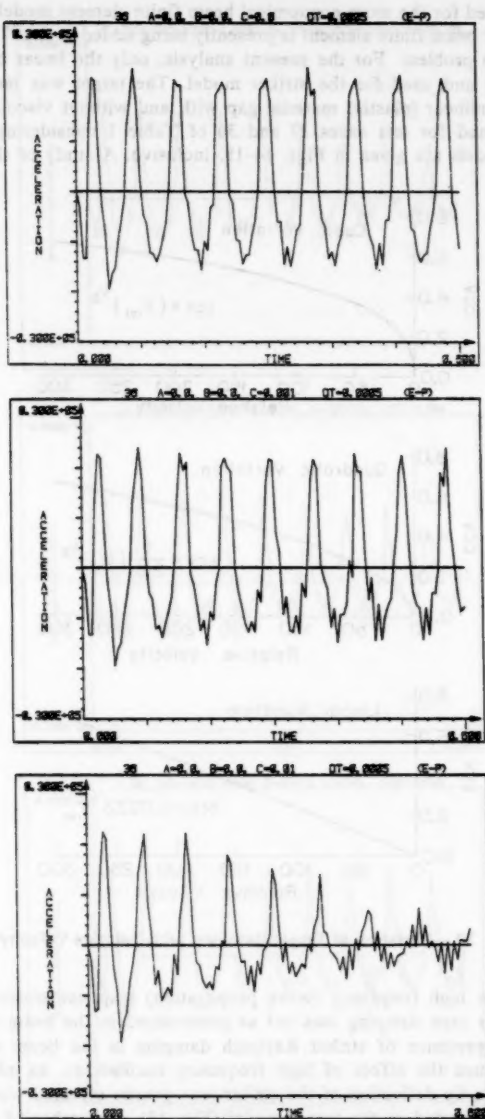
FIG. 19.—Effect of Viscous Damping in Target Material (Constant Variation)

were performed for the more economical beam finite element model.

A nonlinear beam finite element is presently being added to SAP7 to consider the pipe whip problem. For the present analysis, only the linear beam model was available and used for the striker model. The target was modeled as a linear and nonlinear (plastic) material gap with and without viscous damping. Results obtained for test cases 27 and 36 of Table 1 considering both 2/D and beam models are given in Figs. 14–18, inclusive. A study of these results

Cubic Variation

$$ccv = (V_{rel})^{1/3}$$

Quadratic Variation

$$ccv = \frac{1}{2.6}(V_{rel})^{1/2}$$

Linear Variation

$$ccv = 0.0233\, V_{rel}$$
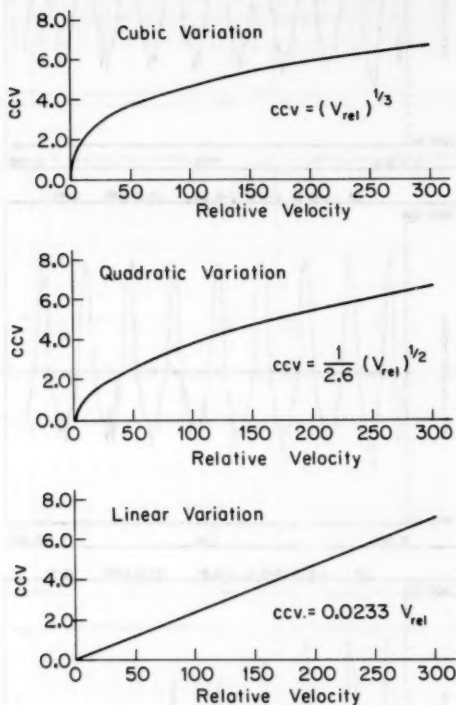
FIG. 20.—Variation of Target Damping with Relative Velocity

shows that the high frequency (wave propagation) response observed in the 2/D model for zero damping was not as pronounced in the beam model and that also the presence of striker Rayleigh damping in the beam model was to further reduce the effect of high frequency oscillations. In addition, the response of the tip deflection of the striker was greatly effected when viscous damping was included in the target model (Fig. 19). A number of tests were performed to study the effect of damping in the target material. Specifically three different nonlinear damping curves representing the damping properties
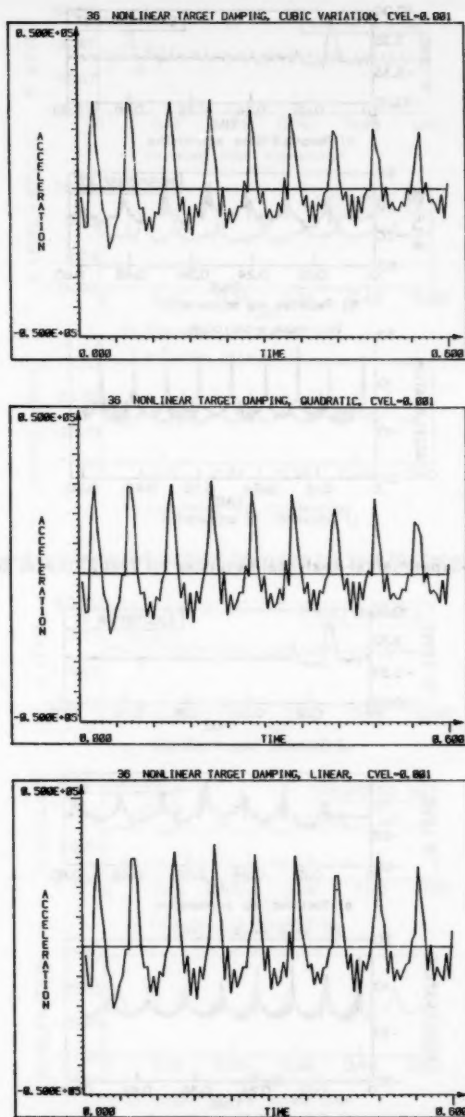
FIG. 21.—Acceleration Response for Different Nonlinear Target Damping Variations

a) Recorded base acceleration

b) Recorded tip acceleration

27 A=0.0, B=0.0, C=0.0

c) Calculated tip acceleration

FIG. 22.—Experimental-Analytical Response for Test 27 (Beam Element)

a) Recorded base acceleration

b) Recorded tip acceleration

27 A=0.0, B=0.0001, C=0.0

c) Calculated tip accelerated
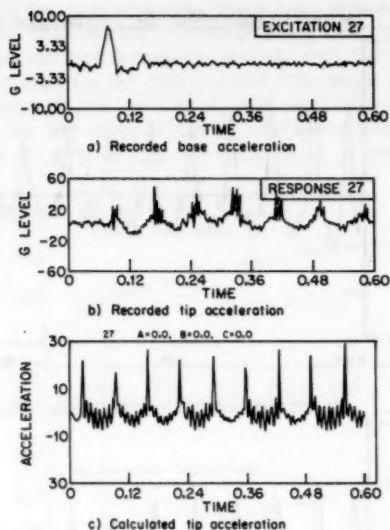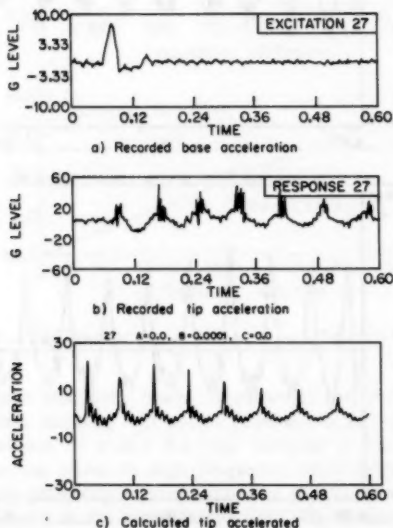
FIG. 23.—Experimental-Analytical Response for Test 27 (Beam Element)
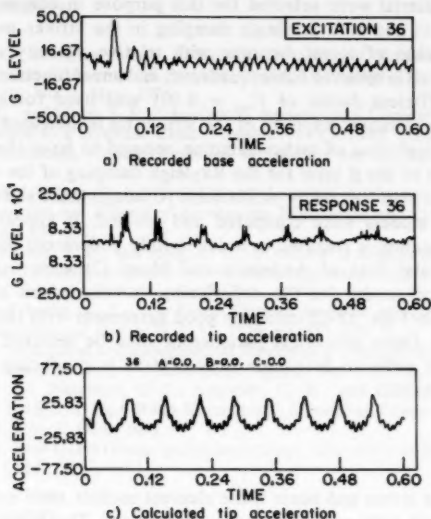
FIG. 24.—Experimental-Analytical Response for Test 36 (Beam Element)
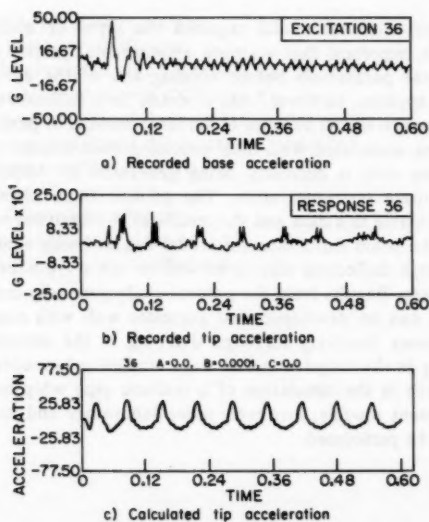
FIG. 25.—Experimental-Analytical Response for Test 36 (Beam Element)

of the target material were selected for this purpose in conjunction with test case 36 (Table 1) and zero Rayleigh damping in the striker material. Fig. 20 shows the variation of target damping with relative velocity as employed in the present analysis in terms of cubic, quadratic, and linear functions, respectively. A damping coefficient factor of $C_{vel} = 0.001$ was used for all three cases. The resulting acceleration response of the striker tip is indicated in Fig. 21.

As seen, the inclusion of target damping seemed to have the same type of influence as that of the β term for the Rayleigh damping of the striker, namely a reduction in the high frequency oscillations. Although these and other nonlinear target damping models were compared and studied, it appears that a more extensive examination is required in order to fully understand the phenomenon.

The experimental data of Anderson and Masri (2) were used to obtain a realistic analytical model for the experiment. A comparison of the recorded tip acceleration in Figs. 22–25 indicates good agreement with the selected finite element models. Other numerical parameters must be selected and studied in future models in order to determine their effects in producing more accurate and objective results.

CONCLUSION

The 2/D plane stress and beam finite element models yield numerical results that correlate well with available experimental data. The beam finite element model yields similar results to the 2/D plane stress model and uses much less computer time. For this reason, further investigation will concentrate on this model.

Since the finite element model requires the input of many experimental parameters, it is important that accurate experimental property measurements are made of these parameters before running any of the dynamic pipe whip experiments. It appears, however, that it would be a difficult task to establish a unique experimental model because of the large number of parameters involved and the problems associated with their precise measurements. Further experimental pipe whip data is currently being generated by Anderson and Masri using more accurate instrumentation. The present finite element models are being used to evaluate this data and the results of the analyses will be published in the future. The beam finite element model is also being modified to include plasticity and large deflection effects as well as other types of impact actions for future analyses. Results from the present study generally indicate that finite element models can be developed that correlate well with experimental data. A number of cases involving Rayleigh damping in the striker and nonlinear viscous damping in the target material were studied independently to evaluate the effect of each in the simulation of a realistic pipe whip model. To refine these finite element models, however, more laboratory and numerical experimentation must be performed.

ACKNOWLEDGMENT

Appendix I.—References

1. Anderson, J. C., and Singh, A. K., "Inelastic Response of Nuclear Piping Subjected to Rupture Forces," *Journal of Pressure Vessel Technology*, Transactions, ASME, Series J, Vol. 98, No. 2, May, 1976.
2. Anderson, J. C., and Masri, S. F., "Analytical/Experimental Correlations of a Nonlinear System Subjected to a Dynamic Load," *Report No. CR-0949*, United States National Regulatory Commission, National Technical Information Service, Springfield, Va., July, 1979.
3. Bathe, K. J., and Wilson, E. I., "Stability and Accuracy Analysis of Direct Integration Methods," *International Journal of Earthquake Engineering and Structural Dynamics*, Vol. 1, 1973, pp. 283–291.
4. Bathe, K. J., Wilson, E. L., and Iding, R. H., *NONSAP, A Structural Analysis Program for Static and Dynamic Response of Nonlinear Systems*, SESM Report No. 74-3, University of California, Berkeley, Calif., Feb., 1974.
5. Ma, M. S., and Bathe, K. J., "On Finite Element Analysis of Pipe Whip Problems," *Nuclear Engineering and Design*, Vol. 37, 1976, pp. 413–430.
6. Masri, S. F., "Analytical and Experimental Studies of a Dynamic System with a Gap," *Journal of Mechanical Design*, Transactions, ASME, Vol. 100, July, 1978, pp. 48–486.
7. Moreadith, F. L., Patterson, G. J., Angstadt, C. E., and Glova, J. F., "Structural Analysis and Design of Pipe Whip Restraints," *Structural Design of Nuclear Power Plants*, ASCE, Vol. 2, Dec., 1973.
8. *SAP7 Manual*, SAP Users Group (preliminary copy), University of Southern California, Los Angeles, Calif., Feb., 1980.

Appendix II.—Notation

The following symbols are used in this paper:

C = damping coefficient matrix;
C_{tot} = total damping coefficient;
C_{dis} = factor associated with CCD (see Eq. 1);
C_{vel} = factor associated with CCV (see Eq. 1);
CCD = damping coefficient due to relative displacement;
CCV = damping coefficient due to relative velocity;
K = stiffness coefficient matrix;
M = mass coefficient matrix;
$2/D$ = two-dimensional element;
$3/D$ = three-dimensional element; and
α, β = Rayleigh damping coefficients.

SEISMIC EFFECTIVENESS OF TUNED MASS DAMPERS

By Amir M. Kaynia,[1] Daniele Veneziano,[2] A. M. ASCE,
and John M. Biggs,[3] M. ASCE

INTRODUCTION

Tuned mass dampers (vibration absorbers) are viscous spring-mass units which are added to vibratory systems to reduce their dynamic motion. Experience with their installment on tall buildings indicates that *wind-induced* oscillations are indeed reduced by these devices (14,16). Their *seismic* effectiveness has been studied by several authors, using a variety of different models for the main structure and for the absorber. Crandall and Mark (6) found that vibration absorbers mounted on single-degree-of-freedom systems are effective in the case of stationary white base acceleration. Gupta and Chandrasekaran (9) used one earthquake record to study the seismic effect of a group of *elasto-plastic* absorbers connected in parallel to simple elastic oscillators. The number of absorbers and their yield levels were found to have only minor influence on peak response. Wirsching and Yao (21,22) used pseudo-random nonstationary earthquake records to quantify the change in seismic response after certain "passive motion-reduction devices" are added to multistory structures. They found that tuned mass dampers are quite helpful. For the case of stationary white noise base acceleration, Wirsching and Campbell (20) calculated the absorber parameters which minimize the response variance of a single-degree-of-freedom system and the first mode response variance of a 5- and 10-story shear structure. The early findings by Den Hartog (7) on simple oscillators with an added damper, excited by harmonic forces, also bear on the problem.

Judged from the available literature, there seems to be a general consensus that tuned mass dampers are useful aseismic control devices. However, evidence is sometimes contradictory and does not cover all aspects of the problem. Objectives of this study are: (1) To investigate *statistically* the effect of tuned mass dampers by subjecting elastic and inelastic systems to a *population* of real earthquakes; and (2) for elastic systems, to evaluate the predictive capability of various analytical models based on random vibration theory.

[1] Grad. Student, Massachusetts Inst. of Tech., Cambridge, Mass. 02139.
[2] Assoc. Prof. of Civ. Engrg., Massachusetts Inst. of Tech. 02139.
[3] Prof. of Civ. Engrg., Massachusetts Inst. of Tech. 02139.

The first objective was motivated by the observation that the peak-response ratio between cases with and without an absorber (a measure of damper effectiveness) has large statistical dispersion over populations of historical earthquakes; as a consequence, the effect of adding an absorber *cannot* be expressed simply through a deterministic response-reduction coefficient. As part of the calculations with historical records, sensitivity analyses were performed to assess the importance of various earthquake, system, and absorber characteristics.

The second objective was added in the course of the study, when it became clear that empirical peak-response ratios do not comply with predictions from conventional steady-state random vibration models (6). Specifically, the latter predictions are consistently too favorable to structures with vibration absorbers. In search for improved analytical models, consideration is given here to the effects of correlation and pseudo-stationarity of the input as well as to the effect of damper-induced broadening of the system transfer function.

Based on these studies, a probabilistic model is formulated for the effect of tuned mass dampers on the probability distribution of elastic response-spectrum ordinates.

Preliminary results are also obtained on the effectiveness of connecting vibration absorbers to simple inelastic systems.

Present findings are generally contrary to common belief and such to discourage indiscriminate use of tuned mass dampers as antiseismic devices.

LINEAR ELASTIC SYSTEMS: STATISTICAL ANALYSES WITH HISTORIC EARTHQUAKES

In this study, the response quantity of interest is always taken to be peak displacement of the top floor relative to the ground. This displacement is primarily contributed by the first dynamic mode (4), which is therefore the only one considered in the analysis. It is also assumed that addition of the mass damper does not significantly affect the original modal shape.

Equations of Motion.—With reference to the idealization of Fig. 1(*a*), the motion of a linear elastic structure with n degrees of freedom and viscous damping subjected to base acceleration, $\ddot{u}_G(t)$, satisfies the equation

$$\mathbf{M}\left[\ddot{\mathbf{U}} + \{1\}\,\ddot{u}_G\right] + \mathbf{C}\dot{\mathbf{U}} + \mathbf{K}_L\mathbf{U} = 0 \quad\ldots\ldots\ldots\ldots\ldots\ldots\ldots\ldots\ldots (1)$$

in which $\mathbf{M}$, $\mathbf{C}$, and $\mathbf{K}_L$ = the mass, damping, and lateral stiffness matrices; $\{1\}$ = the column vector with n unit components; and $\mathbf{U}$ = the column vector of horizontal floor displacements relative to the ground. With the assumption that the structure responds only in its fundamental mode, the vector $\mathbf{U}$ can be written as

$$\mathbf{U} = \begin{Bmatrix} u_1 \\ u_2 \\ \vdots \\ u_n \end{Bmatrix} = \boldsymbol{\phi}\, y \quad\ldots\ldots\ldots\ldots\ldots\ldots\ldots\ldots\ldots\ldots\ldots\ldots\ldots (2)$$

in which y = the modal displacement; and $\boldsymbol{\phi}$ = the vector that defines the shape of the fundamental mode. If $\boldsymbol{\phi}$ is normalized such that $\phi_n = 1$, then $y = u_n$.

Substituting Eq. 2 into Eq. 1 and premultiplying both sides of the latter equation by ϕ^T leads to the scalar equation in y

$$(\phi^T M \phi)\ddot{y} + (\phi^T C \phi)\dot{y} + (\phi^T K_L \phi)y = -\phi^T M \{1\}\ddot{u}_G \quad \ldots \ldots \ldots \quad (3)$$

Finally, denoting by ω_1, ξ_1, and P the natural frequency, damping ratio and

a) BUILDING WITHOUT TUNED MASS DAMPER

b) BUILDING WITH TUNED MASS DAMPER
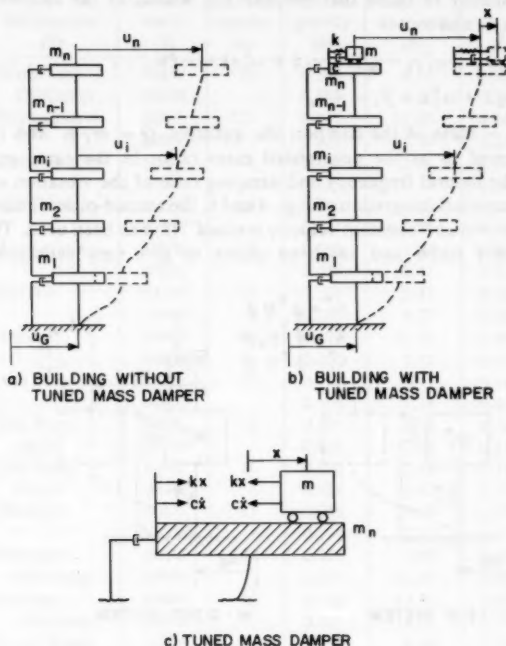
c) TUNED MASS DAMPER

FIG. 1.—Building with and without Tuned Mass Damper

participation factor of the fundamental mode, the equation of motion of the top floor relative to the base simplifies to

$$\ddot{y} + 2\xi_1\omega_1\dot{y} + \omega_1^2 y = -P\ddot{u}_G \quad \ldots \ldots \ldots \ldots \ldots \ldots \ldots \ldots \quad (4)$$

When a tuned mass damper is added [Fig. 1(b)], the equation of motion of the multiDOF system becomes

$$M[\ddot{U} + \{1\}\ddot{u}_G] + C\dot{U} + K_L U - F = 0 \quad \ldots \ldots \ldots \ldots \ldots \ldots \quad (5)$$

This is identical to Eq. 1, except for addition of the vector, $F = \begin{bmatrix} 0 \\ 0 \\ \vdots \\ c\dot{x} + kx \end{bmatrix}$,

of external forces applied to the floors [x, k, and c are the displacement of the vibration absorber relative to the top floor, the associated spring constant, and the associated damping; see Fig. 1(c)].

With the assumption that the tuned mass damper does not modify the fundamental mode shape, one can still write $U = \phi y_1$ with $y_1 = u_n$. Then, operations similar to those that precede Eq. 4 lead to the following coupled equations in y_1 and x

$$\begin{cases} \ddot{y}_1 + 2\xi_1\omega_1\dot{y}_1 + \omega_1^2 y_1 - Q(2\xi_2\omega_2\dot{x} + \omega_2^2 x) = -P\ddot{u}_G & \dots \dots \dots \dots (6a) \\ \ddot{x} + 2\xi_2\omega_2\dot{x} + \omega_2^2 x + \ddot{y}_1 = -\ddot{u}_G & \dots \dots \dots \dots \dots \dots (6b) \end{cases}$$

in which m = mass of the damper; the quantity, $Q = m/\phi^T M\phi$ in Eq. 6(a) will be referred to as the generalized mass ratio. In the same equation, ω_2 and ξ_2 are the natural frequency and damping ratio of the vibration absorber.

For the numerical integration of Eqs. 4 and 6, the second-order finite-difference procedure known as "constant velocity method" (2) has been used. This method is conditionally stable and has been shown to give very satisfactory results

$$M_1^* = \phi^T M \phi$$
$$K_1^* = \phi^T K_L \phi$$
$$C_1^* = \phi^T \underline{C} \phi$$

a) - 1 DOF SYSTEM   b) - 2 DOF SYSTEM
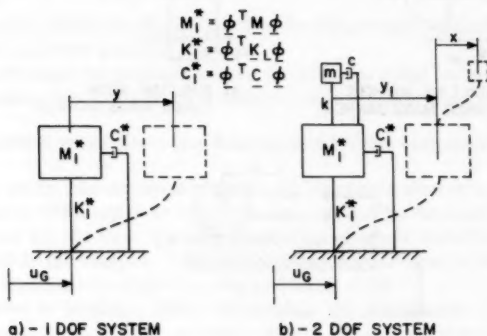
FIG. 2.—1DOF and 2DOF Models

provided that the interval of integration is at least $1/5$–$1/10$ of the natural period of the system (1).

An interesting fact that emerged from the numerical solution of Eqs. 4 and 6 is that the peak-response ratio, $y_{1\,max}/y_{max}$, is not sensitive to the shape of the fundamental mode; i.e., so long as the generalized mass ratio, Q, is unchanged, different values of the participation factor, P, have little effect on $y_{1\,max}/y_{max}$. (See Ref. 12 for numerical results and for an approximate analytical proof of this statement.)

Values of P between 1.0 and 1.5 are usual for buildings with prevalent shear behavior, whereas higher values are found if bending prevails. In the remainder of this study P is taken to be one; in this case Eqs. 4 and 6 are identical to the equations of motion of the 1-DOF and 2-DOF systems shown in Fig. 2. One may therefore gain insight into the seismic effect of tuned mass dampers by studying the modes of vibration of the 2-DOF system in Fig. 2(b) (clearly, if normal modes exist; i.e., for $\xi_1\omega_1 = \xi_2\omega_2$). If ω_1 and ω_2 are widely separated

TABLE 1.—Historical Earthquakes Used in Analysis

C.I.T. number (1)	Earthquake (2)	Component (3)	R, in kilometers (4)	$\ddot{u}_{G\max}$, g = acceleration of gravity (5)	Strong-motion duration, s, in seconds (6)	ξ_g (7)	ω_g, in radians per second (8)
A002-1	Northwest	S44W	53	0.104	4.11	0.317	28.393
A002-2	California	N46W		0.112	4.12	0.293	22.855
A003-1	Kern County	S00E	127	0.047	16.00	0.245	11.183
A003-2		S90W		0.053	23.59	0.217	9.712
A004-1	Kern County	N21E	43	0.156	13.66	0.364	18.462
A004-2		S69E		0.179	10.72	0.346	18.807
A005-1	Kern County	N42E	89	0.090	16.80	0.241	10.599
A005-2		S48E		0.131	6.62	0.211	8.355
A006-1	Kern County	S00W	119	0.055	19.32	0.256	13.902
A006-2		N90E		0.044	35.41	0.317	10.516
A008-1	Eureka	N11W	24	0.168	5.47	0.360	14.164
A008-2		N79E		0.258	4.23	0.287	18.756
A009-1	Eureka	N44E	40	0.159	11.53	0.349	7.465
A009-2		N46W		0.201	3.52	0.361	9.087
A010-1	San Jose	N31W	10	0.102	2.97	0.181	21.769
A010-2		N59E		0.108	1.78	0.064	31.120
A016-1	San Fran-	S09E	14	0.085	2.76	0.163	26.922
A016-2	cisco	S81W		0.056	5.16	0.348	21.407
A017-1	San Fran-	N26E	24	0.040	2.48	0.181	28.929
A017-2	cisco	S64E		0.024	4.82	0.298	27.829
A018-1	Hollister	S01W	21	0.065	18.05	0.276	13.645
A018-2		N89W		0.179	2.72	0.176	18.398
A019-1	Borrego	S00W	64	0.130	7.07	0.476	6.375
A019-2	Mountain	S90W		0.057	31.55	0.491	9.291
A020-1	Borrego	S00W	96	0.030	12.90	0.466	8.685
A020-2	Mountain	N90E		0.029	18.73	0.375	9.836
B021-1	Long Beach	N08E	53	0.133	6.44	0.754	12.627
B021-2		S82E		0.154	2.91	0.479	14.049
B023-1	Southern	S00E	38	0.033	3.53	0.209	20.850
B023-2	California	N90E		0.027	6.76	0.243	18.149
B024-1	Lower	N00E	64	0.160	13.30	0.346	23.158
B024-2	California	N90E		0.183	10.19	0.263	23.388
B026-1	1st n.w.	S45W	55	0.144	1.74	0.257	25.012
B026-2	California	N45W		0.089	4.64	0.229	26.751
B027-1	2nd n.w.	S45W	104	0.062	4.34	0.227	21.058
B027-2	California	N45W		0.039	11.23	0.238	21.226
B030-1	Northern	S44W	43	0.054	9.67	0.337	18.531
B030-2	California	N46W		0.076	4.01	0.268	24.108
B031-1	Wheeler	N21E	43	0.065	3.64	0.282	20.129
B031-2	Ridge	S69E		0.068	4.12	0.189	26.076
B036-1	Parkfield	N50E	38	0.053	12.60	0.775	21.228
B036-2		N40W		0.064	9.55	0.528	30.969
U299-1	Santa	N45E	16	0.238	2.03	0.231	21.247
U299-2	Barbara	S45E		0.176	2.80	0.200	15.715
U300-1	Northern	N45W	50	0.121	2.79	0.288	20.829

TABLE 1.—Continued

(1)	(2)	(3)	(4)	(5)	(6)	(7)	(8)
U300-2	California	S45W		0.116	3.33	0.261	23.321
U312-1	Ferndale	N46W	32	0.105	2.66	0.847	10.552
U312-2		S44W		0.237	0.30	0.291	29.145

(if max $\{\omega_1, \omega_2\}$/min $\{\omega_1, \omega_2\} > 1.2$), then one of the two modes has a natural frequency very close to ω_1 and strongly dominates the response; in this case the response of the structure is not significantly affected by the presence of the mass damper. On the contrary, when $\omega_2/\omega_1 \approx 1$, the frequencies of the two modes, ω_1 and ω_{II}, are both very close to ω_1 with $\omega_1 < \omega_1 < \omega_{II}$ and the modes give comparable contribution to the response. The (small) difference between ω_1 and ω_{II} reduces the probability of coincidence of modal peaks; this is the main mechanism through which vibration absorbers tend to reduce seismic response.

Parametric Analysis on Effectiveness of Tuned Mass Dampers.—The role played by structural parameters and by several earthquake characteristics in determining the effectiveness of tuned mass dampers is investigated by subjecting different systems to the set of historical earthquakes listed in Table 1 (15). These records, which were obtained at western United States sites, were selected so that they would provide wide variability in earthquake characteristics.

The main results concerning structural parameters are displayed in Figs. 3–7. Specifically, Fig. 3 shows how the mean and standard deviation of $y_{1\,max}/y_{max}$ depend on the frequency ratio, ω_2/ω_1, when all other structural parameters are fixed to the values in the figure. Two important conclusions can be drawn. First, maximum mean-value reduction in peak response is obtained when the frequency ratio is about 1; this is consistent with predictions from simple random vibration analysis (6). Second, results from individual earthquakes have relatively large dispersion about the mean response ratio, especially for frequency ratios around 1 (coefficient of variation of about 0.2). This is an important consideration if the safety of buildings with and without dampers is to be compared on a probabilistic basis. For some motions there was no reduction in response.

In a similar format, Figs. 4–7 show sensitivity results with respect to the generalized mass ratio, Q, damping of the building, ξ_1, damping of the vibration absorber, ξ_2, and fundamental period of the building, $T_1 = 2\pi/\omega_1$. All these results have been obtained using the first 20 records of Table 1.

Figs. 4 and 5 suggest that within usual ranges of Q and ξ_1 (Q from 0.005–0.02, ξ_1 from 0.03–0.08) sensitivity to these two parameters is quite small. The effect of ξ_2 on response ratios, which is shown in Fig. 6, is also small. Since this is a parameter which greatly affects the motion of the mass damper itself, its value should be decided on grounds other than reduction of seismic response of the main structure. For example, increasing ξ_2 from 0.05–0.10 produces, on the average, a 30% decrease both in the maximum relative displacement and in the maximum absolute acceleration of the mass damper which may be important design considerations. Finally Fig. 7 suggests that tuned-mass dampers tend to be more effective in buildings with shorter natural period.

In all cases the empirical skewness of the peak-response ratio was found to be negative.

From the results of a limited study on the effect of earthquake characteristics, it seems that the distribution of peak-response ratio does not depend on epicentral distance and central frequency; however, the data is not sufficient to definitely exclude any trend. The same data suggests some dependence of $y_{1\,max}/y_{max}$
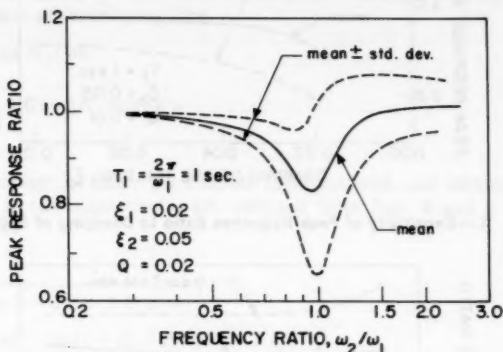
FIG. 3.—Sensitivity of Peak Response Ratio to Frequency Ratio
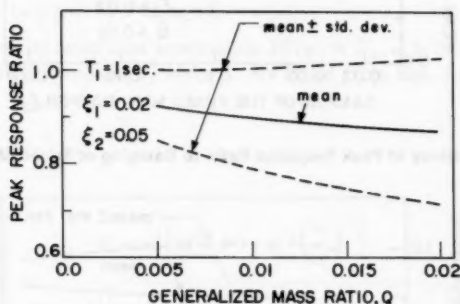
FIG. 4.—Sensitivity of Peak Response Ratio to Generalized Mass Ratio

on strong-motion duration. Empirical evidence and some theoretical results on the effects of this last parameter will be given in the next section.

LINEAR ELASTIC STRUCTURES: RANDOM VIBRATION ANALYSIS

Alternative analytical methods to study the effect of tuned mass dampers are those based on the theory of random vibration. The conceptual appeal of this analytical approach is somewhat counterbalanced in the present case by the fact that useful theoretical results are available only under rather idealized conditions of input and response. The objective of this section is to use a

variety of random vibration analyses, in search of a model that adequately describes the empirical findings. In the course of this search important and
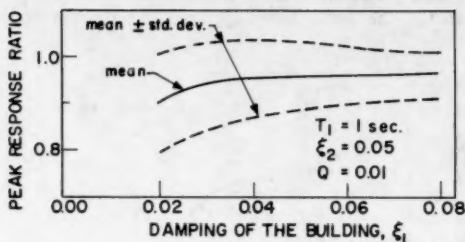
FIG. 5.—Sensitivity of Peak Response Ratio to Damping of Building
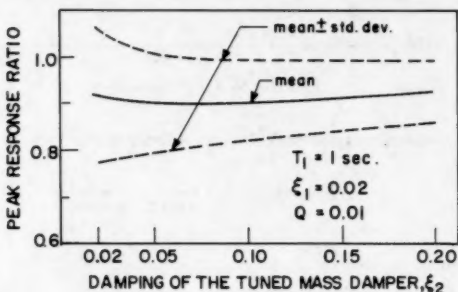
FIG. 6.—Sensitivity of Peak Response Ratio to Damping of Tuned Mass Damper
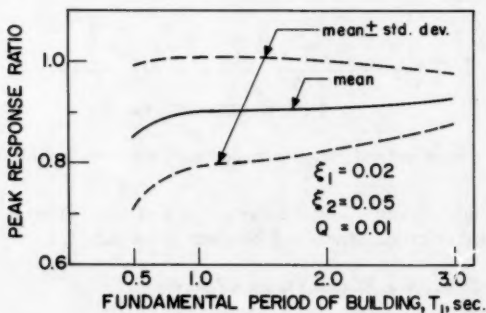
FIG. 7.—Sensitivity of Peak Response Ratio to Fundamental Period of Building

unimportant modeling features are identified.

In all models with stationary (or pseudo-stationary) input motion, the random

process of ground acceleration is characterized at the level of second-moments by assuming zero-mean and by specifying the one-sided spectral density function, $G(\omega)$. Therefore, the input process has variance $\sigma^2 = \int_0^\infty G(\omega)\,d\omega$ and if one denotes by $H_y(\omega)$ the transfer function of the system from ground acceleration to top floor relative displacement, then at steady-state the spectral density function and the variance of the response are

$$G_R(\omega) = G(\omega)\,|H_y(\omega)|^2 \quad\dots\dots\dots\dots\dots\dots\dots\dots\dots\dots\dots (7)$$

and

$$\sigma_R^2 = \int_0^\infty G(\omega)\,|H_y(\omega)|^2\,d\omega \quad\dots\dots\dots\dots\dots\dots\dots\dots (8)$$

respectively.

For the problem at hand, the transfer functions with and without damper, $H_{y_1}(\omega)$ and $H_y(\omega)$ respectively, are obtained from Eqs. 4 and 6 with $P = 1$. They are (6)

$$
\begin{cases}
H_y(\omega) = \dfrac{-1}{(\omega_1^2 - \omega^2) + 2i\xi_1\omega_1\omega} \quad\dots\dots\dots\dots\dots\dots\dots (9a)\\[2ex]
H_{y_1}(\omega) = \dfrac{\omega^2 - i\omega(1+Q)2\xi_2\omega_2 - (1+Q)\omega_2^2}{\begin{array}{l}\omega^4 - i\omega^3\,[2\xi_1\omega_1 + 2(1+Q)\xi_2\omega_2]\\[1ex] -\ \omega^2\,[\omega_1^2 + (1+Q)\omega_2^2 + 4\xi_1\xi_2\omega_1\omega_2]\\[1ex] +\ i\omega\,[2\xi_1\omega_1\omega_2^2 + 2\xi_2\omega_2\omega_1^2] + \omega_1^2\omega_2^2\end{array}} \quad\dots\dots (9b)
\end{cases}
$$

For stationary white noise base acceleration $[G(\omega) \equiv G_0,\ \omega \ge 0]$ the variances of the steady-state response, σ_y^2 and $\sigma_{y_1}^2$, are found from Eqs. 8 and 9. Again from Ref. 6

$$\sigma_y^2 = G_0\,\dfrac{\pi}{4\xi_1\omega_1^3} \quad\dots\dots\dots\dots\dots\dots\dots\dots\dots\dots\dots\dots (10a)$$

$$
\sigma_{y_1}^2 = \pi G_0\ \frac{\left[\begin{array}{l} 2\xi_1\omega_1\omega_2^2\left[Q^2 + Q(1+Q)^2\left(\dfrac{\omega_2}{\omega_1}\right)^2\right]\\[2ex] +\ 2\xi_2\omega_2\omega_1^2\left\{\left[1 - (1+Q)^2\left(\dfrac{\omega_2}{\omega_1}\right)^2\right]^2 + Q(1+Q)^2\left(\dfrac{\omega_2}{\omega_1}\right)^2\right\}\\[2ex] +\ 8\xi_1\xi_2^2\omega_1\omega_2^2(1+Q)^2\left[1 + (1+Q)\left(\dfrac{\omega_2}{\omega_1}\right)^2\right]\\[2ex] +\ 8\xi_2^3\omega_2^3\left[1 + Q + \left(\dfrac{\xi_1}{\xi_2}\right)^2\right](1+Q)^2 \end{array}\right]}{\begin{array}{l} 8\omega_1\omega_2\{Q\omega_1\omega_2(\xi_1\omega_2 + \xi_2\omega_1)^2 + \xi_1\xi_2\,[\omega_1^2 - (1+Q)\omega_2^2]^2\}\\[1ex] +\ 4\xi_1\xi_2\omega_1\omega_2\,[\omega_1\omega_2(\xi_1^2 + (1+Q)\xi_2^2) + \xi_1\xi_2(\omega_1^2 + (1+Q)\omega_2^2)]\} \end{array}}
$$

$$\qquad\qquad\qquad\qquad\qquad\qquad\qquad\qquad\qquad\qquad (10b)$$

Fig. 8 shows the stationary r.m.s. response ratio (for zero-mean input), σ_{y_1}/σ_y, obtained from the last equation as a function of ω_2/ω_1. If one compares this

result with the mean peak-response ratio using 48 historical earthquakes (Fig. 3), then one concludes that the present random vibration analysis underestimates the expected value of $y_{1\,max}/y_{max}$. It is recalled that several assumptions were made in the course of the analysis: (1) Namely, that the input is white and stationary; (2) that the output is stationary; and (3) that $\sigma_{y_1}/\sigma_y = E[y_{1\,max}/y_{max}]$. The approximate validity of these assumptions is investigated next.

Correlated Ground Acceleration.—A nonconstant spectral density function
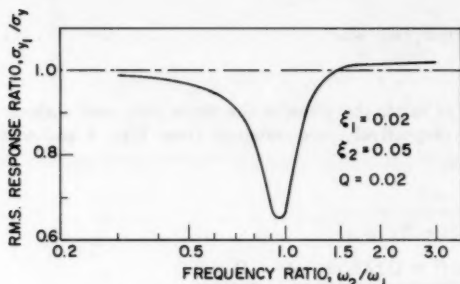
FIG. 8.—R.M.S. Response Ratio as Function of Frequency Ratio; Stationary White Ground Acceleration
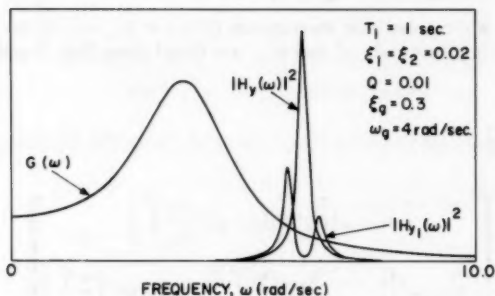
FIG. 9.—Spectral Density Function of Kanai-Tajimi Type and Squared Amplitude of System Transfer Functions with and without Damper

which is frequently used in modeling ground acceleration is that proposed by Kanai and Tajimi (11). It has the general form

$$G(\omega) = G_1 \frac{1 + 4\xi_g^2 \left(\dfrac{\omega}{\omega_g}\right)^2}{\left[1 - \left(\dfrac{\omega}{\omega_g}\right)^2\right]^2 + 4\xi_g^2 \left(\dfrac{\omega}{\omega_g}\right)^2} \quad \ldots \ldots \ldots \ldots \ldots \ldots (11)$$

with parameters ξ_g, ω_g, and G_1.

The associated stationary r.m.s. responses, σ_y and σ_{y_1}, are obtained by numerically integrating Eq. 8 with $G(\omega)$, $H_y(\omega)$, and $H_{y_1}(\omega)$ in Eqs. 11 and 9. Calculations with different combinations of ω_g and ξ_g show that the Kanai-Tajimi model produces values of σ_{y_1}/σ_y that are very similar to those from white noise input, if ω_g is not too close to ω_1. Important differences are found only for very small ξ_g and $\omega_g \approx \omega_1$. The same conclusions can be drawn by examining plots of $|H_y(\omega)|^2$, $|H_{y_1}(\omega)|^2$, and $G(\omega)$ such as those in Fig. 9 and by noticing that due to the sharp peaks of $|H_y(\omega)|^2$ and $|H_{y_1}(\omega)|^2$, σ_y^2 and $\sigma_{y_1}^2$ are mainly influenced by the ordinates of $G(\omega)$ at the location of these peaks. (For further considerations see Ref. 12.)

By fitting a function of the type in Eq. 11 to the squared Fourier amplitude of historical accelerograms (3), one obtains the values of ω_g and ξ_g in the last two columns of Table 1. These values show that ω_g is usually greater than the fundamental frequency of tall buildings (for which ω_1 is less than about 6 rad/sec) and that ξ_g is typically greater than 0.2.

One may therefore conclude that nonwhiteness of the input is not the main cause for departure of the analytical results from the empirical mean peak-response ratios.

Pseudo-Stationarity of Ground Acceleration.—One of the assumptions in the derivation of Eq. 10 is that the response has reached steady state in spite of the fact that for many earthquakes the duration of strong motion is very short. In order to correct for this assumption one may model the input motion as a *finite portion* of stationary white noise (whiteness has already been discarded as a cause of significant inaccuracy). One such process is usually said to be pseudo-stationary.

The transient variance of the response to pseudo-stationary white noise can be conveniently calculated by state-space methods (an alternative approach which uses the notion of evolutionary spectral density can be found in Ref. 10). For the case without damper the result is well known (19) and is given by

$$\sigma_y^2(t) = \frac{\pi G_0}{4\xi_1\omega_1^3} \left[1 - \frac{e^{-2\xi_1\omega_1 t}}{\omega_{1D}^2} (\omega_1^2 - \xi_1^2\omega_1^2 \cos 2\omega_{1D} t \right.$$

$$\left. + \xi_1\omega_1\omega_{1D} \sin 2\omega_{1D} t) \right] \quad \dots \dots \dots \dots \dots \dots \dots \dots \dots \quad (12)$$

in which $\omega_{1D} = \omega_1 \sqrt{1 - \xi_1^2}$ is the damped natural frequency; and t does not exceed the duration of the ground motion.

For a system with two degrees of freedom (Eq. 6 with $P = 1$), modal responses, $a_1(t)$ and $a_{11}(t)$, and participation factors, Γ_1 and Γ_{11}, the response, $y_1(t)$, is given by

$$y_1(t) = \Gamma_1 a_1(t) + \Gamma_{11} a_{11}(t) \quad \dots \dots \dots \dots \dots \dots \dots \dots \dots \dots \quad (13)$$

Therefore $\quad \sigma_{y_1}^2(t) = \Gamma_1^2 \sigma_{a_1}^2(t) + \Gamma_{11}^2 \sigma_{a_{11}}^2(t) + 2\Gamma_1\Gamma_{11} \text{cov} [a_1(t), a_{11}(t)] \quad (14)$

The variance terms, $\sigma_{a_1}^2(t)$ and $\sigma_{a_{11}}^2(t)$, are obtained from Eq. 12 with appropriate

modal parameters (ξ_1, ω_1 and ξ_{11}, ω_{11}), whereas the covariance term is (e.g., Ref. 9)

$$\text{cov}\,[a_1(t), a_{11}(t)] = \frac{\pi G_0}{\omega_{1D}\omega_{11D}} \left[\frac{a + e^{-at}(b \sin bt - a \cos bt)}{2(a^2 + b^2)} \right.$$
$$\left. - \frac{a + e^{-at}(d \sin dt - a \cos dt)}{2(a^2 + d^2)} \right] \quad \ldots \ldots \ldots \ldots \ldots \ldots \ldots \quad (15)$$

in which $\begin{cases} a = \xi_1 \omega_1 + \xi_{11} \omega_{11}; & b = \omega_{1D} - \omega_{11D}; \quad d = \omega_{1D} + \omega_{11D}; \\ \omega_{1D} = \omega_1 \sqrt{1 - \xi_1^2}; & \text{and} \quad \omega_{11D} = \omega_{11} \sqrt{1 - \xi_{11}^2} \quad \ldots \ldots \ldots \quad (16) \end{cases}$

Plot A in Fig. 10 gives the ratio, $\sigma_{y_1}(t)/\sigma_y(t)$, as a function of dimensionless duration (equivalent number of response cycles) for the set of parameters in
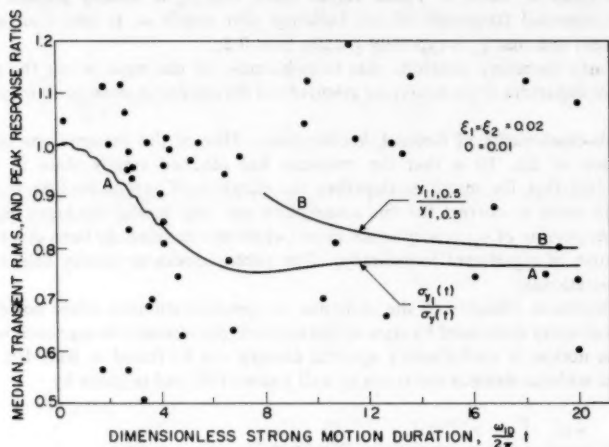
FIG. 10.—Transient R.M.S.: (a) Median Response Ratio; (b) Peak-Response Ratios for Historic Earthquakes of Table 1. Results from Historic Earthquakes are for $T_1 = 2\pi/\omega_1 = 1$ s

the figure. It might be argued that this ratio should be a good approximation to $E\,[y_{1\,max}/y_{max}]$ if t is set equal to the duration of strong motion. However, this is not so: ratios of the latter type are shown in Fig. 10 as dots. They correspond to earthquakes in Table 1 and to duration values according to the definition of Vanmarcke and Lai (18) also given in the table. In spite of the improvement from transient analysis, plot A still lies below any reasonable estimate of $E\,[y_{1\,max}(t)/y_{max}(t)]$ from historic data. An additional correction is made in the next subsection by considering bandwidth of the response process.

An interesting feature of plot A is that for earthquakes with short strong-motion duration (with respect to the first natural period of the building), the transient r.m.s. ratio is significantly larger and is a better estimator of $E\,[y_{1\,max}/y_{max}]$ than the stationary r.m.s. ratio. Fig. 10 also shows that for flexible (e.g., tall)

buildings, one should expect little if any benefit from the addition of a vibration absorber.

Bandwith of Response Process.—Use of the ratio $\sigma_{y_1}(t)/\sigma_y(t)$ as an estimator of $E\,[\,y_{1\,\max}\,/y_{\max}\,]$ for earthquakes with strong-motion duration, t, may be viewed to rest upon two assumptions: (1) That $E\,[\,y_{\max}\,]$ and $E\,[\,y_{1\,\max}\,]$ are proportional to the associated r.m.s. responses at time, t, with the same proportionality constant and; (2) that $E\,[\,y_{1\,\max}\,/y_{\max}\,]\,=\,E\,[\,y_{1\,\max}\,]\,/E\,[\,y_{\max}\,]$. In the analysis that follows, the second assumption is retained, but the first assumption is dropped in consideration of the fact that expected peak response depends also on response bandwidth and that typically this quantity is increased by the addition of a vibration absorber. (E.g., consider white noise input for which the spectral density function of the response is proportional to the squared amplitude of the transfer function and compare $|H_y(\omega)|^2$ and $|H_{y_1}(\omega)|^2$ in Fig. 9.) A wide-banded process displays less time correlation and, for the same variance, a larger expected peak value than a narrow-banded process. This may be an important mechanism that increases the mean peak-response ratio, $E\,[\,y_{1\,\max}\,/y_{\max}\,]$, with respect to the r.m.s. ratio, $\sigma_{y_1}(t)/\sigma_y(t)$.

Under the assumption that high-level crossings occur according to a Poisson process, Vanmarcke (17) derived an approximate expression for the $(1-p)$-fractile of the maximum response to a pseudo-stationary input motion of duration, t. If $y_{t,p}$ denotes this fractile, then the approximate expression is

$$y_{t,p} \approx (2 \ln \{2N\,[1 - \exp(-\delta_y(t)\sqrt{\pi \ln(2N)}]\})^{1/2} \quad\dots\dots\dots\dots\dots (17)$$

in which $$N = \left(\frac{t_0\,\Omega_y(t)}{2\pi}\right)(-\ln p)^{-1} \quad\dots\dots\dots\dots\dots\dots\dots (18)$$

is related to the average number of cycles of response motion, the quantity

$$t_0 = t \exp\left\{-2\left[\frac{\sigma_y^2(t)}{\sigma_y^2\left(\dfrac{t}{2}\right)} - 1\right]\right\} \quad\dots\dots\dots\dots\dots\dots\dots (19)$$

is an "equivalent stationary response" duration, and $\Omega_y(t)$ and $\delta_y(t)$ = shape parameters of the evolutionary response spectral density, at time, t. These last two parameters are defined in terms of the time-dependent spectral moments

$$\lambda_i(t) = \int_0^\infty \omega^i\,G(\omega)|\,H_y(\omega,t)|^2\,d\omega \quad\dots\dots\dots\dots\dots (20)$$

as $$\Omega_y(t) = \left[\frac{\lambda_2(t)}{\lambda_0(t)}\right]^{1/2} \quad\dots\dots\dots\dots\dots\dots\dots\dots\dots\dots (21)$$

$$\delta_y(t) = \left[1 - \frac{\lambda_1^2(t)}{\lambda_0(t)\,\lambda_2(t)}\right]^{1/2} \quad\dots\dots\dots\dots\dots\dots\dots\dots (22)$$

An approximate expression for the time-dependent transfer function, $H_y(\omega,t)$, in Eq. 20 can be obtained by replacing ξ_1 in $H_y(\omega)$ (Eq. 9) with a fictitious time-dependent damping, ξ_{1t}, defined (17)

$$\xi_{1t} = \frac{\xi_1}{(1 - e^{-2\xi_1\omega_1 t})} \quad\dots\dots\dots\dots\dots\dots\dots\dots\dots\dots (23)$$

The same procedure can be followed to obtain $y_{1t,p}$, with $\Omega_{y_1}(t)$ and $\delta_{y_1}(t)$ that correspond to the evolutionary transfer function

$$H_{y_1}(\omega, t) = \frac{-\Gamma_I}{(\omega_I^2 - \omega^2) + 2i\xi_{It}\omega_I\omega} + \frac{-\Gamma_{II}}{(\omega_{II}^2 - \omega^2) + 2i\xi_{IIt}\omega_{II}\omega} \ldots \ldots \ldots (24)$$

and ξ_{It} and ξ_{IIt} obtained from Eq. 23 with ξ_I and ξ_{II}, in place of ξ_1, and ω_I and ω_{II}, in place of ω_1.

Plot B in Fig. 10 corresponds to the median response ratio, $y_{1t,0.5}/y_{t,0.5}$ (values for short durations, t, are omitted because Eq. 17 is not accurate in this case). Peak-response ratios from historical earthquakes in the nearly stationary (right) portion of the figure have a mean value which is only slightly higher than $y_{1t,0.5}/y_{t,0.5}$ in that region.

Improvement of the median ratio over the r.m.s. ratio (plot A) is particularly noticeable for small ξ_1 and ξ_2, whereas if these damping parameters are large, then both $y(t)$ and $y_1(t)$ are wide-banded processes and $y_{1t,0.5}/y_{t,0.5} \approx \sigma_{y_1}(t)/\sigma_y(t)$.

Assumption that $E[y_{1\max}/y_{\max}] = E[y_{1\max}]/E[y_{\max}]$.—Accuracy of the approximation in the title of this subsection depends on the joint probability distribution of $y_{1\max}$ and $y_{\max}$, and not only on the first two moments of the response processes, $y(t)$ and $y_1(t)$.

Results of time history analysis with historical earthquakes normalized to a common peak acceleration support a joint lognormal distribution assumption for $y_{\max}$ and $y_{1\max}$. With this assumption, it can be shown that

$$E\left[\frac{y_1}{y}\right] = \frac{E[y_1]}{E[y]} \cdot \frac{V_y^2 + 1}{\dfrac{\text{cov}(y,y_1)}{E[y] \cdot E[y_1]} + 1} \ldots \ldots \ldots \ldots \ldots \ldots \ldots (25)$$

in which V_y = the coefficient of variation of the random variable, y; and notation is simplified by deleting subscript "max."

Empirical estimates of the second factor in the right-hand side of Eq. 25 from historic data are very close to 1, suggesting that the approximation $E\left[\dfrac{y_1}{y}\right]$ $= \dfrac{E[y_1]}{E[y]}$ is not a source of significant error.

Summary Considerations.—Previous results can be summarized as follows. Steady-state random vibration analysis with stationary white or correlated input gives r.m.s. ratios that are much smaller than empirical mean peak-response ratios. Improvements can be obtained: (1) For ground motions with short duration t, by replacing the stationary r.m.s. ratio with the transient r.m.s. ratio, $\sigma_{y_1}(t)/\sigma_y(t)$; and (2) for lightly damped systems, by accounting for the increase in response bandwidth due to the addition of the absorber and by replacing $\sigma_{y_1}(t)/\sigma_y(t)$ with the median peak-response ratio, $y_{1t,0.5}/y_{t,0.5}$.

There are other characteristics of the ensemble of ground acceleration time histories that might be responsible for inaccuracies of the random-vibration approach; in particular, nonstationarity and time-dependency of frequency content of the input motion. For analytical approximations that make use of Eq. 17,

another source of error is the implicit assumption that the response process is Gaussian.

PROBABILITY DISTRIBUTION OF SPECTRAL ORDINATES FOR OSCILLATORS WITH VIBRATION ABSORBER

A simple probabilistic model is developed, which combines the probability distribution of spectral ordinates for unmodified oscillators with results in previous sections to give the probability distribution of peak response for oscillators with an added damper. This last distribution can be used in connection with conventional seismic risk procedures to obtain the probability that the response of structures modified by vibration absorbers will exceed a given value in a given interval of time.

If one assumes that $r = y_{1\,max}/y_{max}$ and y_{max} have bivariate lognormal distribution, then also $y_{1\,max} = r y_{max}$ has lognormal distribution, with parameters (12)

$$\begin{cases} E\,[\ln y_1] = \ln\left(\dfrac{E\,[y]\cdot E\,[r]}{\sqrt{V_y^2+1}\cdot\sqrt{V_r^2+1}}\right) \\[2mm] \sigma_{\ln}^2 y_1 = \ln\left((V_y^2+1)(V_r^2+1)\left(\dfrac{\operatorname{cov}(y,r)}{E\,[y]\cdot E\,[r]}+1\right)^2\right) \end{cases} \dots\dots\dots (26)$$

in which V_x = the coefficient of variation of x; and subscript "max" has been deleted for simplicity.

Estimates of V_r and $\dfrac{\operatorname{cov}(y,r)}{E\,[y]\cdot E\,[r]}$ from historic data and for several combinations of structural parameters indicate that $V_r^2+1\approx 1$ and $\dfrac{\operatorname{cov}(y,r)}{E\,[y]\cdot E\,[r]}+1\approx 1$ (r has relatively small dispersion and y and r are weakly correlated). With these replacements, Eq. 26 simplifies to

$$\begin{cases} E\,[\ln y_1] \approx \ln\left(\dfrac{E\,[y]\cdot E\,[r]}{\sqrt{V_y^2+1}}\right) \\[2mm] \sigma_{\ln}^2 y_1 \approx \ln(V_y^2+1) \end{cases} \dots\dots\dots\dots\dots\dots\dots\dots (27)$$

Fig. 11 shows histograms of y_{max} and $y_{1\,max}$ for the earthquake records of Table 1 normalized to 0.1 g peak acceleration, and for the structural parameters in Fig. 10. Superposed to the histogram of Fig. 11(b) are lognormal density functions with moments from Eq. 27. In constructing the solid curve, $E\,[y]$ and $E\,[r]$ were set equal to the empirical estimates in Fig. 11(a); whereas the dashed curve corresponds to $E\,[y]$ in Fig. 11(a), and $E\,[r]$ estimated from the median response ratio (plot B in Fig. 10) with a nominal strong-motion duration of 10 sec. In both cases the density functions provide reasonable fits to the empirical data.

The previous analysis gives the distribution of peak response for an oscillator with vibration absorber and for given peak ground acceleration. This last quantity, referred either to a single earthquake or to an interval of time, is highly uncertain in practice, with probability distribution that is the usual output of seismic risk analysis programs (e.g., Ref. 5).

One should be careful in combining probabilistically peak ground acceleration and peak structural response to normalized input motions; the operation is simple if peak acceleration refers to one earthquake, but may be complicated if reference is to a given interval of time. In the latter case, one must address the question whether structural responses to different earthquakes (scaled to the same intensity)
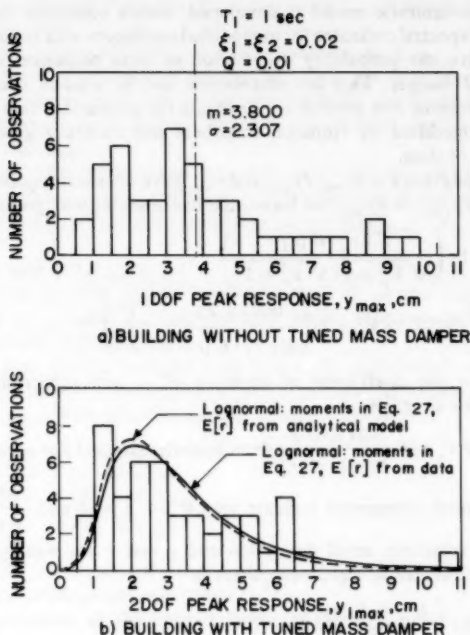
FIG. 11.—Observed and Predicted Distribution of Peak Response for Building with Tuned Mass Damper: $T_1 = 1$ s, $\xi_1 = \xi_2 = 0.02$, Peak Ground Acceleration 0.1 g

are independent or not. It suffices here to mention this problem, which is much too vast to receive fair treatment within the present paper.

SEISMIC EFFECTIVENESS OF VIBRATION ABSORBERS IN SIMPLE INELASTIC SYSTEMS

Assessing the influence of inelastic structural behavior on the control action of tuned mass dampers is a difficult problem due to the great variety of possible inelastic models. With this limitation in mind, a preliminary analysis was undertaken using elastic-perfectly plastic oscillators and linear elastic dampers. It was felt that extension to more sophisticated models would be justified if the results from this simpler analysis had demonstrated the effectiveness of an added damper. This was not the case.

In Ref. 13, Lai suggested that long-term inelastic damage be measured by cumulative yielding ductility, η. With y_{e1} the yielding displacement of the main system and D_i the plastic displacement caused by the ith yielding event, η is defined

$$\eta = \frac{\Sigma |D_i|}{y_{e1}} + 1 \dots \dots \dots \dots \dots \dots \dots \dots \dots \dots \dots \dots \dots \dots \quad (28)$$

In the present study, two quantities are used to measure the effectiveness of tuned mass dampers: the ratio between cumulative yielding ductility in the 2DOF and in the 1DOF system, η_1/η, and the ratio between the associated ductility ratios, μ_1/μ. From the definition of ductility ratio, it is clear that μ_1/μ is the same as peak response ratio.

Parameters of the 1DOF system are: mass M, frequency of small-amplitude response ω_1, damping ratio ξ_1, and yielding displacement y_{e1}; whereas the mass damper is identified as before by the three parameters, m, ω_2, and ξ_2. For several combinations of ω_1 and y_{e1} the sensitivity of η_1/η and μ_1/μ to dimensionless damper parameters (frequency ratio, ω_2/ω_1, mass ratio, m/M, and damping, ξ_2) was investigated by using the set of historical earthquakes in Table 1, normalized to a common peak acceleration. The study, which is documented in detail in Ref. 12, showed that the ratios η_1/η and μ_1/μ have a dependence on the aforementioned parameters similar to that of peak response ratio in elastic systems. There is, however, a quantitative difference; while some reduction is noticed in cumulative yielding ductility due to the vibration absorber, the reduction in ductility ratio is insignificant. Mean values of η_1/η are typically between 0.85 and 0.95 and those of μ_1/μ are typically between 0.95 and 1.05. The tentative conclusion is therefore drawn that the small seismic effectiveness of tuned mass dampers in elastic systems becomes even smaller in the presence of inelastic action.

CONCLUSIONS

Assuming that elastic structural systems respond only in their fundamental mode and that the fundamental mode shape does not change due to the addition of a damper, the equation of motion of a building with and without a tuned mass damper can be reduced to that of a 2DOF and a 1DOF system, respectively. Small changes in the shape of the fundamental mode have negligible effect on the ratio r between the peak relative displacements of the top floor with and without damper, a quantity which is used to measure damper effectiveness.

Sensitivity studies with respect to structural parameters have shown that:

1. $E[r]$ is minimum when the natural frequency of the damper is about equal to fundamental frequency of the structure.

2. Increasing modal damping or period of the main structure decreases the efficiency of the damper.

3. The effectiveness of tuned mass dampers increases with increasing generalized mass ratio (see definition following Eq. 6).

4. An increase in the damping of the vibration absorber slightly increases

the mean response ratio and at the same time decreases considerably the motion of the damper. To the extent that the latter phenomenon is important, higher damping values should be used.

Time history analysis using a catalog of historical earthquakes has revealed two important facts:

1. The mean peak-response ratio is higher than predicted by random vibration theory on the basis of stationary r.m.s. response to stationary white noise ground acceleration.
2. Empirical response ratios are widely scattered, i.e., there is much uncertainty as to the effectiveness of tuned mass dampers for individual earthquakes.

In search for an improved analytical model, several conclusions are arrived at:

1. Compared with correlated ground acceleration having a spectral density function of the Kanai-Tajimi type, the assumption of white noise input is not a major source of inaccuracy.
2. Pseudo-stationarity of the input increases significantly the r.m.s. response ratio for earthquakes that are too short for the system to reach steady state.
3. For systems with small damping, improved (higher) estimates of the mean peak-response ratio are obtained by considering the broadening of the response spectral density due to the damper.
4. Replacing $E[y_{1\,max}]/E[y_{max}]$ with $E[y_{1\,max}/y_{max}]$ does not introduce significant inaccuracy in the analytical models.

In some analytical approximation, bias is also contributed by the fact that real earthquakes are not exactly portions of realizations of stationary Gaussian processes.

A simple model is suggested to incorporate the effect of vibration absorbers into the probability distribution of response spectrum ordinates, given peak ground acceleration. The model uses the knowledge of the same probability distribution for unmodified oscillators, coupled with results from random vibration theory.

Generally speaking, tuned mass dampers seem to be less effective than previously thought, especially on account of the large statistical variability of the peak-response ratio (typical mean values in the range 0.85–0.95 and standard deviations as high as 0.15).

From a pilot study of elastic-perfectly plastic oscillators, it was concluded that seismic effectiveness of vibration absorbers is even smaller in the case of inelastic systems.

All these considerations refer to cases when the response quantity of interest is contributed primarily by the first mode. Additional study is needed to find the effect of tuned mass dampers on higher modes and hence on response quantities such as interstory displacements and local deformations.

APPENDIX I.—REFERENCES

1. Anagnostopoulos, S. A., "Non-linear Dynamic Response and Ductility Requirements of Building Structures Subjected to Earthquakes," *M.I.T. Department of Civil Engineering Research Report R72-54*, Cambridge, Mass., Sept., 1972.
2. Biggs, J. M., *Introduction to Structural Dynamics*, McGraw-Hill Book Co., Inc., New York, N.Y., 1964.
3. Binder, R., "Equivalent Durations and Power Spectral Density Functions for a Set of 39 Ground Motions," *Internal Study Report No. 16, Seismic Safety of Buildings*, M.I.T. Department of Civil Engineering, Cambridge, Mass., Apr., 1978.
4. Clough, R. W., and Benuska, K. L., *FHA Study of Seismic Design Criteria for High-Rise Buildings*, Aug., 1966.
5. Cornell, C. A., and Merz, H. A., "Seismic Risk Analysis of Boston," *Journal of the Structural Division*, ASCE, Vol. 101, No. ST10, Proc. Paper 11617, Oct., 1975, pp. 2027–2043.
6. Crandall, S. H., and Mark, W. D., *Random Vibration in Mechanical Systems*, Academic Press, New York, N.Y., 1973.
7. Den Hartog, J. P., *Mechanical Vibrations*, McGraw-Hill Book Co., Inc., New York, N.Y., 1956.
8. Gasparini, D. A., "Response of MDOF Systems to Nonstationary Random Excitation," presented at the January, 1979, ASCE Specialty Conference on Probabilistic Mechanics and Structural Reliability, held at Tucson, Arizona.
9. Gupta, Y. P., and Chandrasekaran, A. R., "Absorber System for Earthquake Excitations," *Proceedings of the 4th World Conference on Earthquake Engineering*, 1969.
10. Hammond, J. K., "On the Response of Single and Multi-degree of Freedom Systems to Nonstationary Random Excitations," *Journal of Sound and Vibration*, 7, 3, London, England, 1968, pp. 393–416.
11. Kanai, K., "An Empirical Formula for the Spectrum of Strong Earthquake Motions," *Bulletin of the Earthquake Research Institute*, Vol. 39, University of Tokyo, Tokyo, Japan, 1961.
12. Kaynia, A. M., "Effect of Tuned Mass Dampers on the Seismic Response of Buildings," thesis submitted to the Massachusetts Institute of Technology, at Cambridge, Mass., in 1979, in partial fulfillment of the requirements for the degree of Master of Science.
13. Lai, S. P., "On Inelastic Response Spectra for Aseismic Design," *M.I.T. Department of Civil Engineering Research Report R78-18*, Cambridge, Mass., July, 1978.
14. McNamara, R. J., "Tuned Mass Dampers for Buildings," *Journal of the Structural Division*, ASCE, Vol. 103, No. ST9, Proc. Paper 13200, Sept., 1977, pp. 1785–1798.
15. "Strong-Motion Earthquake Accelerograms—Digitized and Plotted Data," California Institute of Technology, Earthquake Engineering Research Laboratory, Vol. II, 1971.
16. "Tuned Mass Dampers Steady Sway of Skyscrapers in Wind," *Engineering News Record*, New York, N.Y., Aug. 18, 1977.
17. Vanmarcke, E. H., *Seismic Risk and Engineering Decisions*, Chapter 8, C. Lomnitz, and E. Rosenblueth, eds., Elsevier Publishing Co., New York, N.Y., 1977.
18. Vanmarcke, E. H., and Lai, S. P., "Strong-Motion Duration of Earthquakes," *M.I.T. Department of Civil Engineering Research Report R77-16*, Cambridge, Mass., July, 1977.
19. Wang, M. C., and Uhlenbeck, G. E., "On the Theory of Brownian Motion II," *Selected Papers on Noise and Stochastic Processes*, N. Wax, ed., Dover Publications, Inc., New York, N.Y., 1954.
20. Wirsching, P. H., and Campbell, G. W., "Minimal Structural Response under Random Excitation Using the Vibration Absorber," *Earthquake Engineering and Structural Dynamics*, Vol. 2, 1974, pp. 303–312.
21. Wirsching, P. H., and Yao, J. T. P., "A Statistical Study of Some Design Concepts in Earthquake Engineering," *Technical Report CE-21 (70) NSF-065*, Bureau of Engineering Research, The University of New Mexico, Albuquerque, N.M., May, 1970.
22. Wirsching, P. H., and Yao, J. T. P., "Safety Design Concepts for Seismic Structures," *Computers and Structures*, Vol. 3, Pergamon Press, Inc., New York, N.Y., 1973, pp. 809–826.

APPENDIX II.—NOTATION

The following symbols are used in this paper:

$a_1(t), a_{11}(t)$ = modal displacements of 2DOF system;

c = damping of vibration absorber;

$\mathbf{C}$ = damping matrix of main system;

$G(\omega)$ = one-sided spectral density function of base acceleration;

G_0 = constant spectral density (white noise input only);

$H(\omega), H_y(\omega), H_{y_1}(\omega)$ = complex transfer functions;

k = spring constant of vibration absorber;

$\mathbf{K}_L$ = lateral stiffness matrix of main system;

m = mass of vibration absorber;

$\mathbf{M}$ = mass matrix of main system;

n = number of degrees of freedom for main system;

P = participation factor in the fundamental mode;

Q = generalized mass ratio; definition following Eq. 6;

T_1 = fundamental period of main system;

$\mathbf{U}$ = displacement vector for main system;

x = displacement of tuned mass damper relative to top floor;

y_1, y = relative displacement of top floor with and without damper;

$y_{1,p}, y_{t,p}$ = $(1 - p)$-fractile of peak system response with and without damper, for earthquakes of duration, t;

y_{el} = yielding displacement of elasto-plastic system;

Γ_1, Γ_{11} = participation factors of 2DOF systems;

δ, Ω = shape parameters of spectral density function; see Eqs. 21 and 22;

η_1, η = cumulative yielding ductility, with and without damper;

μ_1, μ = ductility ratio, with and without damper;

ξ_1 = damping ratio of fundamental mode;

ξ_2 = damping ratio of tuned mass damper;

ξ_1, ξ_{11} = damping ratio for the modes of 2DOF system;

ξ_g, ω_g = parameters of Kanai-Tajimi spectral density function;

$\sigma_{y_1}^2, \sigma_y^2$ = response variances, with and without damper;

ϕ = fundamental mode shape of main system;

ω_{1D}, ω_1 = damped and undamped natural frequencies of fundamental mode;

ω_2 = natural frequency of mass damper; and

ω_1, ω_{11} = natural frequencies of 2DOF system.

POST-ELASTIC DYNAMICS OF THREE-DIMENSIONAL FRAMES

By Antony G. Gillies[1] and Robin Shepherd,[2] F. ASCE

INTRODUCTION

The necessity for frame buildings to dissipate significant amounts of energy inelastically under severe earthquake excitation is widely recognized. Current seismic resistant design involves the prediction of inelastic effects leading to a distribution of beam capacity moments into columns differing from the distribution derived from elastic analyses. Also, to determine axial column loads, the designer must assess the extent of hinging occurring in adjacent stories and in orthogonal directions arising from concurrent earthquake effects. With the object of improving the modeling techniques currently in general use, a computer program has been developed to enable prediction of the time-history response of three-dimensional frame structures to earthquake ground motion. Application is not restricted to a rectangular grid layout, but a completely general structure geometry can be modeled. Yielding is allowed for in both beams and columns by a series of yield surface options selected according to the principal structural actions of the component elements. For a typical beam element, the yield status may be a function of the principal bending moment only, whereas for an exterior column account can be taken of biaxial bending coupled with axial load. In this paper the principles of the analysis procedure are presented and, to demonstrate the implementation of the program, the response of a six-story reinforced concrete ductile frame building is investigated. The results demonstrate that the response based on an equivalent planar frame assumption is modified significantly when account is taken of concurrent earthquake effects.

BACKGROUND

Considerable effort has been expended on inelastic analysis of frame structures to earthquake base motions. Many computer programs have been developed, but most are restricted to planar frame analysis. A number of general purpose

[1] Asst. Engr., Beca, Carter, Hollings & Ferner, Consulting Engrs., Box 3942, Wellington, New Zealand.
[2] Prof. of Civ. Engrg., School of Engrg., Univ. of California, Irvine, Calif. 92717.

three-dimensional programs are available, but some are restricted to examination of linear elastic behavior, and all necessarily exhibit some limitation of structure geometry, material representation, computer capacity or efficiency. These considerations prompted the development of a new program (1) to compute the response time history of a three-dimensional frame by direct integration of the equations of motion with allowances incorporated for inelastic member behavior.

The new coding incorporates efficient algorithms and core storage with a user-oriented emphasis, particularly in regard to handling input and output data. A modular construction facilitates both updating the analysis sections and extending the finite element library. It is believed that the new program is more versatile than other nonlinear ones while being more convenient to use.

PROGRAM SUMMARY

The computer program comprises two main sections. The first controls the input of the problem definition data and solves for the node displacements and member forces due to static applied loads. In the second phase the dynamic load vector is derived, based on the specific earthquake ground acceleration record. Once the dynamic load vector is established, the node displacement increments are found using the tangent stiffness properties which reflect the structure stiffness state at the beginning of the current loading increment.

If no change in element yield status occurs throughout the structure during a particular increment, the predicted displacements correspond to the correct displacement increments consistent with the stiffness and loading assumptions. When some changes in element yield status are observed, the statement of dynamic equilibrium requires additional consideration.

The equations of motion are derived in the finite element representation by considering the statement of equilibrium at time, t. The dynamic equilibrium at time, t, is written as:

$$\mathbf{F}_I(t) + \mathbf{F}_D(t) + \mathbf{F}_E(t) = \mathbf{R}(t) \quad \dots \dots \dots \dots \dots \dots \dots \dots \dots \dots (1)$$

in which $\mathbf{F}_I(t)$ = inertia force vector; $\mathbf{F}_D(t)$ = damping force vector (viscous damping); $\mathbf{F}_E(t)$ = vector of internal member actions; and $\mathbf{R}(t)$ = vector of externally applied loading. Nonlinear effects are introduced in the analysis from the realization that the elements of the mass, damping and stiffness matrices may be dependent on the current displacements of a structure and on its previous loading history. Nonlinear effects in the element stiffness matrices may be due to either large displacement effects or to material yielding behavior or to a combination of both. In the problem considered in this study, nonlinear stiffness effects are restricted to those related to material yielding. The formulation is equally capable of handling both effects without further complication.

In nonlinear problems the structure response is most conveniently derived by a consideration of dynamic equilibrium at two stations, at time, t, and at $t + \Delta t$. Writing Eq. 1 at these two instances yields:

$$\mathbf{F}_I(t) + \mathbf{F}_D(t) + \mathbf{F}_E(t) = \mathbf{R}(t) \quad \dots \dots \dots \dots \dots \dots \dots \dots \dots (2)$$

$$\mathbf{F}_I(t + \Delta t) + \mathbf{F}_D(t + \Delta t) + \mathbf{F}_E(t + \Delta t) = \mathbf{R}(t + \Delta t) \quad \dots \dots \dots \dots \dots (3)$$

The equations of motion may be rewritten in incremental form by considering

the difference between the states at time, t, and time, $t + \Delta t$:

$$\Delta \mathbf{F}_I(t) + \Delta \mathbf{F}_D(t) + \Delta \mathbf{F}_E(t) = \Delta \mathbf{R}(t) \quad \ldots \ldots \ldots \ldots \ldots \ldots \ldots \ldots \quad (4)$$

in which $\Delta \mathbf{F}_I(t) = \mathbf{F}_I(t + \Delta t) - \mathbf{F}_I(t)$; $\Delta \mathbf{F}_D(t) = \mathbf{F}_D(t + \Delta t) - \mathbf{F}_D(t)$; $\Delta \mathbf{F}_E(t) = \mathbf{F}_E(t + \Delta t) - \mathbf{F}_E(t)$; and $\Delta \mathbf{R}(t) = \mathbf{R}(t + \Delta t) - \mathbf{R}(t) = \mathbf{R}(t + \Delta t) - \mathbf{F}_I(t) - \mathbf{F}_D(t) - \mathbf{F}_E(t)$. The member force contribution is given by the term $\Delta \mathbf{F}_E(t)$. If no change in element yield status is observed during the increment then dynamic equilibrium is preserved. Where the status of some elements changes during the increment, the increment in member forces is given by $\Delta \mathbf{F}_E(t)_{NL}$ in which

$$\Delta \mathbf{F}_E(t)_{NL} = \Delta \mathbf{F}_E(t) - \Delta \mathbf{F}_{UB_K} \quad \ldots \ldots \ldots \ldots \ldots \ldots \ldots \ldots \quad (5)$$

where $\Delta \mathbf{F}_E(t)$ = vector of internal member actions based on the element stiffness properties at the start of the increment; $\Delta \mathbf{F}_E(t)_{NL}$ = vector of internal member actions taking into account the change in element yield status during the increment; and $\Delta \mathbf{F}_{UB_K}$ = a vector of fictitious forces which are necessary to restore the dynamic equilibrium balance. Then

$$\Delta \mathbf{R}(t) = \Delta \mathbf{F}_I(t) + \Delta \mathbf{F}_D(t) + \Delta \mathbf{F}_E(t)_{NL} + \Delta \mathbf{F}_{UB_K} \quad \ldots \ldots \ldots \ldots \ldots \quad (6)$$

In order to avoid errors which may arise from accumulating equilibrium unbalances over a series of time steps a number of corrective procedures are possible. One option is to introduce an iterative cycle into the analysis such that, at the end of each time step, the unbalanced forces are redistributed throughout the structure. With the high demand on computer resources, the introduction of additional iterative cycles into each increment is not considered warranted. Therefore a second option, which is to apply a corrective load during the subsequent time interval, is implemented in the new program. Thus, although the equilibrium unbalance is allowed to remain over part of a time step, the out-of-phase corrective loads restore the force balance. In the computer codes developed in this study, the vector of unbalanced forces is determined in a subroutine and is added to the load vector for the subsequent interval.

Damping is taken to be stiffness proportional and is split into two components, one proportional to the initial elastic stiffness properties, and the second a function of the current tangent stiffness. During intervals of extensive yielding, tangent stiffness related damping forces may be low and the solution stability control afforded by structural damping can be negligible. A level of initial stiffness proportional damping ensures that a minimum level of damping is retained throughout the analysis.

Because changes in element yield status modify the structure tangent stiffness matrix, unbalanced forces are generated in the stiffness proportional damping model. The equilibrium damping representation is given by

$$\mathbf{F}_D(t) = [\alpha M + \beta_0 K_0 + \beta_t K_t] \{ \dot{x}(t) \} \quad \ldots \ldots \ldots \ldots \ldots \ldots \ldots \quad (7)$$

in which M = the structure mass matrix; K_t = the current tangent stiffness matrix; K_0 = the original elastic stiffness matrix; and α, β_t and β_0 = constants to be determined. At the beginning of the next increment the damping force is given

$$\mathbf{F}_D(t)_+ = [\alpha M + \beta_0 K_0 + \beta_t K_t'] \{ \dot{x}(t) \} \quad \ldots \ldots \ldots \ldots \ldots \ldots \ldots \quad (8)$$

in which $K'_t = K_t + \Delta K$; and ΔK = change in the tangent stiffness matrix computed at the end of the preceding time step. To restore the equilibrium balance, an additional out-of-plane corrective load, ΔF_{UB_D}, is applied in the next time increment, in which

$$\Delta F_{UB_D} = \beta_t [\Delta K] \{\dot{x}(t)\} \dotfill (9)$$

The constants α and β are defined in Eqs. 10 and 11 by specifying a proportion of critical damping in any two modes. The two modes are selected such that the level of damping is controlled over the frequency spectrum of interest

$$\alpha = \frac{4\pi(T_j \epsilon_j - T_i \epsilon_i)}{(T_j^2 - T_i^2)} \dotfill (10)$$

$$\beta = \frac{T_i T_j (T_j \epsilon_i - T_i \epsilon_j)}{\pi(T_j^2 - T_i^2)} \dotfill (11)$$

in which ϵ_i = the proportion of critical damping in the mode with period T_i; and ϵ_j = the proportion of critical damping in the mode with period T_j. The stiffness proportional damping factor β is subdivided into two components β_0 and β_t such that

$$\beta = \beta_0 + \beta_t \dotfill (12)$$

In the absence of any better substantiated value of the modulus of elasticity, E, its value is derived from the relationship based on cylinder tests and normal weight concrete

$$E_c = 4,700 \sqrt{f'_c}, \quad \text{in Megapascals} \dotfill (13)$$

in which f'_c = specified compressive strength of concrete, in Megapascals.

In selecting values for the section second moment of area, consideration is given to the assumed material deformation state. Since the elastic-perfectly plastic and bilinear hysteresis loops do not include directly the softening due to flexural cracking, the EI values for members subjected to significant deformation are selected to be representative of cracked sections.

The mathematical model which forms the basis of the structural member elements provided for in the program is a three-dimensional one (1) based on an extension of the Giberson (2) one-component model. The inelastic actions are confined to the ends of the element. In order to represent the joint core zones at the ends of the member, rigid end blocks may be specified. Plastic hinges are assumed to form at the beam face of the rigid block. Curvature of the equivalent plastic hinge is derived from an application of small displacement concepts. The element yield status is defined by the specification of a set of yield forces. In addition, if a finite post-elastic stiffness is desired in the model, a stiffness ratio which relates the post-yield stiffness to the initial elastic stiffness is supplied. The model parameters are completed by the derivation of an equivalent plastic hinge length from which the hinge curvature is obtained. A family of five yield surfaces of increasing complexity is included in the program. The surface appropriate to a particular member in a frame may be selected according to the member forces which interact significantly on the yield surface. Particular applications are demonstrated in the following section.

Six-Story Building Analyzed

The two by one bay, six-story reinforced concrete building frame analyzed is shown in Fig. 1. The seismic resistance design level is based on a current loadings code (3) and the member properties assumed in the analysis are summarized in Table 1. The effective section stiffness properties, representative of a cracked section, were calculated assuming an equivalent second moment of area equal to three quarters of the gross uncracked value and assuming the width of the slab effective as a T-beam flange to be one eighth of the span length of the beam. The yield surface parameters selected are summarized. In recognition of the orthogonal frame geometry, the yield moment level of the beam elements is defined by bending in the plane of the two-dimensional subframes and consequently the simplest of the family of available yield surfaces may be used. The design of the structure reflects the capacity design philosophy, where in this instance the beam hinges form the energy-dissipating mechanism. An overstrength capacity factor is applied in the design of the column elements
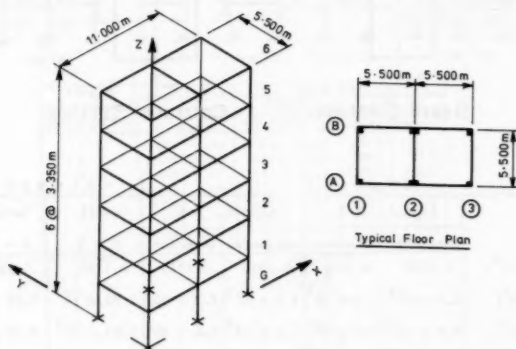
FIG. 1.—Definition of Six-Story Building

to ensure the desired strength hierarchy is achieved which will ensure beam hinging in preference to column hinging.
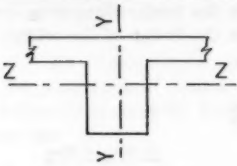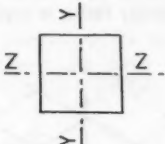
Analyses of plane frame structures indicate that for structures proportioned in accordance with the capacity approach some plastic hinging is frequently unavoidable at the base of the ground floor columns. Since the possibility of hinge formation in this zone cannot be discounted a yield surface is assigned to each of the ground floor columns. When concurrent earthquake loading is applied, the columns are subjected to significant flexural deformation about both principal axes of the section. The axial load level in the columns is influenced by the instantaneous overturning moment resisted at ground level and this, in turn, is a function of the earthquake induced inertial loading on the structure. The yield surface chosen to model the complex interaction of orthogonal bending moments combined with a time varying axial load is shown in Fig. 2.

A lumped mass model is used to represent the mass properties of the structure.

Two distributions are assumed in the analyses, both having the same total mass at each floor level. The first is representative of a balanced structure, with the center of mass and the center of elastic stiffness coincident. The second distribution, given in Fig. 3, corresponds to a 10% static eccentricity between the center of mass and the center of stiffness at each level. The eccentricity is applied in both X and Y global coordinate directions.

To establish the viscous damping allowance, the damping effective in each modal coordinate is specified for two periods with the distribution throughout the frequency spectrum then given by the relationship in Eqs. 10 and 11. The required parameters are established by assigning 10% of critical damping at the periods $T_1 = 0.77$ sec and $T_2 = 0.26$ sec.

TABLE 1.—Summary of Member Section Properties

Beam Section   Column Section

| | BEAMS | | | | COLUMNS | |
| | Levels 1-3 | | Levels 4-6 | | Levels | Levels |
	perimeter	interior	perimeter	interior	G - 3	4 - 6
Area (m^2)	0.1050	0.1050	0.1015	0.1015	0.1250	0.1013
Iyy (m^4)	2.3×10^{3}	2.3×10^{3}	2.3×10^{3}	2.3×10^{3}	3.91×10^{3}	2.56×10^{3}
Izz (m^4)	5.9×10^{3}	5.9×10^{3}	5.4×10^{3}	5.4×10^{3}	3.91×10^{3}	2.56×10^{3}
J (m^4)	1.0×10^{4}	1.0×10^{4}	1.0×10^{4}	1.0×10^{4}	1.0×10^{4}	1.0×10^{4}
Rigid end block (m)	0.300	0.300	0.275	0.275	0.250	0.250
F.E.S.(kN)	25.0	25.0	25.0	25.0	-	-
F.E.M.(kN-m)	20.0	40.0	20.0	40.0	-	-

$$E = 25.0 \times 10^6 \text{ kN/m}^2 \qquad G = 10.4 \times 10^6 \text{ kN/m}^2$$

The dynamic properties of the elastic models are given by the eigenvalue problem solution for the balanced and eccentric mass distribution assumptions. The properties for the first three modes in each instance are summarized schematically in Fig. 4. In the balanced case, the modes correspond to two distinct lateral displacement modes and a torsional mode. For the eccentric model a strong degree of coupling in the displacement components is observed. It is possible to classify the three modes as predominantly displacement or torsional configurations, if comparison with the properties of the balanced model is made.

The horizontal ground acceleration components recorded in the El Centro, May 18, 1940 earthquake provide the source of the input earthquake loading for all the comparisons undertaken in this study. In the elastic case, the structure's response is determined for the first 5 sec of the earthquake time history. In the inelastic studies limitations are imposed because of computer resource restrictions. To remain within the bounds of the scheduled computer allocation, the analyses are confined to approx 4,000 sec of process time. In the case of a yielding structure subjected to concurrent earthquake duration, this corre-
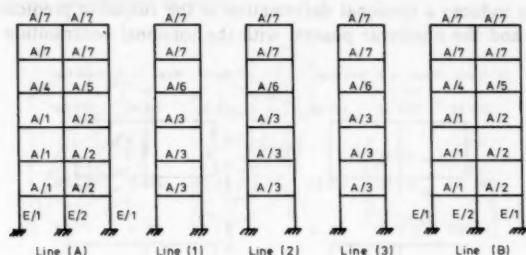
TYPE A YIELD SURFACE SPECIFICATION	HINGE LENGTHS		YIELD MOMENTS			
	END (I) (m)	END (J) (m)	END (I)		END (J)	
			POSITIVE (kN-m)	NEGATIVE (kN-m)	POSITIVE (kN-m)	NEGATIVE (kN-m)
A/1	0.410	0.410	208.0	208.0	190.0	190.0
A/2	0.410	0.410	190.0	190.0	208.0	208.0
A/3	0.410	0.410	208.0	208.0	208.0	208.0
A/4	0.375	0.375	160.0	131.0	115.0	137.0
A/5	0.375	0.375	115.0	137.0	160.0	131.0
A/6	0.375	0.375	160.0	131.0	131.0	160.0
A/7	0.375	0.375	115.0	115.0	115.0	115.0
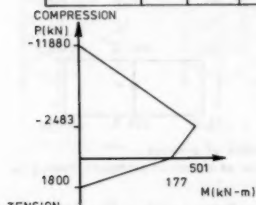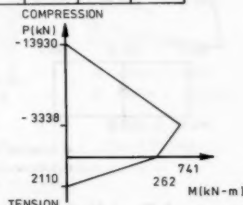
FIG. 2.—Summary of Yield Surface Parameters for Six-Story Building

sponds to approx 3.2 sec of earthquake duration. From a consideration of the elastic response time history it is observed that a relatively small displacement response is induced in the structure during the first second of the earthquake. In order that the structure is subjected to a significant duration of potential nonlinear response analysis time the earthquake ground motion for the first second of the time history is skipped in the nonlinear studies. Five additional linear increments are introduced at the start of the assumed record to avoid a sudden impulse loading on the structure because of the displaced origin.

The peak ground acceleration in the S 00 E component is 3,420 mm/s² at 2.13 sec and, in the S 90 W component, 1,790 mm/s² at 1.91 sec. A comparison between the X and Y directions displacement response time histories given in Fig. 5 demonstrates the significant difference in the peak displacement response components of the structure for fully elastic element behavior.

Summary of Response Characteristics Based on Uniform and Eccentric Mass Distributions.—In Figure 6 the Y direction displacement time history of the top floor (Level 6) of the building is plotted for the two cases representing the balanced and the eccentric mass distributions. The inclusion of 10% static eccentricity induces a torsional deformation in the response prediction in both the elastic and the nonlinear phases, with the torsional contribution becoming
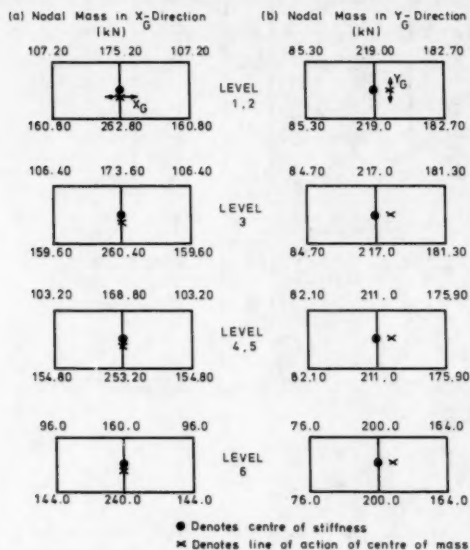
FIG. 3.—Summary of Floor Nodal Masses Representing Six-Story Structure with 10% Static Eccentricity

more dominant in the post-elastic sector. Before the structure is subjected to significant post-elastic deformation, it is possible to relate the response characteristics of the two models. If a torsional deformation is superimposed on the lateral displacements derived from the balanced mode, the displacements of the perimeter frames in the eccentric model can be resolved. Following the onset of yield, the eccentricity between the center of mass and the instantaneous center of stiffness at each level is no longer constant—the instantaneous torque may be increased or decreased depending on the distribution of the yielding elements.

In the initial elastic section of the response, the elastic displacement of the balanced building serves as a useful prediction of the average response charac-

teristics of the eccentric model. In the post-yield section the torsional contribution is the result of a complex interaction between the center of mass and the instantaneous center of stiffness. It is no longer possible to predict the displacement profile on the basis of a projection of the displacement time history produced from an elastic three-dimensional analysis. In a similar manner, the post-elastic response derived from a simplified two-dimensional planar frame idealization does not model the torsional imbalance observed in the response of three-dimensional structures. A significant torsional deformation can be identified in the response of the initially balance structure [Fig. 6(a)], as a consequence of the asymmetric distribution of yield.

MODE 1
$T_2 = 0.91$ secs.

MODE 2
$T_1 = 0.82$ secs.

MODE 3
$T_3 = 0.79$ secs.

(a) Balanced Building - Centre of Mass and Centre of Stiffness Coincident

MODE 1
$T_1 = 0.96$ secs.

MODE 2
$T_2 = 0.84$ secs.

MODE 3
$T_3 = 0.72$ secs.

△ Centre of Mass
○ Centre of Stiffness

(b) Eccentric Building   10% Static Eccentricity between Centre of Mass and Centre of Stiffness.
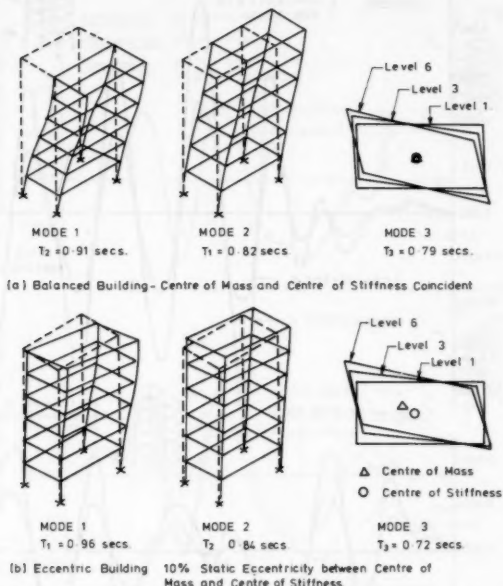
FIG. 4.—Comparison of Modal Properties of Balanced and Eccentric Structures

The results of the limited analyses undertaken in this study are sufficient to demonstrate the significant contribution to the overall structure response which can be attributed to torsional vibration modes. Traditionally the nonlinear response of three-dimensional frame structures has been estimated on the basis of planar frame idealizations. It is now apparent that the response derived on the basis of this planar assumption should be interpreted, in many instances, as a qualitative indication of the hierarchy of the yield strengths of the individual members only. A full three-dimensional analysis is necessary before an accurate prediction of the time-history displacement response of the structure is possible.

The comparison between the balanced and eccentric structural models is considered for the El Centro ground motion with a scale factor of 1.0 applied

to the ground accelerations. At this intensity of earthquake loading short sequences only of post-elastic deformation are observed in the response—particularly in the Y global coordinate direction. In particular, the ground floor columns are subjected to little nonlinear deformation. Subsequent studies of the balanced building model indicate that the torsional response originating from a nonsymmetric distribution of yield is sensitive to the formation of plastic hinges in the ground floor columns. The response of both models should be investigated
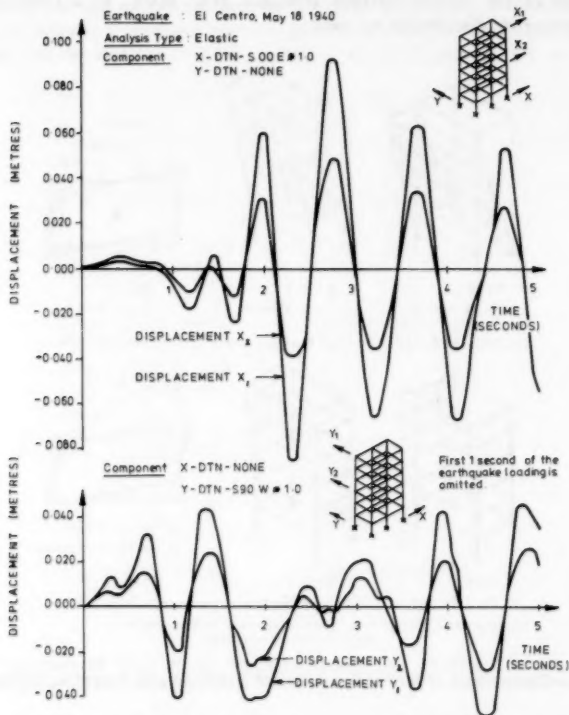
FIG. 5.—Displacement Time-History Comparisons for Elastic Response

further with an increased level of earthquake loading to establish the potential level of torsional amplification in the nonlinear displacement time history.

Summary of Response of Balanced Mass Model.—The time-history displacement summary of the symmetric building subjected to 150% El Centro 1940 unidirectional earthquake loading is shown in Fig. 7. The nonlinear response exhibits the characteristics which have been observed in previous studies on a planar frame idealization. The effective modal period shows a lengthening when compared with the elastic response of the system (see Fig. 5). Following the

onset of yield the structure vibrates about a displaced equilibrium position. The relative location of this instantaneous equilibrium position is dependent upon the time history of the nonlinear deformation. A bias in the positive X direction is clearly evident in the X direction response history. In the Y direction the location of the instantaneous equilibrium position is less obvious although a bias can be detected first in the positive Y coordinate direction, and, laterally, in the opposite direction. The hinge formation in the beams follows the now familiar pattern where a band of plastic hinging migrates up the structure. During instances of strong ground motion the band can extend the full height of the structure.

(a) Centre of Mass (C.M.) and Centre of Stiffness (C.S.) Coincident.

(b) 10% Static Eccentricity between Centre of Mass and Centre of Stiffness.
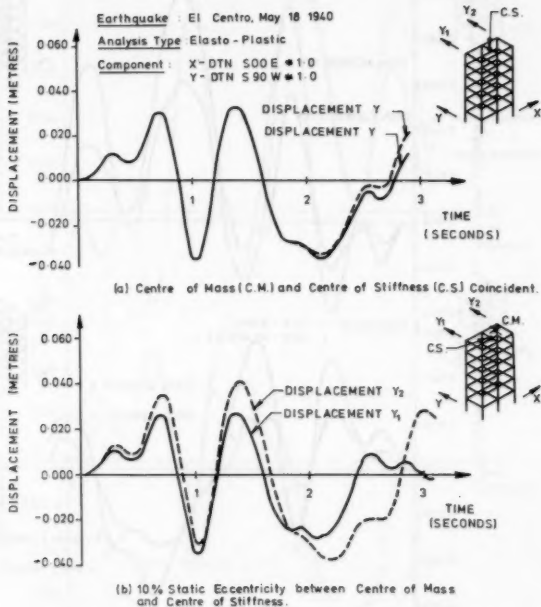
FIG. 6.—Comparison of Top-Story Y Direction Displacements between Balanced and Eccentric Mass Distributions

When the simultaneous occurrence of an orthogonal earthquake component is taken into account the displacement time history is significantly modified. In Fig. 8 the X and Y coordinate displacement time histories for Level 6 of the building are summarized for concurrent earthquake loading. A typical pictorial representation of the structure's yield configuration at selected intervals is shown in Fig. 9. From study of similar figures it was noted that during the early cycles of yield the pattern of hinging is similar to that observed in the unidirectional earthquake analyses. A band of hinges migrates up the structure in both orthogonal directions. The distribution of yield is generally symmetric at each level in

the structure indicating a lateral displacement dominated response, with little torsional induced effects. An asymmetric yield pattern occurs for brief instances, however its duration is insufficient for a torsional response to develop. This response pattern is recognizable also in the displacement time history in Fig. 8. Concurrent loading effects in the early stages of the analysis precipitate the onset of yield and generally extend the duration of yield sequences.
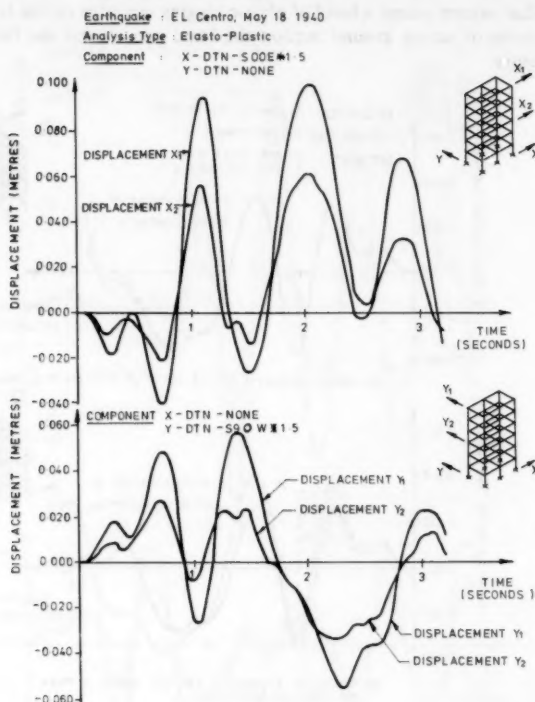
FIG. 7.—Nonlinear Displacement Time Histories for Single Direction Earthquake Components

As the duration of earthquake loading progresses, the concurrent earthquake response diverges from the single component response prediction. When the loading approaches its peak intensity, the yield distribution becomes less uniform because of the interaction of the orthogonal displacement components in defining the locus of the yield point on the assumed yield surface, and a torsional vibration pattern emerges.

The torsional mode is enhanced by the occurrence of hinges in some of the ground floor columns which effect a sudden significant shift in the instanta-

neous center of stiffness at this level which is accompanied by an applied torque about the instantaneous center of stiffness. A study of Fig. 8 demonstrates how the torsional mode becomes more dominant as the analysis progresses. The duration of earthquake loading considered is insufficient to indicate whether the torque asymptotes to a peak value or, alternatively, whether it is damped out by the lateral displacement response.
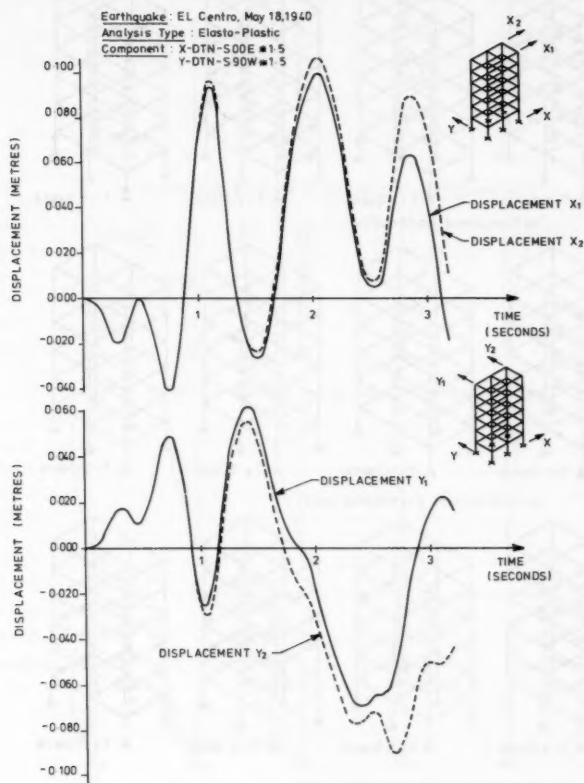
FIG. 8.—Top-Story Displacement Time History for Concurrent Earthquake Loading

In Fig. 10 typical deformed profiles of the structure in the X and Y directions are plotted for the two cases of unidirectional and concurrent earthquake loading. The development of the torsional response is again clearly evident. The formation of plastic hinges in the ground floor columns is seen to increase the displacements in the lower levels but has a less influence further up the structure. Also, in the lower levels the structure displacements reflect the displacement reversals

in the ground motion albeit to a lesser extent than in the case of the unidirectional earthquake loading. The inertia of the structure acts to damp out these reversals further up the structure.

Earthquake: El Centro, May 18 1940 (Scaled by 1·5)

T= 1·0secs   T= 1·2secs   T= 2·1secs   T= 3·0 secs

(a) Concurrent Earthquake

T= 1·0secs   T= 1·2secs   T = 2·1secs   T = 3·0secs

(b) X-Direction Earthquake only

T= 1·0secs   T= 1·2secs   T = 2·1secs   T = 3·0secs
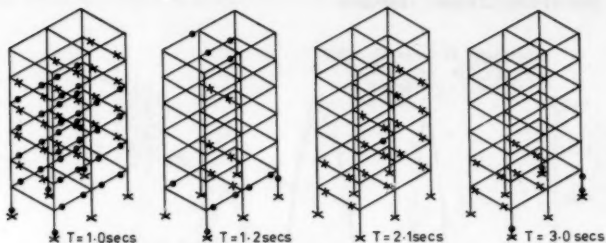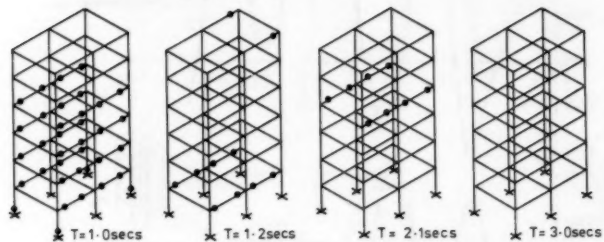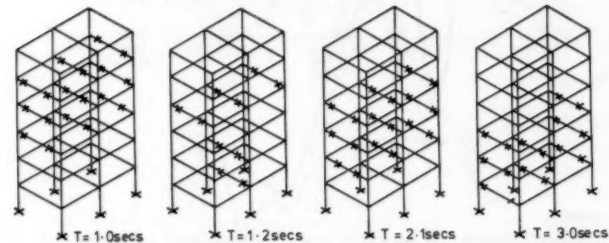
(c) Y-Direction Earthquake Only

  o   Indicates a column hinge

  \   Indicates a beam hinge in frames on Line ① , Line ② or Line ③

  •   Indicates a beam hinge in frames on Line Ⓐ or Line Ⓑ

FIG. 9.—Schematic Comparison of Yield Distribution at Selected Intervals with Unidirectional and Concurrent Earthquake Loading

Although some pattern may be recognized in the sequence of beam hinging, in the latter section time history the migrating band as observed in the initial

yield cycles is less regular. The interaction of the orthogonal displacement components coupled with the additional torsional deformation combine to produce a more complex distribution of element yield.

From a comparison of the unidirectional and concurrent earthquake loading response time histories it is apparent that the nonlinear response predicted by

2 1 secs.   2 2 secs.   2 6 secs.   2 8 secs.   3 0 secs.

(a) X - DIRECTION RESPONSE TO X - DIRECTION EARTHQUAKE ONLY.

LINE Ⓑ

LINE Ⓐ

(b) X-DIRECTION RESPONSE TO CONCURRENT EARTHQUAKE LOADING

(c) Y - DIRECTION RESPONSE TO Y - DIRECTION EARTHQUAKE ONLY.

LINE ①

LINE ③

(d) Y - DIRECTION RESPONSE TO CONCURRENT EARTHQUAKE LOADING
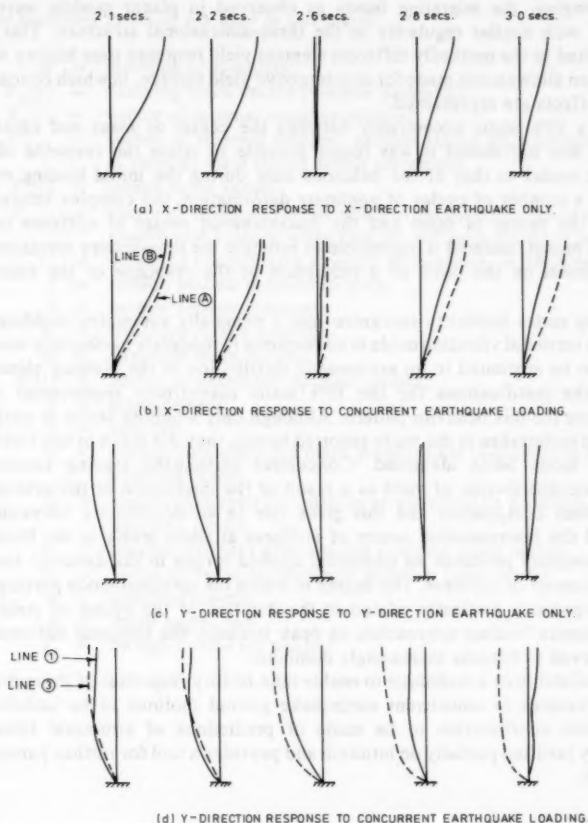
FIG. 10.—Deformed Profile of Structure for Selected Time Intervals

a full three-dimensional analysis is significantly different from the response based on a planar frame idealization. The planar frame model is not able to reproduce all the structural parameters which participate in determining the response of the structure.

SUMMARY

In both the unidirectional and concurrent earthquake loading cases, bands of plastic hinges are found to migrate up and down the structure and the effective modal period elongates, in comparison with the initial elastic period, during cycles of yield. Although a pattern was evident in the distribution of beam plastic hinging, the migrating bands as observed in planar models were not recorded with similar regularity in the three-dimensional structure. This may be attributed to the markedly different element yield response time history which occur when allowance is made for an interactive yield surface, in which concurrent loading effects are represented.

When a 10% static eccentricity between the center of mass and center of stiffness was introduced it was found possible to relate the response of the eccentric model to that of the balanced case during the initial loading cycles but after a number of cycles of nonlinear deformation, the complex interaction between the center of mass and the instantaneous center of stiffness in the eccentric model rendered it impossible to estimate the time-history displacement of this model on the basis of a projection of the response of the balanced model.

Building codes implicitly recognize that a nominally symmetric building can develop a torsional vibration mode in its response to moderate earthquake loading, which can be attributed to an asymmetric distribution of the yielding elements. One of the justifications for the 10% static eccentricity requirement is to compensate for this behavior pattern. Although only a limited series of analyses have been undertaken in the study reported herein, they did result in this torsional response mode being identified. Concurrent earthquake loading causes an asymmetric distribution of yield as a result of the interaction of the orthogonal displacement components and this gives rise to an eccentricity between the mass and the instantaneous center of stiffness at some levels in the building. This eccentricity produces an additional applied torque in the dynamic loading about the center of stiffness. The degree to which the torsional mode participates in the response is evidently related to the duration of the cycles of yield. As the earthquake loading approaches its peak intensity the torsional deformation was observed to become increasingly dominant.

The availability of a technique to enable time-history responses of three-dimensional structures to concurrent earthquake ground motions to be undertaken has enabled confirmation to be made of predictions of structural behavior previously justified partially on intuition and provides a tool for further parameter studies (4).

APPENDIX I.—REFERENCES

1. Gillies, A. G., "Post-Elastic Dynamic Analysis of Three-Dimensional Frame Structures," thesis presented to the University of Auckland, in 1979, in partial fulfillment of the requirements for the degree of Doctor of Philosophy.
2. Giberson, M. F., "The Response of Nonlinear Multi-Storey Structures Subjected to Earthquake Excitation," thesis presented to the California Institute of Technology, in 1967, at Pasadena, Calif., in partial fulfillment of the requirements for the degree of Doctor of Philosophy.
3. "Code of Practice for General Structural Design and Design Loadings for Buildings,"

N.Z.S. 4203, Standards Association of New Zealand, 1976.
4. Gillies, A. G., and Shepherd, R., "Dynamic Inelastic Analysis of a Bridge Structure," *Bulletin of the Seismological Society of America*, Vol. 71, No. 2, Apr., 1981, pp. 517–530.

APPENDIX II.—NOTATION

The following symbols are used in this paper:

E = modulus of elasticity;

$\mathbf{F}_D(t)$ = damping force vector (viscous damping);

$\mathbf{F}_E(t)$ = vector of internal member actions;

$\mathbf{F}_E(t)_{NL}$ = vector of internal member actions taking into account change in element yield status during increment;

$\mathbf{F}_I(t)$ = inertia force vector;

$\mathbf{F}_{UB_K}$ = vector of fictitious forces which is necessary to restore dynamic equilibrium balance when tangent stiffness matrix is updated;

f'_c = specified compressive strength of concrete, in Megapascals;

I = section second moment of area;

J = section torsion constant;

$\mathbf{K}$ = structure stiffness matrix;

$\mathbf{M}$ = structure mass matrix;

$\mathbf{R}(t)$ = vector of externally applied loading;

x = displacement;

$\dot{x}$ = velocity;

α = scaling parameter for mass proportional contribution in viscous damping model;

β = scaling parameter for stiffness proportional contribution in viscous damping model;

β_t = tangent stiffness proportional damping scale factor;

β_0 = initial stiffness proportional damping scale factor;

Δ = small increment;

ϵ = small angle; and

ξ_i = damping ratio for mode i.

COLLAPSE OF PLATE GIRDERS
UNDER EDGE LOADING

By Terence M. Roberts[1] and Chooi K. Chong[2]

INTRODUCTION

In practice, web panels of slender plate girders are often subjected to distributed edge loading and combined bending, as shown in Fig. 1. Such a situation occurs in plate girders which support crane rails or railway tracks directly on top of the compression flange, and in bridge construction where plate girders support steel or relatively thin concrete deck slabs and localized wheel loading distributed through the deck slabs.

In 1967, Bossert and Ostapenko (1) carried out a series of tests on slender plate girders subjected to edge loading uniformly distributed between vertical web stiffeners and combined bending. They also presented solutions for the elastic critical loads of web panels with various boundary conditions and showed that experimental collapse loads may be several times greater than elastic critical loads.

Recently, Roberts and Rockey (5) presented a mechanism solution for the collapse of slender plate girders subjected to partial edge loading for which collapse loads are as high as 15 times the elastic critical load of web panels, assuming the edges to be simply supported (2,4,5). The mechanism solution gives satisfactory agreement with a large number of test results from various sources.

A similar solution is presented in this paper for situations in which the edge loading is uniformly distributed between vertical web stiffeners, since the mode of failure observed by Bossert and Ostapenko was similar to the mode of failure of girders subjected to partial edge loading. The results of the analysis are compared with the test results of Bossert and Ostapenko.

[1] Lect., Dept. of Civ. Engrg., University College, Newport Road, Cardiff, CF2 1TA, Wales.
[2] Grad. Student, Dept. of Civ. Engrg., University College, Newport Road, Cardiff, CF2 1TA, Wales.

THEORY

The mode of failure in Fig. 2 is for a short-span girder with a relatively strong flange, and the idealization of the mode of failure is shown in Fig. 3. It is assumed that plastic hinges form in the flange, two adjacent to and one mid-way between the vertical web stiffeners, and that yield lines form in the web. Stretching the web plate is neglected. Dimensions α and $\beta = b/2$,
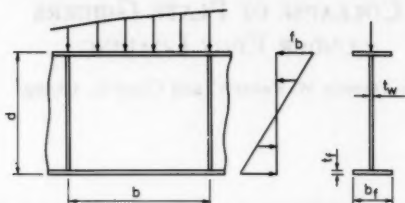
FIG. 1.—Details of Loading and Girder Dimensions
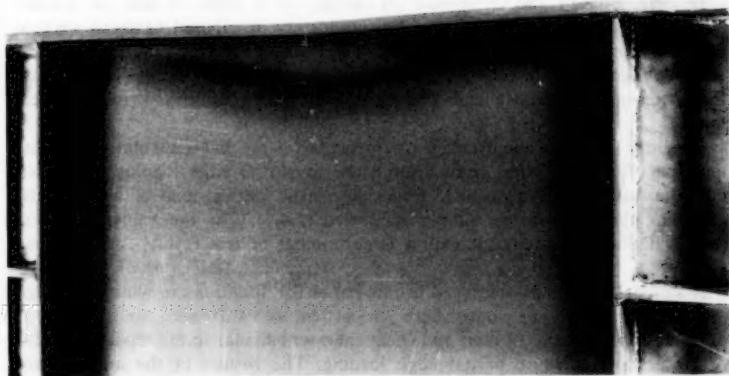
FIG. 2.—Typical Mode of Failure

in which b = the width of the web panel defines the positions of the yield lines in the web and plastic hinges in the flange; and the angle θ defines the deformation of the web just prior to collapse. The variables M_w, M_f, f_{yw}, and f_{yf} = the plastic moments and yield stresses of the web and flange, respectively (plastic moment per unit width of web).

If at the collapse load the central plastic hinge in the flange is assumed to move vertically downwards through a small distance, δv, the rotation, $\delta\phi$, of

the plastic hinges in the flange is $\delta v / \beta$ (twice this value for the central plastic hinge). The corresponding rotation, $\delta\theta$, of the yield lines in the web is $\delta v / 2\alpha \cos\theta$ (twice this value along the central yield line). This can be deduced from the equation for δv

$$\delta v = 2\alpha \sin\theta - 2\alpha \sin(\theta - \delta\theta) \quad\quad\quad\quad\quad\quad\quad\quad (1)$$

which reduces to $\quad \delta v = 2\alpha \cos\theta \, \delta\theta \quad\quad\quad\quad\quad\quad\quad\quad (2)$

if $\delta\theta$ is small. Equating the work done by the applied load, P_u, during the small vertical displacement of the flange, to the internal dissipation of plastic energy gives

$$P_u \frac{\delta v}{2} = 4 M_f \delta\phi + 4\beta M_w \delta\theta \quad\quad\quad\quad\quad\quad\quad\quad (3)$$

Substituting for $\delta\phi$ and $\delta\theta$ in Eq. 3 and cancelling δv gives

$$P_u = \frac{8 M_f}{\beta} + \frac{8\beta M_w}{\alpha \cos\theta} \quad\quad\quad\quad\quad\quad\quad\quad (4)$$

An estimate of the deflection of the flange just prior to collapse can be made using elastic theory. If it is assumed that the moment in the flange varies
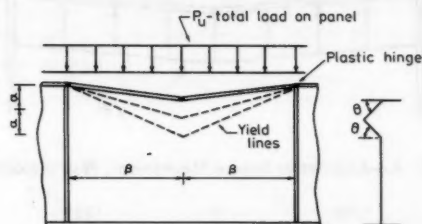
FIG. 3.—Assumed Failure Mechanism

linearly from $+M_f$ at one hinge to $-M_f$ at the adjacent hinge, both hinges forming simultaneously, then the relative deflection is given by $M_f \beta^2 / 6 E I_f$ in which E = Young's modulus; and I_f = the second moment of area of the flange about its centroidal axis. This deflection must be compatible with the deflection of the web below the central plastic hinge given by $2\alpha(1 - \sin\theta)$. Thus, equating these two values and rearranging gives

$$\sin\theta = 1 - \frac{M_f \beta^2}{12 E I_f \alpha} \quad\quad\quad\quad\quad\quad\quad\quad (5)$$

The uniformly distributed edge loading produces compressive membrane stresses, f_m, in the web, which reduce the plastic moment of resistance of the web (3) to $M_w [1 - (f_m/f_{yw})^2]$. If f_m is assumed uniform, then f_m can be deduced from the web contribution to the collapse load, i.e., the second term on the right-hand side of Eq. 1. Thus

$$f_m = \frac{4 M_w}{\alpha \cos \theta \, t_w} \quad \dots \dots \dots \dots \dots \dots \dots \dots \dots \quad (6)$$

and introducing the reduced moment of resistance of the web into Eq. 4 gives, as a first approximation to the collapse load

$$P_u = \frac{8 M_f}{\beta} + \frac{8\beta M_w}{\alpha \cos \theta} \left[1 - \left(\frac{4 M_w}{\alpha \cos \theta \, t_w f_{yw}} \right)^2 \right] \quad \dots \dots \dots \dots \quad (7)$$

If α is chosen empirically, Eqs. 5 and 7 lead to a value for the collapse load. A suitable choice for α, which gives satisfactory predictions for a large number of tests on girders subjected to partial edge loading (2) is

$$\alpha = 25 \, t_w, \quad \left(\alpha < \frac{d}{2} \right) \quad \dots \dots \dots \dots \dots \dots \dots \dots \quad (8)$$

For girders with a slenderness ratio, $d/t_w = 50$, Eq. 8 predicts that the bottom yield line in the web just touches the bottom flange. However, for stocky girders,
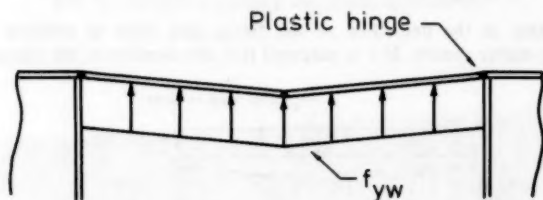
FIG. 4.—Alternative Failure Mechanism: Web Yielding
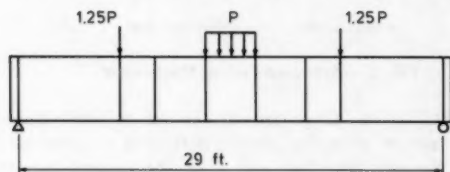
FIG. 5.—Details of Girders Tested by Bossert and Ostapenko (1)

it is possible that failure will be initiated by direct yielding of the web. The solution for this latter case can be obtained by considering the failure mechanism shown in Fig. 4. Equating the work done by the applied load to the internal dissipation of plastic energy gives

$$P_u = \frac{8 M_f}{\beta} + 2\beta f_{yw} t_w \quad \dots \dots \dots \dots \dots \dots \dots \dots \dots \quad (9)$$

The collapse load is taken as the lesser of the values given by Eqs. 7 and 9.

For girders subjected to partial edge loading (5), an allowance can be made

for the coexistent bending stresses, f_b, by reducing the collapse load by a factor $[1 - (f_b/f_{yw})^2]^{1/2}$. It is recommended therefore, that the value of P_u given by Eqs. 7 and 9 be reduced by the same factor.

TABLE 1.—Details of Girders Tested by Bossert and Ostapenko (1) and Comparison of Predicted and Experimental Failure Loads

Test number (1)	b, in inches (2)	d, in inches (3)	t_w, in inches (4)	b_f, in inches (5)	t_f, in inches (6)	f_{yw}, in kips per square inch (7)	f_{yf}, in kips per square inch (8)	f_b, in kips per square inch (9)	P_{expt}, in kips (10)	P_u, in kips (11)	P_{expt}/P_u (12)
EG1.1	28	36	0.1205	8	0.625	43.4	33.7	12.0	49.6	37.3	1.33
EG1.2	28	36	0.1205	8	0.625	43.4	33.7	32.8	28.0	26.4	1.06
EG1.3	28	36	0.1205	8	0.625	43.4	33.7	26.5	36.5	30.7	1.19
EG1.4	28	36	0.1205	8	0.625	43.4	33.7	13.5	41.0	36.6	1.12
EG2.1	43	36	0.1124	8	0.625	43.4	36.4	25.6	30.0	28.3	1.06
EG2.2	43	36	0.1124	8	0.625	43.4	36.4	26.0	57.0	28.2	2.02[a]
EG2.3	43	36	0.1124	8	0.625	43.4	36.4	12.0	46.0	33.6	1.37
EG2.4	43	36	0.1124	8	0.625	43.4	36.4	10.1	43.5	33.7	1.29
EG3.1	57	36	0.1216	8	0.625	43.4	34.1	12.3	45.0	31.2	1.44
EG3.2	57	36	0.1216	8	0.625	43.4	34.1	17.5	38.0	30.1	1.26

[a] Load applied through wooden beam.
Note: 1 in. = 25.4 mm; 1 kip = 1,000 lb = 4,460 N; 1 ksi = 6.91 N/mm².
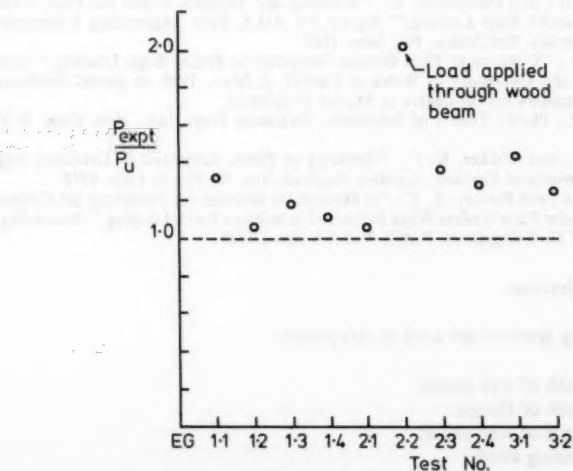
FIG. 6.—Comparison of Predicted and Experimental Failure Loads

COMPARISON WITH TEST RESULTS

Bossert and Ostapenko carried out a series of tests on three slender, long-span girders, with vertical web stiffeners, similar to the girder shown in Fig. 5. The girders were loaded by a uniformly distributed edge load over one panel at a time and by additional loads acting through vertical web stiffeners to vary the magnitude of the coexistent bending stress in the loaded panel. Dimensions, properties, and experimental failure loads, P_{expt}, of the tested panels are given in Table 1 together with the collapse load, P_u, given by Eq. 7, modified to allow for the maximum coexistent bending stress. Also given in Table 1 are the ratios P_{expt}/P_u. The high value of P_{expt}/P_u for test EG 2.2 is due to the fact that the distributed edge load was applied through a wooden beam which transmitted some of the applied load directly to the vertical stiffeners. The ratios P_{expt}/P_u are plotted in Fig. 6.

CONCLUSIONS

The analysis presented gives satisfactory agreement with tests on web panels having a slenderness ratio $d/t_w \simeq 300$ and aspect ratios b/d between approx 0.8 and 1.6. Experience with a similar solution for web panels subjected to partial edge loading indicates that the analysis will prove satisfactory for a wide range of slenderness ratios and aspect ratios of two or less. Further experimental verification is required for web panels with larger aspect ratios and slenderness ratios less than 75.

APPENDIX I.—REFERENCES

1. Bossert, T. W., and Ostapenko, A., "Buckling and Ultimate Loads for Plate Girder Web Plates under Edge Loading," *Report No. 319.1*, Fritz Engineering Laboratory, Lehigh University, Bethlehem, Pa., June, 1967.
2. Chong, C. K., "Collapse of Plate Girders Subjected to Partial Edge Loading," thesis presented to the University of Wales at Cardiff, in Mar., 1980, in partial fulfillment of the requirements for the degree of Master of Science.
3. Horne, M. R., *Plastic Theory of Structures*, Pergamon Press, Inc., New York, N.Y., 1979.
4. Khan, M. Z., and Walker, K. C., "Buckling of Plates Subjected to Localised Edge Loading," *Structural Engineer*, London, England, Vol. 50, No. 6, June, 1972.
5. Roberts, T. M., and Rockey, K. C., "A Mechanism Solution for Predicting the Collapse Loads of Slender Plate Girders When Subjected to in-Plane Patch Loading," *Proceedings*, Institution of Civil Engineers, Part 2, Vol. 67, Mar., 1979.

APPENDIX II.—NOTATION

The following symbols are used in this paper:

b = width of web panel;
b_f = width of flange;
d = depth of web panel;
f_b = bending stress;
f_m = compressive membrane stress in web;
f_{yf} = yield stress of flange;

f_{yw} = yield stress of web;
t_f = thickness of flange;
t_w = thickness of web;
E = Young's modulus taken as 30,000 ksi;
I_f = second moment of area of flange about centroidal axis = $b_f t_f^3/12$ for rectangular flanges;
M_f = plastic moment of resistance of flange = $f_{yf} b_f t_f^2/4$ for rectangular flanges;
M_w = plastic moment of resistance per unit length of web = $f_{yw} t_w^2/4$;
P_{expt} = experimental collapse load;
P_u = predicted collapse load;
α = dimension defining position of yield lines in web;
β = $b/2$;
δv = vertical displacement of loaded flange;
$\delta \theta$ = rotation at yield lines in web;
$\delta \phi$ = rotation of plastic hinges in flange; and
θ = angle defining deformation of web just prior to collapse.

CODE COMPARISONS OF FACTOR DESIGN FOR WOOD

By James R. Goodman,[1] M. ASCE, Zsolt Kovács,[2] and Jozsef Bodig[3]

INTRODUCTION

The objective of this paper is to consider an alternate methodology for the design of wood structures and to use it as the basis for a comparison of existing code requirements in the United States and several countries in Europe. The methodology selected, Load and Resistance Factor Design (LRFD) (1,2,6,8,9,15, 18,23), is currently being applied at various levels of sophistication in the design of steel and concrete structures (11,12,16,25,26,27,30,36). Proposals for using LRFD methodology have been made by many wood researchers (10,29,31,33). The possibility of combining this methodology with reliability analysis offers much promise in developing a rational and unified basis for structural design for all types of materials.

Load and resistance factor design criteria can be expressed in many formats. For simplicity and to provide at least partial consistency with previous developments, the format chosen is given by general equation

$$(\phi R_n) \geq \gamma_I \gamma_o \left(\sum_{i=1}^{j} \gamma_i C_i Q_i \right) \quad \ldots \ldots \ldots \ldots \ldots \ldots \ldots \ldots \ldots (1)$$

in which ϕ = the "resistance" factor; R_n = the "nominal mean member resistance" for a chosen limit state (n); γ_I = member (or structure) "importance" factor; γ_o = "uncertainty" factor to account for overall uncertainties including those of analysis and others such as effects of load combinations; γ_i = load factor for load type Q_i; $C_i Q_i$ = generalized mean member force, i.e., bending moment, axial load, etc., acting on member to be designed (C_i factor converts Q_i load to member force); and j = number of load combinations.

By adjusting the resistance of the structural member (LHS of Eq. 1) or the factored load (RHS of Eq. 1), or both, various levels of structural safety can be achieved. The assignment of "ϕ" and the various "γ" factors is most properly accomplished using some level of probability-based analysis (2,6,8,9,10,31,33). The purpose of this paper, however, is to demonstrate the implied safety levels

[1] Prof. of Civ. Engrg., Colorado State Univ., Fort Collins, Colo. 80523.
[2] Asst. Prof., Univ. of Forestry and Timber Industry, Sopron, Hungary.
[3] Prof. of Wood Sci. and Civ. Engrg., Colorado State Univ., Fort Collins, Colo. 80523.

existing in current codes which are based on allowable stress or limit states design concepts. Through reorganization of current code provisions into a common LRFD format, comparisons between codes can be obtained. This procedure will, perhaps for the first time, demonstrate the current safety levels now in use in various countries. This study will, it is hoped, provide a basis for continued development of design methodology using reliability-based analysis for assigning load and resistance factors.

REVIEW OF LITERATURE

The study of design methodology has been particularly active in recent years with the advent of the work by Cornell (6) and the subsequent efforts by many others (1,2,8,9,10,15,18,23). The extensive effort by Galambos, et al. (11,12,36) in the United States related to design of steel structures has had far-reaching effects in encouraging design innovations for other materials. Several codes and standards in Europe have used a form of "limit states" design for many years (7,9,16,28).

For the design of wood structures, a series of papers mostly aimed at the concept of reliability-based design have been published recently (1,8,10,29,31,33, 37). These papers develop concepts dealing with special wood design problems such as duration of load (creep rupture) (3,4,20,35) and large variability (10). In particular, the work of Barrett and Foschi on duration of load and probability of failure (3,4) and that of Gerhards (13) are of special importance to the extension of the LRFD design methodology. The load and resistance factors in future codes must be based on rational analysis of the probability of failure or other limit criteria. Foschi's recent paper (10) cites problems which may exist with the use of a "safety index" procedure for wood structures using probability-based extensions of the LRFD design methodology as developed. Other papers describing recent additional efforts in this area include Vanderbilt, et al. (33) involving application of probability-based design to wood electrical transmission structures using LRFD methodology and the efforts of Sexsmith and Fox (29) in "limit states" design of wood structures.

Of special interest are the practical applications of probability-based design such as the development of the Ontario Highway Bridge Design Code reported by Nowak and Lind (25). Practice in the United States is most likely to be based on a recent Bureau of Standards publication authored by Ellingwood, et al. (8). These publications are of particular importance and point the way towards the use of probability-based design in the near future.

ADAPTATION OF LRFD METHODOLOGY FOR WOOD COLUMN AND BEAM DESIGN

Introduction.—As described earlier, Eq. 1 has been chosen as the basis for the design format. To relate current code provisions for design of wood members to the LRFD format requires some special considerations. In current codes various levels of safety are implied. To provide a uniform method of treating each of the codes considered, a "reduction factor, R_F" is defined as

$$R_F = \frac{1}{\phi} \gamma_o \gamma_I \quad \ldots \ldots \ldots \ldots \ldots \ldots \ldots \ldots \ldots \ldots \ldots \ldots \ldots \ldots \ldots \ldots \ldots \ldots \ldots \ldots (2)$$

in which ϕ, γ_o, and γ_l are as previously defined in Eq. 1. A calculation of R_F is presented for each code and subsequently the separation of R_F into the appropriate values of ϕ, γ_o, and γ_l is developed to accommodate the LRFD format. Adaptation to the design of long columns, governed by the Euler column formula, and to simple flexural members, governed by bending, is presented. The design factors for Eq. 1 are derived for each case and for each of the several example codes. Finally, a table of these factors is provided to compare the levels of safety present in current codes. The two cases, long columns and beams, represent typical problems in the design of wood structures and serve to illustrate the relative ease with which current codes can be converted to the LRFD format.

Long Column Design.—The design of long wood columns is generally based on the use of Euler's formula with an appropriate reduction factor, R_F. For simple pinned-end columns with no initial eccentricity

$$P_c = \frac{\pi^2 EI}{l_e^2 R_F} \dots\dots\dots\dots\dots\dots\dots\dots\dots\dots\dots\dots\dots\dots\dots\dots\dots (3)$$

in which P_c = maximum load the column can sustain assuming elastic buckling; E = modulus of elasticity; I = moment of inertia of the column about its weak axis; and l_e = effective column length depending on the support conditions.

Eq. 3 is often rewritten by use of the slenderness ratio, λ, in which

$$\lambda = \frac{l_e}{r} \dots\dots\dots\dots\dots\dots\dots\dots\dots\dots\dots\dots\dots\dots\dots\dots\dots\dots\dots (4)$$

where r = radius of gyration $\sqrt{I/A}$; and A = cross-sectional area of the column. Expressing I as a function of r and A, and substituting it into Eq. 3 results in

$$P_c = \frac{\pi^2 A}{\lambda^2 R_F} E \dots\dots\dots\dots\dots\dots\dots\dots\dots\dots\dots\dots\dots\dots\dots\dots (5)$$

This expression can be written as

$$P_c = \frac{A_e E}{R_F} \dots\dots\dots\dots\dots\dots\dots\dots\dots\dots\dots\dots\dots\dots\dots\dots\dots (6)$$

in which A_e = effective area given by $\pi^2 A / \lambda^2$.

A simple form may then be given for the LRFD format (Eq. 1) for rectangular long wood columns, i.e.:

$$\phi(A_e \bar{E}) \geq \gamma_l \gamma_o \left(\sum_{i=1}^{j} \gamma_i P_i \right) \dots\dots\dots\dots\dots\dots\dots\dots\dots\dots\dots (7)$$

in which P_i = the nominal axial column loads; and $\bar{E}$ = mean modulus of elasticity of the wood species or species group. Eq. 7 is the basic expression for long column design to be used in studying the various code provisions and developing implications for the structural safety of single-member wood columns as now prescribed.

Flexural Member Design.—The design of simple wood flexural members controlled by bending strength is generally based on the use of some limiting

value of bending strength as calculated from

$$\frac{\bar{f}_b}{R_F} = \frac{M}{S} \quad \dots \dots \dots \dots \dots \dots \dots \dots \dots \dots \dots \dots \dots (8)$$

in which $\bar{f}_b$ = mean flexural resistance of the wood species or species group often called modulus of rupture (MOR); M = applied governing moment; and S = section modulus ($bd^2/6$ for a rectangular beam of width = b and depth = d). The use of the LRFD format for this case simply involves multiplying the mean flexural resistance, $\bar{f}_b$, by S to give the mean flexural resistance capacity of the wood member resulting in

$$\phi(\bar{f}_b S) \geq \gamma_i \gamma_o \left(\sum_{i=1}^{J} \gamma_i M_i \right) \quad \dots \dots \dots \dots \dots \dots \dots \dots \dots \dots \dots (9)$$

in which M_i = nominal applied bending moments.

Due to the manner in which the mean flexural resistance of wood members is currently being established, a more precise definition of $\bar{f}_b$ is needed. It is also necessary to define the corrections and adjustments included in $\bar{f}_b$ to ensure that the results from the various codes will, in fact, be evaluated on the same basis. In current United States practice, as given by ASTM D245 (21), ASTM D2555 (22), the Wood Handbook (32), and the National Design Specification (NDS 1977) (24), adjustments are made in clear wood bending strength to obtain the member strength accounting for defects, moisture content, depth effect, duration of loading, etc. In particular, the duration of loading effect is not uniformly considered for wood by the various codes. Thus, the simplest procedure is to include the duration of load and other service condition effects, if present, within the load or uncertainty factors.

The precise definition of $\bar{f}_b$ to be used in all the comparison studies is therefore selected to be $\bar{f}_b$ = mean short-term test value of modulus of rupture (MOR) for clear wood adjusted for moisture content, size, defects for grade used (such as knots and slope of grain), and specified service conditions if different from the standard assumed conditions. It should be noted that $\bar{f}_b$ can be obtained from actual ingrade test results for the grade of lumber, moisture content, etc. used rather than by use of small clear specimens given in ASTM D245 (21) and ASTM D2555 (22) resulting in the tabulated values in NDS 1977 (24).

APPLICATION OF LRFD TO CURRENT CODES

Basis of Comparison.—The adaptation of LRFD methodology for the design of long columns of wood results in Eq. 7. This equation is used as the basis for examining the various code provisions for such members.

For design of wood flexural members with adequate lateral bracing, the LRFD methodology leads to Eq. 9. The strength value used in this method is the mean flexural capacity (MOR) of clear wood with all necessary adjustments for moisture content, size, defects, and the particular service conditions. Duration of load effect, if specified by the code, is included within the load or uncertainty factors.

It should be noted that the process of conversion of each code to a common format for comparison requires a complete knowledge of the basis of code

values. In some cases this information is not available, however, every attempt was made to be consistent in defining the ϕ and γ factors to reflect the current practices specified. Values in question are considered. The various problems encountered in this study indicate the need for a more open and clearly understood basis for establishing safe structural design rules.

Design of Long Columns

United States.—The design of long wood columns of rectangular cross section under the rules specified by the National Design Specification (NDS 1977), is governed by

$$F_c' = \frac{0.30\,\bar{E}}{\left(\dfrac{l_e}{d}\right)^2} \quad \ldots\ldots\ldots\ldots\ldots\ldots\ldots\ldots\ldots \quad (10)$$

in which F_c' = allowable axial compressive stress. Thus the load carrying capacity, P_c, is simply

$$P_c = F_c'A = \frac{0.30\,\bar{E}\,A}{\left(\dfrac{l_e}{d}\right)^2} \quad \ldots\ldots\ldots\ldots\ldots\ldots\ldots\ldots \quad (11)$$

When Eq. 5 is converted from λ to l/d for rectangular columns and equated to Eq. 11 a value for R_F of 2.74 results, i.e.:

$$\frac{\pi^2 \bar{E} A}{12\left(\dfrac{l}{d}\right)^2 R_F} = \frac{0.30\,\bar{E}\,A}{\left(\dfrac{l}{d}\right)^2} \quad \text{thus} \quad R_F = \frac{\pi^2}{0.3(12)} = 2.74$$

In this case, R_F is the product of three factors, namely: (1) A "safety (or uncertainty) factor," γ_o, of 1.66; (2) a shear correction factor to obtain the true modulus of elasticity of 1.03; and (3) the reciprocal of the appropriate factor of ϕ to produce a limiting modulus of elasticity, E_{limit}, as defined in Appendix G of NDS 1977 (24). By considering that the modulus of elasticity used in Eq. 7 is the true modulus of elasticity, the adjustment factor of 1.03 can be omitted from R_F which then results in $\phi = 0.589$ after applying Eq. 2 and assuming $\gamma_l = 1.0$. Thus, for NDS 1977

$$E_{\text{limit}} = \phi \bar{E} = 0.589\,\bar{E} \quad \ldots\ldots\ldots\ldots\ldots\ldots\ldots\ldots\ldots \quad (12)$$

This value of E_{limit} corresponds to the lower 5% exclusion limit of a normal E distribution with a COV of 0.25. This result can be computed from statistical equation

$$E_{\text{limit}} = [1 - (t\,\text{COV})]\,\bar{E} \quad E_{\text{limit}} = \phi E \quad \ldots\ldots\ldots\ldots\ldots \quad (13)$$

in which the t value can be taken from statistical tables for a one-tail exclusion limit. Another example can be obtained by considering the lower 5% exclusion limit for a large sample size ($t = 1.645$) combined with a COV = 0.4 resulting in a ϕ value of 0.342. Additional example ϕ values for the lower 5% and 1% exclusion limits for various COV values are tabulated in Table 1. Considering

Eq. 7, a higher value of ϕ indicates either a higher load carrying capacity at the same probability of failure or a less probable failure at the same load level.

It should be noted that one of the difficulties in comparing the various codes is a lack of consistency in defining live load. Live loads in most countries are considered to be all the loads normally occurring with the occupancy of a structure except the weight of the structure which is dead load. However, for wood design in the United States (NDS 1977) live load excludes snow, wind, earthquake, and impact loads.

To place the design of long columns by NDS 1977 into the LRFD format of Eq. 7 requires the separation of the reduction factor R_F of 2.74 into values of uncertainty factor, γ_o, and appropriate exclusion limit, ϕ, as previously outlined. The result of this modification considering, e.g., the combination of

TABLE 1.—Values of Resistance Factor for 1% and 5% Exclusion Limits (Normal Distribution)

Levels of coefficient of variation, (COV) (1)	Resistance Factors, (ϕ)	
	5% exclusion limit (2)	1% exclusion limit (3)
0.40	0.342	0.068
0.35	0.424	0.185
0.30	0.507	0.301
0.25[a]	0.589	0.418
0.20	0.671	0.534
0.15	0.753	0.651
0.11[b]	0.819	0.744
0.10[c]	0.836	0.767
0.05	0.918	0.884

[a] NDS 1977 visually graded sawn lumber.
[b] NDS 1977 machine stress-rated sawn lumber.
[c] NDS 1977 glued laminated timber.

dead load (DL) and live load (LL) to be critical, gives

$$0.589 \, (A_e \bar{E}) \geq \gamma_t (1.66)(1.00 \, P_{DL} + 1.00 \, P_{LL}) \quad \ldots \ldots \ldots \ldots \ldots \ldots \ldots \quad (14)$$

in which $A_e = (\pi^2 A)/\lambda^2$ (see Eq. 6); $\bar{E}$ = the mean true modulus of elasticity for grade and species of lumber used (adjusted for condition of use); P_{DL} = axial column dead load; and P_{LL} = nominal axial column live load (as defined by NDS 1977). The value of ϕ is different for various levels of COV such as, e.g., 0.11 for machined graded lumber and 0.10 for glulam members (NDS 1977) as shown in Table 1.

Table 2 presents comparative column design requirements specified by the various codes. The basis of comparison is the NDS 1977 based on a 5% exclusion limit and a 0.25 COV given for visually graded lumber. For design of columns, no distinction is made between dead load (long duration) and loads of shorter

durations in the NDS 1977, thus the load factors are identical and taken to be unity. The importance factor γ_I is not considered in NDS 1977 and is therefore also taken to be unity.

In addition to the ϕ, γ_I, and γ_o factors, values of γ_I for dead load (γ_{DL}) and live load (γ_{LL}) (NDS 1977), are also incorporated into Table 2. Further, to provide for comparisons of the various codes, the numerical values for product $\gamma_I \gamma_o \gamma_{DL}/\phi$ and $\gamma_I \gamma_o \gamma_{LL}/\phi$, respectively, are also tabulated.

France.—The design of long wood columns in France is governed by the rules specified by Règles C. B. 71 (28). These rules consider a transformed

TABLE 2.—Tabulation and Comparison of Design Factors for Long Columns of Lumber

Code (1)	Format $\phi (A_c \bar{E}) \geq \gamma_I \gamma_o (\gamma_{DL} P_{DL} + \gamma_{LL} P_{LL})$						
	ϕ (2)	γ_I (3)	γ_o (4)	γ_{DL} (5)	γ_{LL} (6)	$\gamma_I \gamma_o \gamma_{DL}$ (7)	$\gamma_I \gamma_o \gamma_{LL}$ (8)
National Design Specification (United States, 1977)	0.589 (5% level COV 25%)	1.00	1.66	1.00	1.00	1.66	1.66
Règles C. B. 71 (France, 1975)	0.589 (5% level COV 25%)	1.00	1.76	1.00	1.21	1.76	2.11
MSz 15025/1-72 (Hungary, 1972)	0.589 (5% level COV 25%)	1.00	1.11	1.10	1.30	1.22	1.43
VOB/StLB Hochbau 9 (ATV DIN18334) (West Germany, 1976)	0.589 (5% level COV 25%)	1.00	1.58	1.00	1.00	1.58	1.58
DIF-Ref. No. NP 118-T (Denmark, 1975)	0.589 (5% level COV 25%)	1.00	1.51	1.00	1.30	1.51	1.96

Note: $\bar{E}$ = Mean pure bending modulus of elasticity at 19% moisture content unless otherwise noted. For Règles C. B. 71 (French 1975) $\bar{E}$ = dynamic modulus of elasticity at 15% moisture content. content.

form of the Euler buckling equation in which the allowable stress is given by

$$F'_c = KF_c \dots\dots\dots\dots\dots\dots\dots\dots\dots \quad (15)$$

in which $K = 3,100/\lambda^2$; and F_c = allowable compressive stress for short columns. On the other hand, the Euler buckling equation with the appropriate reduction factor R_F must also apply. Thus, from Eq. 5

$$F'_c = \frac{P_c}{A} = \frac{\pi^2 \bar{E}}{R_F \lambda^2} \dots\dots\dots\dots\dots\dots\dots \quad (16)$$

By equating Eqs. 15 and 16, the reduction factor of R_F is obtained as

$$R_F = \frac{\pi^2 \bar{E}}{3,100 F_c} \dots\dots\dots\dots\dots\dots\dots\dots \quad (17)$$

According to the French code (28), the load factors assigned to dead and live loads are $\gamma_{DL} = 1.0$ and $\gamma_{LL} = 1.2$, where the live load is considered

as an occupancy load not of "long" duration. To place the design of long columns by Règles C. B. 71 (28) into the format of Eq. 7 requires the separation of resistance factor, ϕ, from the uncertainty factor, γ_o, assuming an exclusion level obtained as a result of the calculation of R_F from Eq. 17. Since the value of R_F depends on the in-service moisture content of the wood, it has been calculated assuming 19% moisture content to be consistent with the assumptions given in NDS 1977. The result of these calculations for common European conifers gives a value for $R_F = 2.99$. Since the desire is to compare the true levels of safety of the various codes assuming the same material property probability levels, a value of $\phi = 0.589$ is assigned as in NDS 1977. Thus with the knowledge of R_F and ϕ the value of the uncertainty factor, γ_o, is computed from Eq. 2 resulting in 1.76 again considering the importance factor γ_I to be unity. The LRFD equation for the French code is, therefore

$$0.589\,(A_e \bar{E}) \geq (1.0\,(1.76)(1.0\,P_{DL} + 1.2\,P_{LL}) \dots \dots \dots \dots \dots \dots (18)$$

The results given in Eq. 18 are tabulated in Table 2 for comparison with the other codes considered.

Hungary.—The Hungarian standards (MSz 15020-71, 15021/1-71, 15025/1-72) (14) for centrally loaded intermediate or long columns call for satisfying equality

$$P_c' = \eta\,F_c A \dots \dots \dots \dots \dots \dots \dots \dots \dots \dots \dots \dots \dots \dots (19)$$

in which $P_c' =$ limiting load the column may support; $F_c =$ limiting stress in short column compression for the wood used (design value); and $\eta =$ function of the column slenderness ratio, i.e.:

$$\eta = \frac{1}{1.1 + \left(\dfrac{\lambda}{60}\right)^2} \dots \dots \dots \dots \dots \dots \dots \dots \dots \dots \dots \dots (20)$$

The resultant compression stress should satisfy

$$F_c' = \frac{P_c'}{A} \geq \frac{\displaystyle\sum_{i=1}^{j} \gamma_i P_i}{A} \dots \dots \dots \dots \dots \dots \dots \dots \dots \dots (21)$$

in which $\sum_{i=1}^{j} \gamma_i P_i =$ most unfavorable combination of applied load; and F_c' = allowable compressive stress for long columns.

Comparing this condition to the formula based on the Euler buckling equation for long columns, i.e., Eq. 2, results in

$$F_c' = \eta\,F_c = \frac{1}{R_F}\,\frac{\pi^2 \bar{E}}{\lambda^2} \dots \dots \dots \dots \dots \dots \dots \dots \dots \dots \dots \dots (22)$$

Substituting Eq. 20 into Eq. 22 results in

$$R_F = \frac{1.1 + \left(\dfrac{\lambda}{60}\right)^2}{\lambda^2}\,\frac{\pi^2 \bar{E}}{F_c} \dots \dots \dots \dots \dots \dots \dots \dots \dots \dots (23)$$

Here, the reduction factor R_F is a function of the slenderness ratio, modulus

of elasticity and the limit stress in compression. Further, since both the value of F_c and $\bar{E}$ are assumed to change as moisture content varies (in the Hungarian code), R_F is a function of this variable as well. Using $\lambda = 100$, and properties of common European conifers, (5,17,19), i.e., $\bar{E} = 9,440$ N/mm^2 mean short column compression strength, $\bar{f}_c = 75$ N/mm^2 and $\eta = 0.258$ (19% moisture content) results in $R_F = 1.884$.

According to the Hungarian standard (14) the factors assigned to loads are $\gamma_{DL} = 1.1$, and $\gamma_{LL} = 1.3$ (mean of the range 1.2–1.4). To place the design of long columns by MSz 15025 into the format of Eq. 7 requires, as described previously for the French code, a proper interpretation of R_F calculated using Eq. 23.

Since the value of γ_o is dependent on the column slenderness ratio, λ, and the in-service moisture content of the wood used, a slenderness ratio of 100 is taken for comparison at the 19% moisture content which is again identical to the value assigned for design by NDS 1977. The importance factor, γ_I, is not considered in the Hungarian standard and is thus taken as unity. Considering these definitions, the LRFD format results in

$$0.589\,(A_c \bar{E}) \geq 1.0\,(1.11)(1.1\,P_{DL} + 1.3\,P_{LL}) \quad \dots \dots \dots \dots \dots \dots \quad (24)$$

These results are tabulated in Table 2 for comparison with other code requirements.

West Germany.—The West German standard for the design of long columns (VOB/StLB Hochbau 9 ATV DIN18334, 1976) (34) is based on a factor, ω, which accounts for the effect of column length and slenderness, much as previously described for French (28) and Hungarian (14) specifications. The ω factor adjusts the long-, intermediate-, and short-column equations to provide a smooth transition curve for all column lengths. In addition, ω appears to contain a "safety factor" to restrict the magnitude of applied stress to that of the allowable stress, i.e.:

$$\frac{\omega(P)}{A} \leq F'_c \quad \dots \dots \dots \dots \dots \dots \dots \dots \dots \dots \dots \dots \dots \dots \dots \dots \dots \quad (25)$$

The ω factor is tabulated (DIN 1052) for different values of the slenderness ratio, λ.

In a manner similar to other specifications, the organization of this method of column design into the form of Eq. 7 requires the calculation of R_F. Relating the Euler equation for long-column buckling to the requirement of Eq. 25 results in

$$R_F = \frac{\omega \pi^2 \bar{E}}{\lambda^2 F'_c} \quad \dots \dots \dots \dots \dots \dots \dots \dots \dots \dots \dots \dots \dots \dots \dots \quad (26)$$

Obviously, the value of R_F depends on the values of $\bar{E}$ and F'_c selected, but it can be shown that R_F is a constant for long columns having the same $\bar{E}$ and F'_c values.

To provide a typical example, the following material properties were used in obtaining R_F for comparison with other codes: (1) $\bar{E}^1 = 10,000$ N/mm^2 (European conifers—DIN 1052); and (2) $F'_c = 10.0$ N/mm^2 (European conifers—DIN 1052). (These design values unadjusted for moisture content are consistent

with the NDS 1977 design values, since a reduction to conditions for use in DIN 1052 is only considered in extreme cases of exposure or initial moisture content of wood.) These values give a result for R_F of 2.69 which may again be interpreted as a product of an assumed exclusion limit times an uncertainty factor, γ_o. These considerations result in the design of long columns by DIN 1052 being organized into the format of Eq. 7 as follows:

$$0.589\,(A_e\bar{E}) \ge (1.0)(1.58)(1.0\,P_{DL} + 1.0\,P_{LL}) \quad\dots\dots\dots\dots\dots\dots \quad (27)$$

in which the load factors of unity are those prescribed under the principle of allowable stress design recognized by the West German standard.

Denmark.—The Danish code for design of wood structures (7) calls for the design of columns with any slenderness ratio (up to $\lambda = 200$) to satisfy

$$F_c' \le K_s F_c \quad\dots\dots\dots\dots\dots\dots\dots\dots\dots\dots\dots\dots\dots\dots \quad (28)$$

in which F_c = design strength function of species moisture content; and load group

$$K_s = K_E \quad \text{for} \quad K_E \le 0.5; \quad K_s = 1 - \frac{0.25}{K_E} \quad \text{for} \quad K_E \ge 0.5 \quad\dots\dots\dots \quad (29)$$

and $\quad K_E = \dfrac{\pi^2 \bar{E}}{F_c \lambda^2} \quad\dots\dots\dots\dots\dots\dots\dots\dots\dots\dots\dots\dots\dots \quad (30)$

To obtain a value of R_F from the Danish code requires selecting a given species, slenderness ratio, and moisture content. In a manner similar to previous computations, values of $\lambda = 100$ and moisture content 19% are selected. For fir, pine, and similar structural lumber, $\bar{E} = 9,000$ N/mm^2 and $F_c = 12.5$ N/mm^2 (17) represent typical values. Substitution of these values into Eq. 20 produces $K_E = 0.276 < 0.5$. Thus Eq. 28 becomes

$$F_c' \le K_E F_c = \frac{\pi^2 \bar{E}}{\lambda^2} \quad\dots\dots\dots\dots\dots\dots\dots\dots\dots\dots\dots\dots \quad (31)$$

Equating this expression to the Euler equation and substituting the numerical values for the variables results in $R_F = 2.575$.

The Danish code calls for $\gamma_{DL} = 1.0$ and $\gamma_{LL} = 1.3$ and does not specify γ_I thus it is taken as unity. Further, by using Eq. 2 with 5% level and COV of 25%, $\gamma_o = 1.51$ and the application of the LRFD format for the Danish code results in

$$0.589\,(A_e\bar{E}) \le (1.0)(1.51)(1.0\,P_{DL} + P_{LL}) \quad\dots\dots\dots\dots\dots\dots \quad (32)$$

As in each previous case, the factors derived are tabulated in Table 2 for comparison to other code values.

Design of Flexural Members

United States.—The design of simple flexural members by the rules of NDS 1977 is based on a limiting deflection and on the allowable stress concept. Consideration here will be limited to the bending-stress limitation as given by Eq. 9.

The process of obtaining the allowable stress from the flexural capacity of

the members (MOR) is specified using the procedures of ASTM D245 (21) and D2555 (22) as mentioned earlier. Thus, adjustments for moisture content, defects, size, etc. are included in the establishment of the flexural capacity. To place all code comparisons on a similar basis, adjustments for load duration, if included, are considered with the load factors, i.e., γ_{DL} and γ_{LL}.

Applying Eq. 9 to the NDS 1977 design of flexural members, and considering the combination of dead and live load to govern results in

$$0.589 \, (\bar{f}_b S) \geq \gamma_I \, 1.3 \, (1.6 \, M_{DL} + 1.6 \, M_{LL}) \quad \ldots \ldots \ldots \ldots \ldots \ldots \ldots \quad (33)$$

in which γ_I is not considered and is assigned a value of unity. The product

TABLE 3.—Tabulation and Comparison of Design Factors for Simple Flexural Members of Lumber

Code (1)	Format $\phi \, (\bar{f}_b S) \geq \gamma_I \gamma_o \, (\gamma_{DL} M_{DL} + \gamma_{LL} M_{LL})$						
	ϕ (2)	γ_I (3)	γ_o (4)	γ_{DL} (5)	γ_{LL} (6)	$\gamma_o \gamma_I / \gamma_{DL}$ (7)	$\gamma_o \gamma_I / \gamma_{LL}$ (8)
National Design Specification (United States, 1977)	0.589 (5% level COV 25%)	1.0	1.3	1.6	1.6	2.08	2.08
Règles C. B. 71 (France, 1975)	0.589 (5% level COV 25%)	1.0	1.62	1.0	1.2	1.62	1.94
MSz 15025/1-72 (Hungary, 1972)	0.589 (5% level COV 25%)	1.0	1.87	1.1	1.3	2.06	2.43
VOB/StLB Hochbau 9 (ATV DIN18334) (West Germany, 1976)	0.589 (5% level COV 25%)	1.0	1.88	1.0	1.0	1.88	1.88
DIF-Ref. No. NP 118-T (Denmark, 1975)	0.589 (5% level COV 25%)	1.0	1.3	1.3	1.3	1.69	1.69

Note: $\bar{f}_b$ = mean short-term test value of lumber flexural strength (MOR) adjusted for moisture content and size effects and including appropriate reduction for grade, etc. from clear wood values; also M_{LL} is based on approximately 2 months duration such as often considered for snow load.

of the value of 1.3 for uncertainty, γ_o, and a value of 1.6 for "normal" 10-yr duration of load results in the traditional value of 2.1 used to assign allowable stresses (ASTM D245). The value of ϕ is again taken to be 0.589 representing the lower 5% exclusion limit and 0.25 for COV.

The results from Eq. 33 are presented in Table 3 for comparison with other codes. The definition of $\bar{f}_b$ is given once more in the notes for Table 3. The importance of the commonality of this definition cannot be overstressed in comparing the various codes.

France.—The design of simple flexural members by the rules of 1975 French codes is based on an allowable stress concept coupled with the use of weighted load factors. Bending strength is calculated assuming elastic behavior.

The allowable stress is obtained from the flexural capacity of the members (MOR) by using a factor of 2.75. This factor is applied to the mean short-term strength and requires further adjustments for moisture content, size, and grade. Adjustment for load duration, however, is only included in calculations of deflections and thus will not be considered here as a part of the load factors (γ_t). Applying Eq. 9 results in

$$0.589 \, (\bar{f}_b S) \geq 1.0 \, (1.620)(1.0 \, \bar{M}_{DL} + 1.2 \, \bar{M}_{LL}) \; \ldots \ldots \ldots \ldots \ldots \ldots \quad (34)$$

in which again ϕ is determined from Table 1 for an assumed exclusion limit of 5% and a COV of 0.25. The importance factor is again not considered in the French code and thus is assigned a value of unity. The results of Eq. 34 are tabulated in Table 3 for comparison with other codes.

Hungary.—The design of simple flexural members by the rules of MSz 15025 is based on the concept of applying limit states for either deflection or stress. In each case elastic behavior is assumed and for the stress limit state an equation analogous to Eq. 8 is used. In this case, however, $\bar{f}_b$ represents the limit stress instead of the allowable stress and M represents the most unfavorable moment loading combination, including appropriate adjustment, factors.

The process of obtaining the limiting stress from the flexural capacity (MOR) of the clear wood members should be first understood to allow proper calculation of the resistance factor and the load factors. These factors must be considered on the same basis as previously done for the NDS 1977. Therefore, this reduction process is considered in some detail.

The limiting stress is derived from the mean short-term test value of a number of samples. This value, unless obtained from ingrade test results, is adjusted for grade and size and further reduced to an exclusion level to obtain a threshold value. This latter result is also divided by a "safety factor" of 1.7 (for the case of bending). Some essential details of the aforementioned process are not adequately manifested in the Hungarian standard and reference books, so assumptions must be made in this paper for the exclusion limit factor and strength ratio involved as well as the adjustment for duration of load.

A reasonable level of exclusion limit is 5% with a COV of 0.25, however, Keldish (16) applies a 1% level with a COV of 0.15 for bending strength value resulting in a reduction fairly close to the former one and perhaps allowing a more realistic strength ratio. The previously mentioned "safety factor" of 1.7 may constitute or perhaps include adjustment for duration of load. An assumed adjustment is considered with the load factors, which, however, does not affect the magnitude of the resulting γ/ϕ ratios.

For the Hungarian standard, the application of Eq. 9 to design of flexural wooden members results in

$$0.651 \, (\bar{f}_b S) \geq \gamma_t (1.7)(1.1 \, M_{DL} + 1.3 \, M_{LL}) \; \ldots \ldots \ldots \ldots \ldots \ldots \quad (35)$$

in which ϕ is determined from Table 1 for an assumed exclusion limit of 1% and a COV of 0.15. The importance factor is again not considered in the standard and is thus assigned a value of unity. These results are presented in Table 3 converted to $\phi = 0.589$ for comparison with other standards.

West Germany.—The design of simple flexural members by the rules of DIN 1052 is based on an allowable stress concept and bending stress is again calculated assuming elastic behavior.

The procedure for obtaining the allowable stress from the flexural capacity of the members (MOR) is not fully explained within DIN 1052. Apparently a factor of safety is applied to the mean short-term strength value. This value is 3.2 (European spruce at 18% moisture content) with the assumption that the strength ratio for the lumber grades is the same as has been used in the French code (28). Adjustment for load-duration effect which is not included in the calculation of stresses, may be included in the apparent safety factor of 3.2. Applying Eq. 9 on this basis results in

$$0.589 \, (\bar{f}_b S) \geq (1.0)(1.88)(1.0 \, M_{DL} + 1.0 \, M_{LL}) \dots \dots \dots \dots \dots \quad (36)$$

in which ϕ is considered at the 5% exclusion level for a COV of 0.25 as in several previously considered cases. The importance factor is not considered in the code and is thus assigned a value of unity. Results of Eq. 36 are tabulated in Table 3 for comparison with other codes.

Denmark.—The Danish code (7) calls for the application of partial load coefficients in equating load and resistance in the form

$$f(\gamma_{DL} C_{DL} Q_{DL} + \gamma_{LL} C_{LL} Q_{LL} + \gamma_{WL} C_{WL} Q_{WL}) \leq \frac{\bar{f}_i}{R_F} = F_i \dots \dots \dots \quad (37)$$

in which f = stress in the structural member calculated on the basis of loads imposed with partial coefficients; γ, C, Q = as defined previously; $\bar{f}_i$ = characteristic strength; and R_F = as defined previously. Two values are given for R_F in the Danish code. For normal load combinations R_F = 1.3 and for exceptional combinations R_F = 1.18. However, for deflection computations the value of R_F is taken as unity. Exceptional load combinations are those which have in addition to dead load, two or more loads acting at the same time and independent of each other. Thus for the case when only dead and live loads are considered, R_F = 1.3 is used. For this case γ_{DL} = 1.3 and γ_{LL} = 1.3.

Considering R_F in the Danish codes to include the same reduction for material variability as the NDS 1977 gives ϕ = 0.589. The load duration adjustment is taken to be 1.67. The safety factor used for lumber is not specifically delineated and is assumed to be 1.3 as given for glulam in the same code. The value of γ_i is again assumed to be unity. Thus, the Danish code for the design of flexural members can be converted to the format of Eq. 9 using these definitives resulting in

$$0.589 \, (\bar{f}_b S) \geq (1.0)(1.3)(1.3 \, M_{DL} + 1.3 \, M_{LL}) \dots \dots \dots \dots \dots \quad (38)$$

This result is summarized in Table 3 for comparison with other codes.

COMPARISON OF VARIOUS FACTORS

The presently used codes for the design of wood structures are based on different approaches and direct comparison of the reduction factors is difficult. On the other hand, the use of an LRFD format permits direct comparisons of the separated individual factors for material variability, load uncertainty, true safety, and importance. In addition, conversion of the present codes into an LRFD format provides a relatively easy method for modifying these factors to adjust the level of safety.

Some difficulty arises in attempting to compare the various codes using only the load factors, γ_i, since each code studied handles the loads and their combinations differently. For simplification, the examples were taken for a nominal dead-load and live-load combination as defined by NDS 1977. To further assist in the comparison, ratios of γ_i, γ_o, γ_{DL}, and γ_i, γ_o, γ_{LL} were determined for both long columns and beam design.

Table 2 is a summary of the factors derived for long columns. By assuming the same resistance probability levels (lower 5% exclusion limit and COV of 0.25) the uncertainty factor, γ_o, can be compared. This value ranges from 1.11 for the Hungarian standard to 1.76 for the French code. However, the γ_o factor should not be interpreted as the true safety factor since the load factors also vary. Thus, values of the product γ_i, γ_o, γ_{DL} and γ_i, γ_o, γ_{LL} are required to make proper comparisons. These products range from 1.22–1.76 for dead load and 1.43–2.11 for live load. It is interesting to note that in the French, Hungarian, and Danish codes the live load is represented by a higher safety factor than the dead load. These higher factors perhaps represent the recognition of the increased uncertainty in determining live load as opposed to dead load.

Table 3 provides a summary for design of beams. A comparison of the values in Table 3 to those in Table 2 reveals some inconsistencies even within the same code for the true safety factors for beams as opposed to long columns. In NDS 1977 a flexural member is designed with a higher level of safety than a column which may support such a beam. The same is true for the Hungarian and West German codes. The French code on the other hand results in a higher safety factor for long columns than for beams, while the Danish code gives a higher safety factor for dead load for beams than for long columns. In the case of design for live load, the reverse is true.

Some caution should be used in interpreting these results since the meaning of the products of γ_i, γ_o, and γ_i needs to be considered carefully. The design loads chosen may be based on different rationale in the various countries. This is especially true for live load. Since the dead load in most cases is the simplest to determine, comparisons of the safety factors for this case may be most valid.

CONCLUSIONS

It should be emphasized that the concept and data presented here are introductory in nature. However, it is hoped this paper will provide a first step in placing the design of wood structures on a probabilistic basis. Importance factors, γ_i, will have to be selected for the various structures and occupancies. The uncertainty factor, γ_o, should be based on rational analysis of the variabilities associated with construction, analysis, maintenance, etc. Further, the load factors, γ_i, should be chosen to properly account for the probability of occurrence of loads and their critical combinations and when combined with the other factors result in a calibrated level of safety.

This paper is meant to serve as a catalyst to encourage additional research. By properly evaluating the concepts on which existing codes are based, the rationale for further probabilistic development of codes for the design of wood structures can be determined. The flexibility of the LRFD format provides

the freedom of choice in the derivation of probability-based factors which will result in proper balance between reliability and economy for a particular structure.

APPENDIX I.—REFERENCES

1. Allen, D. E., "Limit States Design—A Probabilistic Study," *Canadian Journal of Civil Engineering*, Vol. 2, No. 1, Mar., 1975.
2. Ang, A. H-S., and Cornell, C. A., "Reliability Bases of Structural Safety and Design," *Journal of the Structural Division*, ASCE, Vol. 100, No. ST9, Proc. Paper 10777, Sept., 1974, pp. 1755–1769.
3. Barrett, J. D., and Foschi, R. O., "Duration of Load and Probability of Failure in Wood. Part I. Modelling Creep Rupture," *Canadian Journal of Civil Engineering*, Vol. 5, No. 4, 1978.
4. Barrett, J. D., and Foschi, R. O., "Duration of Load and Probability of Failure in Wood. Part II. Constant, Ramp and Cyclic Loadings," *Canadian Journal of Civil Engineering*, Vol. 5, No. 4, 1978.
5. Bölcshei, E., and Dulácska, E., *Statikusok Könyve*, (Book of Structural Engineers), Budapest, Hungary, 1974.
6. Cornell, C. A., "A Probability-Based Structural Code," *Journal of the American Concrete Institute*, Vol. 66, No. 12, Dec., 1969.
7. Code of Practice for the Structural Use of Timber, Dansk Ingeniorforering, DIF-Ref. No. NP-118T, Copenhagen, Denmark, Sept., 1975.
8. Ellingwood, B., Galambos, T. V., MacGregor, J. G., and Cornell, C. A., "Development of a Probability Based Load Criterion for American National Standard A58," *NBS Special Publication 577*, June, 1980.
9. "First Order Reliability Concepts for Design Codes," Committee Europeen du Beton, Bulletin d'Information No. 112, Munich, West Germany, July, 1976.
10. Foschi, R. O., "A Discussion on the Application of the Safety Index Concept to Wood Structures," *Canadian Journal of Civil Engineering*, Vol. 6, No. 4, 1979.
11. Galambos, T. V., and Ravindra, M. K., "Load and Resistance Factor Design Criteria for Steel Beams," *Research Report No. 27*, Civil Engineering Department, Washington University, St. Louis, Mo., Feb., 1976.
12. Galambos, T. V., and Ravindra, M. K., "The Basis for Load and Resistance Factor Design Criteria for Steel Building Structures," *Canadian Journal of Civil Engineering*, Vol. 4, No. 2, 1977.
13. Gerhards, C. C., "Time-Related Effects of Loading on Wood Strength—A Linear Cumulative Damage Theory," *Wood Science*, Vol. 11, No. 3, 1979, pp. 139–144.
14. Magyar szabrány az épületszerkezetek statikai tervezésére. (Hungarian Standards for Statical Design of Load-Carrying Components of Buildings), MSz 15020 General Requirements, 1971; MSz 15021/1 Specific Requirements for Aboveground Construction, 1971; MSz 15025 Wood Structures, 1972.
15. Johnson, A. I., "Strength, Safety and Economical Dimensions of Structures," Royal Institute of Technology, Institute of Byggnadsstatik, Meddelanden, No. 12, Stockholm, Sweden, 1953.
16. Keldysh, V. M., Berechnung von Baukonstructionen nach den Grewzbeanspruchungen, (Design of Building Structures on Limit States Concept), Berlin, Germany, 1953; Lenigrad, 1951.
17. Kollmann, F., Technologie des Holzes und der Holzwerkstoffe, (Technology of Wood and Wood-Based Materials), Vol. 1, Munich, West Germany, 1951.
18. Lind, N. C., "Consistent Partial Safety Factors," *Journal of the Structural Division*, ASCE, Vol. 97, No. ST6, Proc. Paper 8166, June, 1971, pp. 1651–1669.
19. Lugosi, A., *Faipari Kézikönyv*, (*Wood Handbook*), Budapest, Hungary, 1975.
20. Madsen, B., and Barrett, J. D., "Time-Strength Relationship for Lumber," *Structural Research Series Report No. 13*, University of British Columbia, Vancouver, B.C., Canada, 1976.
21. "Methods for Establishing Structural Grades and Related Allowable Properties for Visually Graded Lumber," *D245*, American Society for Testing and Materials.
22. "Methods for Establishing Clear Wood Strength Values," *D2555*, American Society for Testing and Materials.

23. Moses, F., "Reliability of Structural Systems," *Journal of the Structural Division*, ASCE, Vol. 100, No. ST9, Proc. Paper 10780, Sept., 1974, pp. 1813–1820.
24. "National Design Specification for Wood Construction," National Forest Products Association, Washington, D.C., 1977.
25. Nowak, A. S., and Lind, N. C., "Practical Bridge Code Calibration," *Journal of the Structural Division*, ASCE, Vol. 105, No. ST12, Proc. Paper 15061, Dec., 1979, pp. 2497–2510.
26. Ravindra, M. K., Lind, N. C., and Sin, W. W. C., "Illustrations of Reliability-Based Design," *Journal of the Structural Division*, ASCE, Vol. 100, No. ST9, Proc. Paper 10779, Sept., 1974, pp. 1739–1811.
27. Ravindra, M. K., and Galambos, T. V., "Load and Resistance Factor Design for Steel," *Journal of the Structural Division*, ASCE, Vol. 104, No. ST9, Proc. Paper 14008, Sept., 1978, pp. 1337–1353.
28. Règles, C. B. 71, "Règles De Calcul et de Conception des Charpentes en Bois," Editions Eyrolles, 1975.
29. Sexsmith, R. G., and Fox, S. P., "Limit States Design Concepts for Timber Engineering," *Forest Products Journal*, Vol. 28, No. 5, 1978.
30. "Steel Structures for Buildings—Limit States Design," CSA Standard S16.1, 1974.
31. Suddarth, S. K., Woeste, F. E., and Galligan, W. L., "Differential Reliability: Probabilistic Engineering Applied to Wood Members in Bending/Tension," *U.S. Forest Products Lab Research Paper FPL302*, 1978, 16 pp.
32. *Agriculture Handbook No. 72*, United States Department of Agriculture, Forest Products Laboratory Wood Handbook, 1974.
33. Vanderbilt, M. D., Folse, M. D., Goodman, J. R., and Landers, P. G., "Towards Probability-Based Design of Wood Transmission Structures," *Text of Abstract Papers*, IEEE Power Engineering Society, July 1979.
34. "Zimmer-und Holzbauarbeiten," VOB-StLB Hochbau 9, DIN, Beuth Verlag GmbH, Berlin, West Germany, 1976.
35. Wood, L., "Relation of Strength of Wood to Duration of Load," *Forest Products Laboratory Report No. 1916*, Unites States Department of Agriculture, Madison, Wisc., 1951.
36. Yura, J. A., Galambos, T. V., and Ravindra, M. K., "The Bending Resistance of Steel Beams," *Journal of the Structural Division*, ASCE, Vol. 104, No. ST9, Proc. Paper 14014, Sept., 1978, pp. 1355–1370.
37. Zahn, J. A., "Reliability-Based Design Procedures for Wood Structures," *Forest Products Journal*, Vol. 27, No. 3, Mar., 1977, pp. 21–28.

APPENDIX II.—NOTATION

The following symbols are used in this paper:

A = cross-sectional area of column;
A_e = effective column area;
b = beam width;
C_i = conversion factor from load to member force;
d = least column dimension, beam depth;
E = modulus of elasticity;
$\bar{E}$ = mean modulus of elasticity;
E_{limit} = limiting modulus of elasticity;
F_c = allowable compressive stress for short columns;
F_c' = allowable axial compressive stress;
$\bar{f}_b$ = mean flexural resistance (modulus of rupture);
I = moment of inertia of column about weak axis;
K = column design factor;
K_E = column design factor;

K_s = column design factor;
l_e = effective column length;
M = applied moment;
M_i = nominal applied bending moment for ith loading combination;
P_c = maximum column buckling load;
P_c^i = limiting load for column;
P_i = nominal axial column load for ith load combination;
Q_i = member load for ith load combination;
R_F = reduction factor;
R_n = nominal mean member resistance for chosen limit state;
r = radius of gyration for column;
S = section modulus;
γ_i = load factors;
γ_I = importance factor;
γ_o = uncertainty factor;
η = function of slenderness ratio for column;
λ = slenderness ratio for column;
π = ratio of circumference of circle to its diameter;
ϕ = resistance factor; and
ω = column design factor.

Subscripts

DL = dead load;
LL = live load;
WL = wind load;
I = importance;
o = uncertainty;
i,j = index of load combinations; and
n = limit state.

HISTORY OF STRUCTURAL STABILITY
RESEARCH COUNCIL

By Bruce G. Johnston,[1] Hon. M., ASCE

INTRODUCTION

The Column Research Council, which, because of the expanded scope of its coverage became the Structural Stability Research Council in 1976, has had a notable record of activity and achievement over the 40 yr since its initial conception. It has annually provided a forum, now international in its representation, that has brought together research workers in the field of structural stability. The world literature in its field has been reviewed and evaluated. Research projects have been initiated and guided. It has cooperated with specification writing organizations in the application of results in practice. Its example has inspired the formation of similar groups in Japan and Europe.

Three successive editions of the council's design guide have been published and a fourth is underway. Some noteworthy contributions include the recognition and quantification of the residual stress effect on column stability, the definition and application of the strain-hardening modulus in steel, the application of the computer to the determination of maximum inelastic column strength, the participation in the development of load and resistance factor design, and, through its technical memoranda, it has established methods and criteria for tests of columns and metals in compression.

The purpose of this paper is to record the history of the council from its beginnings up to 1981.

ROOTS

The sequence of events that led to the formation of the Column Research Council was initiated in October of 1939 when Jonathan Jones, then Chief Engineer of the Fabricated Steel Construction Division of Bethlehem Steel Corporation, submitted to the ASCE Structural Division a memorandum entitled "Unit Stresses in Columns of High-Yield-Point Steels." At that time the structural carbon steel in common use (ASTM A7) had a minimum specified yield point of 33

ksi. Higher strength structural silicon and structural nickel steels had found limited use in long-span bridges, and some proprietary steels of higher strength were used in certain special applications. It was rightly anticipated that higher strength steels would be used increasingly in both bridges and buildings.

Mr. Jones's memorandum was referred to the ASCE Committee on *Design of Structural Members* which had come into being in January of 1940. A program was already underway to "study the physical properties of four structural alloys in relation to their behavior under varying conditions of stress and shape." Tests for this program were then being carried out at the Fritz Engineering Laboratory of Lehigh University.

The ASCE Committee reviewed Mr. Jones's memorandum and formulated a five-point program covering requirements for additional knowledge in the field of columns. At the suggestion of Mr. Jones, and with the approval of the Structural Division Executive Committee, the scope of the project was enlarged to cover all phases of compression-member behavior.

In 1941 the AISC and ASA, as well as various city building codes, were considering independently the preparation of column-design formulas. Mr. Jones saw the need to give the ASCE program a broader base in order to avoid the impending diversification. Accordingly, in December of 1941, Mr. Jones wrote,

> . . . I urged and do urge that it is a national necessity that as many as possible of the bodies who are interested in writing formulas for steel columns get together in some kind of a central group and carry on the research and analyze the results in a way that will be satisfactory to all.

Action was curtailed by the war during 1942 and 1943 but F. H. Frankland, of AISC, had embraced Mr. Jones's idea and in October of 1943, he wrote

> . . . it is therefore suggested that a Column Research Council be organized under Engineering Foundation.

By early 1944 the Column Research Council concept had germinated and in January of that year the ASCE had agreed to be the sponsoring member under Engineering Foundation. An organizing committee was formed, consisting of Shortridge Hardesty (Chairman), along with C. A. Ellis, F. H. Frankland, S. C. Hollister, Jonathan Jones, and the writer, who was chairman of the ASCE Committee on Design of Structural Members.

The proposed plan for the Council was to have it made up of official representatives of specification writing bodies together with other organizations specifically related thereto. Accordingly, in late 1944 Dr. Hardesty sent out an invitation to prospective organizations, outlining the objectives of the proposed council and asking that they appoint representatives. Dr. Hardesty's prospectus included the 1944 Annual Report of the ASCE Committee on Design of Structural Members but, in his later words, this was ". . . not because we want the Council to follow it, but just so the scope of their work as they organized it would be set forth. In fact . . . this (the Council) is intended to be of much wider scope than the ASCE Committee had planned."

First Meeting of Council

Responding to the 1944 invitation, seventeen organizations sent a total of 32 representatives to the first meeting of the Council, held in the Board Room of the ASME in the Engineering Societies Building of New York City on September 25 and 26 of 1945. In addition, H. E. Wessman was present as an observer for Engineering Foundation. A complete verbatim transcript (5) of this meeting is on file at the Council headquarters at Lehigh University. Those present and the organizations (a list of abbreviations appears as Appendix I, at the conclusion of this paper) they represented were: (1) H. E. Wessman, Engineering Foundation; (2) C. A. Ellis, S. C. Hollister, and B. G. Johnston, ASCE; (3) J. L. Beckel, R. N. Brodie, G. M. Magee, and E. J. Ruble, AAR; (4) L. H. Donnell, and H. L. Whittemore, ASME; (5) O. H. Ammann, S. Hardesty, H. C. Tammen, and F. M. Masters, AICE; (6) F. H. Frankland, H. D. Hussey, and J. Jones, AISC; (7) R. Archibald, Public Roads Administration; (8) H. G. Schlitt, AASHO; (9) W. R. Osgood and H. L. Whittemore, National Bureau of Standards; (10) H. Marcus, Bureau of Yards and Docks; (11) D. F. Windenburg and H. R. Thomas, Bureau of Ships; (12) R. L. Hankinson and E. A. Dubin, United States Coast Guard; (13) E. P. Trask, Society of Naval Architects and Marine Engineers; (14) M. Male, AISI; (15) R. L. Templin and B. J. Fletcher, ALCOA; (16) J. O. Jackson, Steel Plate Fabricators Association; (17) J. S. Newell and E. E. Lundquist, Institute of the Aeronautical Sciences; and (18) T. I. Coe, AIA. (Messrs. Hollister, Beckel, Hardesty, Masters, Frankland, Archibald, Whittemore, Windenburg, Templin, and Newell were members of the initial Executive Committee.)

The adopted plan of organization followed closely that proposed by the organizing committee. The Executive Committee, made up of nine elected members, would not be concerned with technical matters. The Chairman and Vice-Chairman of the Council would also hold the same offices on the Executive Committee on which they would be ex officio members. Every member of the Council would be assigned, according to his preference, to a "category group" that would represent his primary field of interest. These groups were not to be organized as committees but would proclaim the broad scope of the Council and would provide liaison with various specification writing bodies. The following category groups were proposed:

1. Railway bridges.
2. Highway bridges.
3. Tier buildings.
4. Industrial buildings and hangars.
5. Machinery.
6. Derricks and cranes.
7. Military structures.
8. Fixed and floating marine structures.
9. Towers.
10. Aircraft.
11. Ship structures.
12. Mobile equipment.

Reporting to the Executive Committee would be a *Technical Board* that would

include representation of all category groups. Under the *Technical Board* there would be a *Committee on Research* and a *Committee on Recommended Practice*.

Officers elected were: (1) Chairman: S. Hardesty; (2) Vice-Chairman: H. L. Whittemore; (3) Chairman, Technical Board: S. C. Hollister; (4) Vice-Chairman, Technical Board: H. Hussey; (5) Chairman, Research Committee: B. G. Johnston; and (6) Chairman, Committee on Recommended Practice: J. Jones. A committee on finance (S. C. Hollister, Chairman) and a committee to prepare bylaws (F. H. Frankland, Chairman) were established.

Following its initial meeting on September 26, 1945, the Committee on Research proposed that four subcommittees be set up at once, patterned after the column project of the ASCE Committee on Design of Structural Members. These were as follows:

1. Mechanical Properties of Materials.
2. Initial Eccentricities of Compression Elements.
3. Local Buckling of Compression Elements.
4. Columns in Structural Frames.

This organization provided a basis for the recommendation to the ASCE Structural Division that the Committee on Design of Structural Members be disbanded and its work taken over by the Column Research Council through its Research Committee.

ORGANIZATIONAL HISTORY

Jonathan Jones had sown the seed that led to the formation of the Council and Shortridge Hardesty went on to nurture its early growth as chairman for the first 12 yr of its existence. The efforts of these two were of paramount significance to the Council. When, due to ill health, Dr. Hardesty retired from the chairmanship in 1955, he was made an Honorary Member, and when he died a few months later, the following resolution was passed:

<div align="center">

Shortridge Hardesty
September 13, 1884–October 16, 1956

</div>

Column Research Council records with sadness the passing on of Shortridge Hardesty. As Chairman and director for twelve years, Mr. Hardesty gave fully his love, devotion, and material assistance to the organization and continued support of Column Research Council activities. His mind not only grasped the practical problems of engineering application but instinctively went beyond to encompass the fundamental knowledge that underlies research. His influence was a personal inspiration to all who worked in Column Research Council and his kindly spirit will remain with it for so long as it may continue.

Bylaws were adopted in 1946. In practice, the initial scheme of organization proved somewhat unwieldy, and in 1951 the Technical Board and the overall Research Committee were eliminated. New task-oriented research committees

reported directly to the Executive Committee, which then took on both the technical and administrative functions of the Council. In 1960 the designation "research committee" was changed to "task group" with a further narrowing to more specific objectives. In 1961 the bylaws were changed to limit the term of office of the Chairman and Vice Chairman to 3 yr, with an extension of one year permitted if required. The immediate past-chairman and vice-chairman of the council were added to the executive committee as ex officio members. Since 1966, headquarters of the Council has been at the Fritz Engineering Laboratory of Lehigh University where all records are on file. In 1970 Lynn S. Beedle was appointed to be paid part-time director, an office that had been authorized by the bylaws much earlier. See Table 1 for a chronology of the principal officers of the Council.

TABLE 1.—Chronology of Principal Officers of Council

Year (1)	Chairman (2)	Vice-chairman (3)	Director (4)	Technical secretary (5)	Administrative secretary (6)
1945	S. Hardesty	H. L. Whittemore			
1946	S. Hardesty	H. L. Whittemore			
1947	S. Hardesty	H. L. Whittemore		L. S. Beedle	
1948	S. Hardesty	H. L. Whittemore		L. S. Beedle	
1949	S. Hardesty	R. Archibald		L. S. Beedle	
1950	S. Hardesty	R. Archibald		L. S. Beedle	
1951	S. Hardesty	R. Archibald		L. S. Beedle	
1952	S. Hardesty	T. R. Higgins		L. S. Beedle	
1953	S. Hardesty	T. R. Higgins		L. S. Beedle	
1954	S. Hardesty	T. R. Higgins		R. L. Ketter	
1955	S. Hardesty	T. R. Higgins		R. L. Ketter	
1956	B. G. Johnston	T. R. Higgins		R. L. Ketter	
1957	B. G. Johnston	T. R. Higgins		G. V. Berg	
1958	B. G. Johnston	T. R. Higgins		G. V. Berg	
1959	B. G. Johnston	T. R. Higgins		R. B. Harris	
1960	B. G. Johnston	T. R. Higgins		R. B. Harris	
1961	B. G. Johnston	T. R. Higgins		R. B. Harris	
1962	E. H. Gaylord	L. S. Beedle		R. N. Wright	
1963	E. H. Gaylord	L. S. Beedle		R. N. Wright	
1964	E. H. Gaylord	L. S. Beedle		R. N. Wright	
1965	E. H. Gaylord	L. S. Beedle		R. N. Wright	
1966	L. S. Beedle	J. L. Durkee		B. T. Yen	
1967	L. S. Beedle	J. L. Durkee		B. T. Yen	
1968	L. S. Beedle	J. L. Durkee		R. Bjorhovde	
1969	L. S. Beedle	J. L. Durkee		R. Bjorhovde	
1970	T. V. Galambos	G. Winter	L. S. Beedle	R. Bjorhovde	
1971	T. V. Galambos	G. Winter	L. S. Beedle	F. Van der Woude	
1972	T. V. Galambos	G. Winter	L. S. Beedle	G. W. Schulz	
1973	T. V. Galambos	G. Winter	L. S. Beedle	B. G. Freeman	
1974	G. Winter	J. W. Clark	L. S. Beedle	F. Cheong-Siat Moy	
1975	G. Winter	J. W. Clark	L. S. Beedle	F. Cheong-Siat Moy	
1976	G. Winter	J. W. Clark	L. S. Beedle	F. Cheong-Siat Moy	
1977	G. Winter	J. W. Clark	L. S. Beedle	T. Kanchanalai	
1978	J. W. Clark[a]	J. S. B. Iffland	L. S. Beedle	R. Zandonini	L. G. Federinic
1979	J. S. B. Iffland	J. L. Durkee	L. S. Beedle	S. Kitipornchai	L. G. Federinic
1980	J. S. B. Iffland	J. L. Durkee	L. S. Beedle	M. N. Aydinoglu	L. G. Federinic
1981	J. S. B. Iffland	J. L. Durkee	L. S. Beedle	Zu-Yea Shen	L. G. Federinic

[a] Resigned due to ill health

The Executive Committee members serve for 3 yr and are eligible for reelection. Although a few members have served for many years, there has been a large turnover as well. The following have served one or more terms, listed in sequence of their initial election: S. C. Hollister, R. Archibald, J. L. Beckel, F. M. Masters, J. S. Newell; H. D. Hussey, W. R. Osgood, T. R. Higgins, R. W. Crum, B. G. Johnston, G. M. Magee, E. K. Timby, N. J. Hoff, E. L. Erickson, E. F. Ball, R. N. Brodie, E. C. Hartmann, T. C. Kavanagh, D. B. Armstrong, L. S. Beedle, L. K. Irwin, G. Winter, T. Dembie, W. H. Jameson, E. H. Gaylord, J. W. Clark, G. Haaijer, F. R. Shanley, A. Amirikian, J. L. Durkee, T. V. Galambos, C. F. Scheffey, A. I. Westrich, I. M. Hooper, J. S. B. Iffland, W. A. Milek, J. A. Gilligan, G. F. Fox, C. Birnstiel, L. A. Boston, K. P. Buchert, J. Springfield, R. R. Graham, W. J. Austin, S. J. Errera, and R. M. Meith.

From the 32 representative members that were at the first meeting in 1945, the membership of the Council has grown in 1981–205, of which 80 are representatives of Sponsoring or Participating Organizations and Firms. In addition to the 87 members-at-large in 1981 there were 29 "Corresponding Members" who provide continuing contact with relevant work in 24 countries.

Sponsoring / Participating Organizations and Firms

Eighteen organizations, as listed earlier, sent representatives to the first meeting of the Council in 1945. More than half of these organizations still participate (in some instances under a new name that has resulted from reorganization). In recent years engineering firms have been added as participants, each naming one representative member to the council. There are now (1981) 33 sponsoring/participating organizations and 43 participating firms, as noted in Table 2.

Financial Support

Initial financial as well as administrative support came from the Engineering Foundation, which agreed in 1945 to put up $5,000 contingent on the raising of $10,000 by the Council from other sources. This offer was repeated later.

Major sources of funds in support of the Council over the years have been the following: (1) *Engineering Foundation* ($29,000 between 1947 and 1958); (2) *Research Corporation* ($10,000 in 1949); (3) *Association of American Railroads* ($34,500 between 1948 and 1958); (4) *American Institute of Steel Construction* ($141,000); (5) *American Iron and Steel Institute* ($94,000, principally since 1955); (6) *Aluminum Company of America* and (after 1970) the *Aluminum Association* ($6,000); (7) *Canadian Institute of Steel Construction* ($16,000); (8) *National Science Foundation* ($93,000 since 1968, primarily in support of annual technical sessions); (9) *Federal Highway Administration* ($6,000 in support of 1980 annual technical session); and (10) *Urban Mass Transit Administration* ($6,000 in support of 1980 annual technical session).

Additional revenue has accrued from fees paid by participating organizations and firms, dues paid by members-at-large, meeting registration fees, and royalties on the "Guide." (The "Guide," known initially as the "Guide to Design Criteria for Metal Compression Members," will be described later under "Council Publications.")

TABLE 2.—Sponsoring/Participating Organizations and Firms

Sponsoring organizations (1)	Participating organizations (2)	Participating firms (3)
American Institute of Steel Construction	Aluminum Association	Amirikian Engineering Co.
American Iron and Steel Institute	American Institute of Architects	Ammann & Whitney
American Petroleum Institute	American Society of Civil Engineers	Beiswenger, Hoch & Assoc.
Brown & Root, Inc.	American Society of Mechanical Engineers	Martin Berkowitz Assoc.
Canadian Institute of Steel Construction	Canadian Society for Civil Engineering	Blauvelt Engineering Co.
Chevron U.S.A. Inc.	Corps of Engineers, United States Army	Carruthers and Wallace Ltd.
Chicago Bridge & Iron Co.	Earthquake Engineering Research Inst.	Copperweld Tubing Group
Earl & Wright	Engineering Foundation	De Leuw Cather & Co.
McDermott Inc.	European Convention for Constructional Steelwork	Delon Hampton & Assoc.
Metal Building Manufacturers Association	Federal Highway Administration	Dravo Van Houten, Inc.
Mobil Research & Development Corp.	General Services Administration	Edwards and Kelcey, Inc.
National Science Foundation	Institute of Engineers, Australia	Feld, Kaminetzky & Cohen, P.C.
Shell Oil Co.	International Conference of Building Officials	Gannett Fleming Corddry and Carpenter, Inc.
	Langley Research Center, NASA	Gilbert Associates, Inc.
	National Bureau of Standards	Green International, Inc.
	Naval Facilities Engineering Command, United States Navy	Hardesty & Hanover
	Naval Ship Research & Development Center, United States Navy	Hazelet & Erdal
	Steel Joist Inst.	Howard Needles Tammen & Bergendoff
	Structural Engineers Association of California	Iffland Kavanagh Waterbury, P.C.
	Welding Research Council	Bernard Johnson Inc.
		LeMessurier Associates/SCI
		Lev Zetlin Associates, Inc.
		A. G. Lichtenstein & Associates, Inc.
		Lockwood, Andrews & Newman, Inc.
		Loomis and Loomis, Inc.
		Charles T. Main, Inc.
		Modjeski and Masters
		Walter P. Moore & Associates, Inc.
		Parsons, Brinckerhoff, Quade and Douglas, Inc.
		Richardson, Gordon and Assoc.
		Rummel, Klepper & Khal
		Sargent & Lundy
		Seelye, Stevenson, Value & Knecht, Inc.
		Skidmore, Owings & Merrill
		Skilling, Helle, Christiansen, Robertson, P.C.

TABLE 2.—Continued

(1)	(2)	(3)
		Steinman, Boynton, Gronquist & Birdsall
		Sverdrup & Parcel and Associates, Inc.
		Tippetts-Abbett-McCarthy-Stratton
		URS/John A. Blume & Associates, Engineers
		URS/Madigan-Praeger, Inc.
		Vollmer Associates, Inc.
		Weiskopf & Pickworth
		Wiss, Janney, Elstner and Associates, Inc.

The foregoing figures do not include funding made directly to other organizations in support of projects for which the Council acted in an advisory capacity. Records in this category are incomplete, but this funding amounted to $164,000 over the years 1947–1956. Records were also kept for the years 1962–1970 during which time the funding by other organizations of Council-related projects amounted to $1,440,000.

OBJECTIVES AND PURPOSE OF COUNCIL

At the first meeting of the Council in 1945, Shortridge Hardesty had presented his concept of the organization's objectives in the following general statement of purpose:

> The purpose of the Council is to review our existing knowledge of column materials and theory; plan and carry out a program of research and tests; to supplement and develop our knowledge where required; to study the application of results of this program in the practical design of compression members of various types in various kinds of structures; develop a comprehensive series of formulas or rules covering the entire range of compression members; and secure the widest possible adoption of such formulas by specification-writing bodies and by designers.

The statement of purpose was redrafted and made the first section of the Council bylaws, covering essentially the same concepts as those outlined by Dr. Hardesty. Quoting from the bylaws as amended in 1951 and continuing without change until 1962 the statement reads: "The general purposes . . . shall be:

1. "To organize, maintain, and administer a national forum where problems relating to the design and behavior of columns and other compression elements in metal structures can be presented and pertinent structural research problems can be proposed for investigation, with the assurance of an evaluation of all

problems proposed and of support for those projects adjudged important.

2. "To digest critically the world's literature on structural behavior involving compression elements and the properties of metallic materials available for their construction, and make the results widely available to the engineering profession.

3. "To organize and administer cooperative research projects in the field of compression elements.

4. "To stimulate, aid and guide column research projects on the foregoing problems in the engineering colleges, endowed laboratories, and other research laboratories.

5. "To study the application of the results of this program to the design of compression elements.

6. "To develop a comprehensive and consistent set of formulas or rules covering their design.

7. "To promote the widest possible adoption of such formulas by designers and specification-writing bodies.

8. "To publish and disseminate original research information within the field of the Council."

The Council's statement of purpose was substantially revised in 1968 and further minor changes were made in 1976. There is no longer emphasis on developing and promoting specific design rules and formulas as stated in the foregoing items 6 and 7.

In 1980 the statement of purpose read as follows:

1. To maintain a forum where structural stability aspects of the behavior of frames, columns and other compression-type elements in metal and composite structures can be presented for evaluation, and pertinent structural research problems proposed for investigation.

2. To review the world's literature on structural stability of metal and composite structures and study the properties of metals available for their construction, and to make the results widely available to the engineering profession.

3. To organize, administer and guide cooperative research projects in the field of structural stability, and to enlist financial support for such projects.

4. To promote publication and dissemination of research information in the field of structural stability.

5. To study the application of the results of research to stability design of metal and composite structures, and to develop comprehensive and consistent strength and performance criteria and encourage consideration thereof by specification-writing bodies.

DEVELOPMENT OF RESEARCH PROGRAM

As a basis for the establishment of its research program, the Council initially sought answers to the following questions:

1. What are the structural stability problems to which structural engineers are seeking solutions?

2. To what extent does existing information provide solutions to these problems?

3. What is currently being done about the problems?

4. What projects are needed, in the light of past and current research, to give the engineer the answers he needs?

The first project of the Council in 1945 was the distribution of a questionnaire to leading design engineers and researchers requesting detailed information as to what were considered important structural problems involving stability. The questionnaire also asked for suggestions as to needed research and closed with the query "What metals do you expect to use in future structural designs?" A committee chaired by E. E. Lundquist of NACA (Forerunner of NASA) reviewed returns and issued a report in March of 1946 (12). The returns indicated greatest interest in the subject of the column as part of a framed structure. Increasing use of higher strength steels was generally anticipated.

The first sponsored project of the Council was carried out by Dr. Friedrich Bleich, a leading German engineer, under support by the United States Navy Department through the David Taylor Model Basin. This included a literature survey and review of existing information with the objective of answering the second of the four basic questions previously mentioned. The work was carried out in the offices of the firm of Frankland and Lienhard, which entered into a contract with the Navy Department with joint supervision by the Council.

A second questionnaire survey of current research asked the following:

1. What articles have you published since 1942?

2. What research projects have you completed for which results have not yet been published?

3. What programs do you have currently underway or have planned for the immediate future?

With the help of key engineers in nearly every foreign country nearly 2,000 copies of the questionnaire received world-wide distribution. L. S. Beedle and the writer reviewed the returns for the Committee on Research, issuing reports in 1948, 1950, and 1952 (2,3,7). Engineers from abroad who assisted in the work became the initial Corresponding Members of the Council.

A further outgrowth of the Bleich project and the first two questionnaires was the preparation of the Chart of Column Problems, showing column applications for which analytical solutions were available, problems remaining to be investigated, and means for dealing with them.

A chronology of research projects that have been undertaken by the Council is provided in a later section. After the work of the Council became established and widely known, unsolicited proposals became a significant factor in the continuation of research. Such proposals were evaluated by appropriate research committees or task groups and, if approved, were in many cases initiated by small grants of "seed money."

RESEARCH COMMITTEES, TASK GROUPS, AND TASK REPORTERS

Projects originating within the Council were initially planned by the research committees, which, through the questionnaire surveys, established research priorities. The appropriate committee then solicited proposals and financial

support, awarded the project, guided its course, reviewed the resulting reports and approved their release for publication by CRC or other appropriate medium. The first four research committees were initially subcommittees of the overall Research Committee. Three more were added in 1948 and in the 1951 reorganization they all became independent committees, continuing to be active until 1960, when the task group designations took over. The seven research committees were: (1) Mechanical Properties of Materials; (2) Initial Eccentricities of Compression Elements; (3) Local Buckling of Compression Elements; (4) Columns in Structural Frames; (5) Torsional Instability of Structural Elements; (6) Stability of Structural Elements under Dynamic Loading; (7) Stability of Laterally Unsupported Bridge Chords.

The Task Groups that replaced the research committees continued to act in the same capacity, but additional Task Groups took on the responsibility of preparing chapters of the second, and later, the third editions of the Council Guide. Others prepared technical memoranda, special reports, or carried on liaison with other groups.

The Task Groups, with dates of origin, termination, or change of status are listed in the following:

1. Centrally Loaded Columns (1960). (Currently (1981) active task group.)

2. Ultimate Strength of Laterally Loaded Columns (1960–1963).

3. Ultimate Strength of Columns with Biaxially Eccentric Load (1960). Columns with Biaxial Bending (1975 change). (Currently (1981) active task group.)

4. "K" Values for Typical Building Construction and Evaluation of the Factors Affecting Strength of Columns in Actual Structures (1960–1963). Frame Stability and Effective Column Length (Reinstated, 1967). Frame Stability and Columns as Framed Members (1980 change). (Currently (1981) active task group.)

5. Higher Strength Steels (1960). Classification of Steels for Structures (1964 change). (1969 termination)

6. Testing Techniques for Lateral Stability Testing (1960). Test Methods for Compression Members (1963 change). (Currently (1981) active task group.)

7. Tapered Members (Joint with WRC, 1966). (Currently (1981) active task group.)

8. Dynamic Instability of Compression Elements (1967). Dynamic Instability (1968 change). Dynamic Stability of Compression Elements (1975 change). (Currently (1981) active task group.)

9. Curved Compression Members (1967). (1973 Replaced by Task Reporter 15.)

10. Design of Laterally Unsupported Columns (1967). Design of Laterally Unsupported Restrained Beam-Columns (1968 change). (1974 termination)

11. European Column Studies (1967). International Cooperation on Stability Studies (1975 change). (Currently (1981) active task group.)

12. Mechanical Properties of Steel in the Inelastic Range (1967). (Currently (1981) active task group.)

13. Thin-Walled Metal Construction (1967). (Currently (1981) active task group.)

14. Horizontally Curved Girders (1968). (Currently (1981) active task group.)

15. Laterally Unsupported Beams (1969). (Currently (1981) active task group.)

16. Plate Girders (1969). Plate and Box Girders (1971 change). Plate Girders

(1975 change). (Currently (1981) active task group.)

17. Stability of Shell-Like Structures (1969). (Currently (1981) active task group.)

18. Tubular Members (1970). Unstiffened Tubular Members (1975 change). (Currently (1981) active task group.)

19. Stiffened Plate Structures (1970). (1973 Replaced by Task Reporter 16.)

20. Composite Members (1971). (Currently (1981) active task group.)

21. Box Girders (1975). (Currently (1981) active task group.)

22. Stiffened Tubular Members (1975). (Currently (1981) active task group.)

23. Effect of End Restraint on Initially Crooked Columns (1978). (Currently (1981) active task group.)

Task reporters have also been appointed to present annual meeting reports as to the progress of particular research projects or areas of research interest. In many instances the task reporter has been the forerunner of a task group—while in other cases, the task group has given way to a task reporter. The following chronology of task reporters uses the same format as that of the Task Groups:

1. Welded Plate Girders (1963–1968).

2. Strength of Longitudinally Stiffened Plates (1963–1969).

3. Columns in Continuous Frames (1963–1966).

4. Inelastic Lateral-Torsional Buckling of Wide-Flange Beam-Columns (1963–1966).

5. Frame Stability (1963–1968).

6. Stability of Plate and Shell Structures (1963–1966).

7. Truss Bridge Research Project (1963 only).

8. Buckling Strength of Tapered Beams and Columns (1963–1966).

9. Stub Column Test Procedure (1963–1964).

10. Cold-Formed Thin-Walled Metal Construction (1964–1965).

11. Stability of Aluminum Structural Members (1967). (Currently active (1981).)

12. Stability of Box Girders (1968–1970).

13. Local Inelastic Buckling (1970). (Currently active (1981).)

14. Fire Effects on Structural Stability (1971). (Currently active (1981).)

15. Curved Compression Members (1973). (Currently active (1981).)

16. Stiffened Plate Structures (1973). (Currently active (1981).)

17. Laterally Unsupported Restrained Beam-Columns (1974). (Currently active (1981).)

18. Application of Finite Element Methods to Stability Problems (1980). (Currently active (1981).)

RESEARCH PROJECTS

Since its inception, the Council has guided research projects through its committees or task groups. In addition, annual technical sessions have provided increasingly a world-wide forum where researchers can present theoretical and test results and exchange ideas with others in areas of mutual interest with

or without direct sponsorship or authorization by the Council. Major project financing by the Council has diminished, although "seed money" has been authorized frequently to help initiate a beginning project effort.

Since the mid1950s when preparation of the first edition of the Council's "Guide" was initiated, the Guide has become the primary outlet where significant Council-approved research results of both sponsored and nonsponsored projects have been presented. No attempt will be made herein to describe in detail what is already available in the various editions of the Guide. However, a chronological research review will be presented, listing subjects, project workers, and the institution at which the work was carried out. Further information concerning research results based on projects reported herein can be found by reference to the Name Indexes in the various editions of the Guide. The 3rd edition of the Guide, published in 1976, includes primarily references printed before 1975. More recent references are listed in the Annual Proceedings of the Council for 1976 and thereafter.

A general review of Council-related research work will be made under the following categories:

1. Centrally Loaded Columns.
2. Beams and Girders.
3. Beam-Columns.
4. Tapered Members.
5. Built-Up Members.
6. Members with Distributed Lateral Restraints.
7. Members in Frames.
8. Stiffened Plates.
9. Curved Bars and Arches.
10. Tubes and Shells.
11. Local Buckling.
12. Thin-Walled Metal Construction.
13. Composite Columns.

Sponsorship by the Council of the following projects has ranged from little or no support to major financial aid and guidance. All projects listed hereunder have been reported on at one or more of the annual technical sessions of the Council and subsequently summarized in the Annual Reports and Proceedings. Research projects may last from 1 yr to 10 yr or even longer; therefore the dates as listed simply indicate a time when the project had been initiated or was in early progress.

Centrally Loaded Columns.—The earliest work on centrally loaded columns sponsored by the Council concerned the effect of residual stress. The probable importance of residual stress on inelastic column strength had been noted in the late 1940s by researchers at the Fritz Engineering Laboratory, Lehigh University, and the matter was described at the Technical Board Meeting of the Council on November 7 of 1948. A pilot program was authorized and the results led to a series of major studies that are still continuing 32 yr later. The residual-stress effect has also been studied in Canada, Europe, Australia, and Japan.

In the following lists the name of a research worker will be shown only once

in connection with his earliest work. For example, the work of L. Tall at Lehigh University on residual stress effects has continued through the years from 1960–1978, but is listed only for 1960.

1. 1950 C. H. Yang, L. S. Beedle, B. G. Johnston (Lehigh).
2. 1951 W. R. Osgood (National Bureau of Standards).
3. 1954 A. W. Huber (Lehigh).
4. 1955 Y. Fujita (Lehigh).
5. 1958 R. L. Ketter (Lehigh).
6. 1960 L. Tall (Lehigh).
7. 1961 T. V. Galambos, Y. Ueda (Lehigh).
8. 1962 R. H. Batterman (University of Michigan).
9. 1963 F. R. Estuar (Lehigh).
10. 1968 G. Alpsten (Lehigh).
11. 1967 C. K. Yu (Lehigh).
12. 1969 J. Brozzetti (Lehigh).
13. 1969 R. Bjorhovde (Lehigh).
14. 1972 N. Tebedge (Lehigh).
15. 1972 W. F. Chen (Lehigh).
16. 1975 P. C. Birkemoe (University of Toronto).
17. 1978 R. Zandonini (Lehigh).

Effects of initial column curvature or end eccentricities, or both, alone or in combination with residual stress, are especially important in the case of high strength steels. Increasing attention has been given to this subject in recent years: (1) 1950 L. T. Wyly (Purdue); (2) 1962 L. Tall (Lehigh); (3) 1962 R. H. Batterman & B. G. Johnston (University of Michigan); (4) 1969 R. Bjorhovde (Lehigh); (5) 1971 C. Marsh (Sir George Williams University); and (6) 1979 T. V. Galambos (Washington University, St. Louis).

Torsional failure of centrally loaded columns: (1) 1951 W. J. Austin (University of Illinois); (2) 1952 J. Zickel (Brown University); and (3) 1962 G. Winter (Cornell University).

Other centrally loaded column projects involved the relationship between nonlinear stress-strain properties and column strength, including: (1) Effects of cold forming (1963, G. Winter, Cornell); (2) high strength constructional (A514) steels (1956 Y. Fujita and G. Driscoll, Lehigh); (3) use of stainless steel (1964, A. L. Johnson, Cornell); (4) T-shaped aluminum alloy columns (1967, R. Hariri, University of Michigan); (5) design recommendations for multiple column curves (1968, R. Bjorhovde, Lehigh); (6) buckling at elevated temperatures (1970, C. Culver, Carnegie-Mellon University); (7) reversed cyclic loading (1971, R. D. Hanson, University of Michigan); and (8) effects of end restraint on initially curved members (1979, T. V. Galambos, Washington University at St. Louis). Dynamic studies have been reported regularly since 1967 by D. Krajcinovic (University of Illinois at Chicago Circle) and members of his task group. A complete tabulation and classification of all steels then in structural use was prepared in 1967 by CRC Task Group, A. L. Elliot, A. L. Collin, G. Haaijer, and J. L. Walmsley.

Beams and Girders.—In 1945, U.S. design specifications were especially inadequate with respect to laterally unsupported beams and girders. The Council

gave early attention to this problem through the following projects:

1. 1950 R. Templin & H. N. Hill (Aluminum Co. Research Labs.).
2. 1950 R. A. Hechtman & J. L. Tiedemann (University of Washington, at Seattle, Washington).
3. 1951 J. W. Clark (Aluminum Co. Research Labs.).
4. 1953 M. G. Salvadori (Columbia University).
5. 1958 G. C. Lee (Lehigh).
6. 1969 J. A. Yura (University of Texas).
7. 1974 N. S. Trahair (University of Sydney).
8. 1975 C. Marsh (Concordia University, at Montreal, Canada).
9. 1975 M. Ojalvo (Ohio State University).
10. 1976 T. V. Galambos (Washington University, at St. Louis, Washington).

The adoption of tension-field design of plate girder webs in the AISC Specifications was preceded by Council-sponsored research projects: (1) 1958 K. Basler, B. Thurlimann & B. T. Yen (Lehigh); (2) 1968 J. W. Clark (Aluminum Co. Research Labs.); and (3) 1971 A. Ostapenko (Lehigh).

Other girder projects considered the use of longitudinal stiffeners (1964, P. B. Cooper, Lehigh); box girders (1968, P. B. Cooper, Kansas State University); effective flange width (1975, K. P. Chong, University of Wyoming); unsymmetrical girder strength (1967, A. Ostapenko, Lehigh); and cold-formed beams (1965, T. Pekoz & G. Winter, Cornell).

Beam-Columns.—Columns in actual structures usually carry appreciable moment, caused either by lateral load or by end moments and shears induced by frame action. Research on this rather complex problem has been pointed toward the development of design interaction formulas that have a sound theoretical basis and that have been corroborated by test:

1. 1950 R. L. Ketter and L. S. Beedle (Lehigh).
2. 1951 J. W. Clark and H. N. Hill (Aluminum Co. Research Labs.).
3. 1952 W. J. Austin (University of Illinois).
4. 1952 M. Salvadori (Columbia University).
5. 1953 D. C. Drucker & B. Thurlimann (Brown University).
6. 1962 T. V. Galambos (Lehigh).
7. 1969 S. U. Pillai (Royal Military College of Canada).
8. 1969 L. C. Lim (Lehigh).
9. 1972 C. K. Yu and L. W. Lu (St. Louis University).

When biaxial moments occur the problem becomes still more complex:

1. 1960 B. C. Ringo (University of Michigan).
2. 1962 T. V. Galambos (Lehigh).
3. 1962 E. H. Gaylord (Illinois).
4. 1962 C. Birnstiel and J. Michalos (N.Y. University).
5. 1969 W. F. Chen & T. Atsuta (Lehigh).
6. 1974 J. Springfield (Toronto).
7. 1975 S. Vinnakota (Lausanne).

Tubular beam-columns have the advantage of high torsional strength and rigidity: (1) 1964 A. A. Toprac and D. W. Fowler (University of Texas); (2) 1967 D. R. Sherman (University of Wisconsin); and (3) 1976 W. F. Chen (Lehigh University & Purdue).

Tapered Members.—The Council has collaborated in an advisory capacity with the Welding Research Council in a series of projects on single-story rigid frames with tapered members. 1960 C. M. Fogel & R. L. Ketter (State University of New York at Buffalo); 1967 G. C. Lee (State University of New York at Buffalo); 1969 M. L. Morrell (State University of New York at Buffalo); and 1978 C. J. Miller (Case Western Reserve).

Built-Up Members.—In 1949, S. Timoshenko proposed a study of shear effects in built-up laced and battened members, later carried out by J. R. Benjamin at Stanford. In 1956 M. W. White and B. Thurlimann reported for AREA on perforated cover plate design. In 1966 the shear effects in battened and laced members were studied at the University of Michigan by F. J. Lin, E. Glauser, and B. G. Johnston, the latter subsequently making a study of battens that acted only as spacers.

Members with Distributed Lateral Restraints.—Design rules for the top chords of pony truss bridges had been inadequate and from 1950–1957 the Council sponsored work at Penn State University under E. C. Holt, Jr. and R. M. Barnoff. In 1962, at Cornell, S. J. Errera studied double columns connected by shear panels that provided bracing in the weak plane.

Members in Frames.—Most compression members are parts of frames, and the early questionnaires had indicated that the study of overall frame behavior was of top priority. Early work at Cornell and Penn State covered both trusses and continuous building frames. Much of the early work at Lehigh was related to the development of rules for plastic design:

1. 1948 L. S. Beedle (Lehigh University).
2. 1948 T. C. Kavanagh and H. Wessmann (Penn State).
3. 1948 P. P. Bijlaard, G. P. Fisher, and G. Winter (Cornell University).
4. 1951 G. C. Lee (Cornell).
5. 1964 L. W. Lu, M. Ojalvo, Y. Fukumoto, T. V. Galambos, G. C. Driscoll, and V. Levi (Lehigh).
6. 1965 J. A. Yura, J. H. Daniels, P. F. Adams, B. P. Parikh, W. C. Hansell, and B. McNamee (Lehigh).
7. 1966 M. G. Lay (Lehigh).
8. 1974 P. F. Adams (University of Alberta).
9. 1974 C. K. Wang (University of Wisconsin).
10. 1976 Z. Razzag (Arizona State University & Southern Illinois University).

Stiffened Plates.—1958–1964, A. Ostapenko and T. Lee at Lehigh University.

Curved Bars and Arches.—1967 M. Ojalvo & F. Tokarz (Ohio State University); 1968 E. F. Masur (University of Illinois, Chicago Circle); and 1972 W. J. Austin (Rice University).

Tubes and Shells.—1960 L. Tall (Lehigh); 1967 K. P. Buchert (University of Missouri); 1967 Y. Ueda (Lehigh); 1970 D. R. Sherman (University of Wisconsin at Milwaukee); 1972 W. F. Chen (Lehigh University and Purdue); 1975 P. C.

Birkemoe (Toronto); 1976 A. Ostapenko (Lehigh); 1977 R. Bjorhovde (Alberta); and 1978 S. Toma (Purdue).

Local Buckling.—In 1949, E. E. Lundquist (13), a participant at the first meeting of the Council, coauthored a report summarizing significant results of research that had been conducted at the National Advisory Committee for Aeronautics Research Laboratories at Langley Field. Much of the Lehigh work has since been concerned with inelastic behavior as related to plastic design:

1. 1951 B. Thurlimann (Lehigh)
2. 1952 C. H. Yang (Lehigh)
3. 1953 G. Haaijer (Lehigh)
4. 1964 G. Winter (Cornell)
5. 1964 A. Ostapenko (Lehigh)
6. 1968 C. G. Culver (Carnegie-Mellon University)
7. 1969 L. W. Lee (Lehigh University)

Thin-Walled Metal Construction.—1967 G. C. Lee (State University of New York at Buffalo); 1969 E. A. Zanoni and C. G. Culver (Carnegie-Mellon University); 1970 W. W. Yu and C. S. Davis (University of Missouri); 1972 T. Pekoz (Cornell University); and 1978 C. Marsh (Center for Building Studies, Montreal).

Composite Columns.—1972 W. F. Chen (Lehigh); 1974 R. W. Furlong (University of Texas); and 1976 K. P. Chong (University of Wyoming).

Technical Sessions

From 1951–1959 the research report programs were supplemented by technical sessions on a particular theme. In 1969 panel discussions were initiated in the early evening at open meetings to which local engineers and engineering students were invited. At the panel discussions well known experts from design practice have presented prepared papers on a subject appropriate to the geographic location of the meeting, with questions directed to panel members and subsequent open discussion.

Since 1954 the proceedings of technical sessions and panel discussions have been reproduced and distributed to Council members and are currently available on loan upon request to council headquarters.

The following chronology of Council meetings lists the date, location and theme of the technical session or panel discussion. Proceedings for the unlisted years are available but consist primarily of miscellaneous research reports by current investigators:

1. 1951 (New York City) *Columns in Frames.*
2. 1952 (New York City) *Buckling Strength of Metal Structures.* (Bleich's book.)
3. 1953 (New York City) *Torsional Instability of Structural Elements.*
4. 1954 (New York City) *The Philosophy of Column Design.*
5. 1957 (Bethlehem, Pa.) *Lehigh Continuous Frame Project.*
6. 1969 (New York Univ., Bronx) *The Structural Engineer Looks at Column Design.*

7. 1970 (Washington University, St. Louis) *The Structural Engineer Looks at the Stability Provisions of the 1969 AISC Specifications.*

8. 1971 (Pittsburgh, Pa.) *Fire Effects on Structural Stability.*

9. 1972 (Chicago, Ill.) *Stability Problems of Novel Building Systems.*

10. 1973 (Los Angeles) *Frame Stability under Seismic Load.*

11. 1974 (Houston, Texas) *Stability Problems in Offshore Structures.*

12. 1975 (Toronto, Canada) *Stability of Structures during Erection.*

13. 1976 (Atlanta, Georgia) *New Ideas on Stability of Multistory Buildings.*

14. 1977 (Washington, D.C.) International Colloquium on *Stability of Structures under Static and Dynamic Loads.*

15. 1978 (Boston) *Mixed Steel-Con̂rete Structures.*

16. 1979 (Pittsburgh) Panel Discussion: *Stability of Space Frame Structures.*

17. 1980 (New York City) *Bridge Stability Problems.*

18. 1981 (Chicago) *Stability of Tall Buildings.*

19. 1982 (New Orleans) *Stability of Offshore Structures.*

INTERACTION WITH OTHER ORGANIZATIONS

Council activities have interacted with other groups as indicated in the following chronology of events:

1947.—In Japan, an independent "Column Research Council of Japan" was organized and in 1951 a "Handbook on Elastic Stability" was published. In 1971 a 2nd edition was produced in both Japanese and English under the title "Handbook of Structural Stability."

1951.—In response to an invitation by the Structural Engineers Association of California, the writer presented "A Survey of Progress: 1944-1951" at the 1951 Annual Convention, later published as Bulletin No. 1 of the Council (8).

1953.—In response to a request, the Council reported to the AREA regarding proposed amendments to its bridge specifications. Since the early years of its existence the Council has had a representative on AREA Committee 15—Steel Bridges.

1959.—Organized a joint symposium with ASCE on Metal Compression Members.

1961.—The revised AISC Specifications introduced new stability provisions for columns and laterally unsupported beams that were based on Council recommendations and validated by the 1st edition of the Council "Guide."

1961.—As part of a joint working group with the International Institute of Welding, the Council collaborated in a revision of its Technical Memorandum No. 3. (See next section on "Publications.")

1968.—L. S. Beedle, then Council Chairman, presented talks on the Council at the 1968 Annual Meeting of the Highway Research Board and at the Annual Meeting of the AISI.

1968.—The Council cosponsored joint sessions with ASCE on "Compression Members" at meetings in San Diego and in Pittsburgh.

1969.—Cosponsored joint sessions with the ASCE at meetings in Washington, D.C., and in New Orleans.

1969.—Cosponsored with AWS a joint panel discussion on residual stress effects at their New Orleans meeting.

1970.—Cosponsored a joint session with ASCE at their Boston meeting in

July and conducted a panel discussion at the ASCE Specialty Conference at Columbia, Mo.

1971.—Council representatives participated in the IABSE Colloquium on Design of Plate and Box Girders in London.

1971.—Cosponsored the 1st Specialty Conference on Cold-Formed Steel Structures.

1972.—Along with the ECCS, IABSE, and the Column Research Council of Japan, the Council cosponsored the First Colloquium on Column Strength in Paris.

1973.—Cosponsored the 2nd Specialty Conference on Cold-Formed Structures in Rolla, Mo.

1974.—Cosponsored with ASCE a session on Dynamic Stability in Los Angeles.

1975.—Acted as a cooperating organization in the conduct of the 3rd International Specialty Conference on Cold-Formed Steel Structures in St. Louis, Mo.

1976.—Participating in a "presession" of the 2nd International Colloquium on Stability of Steel Structures in Tokyo.

1977.—Cosponsored the 2nd International Colloquium on Stability of Steel Structures in Liege, Belgium.

1977.—Cosponsored the International Colloquium on Stability of Steel Structures under Static and Dynamic Loads, in Washington, D.C.

1977.—Cosponsored a regional Colloquium on Stability of Steel Structures in Budapest, Hungary.

1978.—Cosponsored the 4th International Specialty Conference on Cold-Formed Steel Structures in St. Louis, Mo.

COUNCIL PUBLICATIONS

Official Council publications include principally the Technical Memoranda and the various editions of the Guide.

Technical Memoranda

T.M. 1.—"The Basic Column Formula" was issued in May of 1952. In conjunction with this release a statement as to the desirability of the tangent modulus formula as a suitable expression for determining the buckling load of a straight, prismatic, axially loaded member was published in the July 17, 1952 issue of the Engineering News-Record.

T.M. 2.—"Notes on the Compression Testing of Metals" was published initially in July 1956 ASTM Bulletin, p. 61.

T.M. 3.—"Stub-Column Test Procedure" issued initially as an appendix to T.M. 2, was revised in 1962 by an International Institute of Welding Working Group and later was further revised in 1974 by Task Group 6.

T.M. 4.—"Procedure for Testing Centrally Loaded Columns" was prepared by Task Group 6 of the Council and was based on an earlier report authored by N. Tebedge and L. Tall (1970).

T.M. 5.—"General Principles for the Stability Design of Metal Structures." Completed in 1979 by an Ad-hoc Committee on Column Problems, under the chairmanship of T. V. Galambos, this memorandum updates and re-establishes the basic philosophy of the Council regarding column design. (Published by Civil Engineering Magazine, Feb. 1981, p. 53.)

T.M. 6.—"Determination of Residual Stresses." Completed in 1979 by Task Group 6, this memorandum is based on earlier work at Lehigh by L. Tall and associated research workers. (To be published by the Society for Experimental Stress Analysis.)

Design Guides.—Dr. Friedrich Bleich's book on "Buckling Strength of Metal Structures" has been described earlier in connection with its function as a major first step in the development of the Council's research program. It was also a forerunner of the design guides. After Dr. Bleich's sudden death in February of 1950, the book was completed later that year by his son, Dr. Hans Bleich, who was employed at the time by the firm of Hardesty and Hanover. The book is still widely used as a reference.

The concept of a "design guide" was introduced in 1956 by Jonathan Jones and L. S. Beedle. The purpose was to provide an authoritative source of stability design information for engineers and specification writing bodies. The first two editions were titled "The Guide to Design Criteria for Metal Compression Members" and the third edition, in keeping with the changed name of the Council, was titled "Guide to Stability Design Criteria for Metal Structures" (11). The following comparative summary illustrates the growth of the Guide:

Edition:	1	2	3
Year published	1960	1966	1976
Number of chapters	5	7	19
Number of pages	93	217	616
Number of references	157	327	902

APPLICATION TO DESIGN

The Council's efforts to achieve its primary early goal of upgrading and unifying stability design procedures has involved the following:

1. Direct cooperation with specification writing bodies.

2. Provision in the Guide of alternative design formulas and procedures of varying degrees of complexity.

3. Meetings and panel discussions have provided interaction between research workers, educators, and practicing engineers; many of the latter having had their own expertise upgraded by practicipation in Council committee and task group work.

4. Many research workers trained on Council projects have gone into industry; others have written books on design and stability.

Item 3 and 4 of the foregoing are largely intangible. Some specific examples of the Council's efforts with respect to items 1 and 2 are as follows:

1. 1953. Reported to AREA on proposed amendments to buckling provisions.

2. 1954. Prepared a study of columns with perforated cover plates for the AREA.

3. 1961. Provided input for stability design provisions for the 1961 revision of the AISC Building Specifications.

4. 1968. Provided material for stability design provisions of the AISC Manual

on "Plastic Design of Braced Multi-story Steel Frames."

5. 1969. Participated in the 1969 revision of the AISC Building Design Specifications.

6. 1974. The National Building Code of Canada, in their Limit States Design Standard, adopted curve 2 of the SSRC proposed multiple column curves.

7. 1978. Participated in the 1978 revision of the stability provisions of the AISC Building Design Specifications.

8. 1979. Developed design provisions for composite columns consistent with both reinforced concrete and steel design specifications.

9. 1980. The National Building Code of Canada adopted Curve 1 of the proposed SSRC multiple column curves for hollow heat-treated structural sections.

CLOSURE AND ACKNOWLEDGMENT

Currently, in 1981, the Structural Stability Research Council is recognized throughout the world for its objective approach and for the technical excellence of its work. This historical review of the Council's activities was prepared by the writer upon request by the Executive Committee of the Council and was made possible by the help and cooperation of the current Council Officers and Headquarters Staff, including J. S. B. Iffland, J. L. Durkee, L. S. Beedle, M. N. Aydinoglu, and L. G. Federinic. For the writer, it has been a unique privilege not only to have been associated with the Council since its founding but also to have had the opportunity to prepare this report. Refs. 2, 3, 4, 5, 6, 7, 8, and 9 are available for loan upon request to council headquarters, Fritz Engineering Laboratory, Lehigh University, Bethlehem, Pa. 18015.

APPENDIX I.—ABBREVIATIONS

The following are abbreviations used in this paper:

AAR = Association of American Railroads.
AASHO = American Association of State Highway Officials.
AASHTO = American Association of State Highway and Transportation Officials.
AIA = American Institute of Architects.
AICE = American Institute of Consulting Engineers.
AISC = American Institute of Steel Construction.
AISI = American Iron and Steel Institute.
ALCOA = Aluminum Company of America.
ASA = American Standards Association.
ASCE = American Society of Civil Engineers.
ASME = American Society of Mechanical Engineers.
CRC = Column Research Council.
NACA = National Advisory Committee for Aeronautics
NASA = National Aeronautic and Space Administration.
SSRC = Structural Stability Research Council.

APPENDIX II.—REFERENCES

1. ASCE Committee on Design of Structural Members, Progress Report, ASCE Proc. Vol. 68, No. 4, Apr., 1942.

2. Beedle, L. S., Johnston, B. G., "Questionnaire Survey on Current Research, Fourth Interim Report," (Mimeographed) May 22, 1950, 39 pp.

3. Beedle, L. S., Ketter, R. L., and Johnston, B. G., "Questionnaire Survey on Current Research, Fifth Interim Report," (Mimeographed) Mar., 1952, 61 pp.

4. Beedle, L. S., "The Formation of Column Research Council and its Program," *Proceedings of the Fifth Technical Session of Column Research Council,* May, 1955, p. 1.

5. Council organization meeting. Verbatim transcript of proceedings of the first meeting of the council, Sept. 25-26, 1945.

6. Hardesty, S., and Beedle, L. S., "Column Research Council of Engineering Foundation—Prospectus," as issued by the Council in 1952 and revised in 1953.

7. Johnston, B. G., Beedle, L. S., "Questionnaire Survey on Current Research, Third Interim Report," (Mimeographed) Sept. 1, 1948, 49 pp.

8. Johnston, B. G., "Column Research Council of Engineering Foundation—A Survey of Progress 1944–1951," *Bulletin No. 1,* Issued by the Council in Jan., 1952.

9. Johnston, B. G., "Summary of the Activities of the Column Research Council," *Journal of the Structural Division,* ASCE, Vol. 86, No. ST1, Proc. Paper 2345, Jan., 1960, pp. 13–18.

10. Johnston, B. G., "Third SSRC Guide with Column Design Applications," *Journal of the Structural Division,* ASCE, Vol. 103, No. ST7, Proc. Paper 13071, July, 1977, pp. 1359–1376.

11. Johnston, B. G., "Guide to Stability Design Criteria for Metal Structures," 3rd ed., John Wiley & Sons, Inc., New York, N.Y., 1976.

12. Lundquist, E. E., Johnston, B. G., Jones, J., Tammen, H. C., "Summary of Answers to Questionnaire: Important Structural Problems Involving Stability," (Mimeographed) Mar. 25, 1946, 12 pp.

13. Stowell, E. Z., Heimerl, G. J., Libove, C., and Lundquist, E. E., "Buckling Stresses for Flat Plates and Sections," *Transactions,* ASCE, Vol. 117, Separate Paper 2506, 1952, p. 545.

INELASTIC LATERAL TORSIONAL BUCKLING OF BEAMS

By Bruce A. Hollinger,[1] and C. P. Mangelsdorf,[2] M. ASCE

INTRODUCTION

The purpose of this paper is to present an approximate procedure suitable for general elastic and inelastic lateral torsional buckling solutions of beams with complex loading and restraint conditions. An approximate tangent modulus is used to account for the partial yielding of the cross section due to the existence of residual stresses. An estimate of the effect of a shift in the shear center due to partial yielding is also included. Computer generated finite difference solutions to the differential equations defining initiation of lateral torsional buckling are presented. A comparison of the computer solutions with 123 test results from Japan, Great Britain, Australia, and the United States are included to show the applicability of the approximations.

PREVIOUS THEORETICAL WORK

Compared to inelastic behavior, elastic buckling has received the far greater attention by past investigators. Solutions to the elastic lateral torsional buckling problem have been found for various loading cases and end boundary conditions by using analytical differential equation solutions, energy solutions, finite element analysis, and the finite difference method (1). However, inelastic lateral torsional buckling has only been investigated for a few different load and support cases. The inelastic buckling solution for wide flange beams has been published for the case of single curvature loading and for a simply supported beam with a point load at the center (2,3). These load cases have also been examined by full scale experimental tests.

An ideal beam in the inelastic range undergoes no lateral deflection or twist until the critical moment, M_{cr}, is reached. At this point, bifurcation of equilibrium takes place causing lateral deflection and twist. The beam will still be able to support a small increase in moment (Fig. 1) to M_m due to elastic unloading of previously yielded fibers (1). However, the solution procedure presented

FIG. 1.—Moment—Lateral and Torsional Displacement Curve

in this paper will be concerned only with predicting the initiation of lateral torsional buckling at point, M_{cr}.

ELASTIC CORE SOLUTIONS

The elastic core solutions as presented by Galambos has received a great deal of attention because of its favorable agreement with test results (2,4). The following assumptions underlie the elastic core theory for uniform moment, single curvature, loading (2):

1. No external lateral forces are applied to the beam between supports.
2. The beam is initially straight and free of imperfections.
3. The cross section retains its original shape during buckling.
4. The ends of the beam may not translate or twist but are free to warp.
5. Vertical deflections are small.
6. The beams are as-rolled steel wide flange shapes.
7. The cross-sectional and material properties are uniform along the whole length of the beam.
8. The stress strain curve is the idealized perfectly elastic and perfectly plastic curve for mild steel.
9. The assumed residual stress pattern is as shown in Fig. 2.

Using these assumptions, Galambos derived equations defining the torsional and weak axis bending rigidities for the elastic core of a partially yielded cross section as a function of a given moment. By substitution of these equations for inelastic rigidities in the Timoshenko elastic equation, the critical inelastic buckling moment could then be determined (2).

Galambos also derived a reduced moment method developed from the Column Research Council (CRC) basic strength curve for columns, to approximate beam buckling in the inelastic range for simple span beams under uniform moment.

He observed a close comparison of the elastic core solution with the reduced moment method for that case.

A widely recognized approximate tangent modulus equation for inelastic columns can be derived by substitution of the Euler equation into the CRC equation for basic column strength. The result is

$$E_t = \frac{4EF_{cr}}{F_y}\left(1 - \frac{F_{cr}}{F_y}\right) \dots\dots\dots\dots\dots\dots\dots\dots(1)$$

in which F_{cr} = the axial stress when buckling occurs. Eq. 1 is valid within the Range $F_y/2 \le F_{cr} \le F_y$. The inelastic buckling of beams can be approximated by a similar parabolic approximation for E_t and G_t. Substituting the bending moment, M, and the plastic moment, M_p, for F_{cr} and F_y respectively, in Eq.
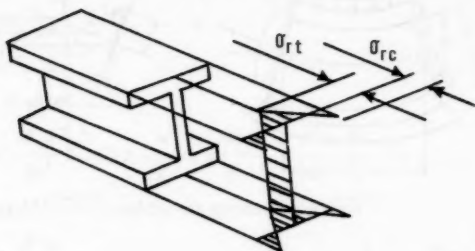
$$\sigma_{rc} = .3\sigma_y$$

$$\sigma_{rt} = \left[\frac{bt}{bt + w(d - 2t)}\right]\sigma_{rc}$$

FIG. 2.—Assumed Residual Stress Distribution

1, the following expressions for E_t and G_t are obtained

$$E_t = \frac{4EM}{M_p}\left(1 - \frac{M}{M_p}\right) \dots\dots\dots\dots\dots\dots\dots\dots\dots\dots(2)$$

$$G_t = \frac{4GM}{M_p}\left(1 - \frac{M}{M_p}\right) \dots\dots\dots\dots\dots\dots\dots\dots\dots\dots(3)$$

Eqs. 2 and 3 are taken to be valid within the range $M_p/2 \le M \le M_p$.

Substitution of Eqs. 2 and 3 into the Timoshenko elastic equation yields an approximate equation for the inelastic ultimate moment. Solutions from this approximate equation provide exactly the same result as the reduced moment method used by Galambos.

DERIVATION OF ELASTIC BUCKLING EQUATIONS

The solution to both the elastic and inelastic buckling cases for a variety of boundary conditions requires a fairly general set of equations. The solution must take into account not only redundant restraint conditions in the plane of buckling but also variations in beam stiffness due to variations in yielding along the beam.

Referring to Fig. 3(a), which shows a beam segment, AA_1, in a buckled position, it can be seen that the internal moment, M_x, in the YZ-plane gives rise to moment components, M'_x, M'_y, and M'_z, at end A, about the x'-, y'-,
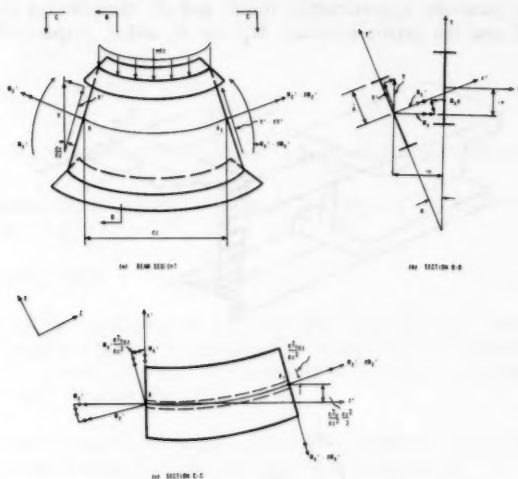
FIG. 3.—Deformed Beam Segment AA1: (a) Beam Segment; Section B-B; (c) Section C-C

and z'-axes, respectively. Assuming small angle theory, the bending in the $y'z'$-plane may be written as

$$EI_x \frac{d^2 v}{dz^2} = M'_x = M_x \quad \ldots \ldots \ldots \ldots \ldots \ldots \ldots \ldots \ldots \ldots (4)$$

Also the moment curvature relationship in the $x'z'$ plane is

$$EI_y \frac{d^2 u}{dz^2} = M_x \phi \quad \ldots \ldots \ldots \ldots \ldots \ldots \ldots \ldots \ldots \ldots \ldots (5)$$

(This moment-curvature relation is not valid in this plane when one or more of the lateral restraints are redundant. The more general equation need not be included here because it is not used.) Eq. 5 will then be differentiated twice

so that numerical solutions to indeterminate lateral restraint conditions may be obtained

$$(EI_y) \frac{d^4 u}{dz^4} + 2 \frac{d(EI_y)}{dz} \frac{d^3 u}{dz^3} + \frac{d^2(EI_y)}{dz^2} \frac{d^2 u}{dz^2}$$

$$= M_x \frac{d^2 \phi}{dz^2} + 2 \frac{dM_x}{dz} \frac{d\phi}{dz} + \frac{d^2 M_x}{dz^2} \phi \quad \ldots \ldots \ldots \ldots \ldots \ldots \ldots \ldots (6)$$

An expression for the change in torque is achieved by summing torques about the z'-axis through A_1 over the length of the beam segment. [Figs. 3(a) and 3(b)]

$$M_z' + dM_z' + M_x' \frac{d^2 u}{dz^2} dz + w dz \, \bar{a} \left(\phi + \frac{d\phi \, dz}{dz 2} \right)$$

$$- M_z' - V \frac{d^2 u}{dx^2} \frac{dz^2}{2} = 0 \quad \ldots \ldots \ldots \ldots \ldots \ldots \ldots \ldots \ldots \ldots \ldots (7)$$

Dividing by dz gives

$$\frac{dM_z'}{dz} = -M_x' \frac{d^2 u}{dz^2} - w \, \bar{a} \, \phi - \frac{w}{2} \, dz \, \bar{a} \frac{d\phi}{dz} + V \frac{d^2 u}{dz^2} \frac{dz}{2} \quad \ldots \ldots \ldots \ldots (8)$$

Realizing that $M_x' \approx M_x$ and for dz approaching zero

$$\frac{dM_z'}{dz} = -M_x \frac{d^2 u}{dz^2} - w \, \bar{a} \, \phi \quad \ldots \ldots \ldots \ldots \ldots \ldots \ldots \ldots \ldots \ldots \ldots (9)$$

Timoshenko's equilibrium equation for moments about the z'-axis

$$GK \frac{d\phi}{dz} - EI_w \frac{d^3 \phi}{dz^3} = M_z' \quad \ldots \ldots \ldots \ldots \ldots \ldots \ldots \ldots \ldots \ldots (10)$$

can be differentiated once to yield

$$\frac{d(EI_w)}{dz} \frac{d^3 \phi}{dz^3} + EI_w \frac{d^4 \phi}{dz^4} - \frac{d(GK)}{dz} \frac{d\phi}{dz} - GK \frac{d^2 \phi}{dz^2} = \frac{-dM_z'}{dz} \quad \ldots \ldots \ldots (11)$$

Substituting Eq. 9 into Eq. 11 leaves

$$\frac{d(EI_w)}{dz} \frac{d^3 \phi}{dz^3} + EI_w \frac{d^4 \phi}{dz^4} - \frac{d(GK)}{dz} \frac{d\phi}{dz} - GK \frac{d^2 \phi}{dz^2} = M_x \frac{d^2 u}{dz^2} + w \, \bar{a} \, \phi \quad (12)$$

Eqs. 4, 6, and 12 may be solved to determine initiation of beam buckling. These equations agree with those derived by Bleich (5).

BOUNDARY CONDITIONS

Only beams with two simple vertical support locations in the yz-plane are considered in this paper. This makes the solution of the major axis static moment, M_x, a determinate problem. It also eliminates the need for the solution of Eq. 4. Furthermore, only beams with warping allowed at the ends are considered.

The following boundary conditions are required for the stated end and interior restraint conditions, for Eqs. 6 and 12:

1. Lateral support at the end of the beam:

$$u_o = 0. \quad \text{and} \quad \frac{d^2 u_o}{dz^2} = 0. \quad \dots \quad (13)$$

2. No lateral support at the end of the beam:

$$\frac{d^2 u_o}{dz^2} = 0. \quad \text{and} \quad \frac{d^3 u_o}{dz^3} = 0. \quad \dots \quad (14)$$

3. Rotational support at the end of the beam:

$$\phi_o = 0. \quad \text{and} \quad \frac{d^2 \phi_o}{dz^2} = 0. \quad \dots \quad (15)$$

4. No rotational support at the end of the beam:

$$\frac{d^2 \phi_o}{dz^2} = 0. \quad \text{and} \quad GK \frac{d\phi_o}{dz} - EI_w \frac{d^3 \phi_o}{dz^3} = 0. \quad \dots \quad (16)$$

5. Lateral support at an interior point in the span:

$$u_n = 0. \quad \dots \quad (17)$$

6. Rotational support at an interior point in the span:

$$\phi_n = 0. \quad \dots \quad (18)$$

A point load applied above or below the shear center, at an interior point along the beam span, causes a discontinuity in the distributed torque Eq. 12. Resolution of this difficulty is achieved by considering the boundary conditions immediately to the left and right of the applied load.

The following boundary conditions are required (6).

The change in internal torque at the load point is equal to the applied torque

$$\left(GK \frac{d\phi}{dz} - EI_w \frac{d^3 \phi}{dz^3} \right)_R - \left(GK \frac{d\phi}{dz} - EI_w \frac{d^3 \phi}{dz^3} \right)_L = Pa\phi_p \dots \quad (19)$$

and the warping moment immediately to the left of the point equals the warping moment immediately to the right

$$\left(EI_w \frac{d^2 \phi}{dz^2} \right)_R = \left(EI_w \frac{d^2 \phi}{dz^2} \right)_L \quad \dots \quad (20)$$

The following boundary conditions are required for the point torque condition at the end of a beam with no rotational support (6)

$$GK \frac{d\phi_o}{dz} - EI_w \frac{d^3 \phi_o}{dz^3} = P\bar{a}\phi. \quad \dots \quad (21)$$

and $\dfrac{d^2 \phi_o}{dz^2} = 0.$ . . . . (22)

INELASTIC BUCKLING

The inelastic solution to the differential equations must be achieved by an iterative technique. Iterations are required because the approximate tangent modulus is a function of the failure load which is not known to start with. The finite difference method is convenient because it allows variations in beam properties along the length. Finite difference equations are written at each node point using the beam's rigidity at that point based upon an assumed failure load. The major axis moment at every node is examined to determine if it falls between $0.5M_p$ and M_p. If so, the approximate tangent moduli, E_t and G_t, are calculated, for that point, based on Eqs. 2 and 3. The values for E_t and G_t are then substituted for values E and G. The failure load is then determined and compared with the assumed value. The process is repeated until the assumed and calculated values agree.

SHEAR CENTER ADJUSTMENT

Investigators who have studied the geometry of partially yielded cross sections have found the shear center location to vary in the inelastic range. For a doubly-symmetrical wide flange beam, the shear center is coincidental with the centroid at the center of the elastic cross section. An increase in the major axis moment above $0.5M_p$ will cause the location of the shear center and the centroid to move from the center of the beam toward the bottom flange (2).

Fig. 4 shows a shear center location plot for a parabolic residual stress pattern in a 10UB29 as calculated by Kitipornchai and Trahair (3). As can be seen, the shear center distance from the beam center has almost a linear relationship with the major axis moment. The approximate variation shown in Fig. 4 can be calculated very simply and is in fairly close agreement with the calculated variation.
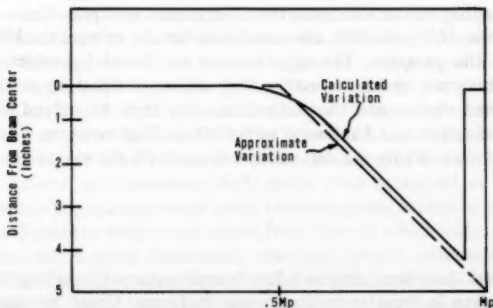
FIG. 4.—Shear Center Location Curve

The drop in the shear center location will increase the applied torque for any load above the shear center. This effect can be accounted for by using the approximate variation curve in Fig. 4 to adjust $\bar{a}$ in the inelastic range.

The adjustment in shear center location in conjunction with the approximate tangent modulus method has not been previously investigated. For this reason, the approximate tangent modulus method concept by itself is presented as Method 1. Method 2 will include the shear center adjustment.

NUMERICAL SOLUTION

The subject program automatically breaks the input beam into 200 segments and 201 nodes. The first order central finite difference equations for Eqs. 6 and 12 are written at each node. This requires two simultaneous equations at each node for a total of 402 simultaneous equations for the entire beam. The program assembles the coefficients for these equations into a rectangular banded matrix with a full band width of nine coefficients.

The coefficient matrix has coefficients for two exterior fictitious nodes at both ends of the beam which must be eliminated by using end boundary conditions. This elimination can be accomplished by writing the central difference equations for the required two boundary conditions stated previously.

Interior restraint points are accounted for by modifying the coefficient matrix. The program locates lateral and torsional restraints at the nearest node point and then with the exception of the diagonal terms, zeros out the appropriate rows of the coefficient matrix.

This set of 402 homogeneous simultaneous equations has a nontrivial solution for deflection vectors, $\{U\}$ and $\{\Phi\}$, when the determinant of the coefficient matrix equal zero (7). The determinant is equal to the product of the diagonal terms on the upper triangular coefficient matrix. Gaussian elimination is used to transform the rectangular coefficient matrix into an upper triangular matrix.

A linear relationship does not occur between the loading and the determinant of the coefficient matrix in either the elastic or inelastic range. Because of this nonlinearity, a search procedure was developed for the program to find the loading at which the determinant equals zero. A procedure using incremental search and linear interpolation was used. The first mode of failure occurs at the lowest loading which will cause the determinant to equal zero.

Eigenvectors, $\{U\}$ and $\{\Phi\}$, are calculated for the critical buckling load and published by the program. The eigenvectors are found by selecting a degree of freedom between restraint points, and setting it equal to unity. This will generate a load vector and the deflections can then be solved for by using Gaussian elimination and backward substitution. Eigenvectors, $\{U\}$ and $\{\Phi\}$, are solved by normalizing the deflection vectors with the maximum value equal to unity.

TEST DATA

Experimental data was obtained for lateral torsional buckling tests on 123 beams. The data is from tests conducted in Japan, Great Britain, Australia, and the United States and covers a variety of beam stiffness, loading conditions, unsupported lengths, and restraints. Data points are compared for elastic and

inelastic buckling, although the majority of the data falls in the inelastic range. The data is broken down into two categories for graphical comparison with the program solutions. The first category (A) includes all test beams with full lateral and torsional restraint at the point of load application. The second category (*B*) includes all test beams without restraint at point of loading. The second category is separated from the first for comparison with Method 1 and Method 2, as previously described. The solutions using Method 1 and Method 2 will be identical for Category A since restraint is provided at the point of load application.

CATEGORY A RESULTS

Category A includes tests from Great Britain, Japan, and the United States. The British tests were carried out by Dibley in 1969 (8,9). These tests covered 30 test points for four shapes of high-strength DL 30 steel with an average yield strength of 65 ksi (447 N/mm^2). The shapes were an 8 × 8 UC 58 lb/ft (846 N/m), 6 × 6 UC 20 lb/ft (292 N/m), 8 × 5-1/4 UB 17 lb/ft (248 N/m), and a 12 × 4 UB 19 lb/ft (277 N/m).

s - Lateral - Rotational Restraint
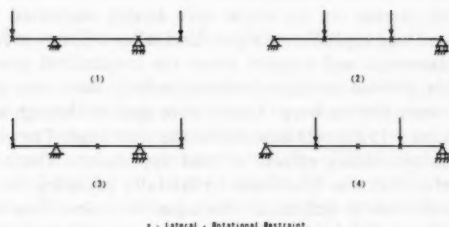
FIG. 5.—Loading and Restraint Conditions of Tests From Ref. 8

Two point symmetrical loading at the ends of the beam was used with two interior vertical supports so that the center span carried a uniform bending moment. Lateral and torsional restraint was provided at the two load points and two vertical restraint points while the ends of the beam were free to warp. The ends of the beam were constrained in guides to move vertically only and the load was applied by hydraulic jacks. The critical load was determined as the maximum loading the beam was able to carry. The published critical bending moment was corrected for dead load of the beam and for estimated error. The estimated error was calculated from measured friction in the testing equipment. Lateral and rotational deflections were measured at the center of the beam and no adjustments were made to compensate for initial imperfections.

Thirty-six Japanese tests were taken from Ref. 8 which only published the beam dimensions, loading conditions, restraints, plastic moments, and critical moments. The English translations for the original references of these tests could not be obtained. Four different loading and restraint conditions were used for these Japanese tests and are shown in Fig. 5. The test had an average measured yield stress of about 40 ksi (275 N/mm^2).

Four United States data points were taken from tests conducted at the University of Pittsburgh in 1979. These tests covered a 3S5.7 shape with an average measured yield stress of approx 46 ksi (316 N/mm²). The buckling tests were carried out on single span simply supported beams with a concentrated load applied at midspan. The ends of the beam were free to warp and lateral deflection and rotation about the longitudinal axis were restrained at the beam ends and at midspan. Two beams of 21 ft (6.41 m) and 24 ft (7.32 m) length each were investigated.

CATEGORY B RESULTS

Category B includes tests from Australia, Japan, and the United States. The Australian tests were carried out by S. Kitipornchai and N. Trahair in 1975 (8,10). These tests provided four data points for a 10UB29 with an average measured yield stress of 45 ksi (310 N/mm²). Kitipornchai and Trahair made an effort to reduce or eliminate some uncertainties in restraint exerted by loading devices and supporting fixtures, in imperfections of the test beams, and in rates of loading which were responsible for much of the scatter of results from similar tests done by earlier investigators.

The tests were carried out on single span simply supported beams with a single concentrated load applied at midspan. End roller supports prevented vertical and lateral displacement and rotation about the longitudinal axis. The flanges of the beam were allowed to rotate independently in their own planes, so that the beams ends were free to warp. Loads were applied through a loading yoke with a bearing point 3-1/2 in. (89 mm) above the top flange. The yoke eliminated almost all of the restraining effects of load application. The effect of beam alignment imperfections was overcome by laterally adjusting the yoke bearing location so that the lateral deflection was equal to or less than 0.1 in. at 80% of the maximum load. The published critical moments were adjusted to account for beam and apparatus dead weight.

The 12 Japanese tests were also taken from Ref. 8. The data was also for single span simply supported beams with a concentrated load at midspan. The load was applied at the top flange for three tests, at the center for seven tests, and at the bottom flange for the last two tests. Lateral and torsional restraint was provided at the beam ends with the flanges free to warp. The data covered varying lengths of a beam section with an average measured yield stress of 43 ksi (296 N/mm²).

The United States data comes from two references. Thirty-three data points are from tests done by Hechtman, Hattrup, Styer, and Tiedemann carried out in 1955 (11). Four more data points are from tests conducted at the University of Pittsburgh. The 33 Hechtman tests covered four sections of ASTM (American Society for Testing and Materials) A7-51T structural steel with an average measured yield stress of 37 ksi (255 N/mm²). The shapes were 10S25.4, 10WF15, 12WF27, and a 18WF50. The buckling tests were carried out on single span simply supported beams with two equal concentrated loads at the two end quarter points applied on the top flange. End roller supports prevented vertical displacement. Lateral displacement and rotation about the longitudinal axis was resisted by lateral restraints on the toes of the flanges. These restraints allowed the flanges to warp freely at the beam ends. Test loads were applied through a

loading yoke with a knife edge bearing point at the top flange. The restraining effects of load application were reduced by manual adjustment of the loads in the lateral direction to keep their lines of action vertical. The effect of beam alignment imperfections were overcome by initially centering the bearing point. Centering involved adjusting the yoke laterally until the cross sections under the loads and at midspan showed very little or no rotation at a load estimated to be 25% of the buckling load. Centering was used for the 10WF15 beam shape only. The load points were located at the center line of the web for the other three beam sections.

The four University of Pittsburgh tests covered a 3S5.7 shape with an average measured yield stress of 50 ksi (344 N/mm^2). The buckling tests were conducted for a single span simply supported beam with concentrated load at midspan applied above the top flange. The ends of the beam were free to warp and lateral and rotational movement was restrained at the beam ends. Test loads were applied through a loading yoke with a bearing point 4.5 in. (114 mm) above the top flange. The loading yoke was attached to a mechanism that allowed lateral movement of the applied load with minimal lateral restraint to beam deflection. Imperfections in beam alignment were accounted for by manual lateral adjustment in yoke location during loading.

COMPARISON OF PROGRAM SOLUTIONS AND EXPERIMENTAL RESULTS

Computer program solutions were obtained for the 123 buckling tests. Beam cross-sectional properties were calculated from the dimensions of the Japanese and British beams and taken from published design properties for the Australian and United States beams. A modulus of elasticity of 29,000 ksi (199,500 N/mm^2) and a modulus of rigidity of 11,154. ksi (76,728. N/mm^2) were used for all beam solutions. The modulus of elasticity was measured for 64 of the tests and ranged from 27,354. ksi (188,168. N/mm^2)–32,959. ksi (226,725. N/mm^2) with an average value of 29,900. ksi (205,682. N/mm^2). The plastic moment used for the Tangent Modulus method was calculated from the measured yield stress in the flanges for each test beam. It should be noted that where measured, the yield stress in the web varied from the yield stress in the flanges by as much as 10%–20%. Due to all the various differences between actual properties and those used in the program, errors as large as 5% could exist.

Although longitudinal symmetry was present in all of the test beam problems, the finite difference matrix was generated for the entire beam. The program was written this way for versatility in problem solutions. The program will allow up to 500 segments but it was found that there was virtually no change in solutions achieved using 200 segments in comparison to using 500. The number of segments required is dependent on the complexity of the buckled shape. The complexity of this shape is dependent on the number of restraints used and variation of the moduli in the inelastic range. A 5% change in results was noted for increasing the number of segments from 100–200 for one particular inelastic solution for a beam with four points of lateral and torsional restraint.

GRAPHICAL REPRESENTATION OF RESULTS

Past investigators have used the nondimensional plotting method of comparing

the ultimate moment to plastic moment ratio, M_u/M_p, versus the ratio $\sqrt{M_p/M_E}$, where M_E is the elastic buckling moment. This method allows one curve to represent all beam buckling solutions in the elastic range but generates separate curves for different beam geometries, loading and restraint conditions in the inelastic range.

The nondimensional coordinates used here allows one curve to represent all solutions in the elastic and inelastic range. The program maximum moment to plastic moment ratio, $M_u - \text{prog}/M_p$, and the test maximum moment to plastic moment ratio, $M_u - \text{test}/M_p$, are compared against the ratio $\sqrt{\text{Log}\sqrt{M_p/M_u - \text{prog}}}$. The lower bound of the ratio, $M_p/M_u - \text{prog}$ is 1.0 and the Log of this value was taken in order for the origin of the abscissa to begin at 0.0. The nondimensional program curve takes on a shape similar to the classical column stability curves. The inelastic buckling range is the region between abscissa values 0.0 and 0.388, and the elastic buckling range is the region with abscissa values greater than 0.388. Three plots were used to represent all the test data versus program solutions and are shown in Figs. 6, 7, and 8. A band of 10% above and 10% below the program solutions is represented by two curves. These curves are plotted to show the degree of test data scatter about the program curve.

Graphical representation of Category A, which are beams with restraint at point of load, is shown in Fig. 6. Only five of the 66 plotted test points fall completely outside of the 10% bands. Many of the test data points with abscissa values less than 0.12 have achieved maximum moments greater than their full plastic moment. The failure in this region are entering the strain-hardening range of buckling.
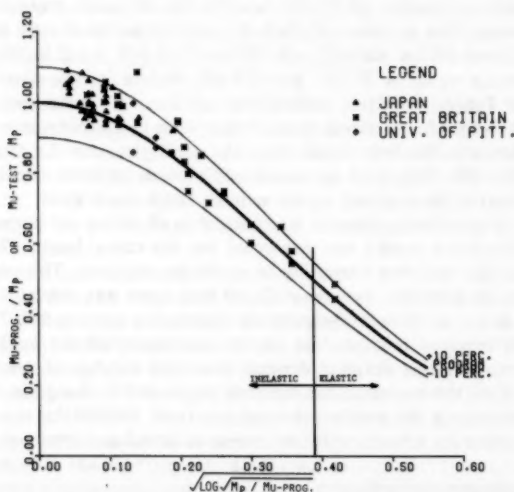
FIG. 6.—Comparison of Category A Test Results with Program Solution

The Japanese beams all failed near their full plastic moment. Good comparison with the program solutions would be expected in this region except for the influence of strain-hardening. The determinant of the finite difference matrix would be forced to zero as the tangent moduli approach zero near the full plastic moment.

The British data covers the full range of inelastic buckling and even has a few points in the elastic region. It should be noted that the British test beams were loaded under uniform moment for the entire center span between vertical and lateral torsional restraints. Good comparison would be expected for this data since past investigators have found favorable comparison between the approximate tangent modulus concept and uniform bending moment test data.

The four University of Pittsburgh data points are all well within the inelastic range. These points compare favorably with the program solution curve with all four points falling inside the 10% bands. This group is significant because within this category the beams were subjected to the most severe bending moment gradient. The results indicate that the tangent modulus concept generates good beam buckling solutions for beams under a moment gradient as well as those in uniform bending.

Category B includes the beam buckling tests without restraint at the point of loading. Testing beam buckling in this category is difficult due to uncertainties in amount of restraint developed by loading or supporting devices and imperfections in beam alinement. A load applied to a beam with a lateral misalinement of u_p at point of loading will generate an added torque of Pu_p. This added torque will generate warping stresses which can cause additional yielding of the beam cross section. The program solutions are for perfectly straight beams. Beam buckling tests that do not adjust for misalinement will therefore have buckling loads lower than those predicted by the program. This condition will greatly effect inelastic buckling but will have very little effect on buckling in the elastic range. Partial restraint generated by loading or supporting devices will give test buckling loads higher than those predicted by the program. This additional restraint will effect buckling in both the elastic and inelastic range.

Test data in this category are compared against program solutions using Method 1 and Method 2. Graphical representations of these two Methods are shown in Figs. 7 and 8.

The Japanese data points are above the upper 10% curve for failures either in or near the elastic buckling range. This would suggest that some restraint was generated by loading or support devices. Method 1 appears to give closer solutions than Method 2 for the Japanese data in the inelastic range. This would be expected since Method 1 gives higher inelastic buckling solutions than Method 2.

The single elastic Australian data point falls almost directly on the program solution. As was previously described Kitipornchai and Trahair recognized and tried to minimize the effects of loading device partial restraint. Method 1 gives solutions higher than the Australian inelastic data points with one point falling outside the lower 10% curve. Method 2 (Fig. 8), gives a good curve fit through the three inelastic points with one point falling on the curve and the other two lying on either side.

The Hechtman, United States data points compare very favorably with the program solutions in the elastic range with only three of the 14 points falling
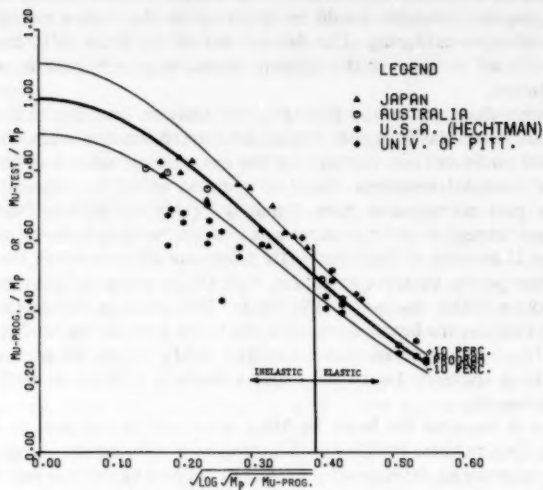
FIG. 7.—Comparison of Category B Test Results with Program Solution Using Method 1
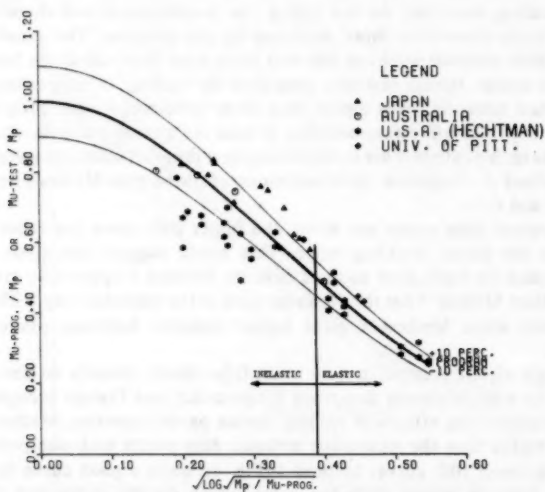
FIG. 8.—Comparison of Category B Test Results with Program Solution Using Method 2

outside the 10% curves. This would indicate that very little partial restraint was generated by the loading devices for these test beams. The majority of the inelastic data points are much lower than the program solutions using both Method 1 and Method 2. These poor comparisons are probably due to beam misalinement. Beam alinement was adjusted for by centering of the load for only four of the 19 inelastic points. Centering was used for the 10WF15 beams and these inelastic test results had the average percentage difference from the program solutions of 9.2% for Method 1 and 7.4% for Method 2.

The four data points from the University of Pittsburgh tests are all either very near to or in the elastic buckling range. These test solutions are all above the upper 10% curve. This would indicate that partial restraint was generated by the loading or support devices.

Conclusions

The principle findings and results of this study may be summarized as follows:

1. Good comparison was found between the program solutions and beam buckling tests in the elastic range. Comparison in both Categories A and B were favorable with the exception of the effects of probable loading device restraint and beam misalinement. The influence of major axis curvature has not been considered.

2. The program solutions compared very well with the inelastic buckling test results in Category A. Beam misalinement and loading device partial restraint were likely responsible for much of the test data scatter in Category B. The Australian data is believed to be the most accurate in this category since the investigators recognized and tried to minimize these affects. The Australian data compared best with Method 2 which used the shear center adjustment.

3. The comparisons made by this study indicate that the approximate tangent modulus method is an applicable technique for predicting inelastic beam buckling. The shear center adjustment appeared to improve the accuracy of the approximate tangent modulus method. The shear center adjustment gives a more conservative program solution and therefore is a safer prediction to use. The use of the shear center adjustment method causes a negligible increase in computer central processing seconds and therefore is recommended as a worthwhile enhancement to the tangent modulus method.

4. The computer aided program using the finite difference method and matrix algebra is both a convenient and financially feasible technique for obtaining solutions to elastic and inelastic beam buckling problems. An average solution to a beam buckling problem required approximately three central processing seconds on a Control Data Corporation Cyber 175. The variation in beam stiffness and parameters along the beam span were easily accounted for in the inelastic range by using the finite difference method to solve the differential equations of buckling.

Acknowledgments

in the development of the computer program. We wish to thank Wayne Schaper, Michael Ball, and Dave Sheridan, students at the University of Pittsburgh, for their assistance in conducting the recent tests reported herein.

Appendix I.—References

1. Lee, C. G., "A survey of Literature on the Lateral Instability of Beams," *Welding Research Council*, Bulletin, No. 63, New York, N.Y., Aug., 1960, pp. 50–59.
2. Galambos, T. V., "Inelastic Lateral Buckling of Beams," *Journal of the Structural Division*, ASCE, Vol. 89, No. ST5, Proc. Paper 3683, Oct., 1963, pp. 217–241.
3. Kitipornchai, S., and Trahair, N. S., "Buckling of Inelastic I-Beams Under Moment Gradient," *Journal of the Structural Division*, ASCE, Vol. 101, No. ST5, Proc. Paper 11295, May, 1975, pp. 991–1005.
4. Clark, J. W., and Jombock, J. R., "Lateral Buckling of I-Beams Subjected to Unequal End Moments," *Journal of the Engineering Mechanics Division*, ASCE, Vol. 83, No. EM3, Proc. Paper 12971, July, 1957, pp. 1291-1–1291-19.
5. Bleich, F., *Buckling Strength of Metal Structures*, McGraw-Hill Book Co., Inc., New York, N.Y., 1952.
6. Heins, C. P., *Bending and Torsional Design in Structural Members*, Lexington Books, Lexington, Mass., 1975.
7. Ugural, A. C., and Fenster, S. K., *Advanced Strength and Applied Elasticity*, Elsevier North-Holland Publishing Co., Inc., New York, N.Y., Oxford, England, Amsterdam, The Netherlands, 1952.
8. *Stability of Structures Under Static and Dynamic Loads*, ASCE, 1977, pp. 532–562.
9. Dibley, J. E., "Lateral Torsional Buckling of I-Sections in Grade 55 Steel," *Proceedings, Institution of Civil Engineers*, Vol. 43, Aug., 1969.
10. Kitipornchai, S., and Trahair, N. S., "Inelastic Buckling of Simply Supported Steel I-Beams," *Journal of the Structural Division*, ASCE, Vol. 101, No. ST7, Proc. Paper 11419, July, 1975, pp. 1333–1347.
11. Hechtman, R. A., Hattrup, J. S., Styer, E. F., and Tiedman, J. L., "Lateral Buckling of Rolled Steel Beams," *Transactions*, ASCE, Vol. 122, Paper No. 2886, 1957, pp. 823–843.
12. Johnston, B. G., "Design Criteria for Metal Compression Members," 2nd Ed., John Wiley & Sons, Inc., New York, N.Y., 1966.
13. Dux, P. F., and Kitipornchai, S., "Approximate Inelastic Buckling Moments for Determinate I-Beams," *Civil Engineering Transactions*, The Institution of Engineers, Vol. CE 20, No. 2, Sidney, Australia, 1978, pp. 128–133.
14. Razzaq, Z., and Galambos, T. V., "Biaxial Bending of Beams With or Without Torsion," *Journal of the Structural Division*, ASCE, Vol. No. ST11, Proc. Paper 14972, Nov., 1979, pp. 2145–2161.
15. Razzaq, Z., and Galambos, T. V., "Biaxial Bending Tests With or Without Torsion," *Journal of the Structural Division*, ASCE, Vol. 105, No. ST11, Proc. Paper 14973, Nov., 1979, pp. 2163–2185.
16. Yoshida, H., and Imoto, Y., "Inelastic Lateral Buckling of Restrained Beams," *Journal of the Engineering Mechanics Division*, ASCE, Vol. 103, No. EM2, Proc. Paper 9666, Apr., 1973, pp. 343–366.
17. Nethercot, D. A., and Trahair, N. S., "Design Rules for the Lateral Buckling of Steel Beams," *Civil Engineering Transactions*, The Institution of Engineers, Vol. CE 19, No. 2, Sidney, Australia, 1977, pp. 162–165.
18. Nethercot, D. A., and Trahair, N. S., "Lateral Buckling Calculations for Braced Beams," *Civil Engineering Transactions*, The Institution of Engineers, Vol. CE 19, No. 2, Sidney, Australia, 1977, pp. 211–214.

Appendix II.—Notation

The following symbols are used in this paper:

E = modulus of elasticity;

E_t = approximate tangent modulus of elasticity;

F_{cr} = critical column buckling axial stress;

F_y = yield stress;

G = modulus of rigidity;

G_t = approximate tangent modulus of rigidity;

I_x = moment of inertia about beam's x-axis;

I_y = moment of inertia about beam's y-axis;

I_w = warping moment of inertia;

K = torsional constant;

M_p = plastic bending moment;

M_u = ultimate buckling bending moment;

M_x = bending moment about beam's x-axis;

M_z = torsional moment about beam's z-axis;

V = vertical shear in beam;

$\{U\}$ = lateral deflection vector;

$\{\Phi\}$ = rotational deflection vector;

r = radius of gyration;

u = lateral deflection in positive x-axis direction;

v = vertical deflection in positive y-axis direction;

ϕ = rotation about longitudinal z-axis;

M_{cr} = bending moment causing initiation of lateral deflection and twist;

M_m = post buckling ultimate bending moment;

σrc = compressive residual stress; and

σrt = tensile residual stress.

TORSIONAL COUPLING AND EARTHQUAKE RESPONSE
OF SIMPLE ELASTIC AND INELASTIC SYSTEMS

By Christopher L. Kan[1] and Anil K. Chopra,[2] M. ASCE

INTRODUCTION

Lateral and torsional motions are coupled in the response of buildings to earthquake ground motion if the centers of story resistance do not coincide with the centers of floor masses. Assuming linearly elastic force-deformation relations, the earthquake response of idealized buildings with eccentric centers of mass and resistance has been the subject of many studies (see Refs. 4 and 5 for an extensive bibliography). Results of these studies of linear response are not directly applicable to calculating the design forces for buildings because they are usually designed to deform significantly beyond the yield limit during moderate to very intense ground shaking. Thus, there is a need to study the response beyond the linearly elastic range of behavior of torsionally coupled buildings.

Previous studies (1,7) have been concerned with one-story structures with each resisting element (column or wall) idealized by two springs acting independently in two perpendicular, lateral directions and each spring having an elastic-perfectly-plastic force-deformation relationship. Whether it is reasonable to neglect the influence of interaction of forces on yielding behavior is a question that apparently has not been studied. Although these studies have provided valuable information concerning the response of particular systems, it has not been possible to generalize the results and to arrive at widely applicable conclusions because of the many parameters affecting the behavior of such systems.

This study is concerned with systems in which torsional coupling in the linearly elastic range of behavior arises only from eccentricity between center of mass and center of resistance, and with input ground motions that are uniform over the base of the structure and contain no rotational components. The objectives of this study of earthquake response of torsionally-coupled systems in both elastic and inelastic ranges of behavior are: (1) To investigate the influence

[1] Asst. Research Engr., Dept. of Civ. Engrg., Univ. of California, Berkeley, Calif. 94720.

[2] Prof. of Civ. Engrg., Dept. of Civ. Engrg., Univ. of California, Berkeley, Calif. 94720.

of the basic system parameters on the response; and (2) to evaluate the effects of torsional coupling on lateral and torsional deformations of the system and on deformations of individual resisting elements.

SYSTEMS, GROUND MOTION, AND METHOD OF ANALYSIS

One-Story System.—The idealized one-story structure in Fig. 1(a) consists of a rigid deck supported on massless, axially inextensible columns and walls. The three degrees of freedom of the system are lateral displacements u_x and u_y of the center of mass (CM) of the deck, relative to the ground, along the
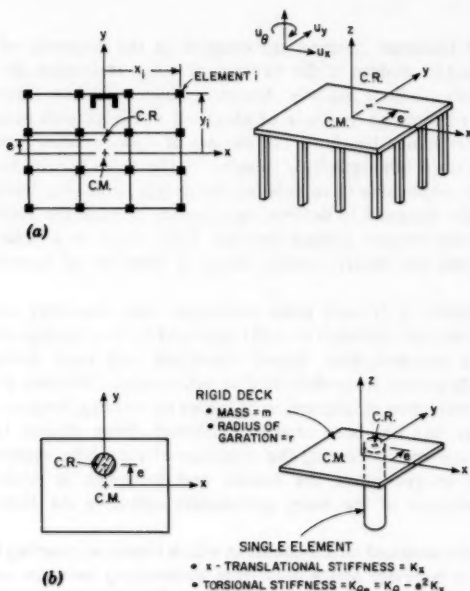
FIG. 1.—(a) Idealized One-Story System; and (b) Its Single-Element Model

principal axes of resistance of the structure, x and y; and the torsional displacement (rotation) u_θ of the deck about the vertical axis.

Let k_{ix} and k_{iy} represent the lateral stiffness of the ith resisting element (column or wall) along the principal axes of resistance x and y, respectively. Then

$$K_x = \sum_i k_{ix} \quad \text{and} \quad K_y = \sum_i k_{iy} \quad \ldots \ldots \ldots \ldots \ldots \ldots \ldots \ldots \ldots (1)$$

are the lateral stiffnesses of the structure in the x and y directions, respectively. With the origin at the center of mass, let (x_i, y_i) define the location of the

ith resisting element [Fig. 1(a)]. Then

$$K_\theta = \sum_i k_{ix} y_i^2 + \sum_i k_{iy} x_i^2 \quad \dots \dots \dots \dots \dots \dots \dots \dots \dots \dots \dots \dots (2)$$

is the torsional stiffness of the structure defined at the center of mass. The torsional stiffnesses of the individual resisting elements are not included because they are negligible.

The center of resistance (CR) is the point in the plan of the rigid deck through which a horizontal force must be applied in order that it may cause translation without torsion. For a system with discrete resisting elements, the center of resistance is located at distances e_x and e_y, the static eccentricities, in which

$$e_x = \frac{1}{K_y} \sum_i x_i k_{iy} \quad \text{and} \quad e_y = \frac{1}{K_x} \sum_i y_i k_{ix} \dots \dots \dots \dots \dots \dots \dots (3)$$

measured from the center of mass along the x-and y-axes.

The structure is assumed to be symmetric with respect to one of the principal axes of resistance, the y-axis [Fig. 1(a)]; consequently, $e_x = 0$ and translational motions of the structure in the y direction are not coupled with the torsional motions and may be considered separately. The two degrees of freedom in which coupling occurs are: (1) Lateral displacement u_x; and (2) torsional displacement u_θ.

Within the range of linear behavior, the coupled lateral-torsional response of the system of Fig. 1(a) to ground acceleration along the x-axis is characterized by the following system parameters: e/r in which $e = e_y$ and r = radius of gyration of the deck about a vertical axis through the center of mass

$$\omega_x = \sqrt{\frac{K_x}{m}} \quad \text{and} \quad \omega_\theta = \sqrt{\frac{K_\theta}{mr^2}} \quad \dots \dots \dots \dots \dots \dots \dots \dots \dots \dots (4)$$

in which m = mass of the deck; and the damping ratio ξ, assumed to be the same in each mode of vibration. The two frequency parameters ω_x and ω_θ may be interpreted as the uncoupled frequencies of the system, the natural circular frequencies of the system if the system were torsionally uncoupled $(e = 0)$.

The resisting elements in the system are assumed to be elastic-perfectly-plastic. For each column, the elastic stiffnesses in the x and y directions are the same. Similarly, the yield shears of each column in the x and y directions are assumed to be the same. Yield shears for individual columns are proportional to their stiffnesses. The fully plastic shear and torque for the system are V_{xp} and T_{Rp}. The system will become a mechanism under the separate action of V_{xp} at the CR and T_{Rp} about the CR.

Single Element Model.—It has been shown (6) that the multi-element system of Fig. 1(a) and the single element model of Fig. 1(b) are equivalent for purposes of calculating linear response—lateral and torsional deformations u_x and u_θ at the CM and the associated total shear and torque—provided the values for the parameters ω_x and ω_θ, and e/r and ξ are the same for the two systems.

Response in the inelastic range of behavior is controlled by the yield shear and torque and the basic parameters of the corresponding linear system. It has been shown (6) that the inelastic response of a multi-element system can

be determined to a useful degree of approximation by analyzing a single-element model with the following properties. Parameters ω_x, ω_θ, e/r, and ξ in the linearly elastic range of behavior are the same as those for the multi-element system; a single yield surface defined in terms of the total forces for the system shear V_x in the x direction and torque T_R defined at the center of resistance (shear V_y in the y direction = 0) as follows:

$$\left(\frac{V_x}{V_{xp}}\right)^2 + \left(\frac{T_R}{T_{Rp}}\right)^2 = 1 \quad \dots \dots \dots \dots \dots \dots \dots \dots \dots \dots \dots \dots \dots \dots (5)$$

with yield shear V_{xp} the same as for the multi-element system and yield torque T_{Rp} given by

$$\frac{T_{Rp}}{r V_{xp}} = q \left[\left(\frac{\omega_\theta}{\omega_x}\right)^2 - \left(\frac{e}{r}\right)^2 \right] \quad \dots \dots \dots \dots \dots \dots \dots \dots \dots \dots \dots \dots (6)$$

in which q = a coefficient between 0.58 and 0.86 that depends on the number, type, and location of resisting elements in the structure.

System Properties.—Values were selected for the parameters of the single element system [Fig. 1(b)]: $T_x (= 2\pi/\omega_x)$ = several values in the range 0.5 sec–2.0 sec; ω_θ/ω_x = 0.8, 1.0, 1.25, and 2.0; e/r = 0, 0.2, and 0.4, and ξ = 0.02. The first of the e/r values indicates no torsional coupling and provides a basis for evaluating the effects of torsional coupling.

The selected values for T_x span a range of vibration periods which would include many multistory buildings. Measured natural frequencies of vibration of buildings (2) indicate that the ratio of the natural frequency of the lowest torsion-dominant mode to that of the lowest translation-dominant mode of vibration varies between 1.0 and 1.8. If these measurements were for the system of Fig. 1, it could be concluded that ω_θ/ω_x values would be within the range of 1.0 and 1.8 (4,5). Considering the one-story system of Fig. 1 to be a three degree-of-freedom model to represent the three lowest vibration modes of a multistory building, the aforementioned conclusion forms the basis for the chosen range of values for ω_θ/ω_x. Because $\omega_\theta/\omega_x < 1$ is uncommon unless the major resistance to lateral loads is provided by a central core, and $\omega_\theta/\omega_x > 2$ implies negligible torsional coupling (4), values for ω_θ/ω_x were chosen in the range 0.8–2.0. The chosen eccentricity ratios e/r = 0.2 and 0.4 represent significant eccentricities between centers of mass and resistance (for a rectangular building plan, e/r = 0.4 represents eccentricity of 11.5%–16.3% of the longer plan dimension) and e/r = 0 represents the corresponding torsionally-uncoupled system. Because effects of torsional coupling decrease as damping increases (4), the damping ratio was assigned a value which is on the low side but yet reasonable for many buildings.

Corresponding to each linearly elastic system with specified parameters ω_x (or $T_x = 2\pi/\omega_x$), ω_θ/ω_x, e/r and ξ, an inelastic system is defined to have the same properties in its linear range of behavior. The yield shear in translation is specified in Table 1 as the base shear determined from Fig. 2(b), corresponding to the natural period T_x of the corresponding torsionally-uncoupled system and ductility factor μ = 5. Yield torque for the system is specified as the torque determined from Eq. 6 with q = 0.75.

Ground Motion.—The ground motion considered is the first 30 sec of the

TABLE 1.—Yield Shears for Inelastic Systems

Uncoupled period, T_x, in seconds (1)	(Yield shear, V_{xp}/mg) 100 (2)
0.5	13.81
0.6	16.34
0.7	17.52
0.8	15.51
0.9	11.87
1.0	9.13
1.2	6.85
1.4	5.43
1.6	4.66
1.8	4.24
2.0	3.90
2.25	3.05
2.5	2.40
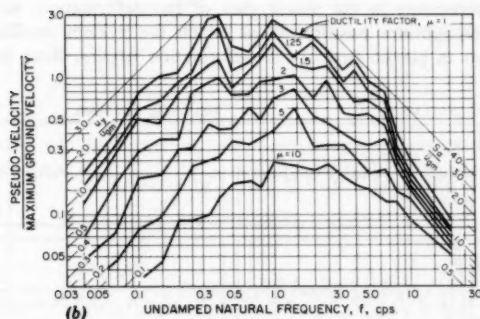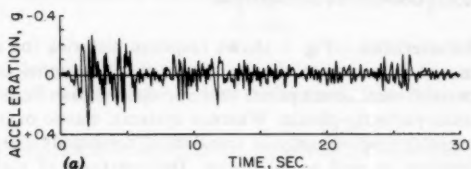
FIG. 2.—(a) SOOE Component of Imperial Valley Earthquake, May 18, 1940, El Centro, Imperial Valley Irrigation District; and (b) Deformation Spectra for Elastic-Perfectly Plastic Systems with 2% Critical Damping Subjected to El Centro Earthquake (from Ref. 8): Maximum Ground Displacement, $u_{gm} = 8.28$ in.; Maximum Ground Velocity = 13.68 in./sec; Maximum Ground Acceleration, $\ddot{u}_{gm} = 0.32$ g; and u_y = Yield Displacement

SOOE component of the El Centro record obtained during the Imperial Valley earthquake of May 18, 1940. The ground acceleration history presented in Fig. 2(a) is the most recent digitization with "standard" base line correction (3). However, the response spectra of Fig. 2(b) (8) from which the yield shears were obtained above is based on an earlier digitization of the record with parabolic base line correction.

Method of Analysis.—Earthquake response of each single element system, with properties mentioned earlier, to the El Centro ground motion is determined by solving the equations of motion by a numerical integration procedure (5,6). The time scale is discretized into equal intervals, small enough (0.02 sec or less) to define the earthquake accelerogram accurately, and no more than a small fraction (1/20th) of the shorter natural period of linearly elastic vibration of the system. Within each small time interval, the lateral and torsional accelerations of the deck were assumed to vary linearly. For the time intervals during which transition from elastic to plastic state or from one plastic state to another occurred, the tangent stiffness was reevaluated and a predictor-corrector iteration procedure was used to reduce force unbalances created by the numerical approximation to an acceptably small value.

EFFECTS OF TORSIONAL COUPLING ON DEFORMATIONS

Response Characteristics.—Fig. 3 shows response histories for a torsionally-coupled system and the corresponding system with no torsional coupling, each analyzed for two different assumptions of force-deformation behavior, linearly elastic, and elastic-perfectly-plastic. Whereas systems, elastic or inelastic, with no torsional coupling respond only in translation, torsionally-coupled systems deform in translation as well as in torsion. Deformations of elastic systems, with or without torsional coupling, are oscillations about the initial equilibrium position. On the other hand, responses of inelastic systems are characterized by several increments in the plastic part of the deformation, each causing a shift in the equilibrium position about which the system oscillates until the next increment in plastic part of the deformation occurs. Both the oscillatory
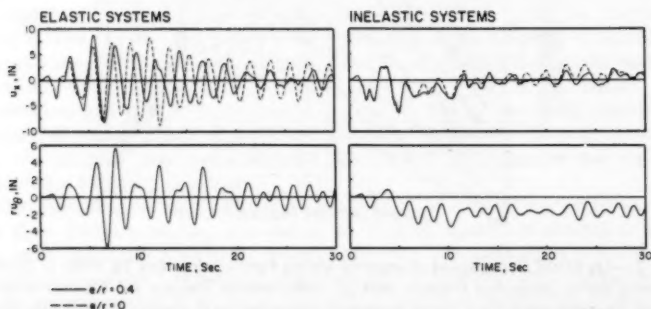
FIG. 3.—Response of Elastic and Inelastic Systems to El Centro Earthquake, System Properties: $T_x = 2$ sec; $\omega_\theta/\omega_x = 1.25$; and $\xi = 2\%$ (1 in. = 25.4 mm)
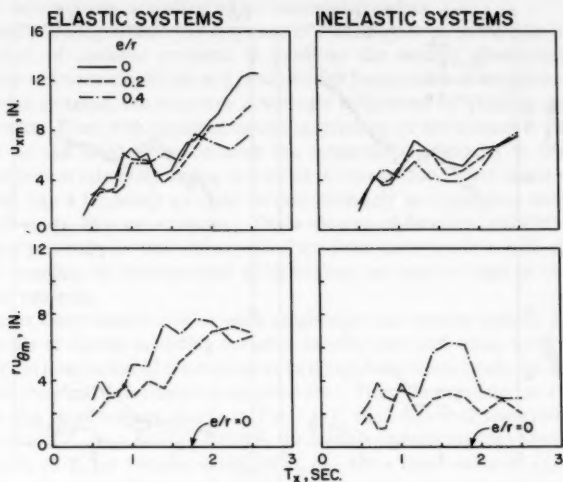
FIG. 4.—Maximum Lateral and Torsional Displacements for Elastic and Inelastic Systems with $\omega_\theta/\omega_x = 0.8$ Subjected to El Centro Earthquake (1 in. = 25.4 mm)
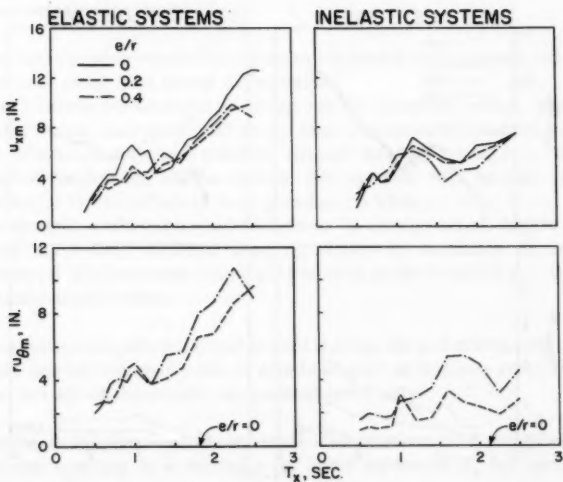
FIG. 5.—Maximum Lateral and Torsional Displacements for Elastic and Inelastic Systems with $\omega_\theta/\omega_x = 1$ Subjected to El Centro Earthquake (1 in. = 25.4 mm)
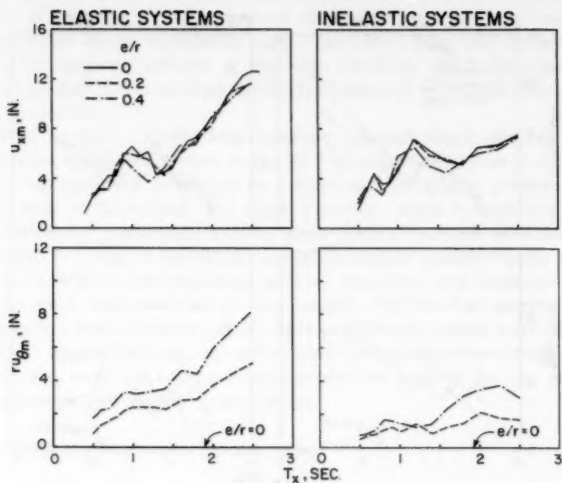
FIG. 6.—Maximum Lateral and Torsional Displacements for Elastic and Inelastic Systems with $\omega_\theta/\omega_x = 1.25$ Subjected to El Centro Earthquake (1 in. = 25.4 mm)
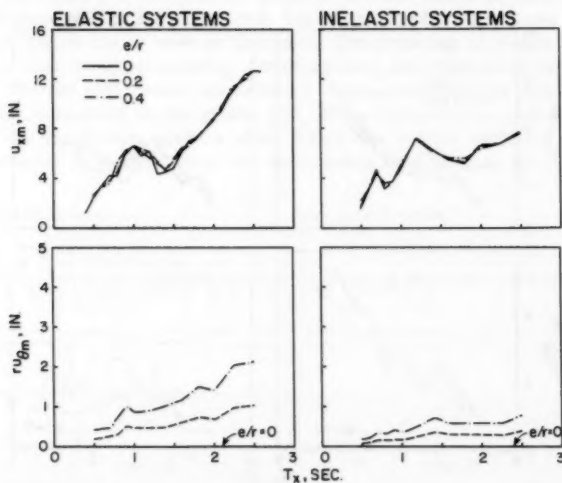
FIG. 7.—Maximum Lateral and Torsional Displacements for Elastic and Inelastic Systems with $\omega_\theta/\omega_x = 2$ Subjected to El Centro Earthquake (1 in. = 25.4 mm)

part of the lateral deformation and the drift of the equilibrium position due to plastic deformation, are affected by torsional coupling.

Torsional coupling affects the response of elastic systems more than it affects the response of inelastic systems. It modifies the natural vibration periods, and thus the response amplitude and predominant frequencies of inelastic systems. For inelastic systems, the response is strongly influenced by yielding properties of the system. Even with torsional coupling, yielding of the system is controlled primarily by the yield shear because the response is primarily in translation and the system is relatively strong in torsion. Consequently, after initial yielding, the system has a tendency to yield further primarily in translation and behave more and more like an inelastic, single degree-of-freedom (SDOF) system responding primarily in translation; thus, torsional deformations and effects of torsional coupling on translational deformations are not as large as they were for elastic systems.

Maximum Deformations.—For each single-element system defined earlier, a complete set of results including variation of response with time, were obtained by numerical integration of the equations of motion. However, only the maximum lateral and torsional deformations are presented. They are presented as a function of T_x for the three values of e/r in Figs. 4–7; each figure is for systems with a fixed value of ω_θ/ω_x. In Figs. 8 and 9, the maximum deformations are presented as functions of T_x for varying values of ω_θ/ω_x but a fixed value of e/r.

In order to interpret these results, it is useful to summarize selected conclusions from an earlier investigation on maximum responses of linearly elastic systems determined for two idealized response spectra, flat (or period-independent) pseudo-acceleration spectrum and hyperbolic pseudo-acceleration spectrum (or flat pseudo-velocity spectrum) (4).

1. Torsional coupling results in torque (and torsional deformation) and smaller values for base shear (and lateral deformation).

2. As e/r increases, torsional coupling has an increased effect, shear (and lateral deformation) decreases, and torque (and torsional deformation) increases.

3. The effects of torsional coupling depend strongly on ω_θ/ω_x, the ratio of uncoupled frequencies of the system. For systems with smaller values of e/r (less than 0.4), this effect is most pronounced when $\omega_\theta = \omega_x$.

4. For systems with uncoupled frequency in torsion much higher than in translation, $\omega_\theta > 2\omega_x$, torsional coupling results in essentially no reduction in base shear; furthermore the torque is essentially proportional to e/r, indicating little dynamic amplification.

In this investigation wherein actual ground motions instead of idealized response spectra are considered, responses of elastic as well as inelastic systems exhibit some, but not all, of the results summarized previously.

1. Torsional coupling causes torsional deformations and modifies lateral deformations resulting in a decrease for some values of T_x but increase for others (Figs. 4–7).

2. As e/r increases, the effects of torsional coupling may or may not increase; lateral deformations decrease for some values of T_x but increase for other values; and torsional deformations increase for almost all values of T_x (Figs. 4–7).
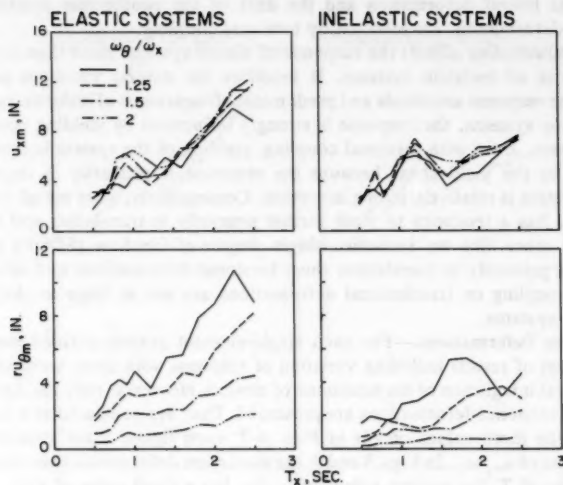
FIG. 8.—Maximum Lateral and Torsional Displacements for Elastic and Inelastic Torsionally Coupled Systems with $e/r = 0.4$ Subjected to El Centro Earthquake (1 in. = 25.4 mm)
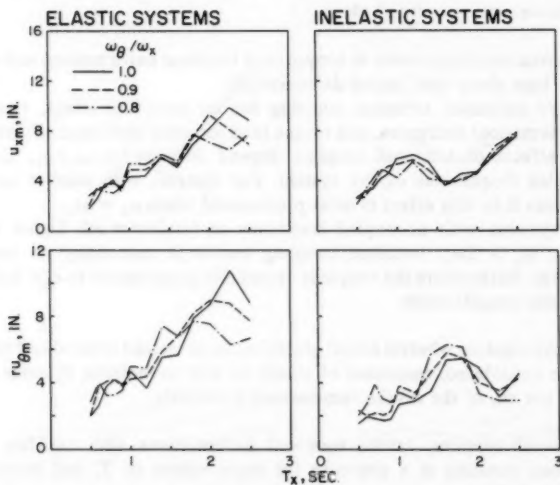
FIG. 9.—Maximum Lateral and Torsional Displacements for Elastic and Inelastic Torsionally Coupled Systems with $e/r = 0.4$ Subjected to El Centro Earthquake (1 in. = 25.4 mm)

3. For systems with $\omega_\theta / \omega_x = 2$, torsional coupling produces little modification in the lateral deformation and the torsional deformation is essentially proportional to e/r, indicating no dynamic amplification (Fig. 7).

4. The effects of torsional coupling—change in lateral deformation and increase in torsional deformation—depend on ω_θ / ω_x (Figs. 8 and 9) but not as strongly, nor in as simple a manner, as was previously mentioned for idealized response spectra. As ω_θ / ω_x approaches one from above, the torsional deformation of elastic systems and almost all inelastic systems increase over the entire range of T_x considered; however, there is no consistent variation in the lateral deformation, which decreases for some values of T_x and increases for others. As ω_θ / ω_x approaches one from below, the effects of torsional coupling vary with ω_θ / ω_x in an apparently unsystematic manner.

The general impression that emerges from the aforementioned results is that effects of torsional coupling on earthquake response are similar to, but not as simple as, those observed from maximum responses determined for idealized response spectra. Complications arise because the response spectrum of an actual ground motion is irregular compared to the flat or hyperbolic shapes assumed for the idealized acceleration response spectrum. Torsional coupling affects the natural periods of vibration of the system and thus the corresponding spectrum ordinates. Depending on the variation of the response spectrum in the neighborhood of T_x, these ordinates may increase or decrease by varying degrees, resulting in another factor influencing the differences between the responses of torsionally-coupled and uncoupled systems.

Torsional coupling influences the maximum deformation response of inelastic systems less than it influences linearly elastic systems (Figs. 4–9), for reasons mentioned under "Response Characteristics." Except for that one difference, inelastic and elastic systems are affected similarly by torsional coupling.

EFFECTS OF TORSIONAL COUPLING ON COLUMN DEFORMATIONS

The deformation of a resisting element (column or wall) results from the combined effect of lateral and torsional displacements at the CM. In the preceding section the effects of torsional coupling on displacement response at the CM were studied. Results for the deformations of corner columns are presented and interpreted in this section. Recall that the displacements at the CM of a torsionally-coupled system were determined from analysis of a single-element model of the system. For a specified set of overall system parameters, the plan geometry did not affect the displacements at the CM but will influence the deformations of corner columns.

Column Deformations and Displacements at Center of Mass.—Considering rectangular plans with several resisting elements including columns at the four corners, u_{ix} and u_{iy}, the x and y components of the deformation of column i (displacement of the top of the column relative to its bottom) can be expressed in terms of u_x and u_θ, the lateral and torsional displacements at the CM simply from the geometry of displacement (Fig. 10)

$$\frac{u_{ix}}{u_x} = 1 - \frac{a}{r}\left(\frac{ru_\theta}{u_x}\right), \ i = 1, 2; \quad \frac{u_{ix}}{u_x} = 1 + \frac{a}{r}\left(\frac{ru_\theta}{u_x}\right), \ i = 3, 4;$$
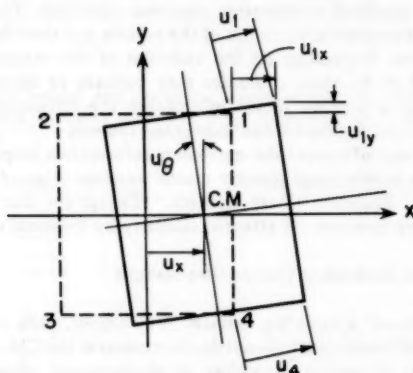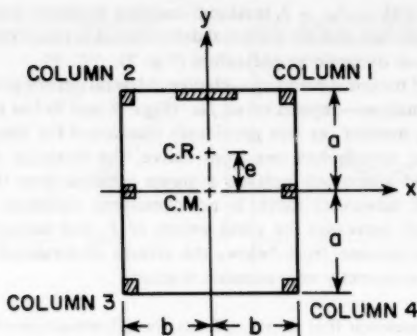
FIG. 10.—Rectangular Plan and Its Displaced Configuration

$$\frac{u_{iy}}{u_x} = \frac{b}{r}\left(\frac{ru_\theta}{u_x}\right), \ i = 1, 4; \quad \frac{u_{iy}}{u_x} = -\frac{b}{r}\left(\frac{ru_\theta}{u_x}\right), \ i = 2, 3 \ \ldots \ldots \ldots \ldots (7)$$

The total vector deformation of the column i

$$u_i = \sqrt{u_{ix}^2 + u_{iy}^2} \ \ldots \ldots \ldots \ldots \ldots \ldots \ldots \ldots \ldots \ldots \ldots \ldots \ldots (8)$$

It is necessary to examine the results for only two columns, say column 1 and column 4, because from Eqs. 7 and 8

$$u_1 = u_2 \quad \text{and} \quad u_3 = u_4 \ \ldots \ldots \ldots \ldots \ldots \ldots \ldots \ldots \ldots \ldots \ldots (9)$$

Column 1 is located closer to the CR than is column 4.

Response to Static Lateral Force.—To aid in interpreting the results to be

presented later for column deformations in torsionally-coupled systems subjected to earthquake ground motion, it will be useful to consider first the effects of a static lateral force, V_x, applied at the CM. The resulting deformations, u_i, of the four columns, expressed as ratios with u_x, are given by Eqs. 7 and 8 wherein it can be easily shown

$$\frac{r u_\theta}{u_x} = \frac{e}{r} \left(\frac{\omega_x}{\omega_\theta} \right)^2 \dots \dots \dots \dots \dots \dots \dots \dots \dots \dots \dots (10)$$

Furthermore, for rectangular plans

$$\frac{a}{r} = \sqrt{\frac{3}{1 + \left(\frac{b}{a} \right)^2}} \quad \text{and} \quad \frac{b}{r} = \frac{b}{a} \left(\frac{a}{r} \right) \dots \dots \dots \dots \dots (11)$$

Consequently, ratios u_i/u_x depend only on the dimensionless parameters e/r, ω_θ/ω_x, and a/b. They are presented as functions of ω_θ/ω_x for selected values
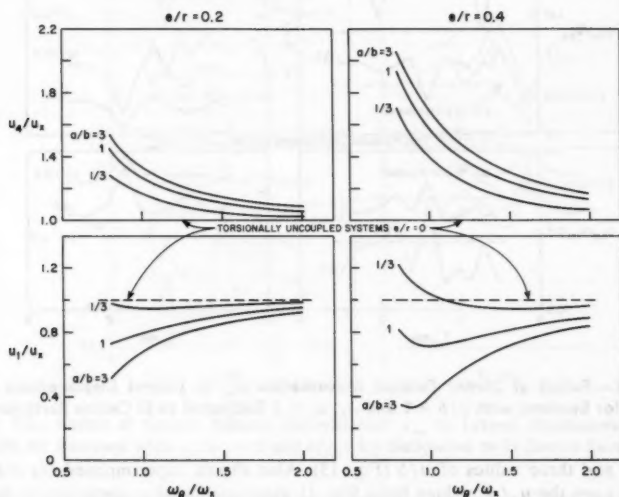
FIG. 11.—Ratios of Corner Column Deformations to Lateral Displacement at CM for Static Shear Force Applied at CM

of e/r and a/b (Fig. 11). If the system is torsionally uncoupled, $u_i/u_x = 1$, differences between this value and those presented in Fig. 11 may therefore be interpreted as effects of torsional coupling on column deformations. Torsional coupling causes an increase in the deformation of the column farthest from the CR but generally a decrease in the deformation of the column nearest the CR. Torsional coupling has increased effects, i.e., u_4/u_x increases and u_1/u_x

decreases, with increasing e/r for fixed a/b and with increasing a/b for fixed e/r.

Earthquake Responses.—Responses of an elastic and corresponding inelastic single-element system to the El Centro ground motion acting along the x-axis were obtained in the preceding section for several values of the system parameters: T_x, ω_θ/ω_x, and e/r. From the history of displacements at the CM of each system (specified T_x, ω_θ/ω_x, and e/r) deformations of corner columns were determined by applying Eqs. 7 and 8 at each instant of time. Ratios u_{im}/u_{xm}, in which u_{im} and u_{xm} are, respectively, the maximum values of displacements during the earthquake at column i and at the CM, were then computed for several different values of the aspect ratio a/b of the rectangular plan.

Results for systems with $\omega_\theta/\omega_x = 2$ are presented as functions of T_x for a fixed value of a/b and two values of e/r (Fig. 12) and for a fixed value

FIG. 12.—Ratios of Corner Column Deformation u_{im} to Lateral Displacement u_{xm} at CM for Systems with $a/b = 1$ and $\omega_\theta/\omega_x = 2$ Subjected to El Centro Earthquake

of e/r and three values of a/b (Fig. 13). Also shown superimposed for elastic systems are the u_i/u_x values from Fig. 11 associated with a static lateral force acting at the CM. Whereas these are independent of T_x, the u_{im}/u_{xm} values obtained from response to earthquake ground motion are not. This dependence on T_x is, however, weak, and is associated with changes in earthquake responses due to changes in vibration periods caused by torsional coupling. Torsional coupling causes increase and decrease in the deformations of columns farthest and nearest, respectively, from the CR (Figs. 12 and 13) and the effects of torsional coupling increase with increasing e/r (Fig. 12) and increasing a/b (Fig. 13). These effects are similar to those observed in systems subjected to static force. It is therefore concluded that for systems with $\omega_\theta/\omega_x = 2$ the effects of torsional coupling on column deformations are similar whether

the deformations are induced by earthquake motion or static lateral force. This observation is consistent with the one of the preceding section, indicating that for systems with $\omega_\theta / \omega_x \geq 2$ effects of torsional coupling on displacements at the CM are similar whether they are due to earthquake motion or static lateral force.

In Figs. 12 and 13, the effects of torsional coupling on deformations of corner columns are less for inelastic systems than for elastic systems. Because the yield torque increases with the square of ω_θ / ω_x (Eq. 6), systems with $\omega_\theta / \omega_x = 2$ are relatively strong in torsion. As a result, it is the yield shear that controls the initial yielding, and subsequently the system has a tendency to yield further primarily in translation and behave more and more like an inelastic, single

FIG. 13.—Ratios of Corner Column Deformation u_{im} to Lateral Displacement u_{xm} at CM for Systems with $\omega_\theta / \omega_x = 2$ and $e/r = 0.4$ Subjected to El Centro Earthquake

degree-of-freedom system, responding primarily in translation. Thus, the effects of torsional coupling on column deformations are not as large as they are for elastic systems.

The deformation ratios u_{im} / u_{xm} are presented for systems with $\omega_\theta / \omega_x = 1$ as functions of T_x for a fixed value of a/b but two values of e/r (Fig. 14) and for a fixed value of e/r but several values of a/b (Fig. 15). As apparent in the preceding section, the effects of torsional coupling are especially pronounced for systems with $\omega_\theta = \omega_x$, and this is reflected in the results for column deformations, i.e., u_{im} / u_{xm} are considerably different than one, the value with no torsional coupling. It is of interest to compare the ratio u_i / u_x obtained from deformations due to: (1) A static lateral force through the CM
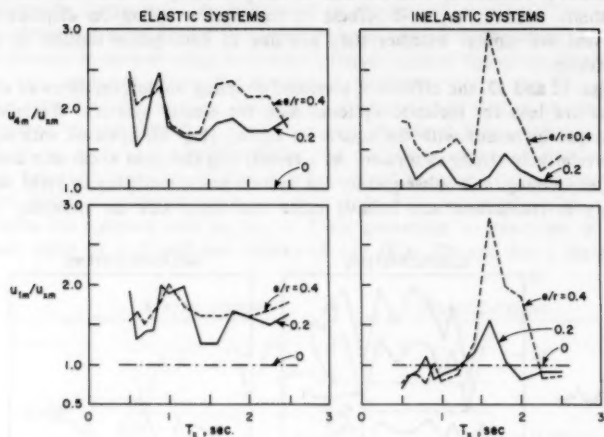
FIG. 14.—Ratios of Corner Column Deformation u_{im} to Lateral Displacement u_{xm} at CM for Systems with $a/b = 1$ and $\omega_\theta/\omega_x = 1$ Subjected to El Centro Earthquake
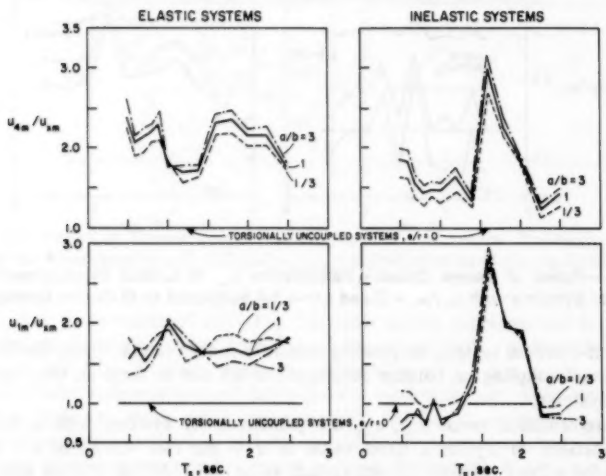
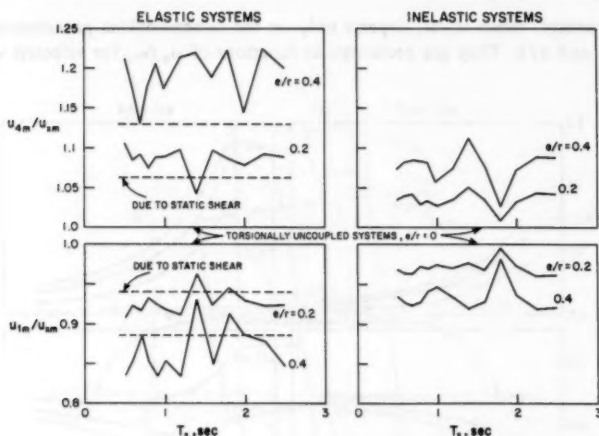FIG. 15.—Ratios of Corner Column Deformation u_{im} to Lateral Displacement u_{xm} at CM for Systems with $\omega_\theta/\omega_x = 1$ and $e/r = 0.4$ Subjected to El Centro Earthquake

(Fig. 11); and (2) earthquake ground motion (Figs. 14 and 15). Whereas in the former case the u_1/u_x ratio is typically smaller than 1 and $u_4 > u_1$ (Fig. 11), in the latter case $u_1/u_x > 1$ and for some systems $u_4 < u_1$, a consequence of the large earthquake-induced torques in systems with $\omega_\theta/\omega_x = 1$. The deformation ratios u_{im}/u_{xm} tend to increase with e/r (Fig. 14) and also have some, but not consistent, tendency to increase with a/b (Fig. 15).

For systems with parameter values $\omega_\theta/\omega_x = 1$ and $e/r = 0.2$, torsional coupling affects column deformations in inelastic systems less than column deformations in elastic systems (Fig. 14). This result is similar to the one observed earlier for systems with $\omega_\theta/\omega_x = 2$ (Figs. 12 and 13). However, inelastic systems can be affected to a greater degree; witness the large peak in the neighborhood of $T_x = 1.6$ sec for systems with $e/r = 0.4$. This very pronounced effect of torsional coupling is a consequence of especially unfavorable phasing of
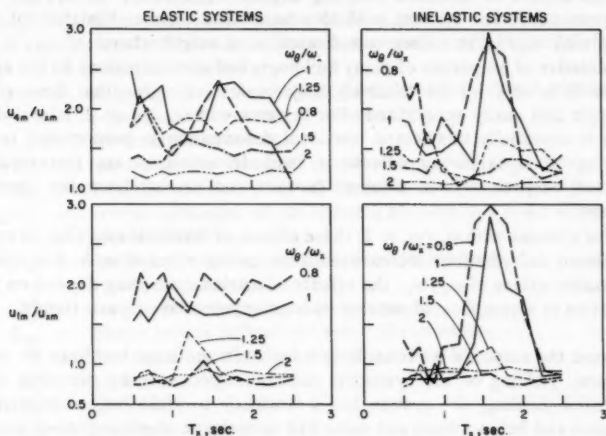
FIG. 16.—Ratios of Corner Column Deformation u_{im} to Lateral Displacement u_{xm} at CM for Systems with $a/b = 1$ and $e/r = 0.4$ Subjected to El Centro Earthquake

u_x and u_θ in this particular case, causing their maximum values to occur almost simultaneously.

As noted in the preceding section, the effects of torsional coupling on u_x and u_θ, the lateral and torsional displacements of the CM, depend on ω_θ/ω_x in a complicated manner. Because column deformations u_i depend on u_x and u_θ, variation of deformation ratios u_{im}/u_{xm} with ω_θ/ω_x is similarly complicated (Fig. 16). Because of torsional coupling, column deformations can be amplified by a factor as large as two–three for systems with $\omega_\theta/\omega_x = 1$ (Fig. 16).

CONCLUSIONS

The principal conclusions of this study concerned with coupled lateral (x)-torsional (θ) response of one-story structures, symmetric about the y principal

axis of resistance, to ground motion along the x-axis may be summarized as follows.

The effects of torsional coupling on the maximum deformation response of inelastic systems are, in general, qualitative terms similar to those for elastic systems. These effects depend in a complicated manner on the system parameters with few apparent systematic trends. The more important of these effects may be summarized as follows.

1. Torsional coupling causes torsional deformation in the system and modifies, increases, or decreases, the lateral deformation of the system. Deformation of an individual column is also modified compared to the lateral deformation of the system. The latter quantity is also the column deformation in torsionally uncoupled systems.

2. The effects of torsional coupling depend significantly on ω_θ / ω_x, being most pronounced for systems with this ratio close to one. Variation of these effects with ω_θ / ω_x is rather complicated in a neighborhood of $\omega_\theta / \omega_x = 1$, representative of properties of many buildings, and generalizations do not appear possible. It is only for the relatively larger values of ω_θ / ω_x that these effects are simple and easily generalized. For systems with $\omega_\theta / \omega_x \geq 2$, lateral deformation is essentially unaffected, torsional deformation is proportional to e/r, indicating no dynamic amplifications, and deformations are increased and decreased, respectively, in columns farthest and nearest from the center of resistance.

3. For systems with $\omega_\theta / \omega_x \geq 2$, these effects of torsional coupling on system and column deformations increase with increasing e/r and a/b. For systems with smaller values of ω_θ / ω_x, the effects of torsional coupling depend on these parameters in a complicated manner with no apparent systematic trends.

Because the response is primarily in translation and most buildings are strong in torsion, yielding of the system is controlled primarily by the yield shear; after initial yielding, the system has a tendency to yield further primarily in translation and behave more and more like an inelastic single-degree-of-freedom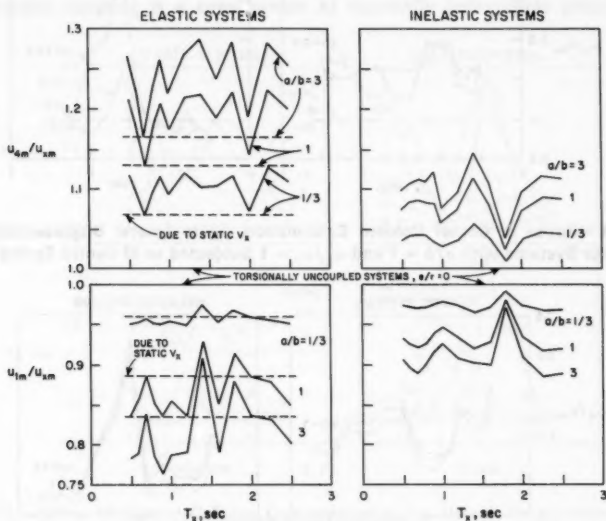 system, responding primarily in translation. Thus, torsional coupling generally affects maximum deformations in inelastic systems to a lesser degree compared to corresponding linearly elastic systems.

APPENDIX I.—REFERENCES

1. Erdik, M. O., "Torsional Effects in Dynamically Excited Structures," *Ph.D. Thesis*, Rice University, Houston, Texas, May, 1975.
2. Hart, G. C., DiJulio, R. M., Jr., and Lew, M., "Torsional Response of High-Rise Buildings," *Journal of the Structural Division*, ASCE, Vol. 101, No. ST2, Proc. Paper 11126, Feb., 1975, pp. 397–416.
3. Hudson, D. E., and Brady, A. G., "Strong Motion Earthquake Accelerograms," *Report No. EERL 71-50*, Earthquake Engineering Research Laboratory, California Institute of Technology, Pasadena, Calif., Sept., 1971.
4. Kan, C. L., and Chopra, A. K., "Effects of Torsional Coupling on Earthquake Forces in Buildings," *Journal of the Structural Division*, ASCE, Vol. 103, No. ST4, Proc. Paper 12876, Apr., 1977, pp. 805–819.
5. Kan, C. L., and Chopra, A. K., "Linear and Nonlinear Earthquake Response of Simple Torsionally Coupled Systems," *Report No. UCB/EERC-79/03*, Earthquake

Engineering Research Center, University of California, Berkeley, Calif., Feb., 1979, 102 pp.
6. Kan, C. L., and Chopra, A. K., "Simple Model for Earthquake Response Studies of Torsionally Coupled Buildings," *Journal of the Engineering Mechanics Division,* ASCE, in press.
7. Shibata, A., Onose, J., and Shiga, T., "Torsional Response of Buildings to Strong Earthquake Motions," *Proceedings of the Fourth World Conference on Earthquake Engineering,* Vol. 2, Santiago, Chile, 1969, pp. A4-123–A4-138.
8. Veletsos, A. S., and Newmark, N. M., "Design Procedures for Shock Isolation Systems of Underground Protective Structures," *Report RTD-TDR-63-3096,* Vol. 3, Air Force Weapons Laboratory, Albuquerque, N.M., June, 1964.

APPENDIX II.—NOTATION

The following symbols are used in this paper:

a, b = dimensions of rectangular building plan;

e = static eccentricity, distance measured from center of mass to center of resistance;

e_x, e_y = static eccentricities, distances measured from center of mass along x-and y-axes to center of resistance;

g = gravitational constant;

K_x, K_y = translational stiffness of structure in x and y directions;

K_θ = torsional stiffness of structure defined at center of mass;

k_{ix}, k_{iy} = lateral stiffnesses of ith resisting element in x and y directions;

m = mass of deck;

q = coefficient relating yield torque to yield shear;

r = radius of gyration of deck;

T_R = torque defined at center of resistance;

T_{Rp} = plastic torque defined at center of resistance;

T_x = uncoupled translational period in x direction;

$\ddot{u}_g$ = ground acceleration along x-axis;

u_i = displacement of column i;

u_{im} = maximum value of u_i;

u_{ix}, u_{iy} = displacements of column i in x and y directions;

u_x = horizontal displacement of center of mass, relative to ground, in x direction;

u_{xm} = maximum value of u_x;

u_{xy} = yield displacement in translation;

u_θ = rotation of deck about vertical axis;

$u_{\theta m}$ = maximum value of u_θ;

V_x = base shear of structure in x direction;

V_{xp} = plastic shear of structure;

x_i, y_i = distances of ith resisting element from center of mass;

μ = ductility factor;

ξ = viscous damping factor;

ω_x = uncoupled translational circular frequency; and

ω_θ = uncoupled torsional circular frequency.

Subscripts

i = column or resisting element number;

m = maximum;
p = plastic;
x, y = principal axes of resistance; and
θ = rotation.

APPROXIMATE METHOD FOR LATERAL LOAD
ANALYSIS OF HIGH-RISE BUILDINGS

By Fernand K. E. C. Mortelmans,[1] Guido P. J. M. de Roeck,[2]
and Dionys A. Van Gemert[3]

INTRODUCTION

High buildings are almost exclusively planned as residential or office blocks, or both. Floor live loads are typically small compared to dead loads. Under the influence of dead and live loads, a nonsymmetrical structure can undergo horizontal displacements which are small compared to the horizontal displacement of the floors under wind loading. The higher the building, the more sensitive it becomes to wind action. These wind actions are carried by "wind stiffeners" such as elevator shafts, staircase walls, and transverse partition or gable walls. Without stiffening the dimensions of the columns increase to such an extent that they are no longer justifiable from an architectural point of view.

The placing of the stiffening walls in many cases disturbs the symmetry in the plan of the structure. Fig. 1 shows a typical example of the disposition of transverse stiffeners.

The transverse stiffening is obtained by means of the staircase wall S, the elevator shaft E, and the gable wall W. Assume that the length of the building is large in relation to the depth. The wind direction is perpendicular to the longitudinal wall; h = the uniformly distributed wind load per unit of area. For each floor R is the resultant of the wind forces.

Consider a building with an asymmetrical distribution of the stiffnesses in plan (Fig. 1). Under wind load this building translates in the y direction and the floors rotate in the yoz plane. Consider first the distribution of column forces, assuming only a horizontal displacement in the y direction. Because of the asymmetrical stiffness distribution the transverse forces in the columns and walls of a given floor are also distributed asymmetrically. The resultant of these transverse forces acts at the "shear center" C, at a distance e from the center of the longitudinal wall. The position of the shear center can vary from floor to floor. A true translation in the y direction is only possible if

[1] Prof. of Struct. Engrg., Struct. Engrg. Dept., Katholieke Universiteit Leuven, Belgium.
[2] Lect., Hoger Instituut de Nayer, Mechelen, Belgium.
[3] Prof. of Numerical Analysis of Structures, Katholieke Universiteit Leuven, Belgium.

on each floor the torsional moment $T = R \cdot e$ is compensated.

From this it follows that the building undergoes a rotation under the action of the torsional moments T. Considering this twisting phase separately, we note that the rotation of each floor takes place round its own twisting center, which generally does not coincide with the shear center C of the bending phase. If the twisting phase is to be analyzed, the location of this center of twist is indispensable. This leads, however, to a nonlinear system, which can be solved, for instance iteratively (2,5).

These difficulties are obviated by a global treatment of the bending and twisting phases in one process of calculation. For buildings in which no torsion can occur ($e = 0$), a simple but accurate approximation method for the analysis of bending of symmetrical high-rise frameworks under uniformly distributed wind loading has been developed by Mortelmans (3) and generalized for frame-
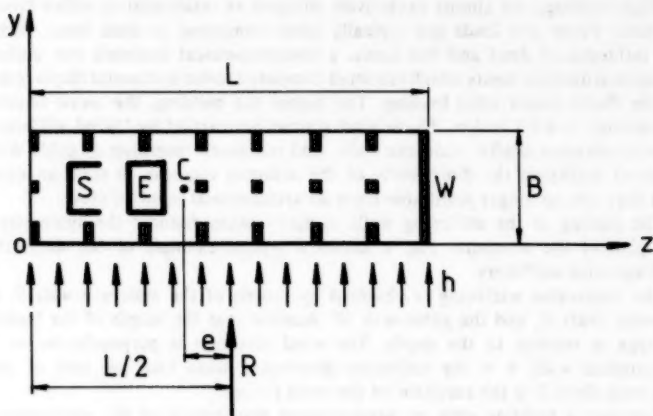
FIG. 1.—Asymmetrical Disposition of Transverse Stiffeners

works in which the column sections and the wind pressure need not be constant over the height of the building (4).

Reported herein is an approximate calculation method for the combined bending and twisting of long, high-rise buildings under wind loading. The method reduces to the solution of a linear system of four equations with four unknowns, which enables the determination of all bending and twisting moments in any element of the structure, regardless of the number of floors, with a surprisingly high degree of accuracy.

APPROXIMATION METHOD PROPOSED

Assumptions.—The method proposed is based upon the following assumptions.

1. The uniformly distributed wind loading acts perpendicularly to the longitudinal wall.

2. The material is homogeneous and linearly elastic.

3. The column and wall sections are constant from the foundation to the roof. The section can, however, vary from one column (wall) to another.

4. The cross beams of the floors between two columns of one frame all have the same moment of inertia.

5. The floors act as diaphragms which are rigid in the horizontal plane.

6. The story height is constant (λ).

7. All columns and walls are fixed at the foundation.

Bending Theory for Symmetric Framework.—Consider first a single plane frame as shown in Fig. 2. It has $n + 1$ columns.

FIG. 2.—Plane Frame
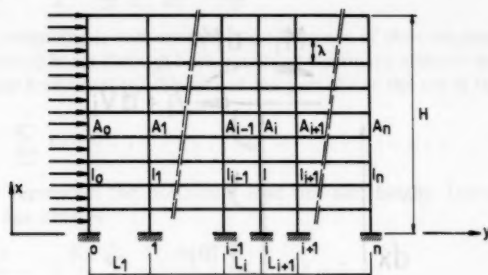
point of contraflexure
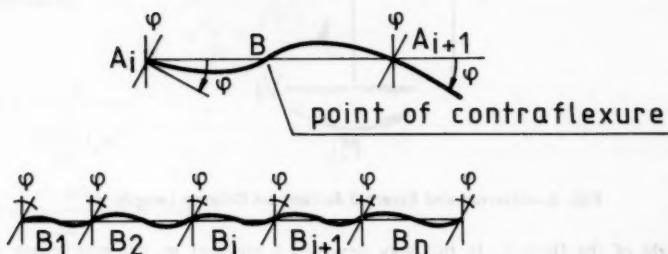
FIG. 3.—Simplified Line of Deformation of Members

Let $I_0, I_1, I_2, \ldots I_n$ be the moments of inertia, respectively, of the columns $0, 1, 2, \ldots n$, and $L_1, L_2, \ldots L_n$ be the distances between successive columns, as shown in Fig. 2. The moment of inertia of each horizontal member is J.

Assuming axial deformations are negligible, all connections of any given member undergo equal horizontal displacements y due to the horizontal wind loading h. Since for high-rise buildings the number of floors is large, it may be assumed for the present that all nodes of any given floor undergo the same rotation ϕ as shown in Fig. 3. The line of deformation of all columns is practically the same, because the height of the floor λ is small in relation to the total

height of the building. In the section on relaxation of nodes a method will be described to take into account the additional deformations, due to the difference in span lengths and stiffnesses.

At the midpoint of a member between two successive columns there is formed a point of contra flexure B, where the vertical displacement is zero. At columns $i - 1$ and i there develops in the member $\overline{A_{i-1}A_i}$ a moment M, equal to

$$M = \frac{6EJ}{L_i} \phi = \frac{6EJ}{L_i} \frac{dy}{dx} \dots \dots \dots \dots \dots \dots \dots \dots \dots \dots \dots \dots \dots (1)$$

This moment M acts as an isolated action on each of columns $i - 1$ and i. If the number of floors is great, these moments can be distributed over the
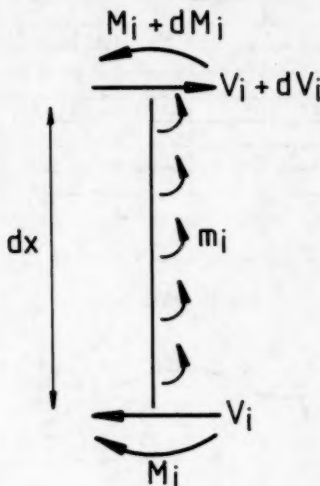
FIG. 4.—Internal and External Actions on Column Length, dx

height of the floor λ. In this way develops a moment m_i per unit length of column i, resulting from the bending of the members $\overline{A_{i-1}A_i}$ and $\overline{A_iA_{i+1}}$ with respective lengths L_i and L_{i+1}. Thus the distributed moment acting on column i is given by

$$m_i = \frac{6EJ}{\lambda} \frac{dy}{dx} \left(\frac{1}{L_i} + \frac{1}{L_{i+1}} \right) \dots \dots \dots \dots \dots \dots \dots \dots \dots \dots (2)$$

From equilibrium of moments of the elementary particle, dx, shown in Fig. 4 results

$$-\frac{dM_i}{dx} - m_i + V_i = 0 \dots \dots \dots \dots \dots \dots \dots \dots \dots \dots \dots \dots \dots (3)$$

From Eq. 2, and using $M_i = -EI_i(d^2 y)/(dx^2)$, Eq. 3 can be written as

$$EI_i \frac{d^3 y}{dx^3} - 6 \frac{EJ}{\lambda} \left(\frac{1}{L_i} + \frac{1}{L_{i+1}} \right) \frac{dy}{dx} + V_i = 0. \quad\ldots\ldots\ldots\ldots\ldots\ldots \quad (4)$$

For any x, the displacement y for all columns is the same due to the rigid diaphragm assumption. The derivatives $(dy)/(dx)$ and $(d^3/y)/(dx^3)$ are then equal for all columns as well.

Summing the equilibrium equations (Eq. 4) for each column (at the same distance x from the origin) gives

$$E \sum_{i=0}^{N} I_i \frac{d^3 y}{dx^3} - \frac{12EJ}{\lambda} \sum_{i=1}^{n} \frac{1}{L_i} \frac{dy}{dx} + \sum_{i=0}^{n} V_i = 0 \quad \ldots\ldots\ldots\ldots\ldots \quad (5)$$

This line of reasoning is now extended to all frames of the complete framework. If the framework is cut through horizontally at a distance x above the foundation, then from the horizontal equilibrium of the part above the cut it follows

$$(H - x) h - \sum_{i=0}^{n} V_i = 0 \quad \ldots\ldots\ldots\ldots\ldots\ldots\ldots\ldots \quad (6)$$

In Eq. 6 h represents the horizontal load per unit height. Introducing Eq. 6 into Eq. 5, one obtains

$$E \sum_{i=0}^{n} I_i \frac{d^3 y}{dx^3} - 12 \frac{EJ}{\lambda} \sum_{i=1}^{n} \frac{1}{L_i} \frac{dy}{dx} + (H - x)h = 0 \quad \ldots\ldots\ldots\ldots \quad (7)$$

Assuming $\quad a = \sqrt{\dfrac{12J}{\lambda \sum\limits_{i=0}^{n} I_i} \sum\limits_{i=1}^{n} \dfrac{1}{L_i}} \quad \ldots\ldots\ldots\ldots\ldots\ldots\ldots \quad (8)$

$$b = \frac{h}{E \sum\limits_{i=0}^{n} I_i a^4} \quad \ldots\ldots\ldots\ldots\ldots\ldots\ldots\ldots\ldots \quad (9)$$

$$q = \frac{Hh}{E \sum\limits_{i=0}^{n} I_i a^3} = Hab \quad \ldots\ldots\ldots\ldots\ldots\ldots\ldots\ldots \quad (10)$$

$$\alpha = ax \quad \ldots\ldots\ldots\ldots\ldots\ldots\ldots\ldots\ldots\ldots\ldots\ldots \quad (11)$$

then Eq. 7 simplifies to

$$\frac{d^3 y}{d\alpha^3} - \frac{dy}{d\alpha} + q - \alpha b = 0 \quad \ldots\ldots\ldots\ldots\ldots\ldots\ldots\ldots \quad (12)$$

Note that α is dimensionless.

The general solution of this differential equation is

$$y = C_1 e^{\alpha} + C_2 e^{-\alpha} + C_3 - \frac{b}{2} \alpha^2 + q\alpha \quad \ldots\ldots\ldots\ldots\ldots\ldots \quad (13)$$

with C_1, C_2, and C_3 three integration constants to be determined. The boundary conditions may be assumed as follows: for $x = 0$ ($\alpha = 0$), $y = 0$ and $(dy)/(dx) = 0$ (or $(dy)/(d\alpha) = 0$; and for $x = H$ ($\alpha = \alpha_1$): $M = 0$ (or $(d^2y)/(d\alpha^2) = 0$). From this follows

$$C_1 = \frac{b(1 - \alpha_1 \exp(-\alpha_1))}{\exp(\alpha_1) + \exp(-\alpha_1)} \dots \dots \dots \dots \dots \dots \dots \dots \dots \dots \dots \quad (14)$$

$$C_2 = \frac{b(1 + \alpha_1 \exp(\alpha_1))}{\exp(\alpha_1) + \exp(-\alpha_1)} \dots \dots \dots \dots \dots \dots \dots \dots \dots \dots \dots \quad (15)$$

$$C_3 = -b \frac{2 - \alpha_1(\exp(-\alpha_1) - \exp(\alpha_1))}{\exp(\alpha_1) + \exp(-\alpha_1)} \dots \dots \dots \dots \dots \dots \dots \dots \quad (16)$$

If these integration constants are introduced into Eq. 13, then the displacement of the framework can be expressed in closed form as a function of α (and consequently of x).
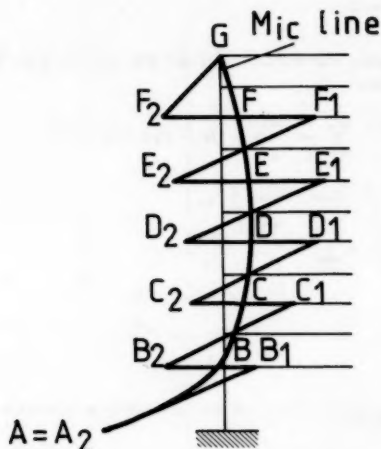
FIG. 5.—Determination of Column Moments

The bending moment in the member $\overline{A_{i-1}A_i}$ at column i can now be derived as

$$M_i = \frac{6EJa}{L_i} \frac{dy}{d\alpha} \dots \dots \dots \dots \dots \dots \dots \dots \dots \dots \dots \dots \dots \dots \dots \dots \dots \quad (17)$$

The exact moment diagram for any given column (i) as shown in Fig. 5 could be determined from the knowledge of the rotations and horizontal displacements of the nodes.

A "smeared out" moment diagram M_{ic} for column i can be calculated from

$$a^2 EI_i \frac{d^2 y}{d\alpha^2} = -M_{ic} \dots\dots\dots\dots\dots\dots\dots\dots\dots\dots\dots\dots\dots\dots\dots (18)$$

Thus the smooth curve $ABCDEFG$ is obtained (Fig. 5). At the height of the first floor the lengths $|BB_1| = |BB_2| = 1/2 \, |\Delta M_i|_1$ are plotted, respectively, to the right and to the left of the point B on the curve; ΔM_i = the sum of the bending moments at node i for the beams meeting at this node. Thus the well known "saw-tooth" line $AB_1B_2C_1C_2$ ... is obtained as the final moment diagram. For practical purposes this simple method appears to be sufficiently accurate. In Refs. 3 and 4 the method is worked out for various typical frames and is tested for its accuracy.

Relaxation of Nodes.—So far it has been implicitly assumed that the column stiffness was great in relation to that of the members and that the moment from the beams acts continuously on the columns. However, in consequence of the fact that the members do not act continuously, additional deformations develop. In fact, the deflection curve y is an oscillation curve with points of
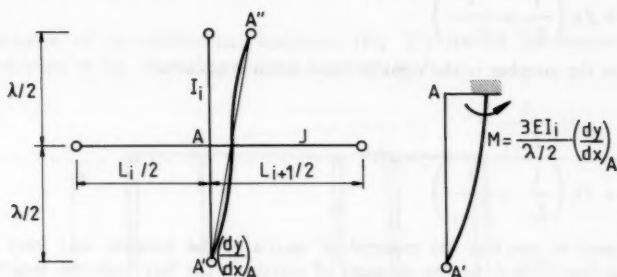
FIG. 6.—Additional Deformation Due to Relaxation

contraflexure approximately in the middle of the story height (Fig. 6). So far we have calculated a smooth curve going through all these points of contraflexure. Subsequently the question arises as to what's the relation between the real rotation θ_A of node A and the inclination $(dy)/(dx)A$ of the smooth curve. In Fig. 6 the assumed points of contraflexure in columns and beams are indicated. The relative displacements of A' and A'' cause the following fixed-end moments in the column

$$M = 2 \left(\frac{3EI_i}{\frac{\lambda}{2}}\right) \left(\frac{dy}{dx}\right) A = \frac{12EI_i}{\lambda} \left(\frac{dy}{dx}\right) A$$

while relaxation of node A gives the result

$$\theta_A = \frac{I_i \dfrac{2}{\lambda}}{2\dfrac{I_i}{\lambda} + \dfrac{J}{L_i} + \dfrac{J}{L_{i+1}}} \left(\frac{dy}{dx}\right) A \dots\dots\dots\dots\dots\dots\dots\dots\dots (19)$$

This becomes for $I_i \to \infty$ or $\theta_A = (dy)/(dx)A$. This indicates that our prior calculations were good, as far as the column stiffness is great in comparison to the beam stiffness. The moment of the member to the left of the column i becomes

$$\frac{12EI_i}{\lambda}\left(\frac{dy}{dx}\right)A \frac{\dfrac{J}{L_i}}{2\dfrac{I_i}{\lambda} + \dfrac{J}{L_i} + \dfrac{J}{L_{i+1}}} \dots \dots \dots \dots \dots \dots \dots \quad (20)$$

This equation replaces Eq. 1. Everything happens as if the moment of inertia of the member to the left of the column i is equal to

$$J \frac{2I_i\dfrac{\lambda}{L_i}}{2I_i + J\lambda\left(\dfrac{1}{L_i} + \dfrac{1}{L_{i+1}}\right)} = J\beta_1 \dots \dots \dots \dots \dots \dots \quad (21)$$

and for the member to the right of the column is equal to

$$J \frac{2I_i\dfrac{\lambda}{L_{i+1}}}{2I_i + J\lambda\left(\dfrac{1}{L_i} + \dfrac{1}{L_{i+1}}\right)} = J\beta'_1 \dots \dots \dots \dots \dots \dots \quad (22)$$

It is easy to see that the moment of inertia of the member may vary from bay to bay. Let J_i be the moment of inertia in the bay with the length L_i, then there can be written generally

$$a = \sqrt{\frac{6E}{\lambda \sum\limits_{i=0}^{n} I_i}\left(\frac{\beta'_0 J_1}{L_1} + \frac{\beta_1 J_1}{L_1} + \frac{\beta'_1 J_2}{L_2} + \frac{\beta_2 J_2}{L_2} + \dots + \frac{\beta_n J_n}{L_n}\right)} \dots \dots \quad (23)$$

However, for each bay the moment of inertia of the member must be equal for all floors.

Bending and Twisting of Long, Nonsymmetric Building.—Given a nonsymmetric structure, as shown in Fig. 7, over the length of the building there are m plane frames. If the building is long, everything happens as if each plane frame under the influence of wind loading deforms in the y direction and rotates through an angle ω.

As the floors are assumed rigid in the horizontal plane, all plane frames and consequently all columns at a given height rotate through the same angle ω. The resulting y displacement of frame j is

$$y_j = y_1 + z_j \omega \dots \dots \dots \dots \dots \dots \dots \dots \dots \dots \dots \dots \dots \quad (24)$$

in which y_1 = the displacement of frame 1; and z_j = the distance from frame 1 to frame j, measured parallel to the longitudinal wall of the structure. The general differential equation for the frame j is

$$EI_J \frac{d^3 y_J}{dx^3} - \frac{12EJ_J}{\lambda} \frac{1}{L_J} \frac{dy_J}{dx} + V_J = 0 \quad \ldots \ldots \ldots \ldots \ldots \ldots \quad (25)$$

in which $I_J = \sum_{i=0}^{n} I_{ij}$ $\ldots \ldots \ldots \ldots \ldots \ldots \ldots \ldots \ldots \ldots \ldots$ (26)

$\dfrac{1}{L_J} = \sum_{n=1}^{n} \dfrac{1}{L_{i,j}}$ (if necessary, adapted owing to relaxation of the nodes) (27)

$V_J = \sum_{i=0}^{n} V_{ij}$ $\ldots \ldots \ldots \ldots \ldots \ldots \ldots \ldots \ldots \ldots \ldots \ldots \ldots$ (28)

From horizontal equilibrium, parallel to the wind direction, of everything above a horizontal cut at a height x above the foundation (Fig. 8) it follows

$$\sum_{j=1}^{m} V_j = (H - x) hL \quad \ldots \ldots \ldots \ldots \ldots \ldots \ldots \ldots \ldots \ldots \quad (29)$$

Summation of the differential equations (Eq. 25) for all the frames, and introduction of Eq. 29 in the resulting equation, leads to
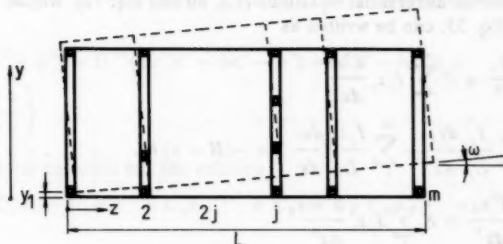
FIG. 7.—Displacement of Floor of Asymmetric Framework
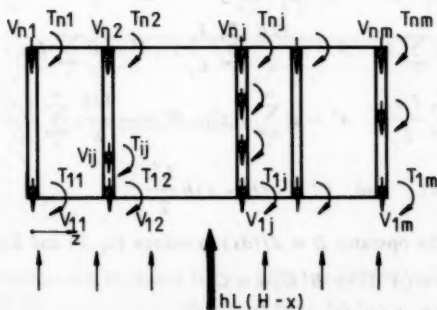
FIG. 8.—Distribution of Forces at Height, x

$$E \sum_{1}^{m} I_j \frac{d^3 y_j}{dx^3} - \frac{12E}{\lambda} \sum_{1}^{m} \frac{J_j}{L_j} \frac{dy_j}{dx} + (H - x) hL = 0 \quad \dots \dots \dots \dots \quad (30)$$

The twisting equilibrium of the isolated part of the building is

$$\sum V_j z_j + \sum \sum T_{ij} - (H - x) h \frac{L^2}{2} = 0 \quad \dots \dots \dots \dots \dots \quad (31)$$

In this equation h represents the horizontal load per square meter.

If we multiply Eq. 25 with z_j and sum for all frames, according to j, we obtain, taken into account Eq. 31

$$E \sum_{1}^{m} I_j z_j \frac{d^3 y_j}{dx^3} - \frac{12E}{\lambda} \sum_{1}^{m} \frac{J_j z_j}{L_j} \frac{dy_j}{dz} - \sum_{i=0}^{n} \sum_{j=1}^{m} T_{ij} + (H - x) \frac{hL^2}{2} = 0 \quad \dots \quad (32)$$

The total resisting moment of torsion from the columns and walls can be written as

$$\sum_i \sum_j T_{ij} = G \sum_i \sum_j K_{ij} \frac{d\omega}{dx} = GK \frac{d\omega}{dx} \quad \dots \dots \dots \dots \quad (33)$$

in which G = the shear modulus. The two equilibrium conditions lead to the two simultaneous differential equations (Eq. 30 and Eq. 31), which, considering Eq. 32 and Eq. 33, can be written as

$$E \sum_{1}^{m} I_j \frac{d^3 y_1}{dx^3} + E \sum_{j}^{m} I_j z_j \frac{d^3 \omega}{dx^3}$$
$$- \frac{12E}{\lambda} \left[\sum_{1}^{m} \frac{I_j}{L_j} \frac{dy_1}{dx} + \sum_{1}^{m} \frac{I_j z_j}{L_j} \frac{d\omega}{dx} \right] = -(H - x) hL \quad \dots \dots \dots \quad (34)$$

$$E \sum_{1}^{m} I_j z_j \frac{d^3 y_1}{dx^3} + E \sum_{1}^{m} I_j z_j^2 \frac{d^3 \omega}{dx^3}$$
$$- \frac{12E}{\lambda} \left[\sum_{1}^{m} \frac{J_j z_j}{L_j} \frac{dy_1}{dx} + \sum_{1}^{m} \frac{J_j z_j^2}{L_j} \frac{d\omega}{dx} \right] - GK \frac{d\omega}{dx} = -(H - x) h \frac{L^2}{z} \quad \dots \quad (35)$$

Define $\quad A = E \sum_{1}^{m} I_j; \quad B = -\frac{12E}{\lambda} \sum_{1}^{m} \frac{I_j}{L_j}; \quad A' = E \sum_{1}^{m} I_j z_j;$

$$B' = -\frac{12E}{\lambda} \sum_{1}^{m} \frac{I_j z_j}{L_j}; \quad A'' = E \sum_{1}^{m} I_j z_j^2; \quad B'' = -\frac{12E}{\lambda} \sum_{1}^{m} \frac{I_j z_j^2}{L_j} - GK;$$

$$C = -(H - x) hL; \quad \text{and} \quad C' = -(H - x) b \frac{L^2}{2} \quad \dots \dots \dots \dots \quad (36)$$

and introduce the operator $D = d/(dx)$ to reduce Eq. 34 and Eq. 35 to

$$(AD^3 + BD) y_1 + (A' D^3 + B' D) \omega = C \quad \dots \dots \dots \dots \dots \quad (37a)$$

$$(A' D^3 + B' D) y_1 + (A'' D^3 + B'' D) \omega = C' \quad \dots \dots \dots \dots \dots \quad (37b)$$

Solution of System of Differential Equations.—The following transformations

make the coefficients and the unknown functions of the system of differential equations (Eq. 37) dimensionless:

$$a = \frac{A}{A} = 1; \quad b = \frac{BH^2}{A}; \quad a' = \frac{A'}{AL}; \quad b' = \frac{B'H^2}{AL}; \quad a'' = \frac{A''}{AL^2};$$

$$b'' = \frac{B''H^2}{AL^2}; \quad h' = \frac{hH^4}{A}; \quad c = \frac{CH^3}{AL} = -h'(1 - x');$$

$$c' = \frac{CH^3}{AL^2} = -\frac{h'}{2}(1 - x'); \quad x' = \frac{x}{H}; \quad z' = \frac{z}{L}; \quad y_1' = \frac{y_1}{L}; \quad \omega' = \omega;$$

$$D' = \frac{d}{dx'}; \quad \text{and} \quad D'^3 = \frac{d^3}{(dx')^3}. \quad \ldots \ldots \ldots \ldots \ldots \quad (38)$$

The system (Eq. 37) becomes

$$(D'^3 + bD')y_1' + (a'D'^3 + b'D')\omega' = c \quad \ldots \ldots \ldots \ldots \quad (39a)$$

$$(a'D'^3 + b'D')y_1' + (a''D'^3 + b''D')\omega' = c' \quad \ldots \ldots \ldots \ldots \quad (39b)$$

This system of two cubic differential equations becomes through the operation $(39a) \times (a'D'^3 + b'D) - (39b) \times (D'^3 + bD')$ an equation of the sixth degree:

$$D'^2(D'^4(a'^2 - a'') + D'^2(2a'b' - ba'' - b'') + (b'^2 - bb''))\omega'$$

$$= h'\left(b' - \frac{b}{2}\right) \quad \ldots \ldots \ldots \ldots \ldots \ldots \ldots \ldots \quad (39c)$$

This differential equation has the solution

$$\omega' = C_1 + C_2 x' + C_3 e^{d_1 x'} + C_4 e^{-d_1 x'} + C_5 e^{d_2 x'} + C_6 e^{-d_2 x'} + \omega_p' \quad \ldots \quad (40)$$

in which

$$d_1 = \sqrt{\frac{-2a'b' + b'' + ba''}{2a'^2 - 2a''} + \sqrt{\frac{(-2a'b' + b'' + ba'')^2 - 4(b'^2 - bb'')(a'^2 - a'')}{4(a'^2 - a'')^2}}} \quad \ldots \quad (41)$$

$$d_2 = \sqrt{\frac{-2a'b' + b'' + ba''}{2a'^2 - 2a''} - \sqrt{\frac{(-2a'b' + b'' + ba'')^2 - 4(b'^2 - bb'')(a'^2 - a'')}{4(a'^2 - a'')^2}}} \quad \ldots \quad (42)$$

These roots are real. The particular solution ω_p' is

$$\omega_p' = \frac{h'\left(b' - \dfrac{b}{2}\right)}{(b'^2 - bb'')} \frac{x'^2}{2} - r_1 x'^2 \quad \ldots \ldots \ldots \ldots \ldots \ldots \quad (43)$$

An analogous solution can be found for y_1' $[(39a) \times (a''D'^3 + b''D') - (39b) \times (a'D'^3 + b'D')]$:

$$y_1' = K_1 + K_2 x' + K_3 e^{d_1 x'} + K_4 e^{-d_1 x'} K_5 e^{d_2 x'} + K_6 e^{-d_2 x'} + y_{1p}' \quad \ldots \quad (44)$$

$$y'_{1p} = r_2 x'^2 = \frac{h'\left(\dfrac{b'}{2} - b''\right)}{2(b'^2 - bb'')} x'^2 \quad \dots \dots \dots \dots \dots \dots \quad (45)$$

The substitution of ω' (Eq. 40) and y'_1 (Eq. 44) in Eq. 39a and Eq. 39b gives a series of relations between the coefficients C and K, which can be reduced to the following six relations:

$$C_2 = -\frac{h'\left(b' - \dfrac{b}{2}\right)}{b'^2 - bb''} = -2r_1 \quad \dots \dots \dots \dots \dots \dots \quad (46)$$

$$K_2 = -\frac{h'\left(\dfrac{b'}{2} - b''\right)}{b'^2 - bb''} = -2r_2 \quad \dots \dots \dots \dots \dots \dots \quad (47)$$

$$C_3 = -K_3 \frac{d_1^2 + b}{a' d_1^2 + b'} = -K_3 d_3 \quad \dots \dots \dots \dots \dots \dots \quad (48)$$

$$C_4 = -K_4 \frac{d_1^2 + b}{a' d_1^2 + b'} = -K_4 d_3 \quad \dots \dots \dots \dots \dots \dots \quad (49)$$

$$C_5 = -K_5 \frac{d_2^2 + b}{a' d_2^2 + b'} = -K_5 d_4 \quad \dots \dots \dots \dots \dots \dots \quad (50)$$

$$C_6 = -K_6 \frac{d_2^2 + b}{a' d_2^2 + b'} = -K_6 d_4 \quad \dots \dots \dots \dots \dots \dots \quad (51)$$

If the building is symmetric, the denominator in Eq. 50 and Eq. 51 is zero and

$$a' = 0.5 \quad \dots \dots \dots \dots \dots \dots \dots \dots \dots \dots \dots \dots \dots \dots \quad (52)$$

$$b' = 0.5b \quad \dots \dots \dots \dots \dots \dots \dots \dots \dots \dots \dots \dots \dots \quad (53)$$

$$d_2 = \sqrt{-b} \quad \dots \dots \dots \dots \dots \dots \dots \dots \dots \dots \dots \dots \quad (54)$$

$$d_2^2 + b = a' d_2^2 + b' = 0 \quad \dots \dots \dots \dots \dots \dots \dots \dots \dots \quad (55)$$

For a symmetric building

$$C_5 = C_6 = 0 \quad \dots \dots \dots \dots \dots \dots \dots \dots \dots \dots \dots \dots \quad (56)$$

Thus it follows that d_4 in Eq. 50 and Eq. 51 is zero.

The six remaining coefficients C_1, K_1, K_3, K_4, K_5, and K_6 can be determined from the six boundary conditions:

$$x' = 0, \ \omega' = 0; \quad C_1 + C_3 + C_4 + C_5 + C_6 = 0 \quad \dots \dots \dots \dots \quad (57)$$

This equation determines C_1. Also

$$x' = 0, \ y'_1 = 0; \quad K_1 + K_3 + K_4 + K_5 + K_6 = 0 \quad \dots \dots \dots \dots \quad (58)$$

This equation determines K_1. Also

$$x' = 0, \quad \frac{d\omega'}{dx'} = 0; \quad C_2 + d_1 C_3 - d_1 C_4 + d_2 C_5 - d_2 C_6 = 0 \quad \ldots \ldots \ldots \quad (59)$$

or, converted according to the coefficients K:

$$-K_3 d_1 d_3 + K_4 d_1 d_3 - K_5 d_2 d_4 + K_6 d_2 d_4 = 2r_1 \quad \ldots \ldots \ldots \ldots \quad (60)$$

$$x' = 0, \quad \frac{dy_1'}{dx'} = 0; \quad K_2 + d_1 K_3 - d_1 K_4 + d_2 K_5 - d_2 K_6 = 0 \quad \ldots \ldots \quad (61)$$

$$x' = 1 (x = H), \quad T = GK \frac{d\omega}{dx} = \frac{GK}{H} \frac{d\omega'}{dx'} = 0;$$

$$2r_1 + C_2 + d_1 e^{d_1} C_3 - d_1 e^{-d_1} C_4 + d_2 e^{d_2} C_5 - d_2 e^{-d_2} C_6 = 0 \quad \ldots \ldots \quad (62)$$

or, converted according to the coefficients K:

$$K_3 d_1 d_3 e^{d_1} - K_4 d_1 d_3 e^{-d_1} + K_5 d_4 d_2 e^{d_2} - K_6 d_4 d_2 e^{-d_2} = 0 \quad \ldots \ldots \quad (63)$$

$$x' = 1 (x = H); \quad \sum_j EI_j \frac{d^2 y_j}{dx^2} = 0;$$

$$\frac{L}{H^2} \sum_j EI_j \frac{d^2(y_1' + z_j' \omega')}{dx'^2} = 0; \quad \frac{d^2 y_1'}{dx'^2} + a' \frac{d^2 \omega'}{dx'^2} = 0 \quad \ldots \ldots \ldots \quad (64)$$

or after the introduction of Eqs. 48–51

$$K_1 d_1 e^{d_1}(d_1 - a' d_1 d_3) + K_2 d_1 e^{-d_1}(d_1 - a' d_1 d_3)$$
$$+ K_3 d_2 e^{d_2}(d_2 - a' d_2 d_4) + K_4 d_2 e^{-d_2}(d_2 - a' d_2 d_4) = -2r_2 - 2r_1 a' \quad (65)$$

The fifth and sixth boundary conditions result from the distribution of member moments over the column height. Finally, a system of six equations with six unknowns is obtained (K_1, K_2, K_3, K_4, K_5, K_6) (Eqs. 47, 58, 60, 61, 63, 65). These six equations can be converted into a system of four equations ($\underline{A} \underline{B} = \underline{B}$), as K_2 results explicitly from Eq. 47 and K_1 for Eq. 58 can be expressed as a function of K_3, K_4, K_5, and K_6. The coefficients C can then be determined from Eqs. 48, 49, 50, 46, and 57.
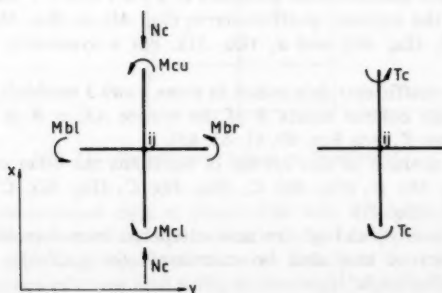

FIG. 9.—Internal Actions on Node ij

Derivation of Internal Actions.—Considering $y = y_1 + z\,\omega$, the internal actions can be written as (see Fig. 9)

$$M_{bl} = \frac{6EJ}{L_i}\,\beta_{ij}\left(\frac{L}{H}\frac{dy_1'}{dx'} + \frac{z_j}{H}\frac{d\omega'}{dx'}\right) \quad\ldots\ldots\ldots\ldots\ldots\ldots\ldots\ldots (66)$$

$$M_{br} = \frac{6EJ}{L_{i+1}}\,\beta_{ij}'\left(\frac{L}{H}\frac{dy_1'}{dx'} + \frac{z_j}{H}\frac{d\omega'}{dx'}\right) \quad\ldots\ldots\ldots\ldots\ldots\ldots\ldots (67)$$

$$M_{cl} = -EI_{ij}\left(\frac{L}{H^2}\frac{d^2y_1'}{dx'^2} + \frac{z_j}{H^2}\frac{d^2\omega'}{dx'^2}\right) + \frac{M_{bl}+M_{br}}{2} \quad\ldots\ldots\ldots (68)$$

$$M_{cu} = -EI_{ij}\left(\frac{L}{H^2}\frac{d^2y_1'}{dx'^2} + \frac{z_j}{H^2}\frac{d^2\omega'}{dx'^2}\right) - \frac{M_{bl}+M_{br}}{2} \quad\ldots\ldots\ldots (69)$$

As mentioned before, the moment change in the column due to the member moments is distributed equally over upper and lower column. The twisting moments and axial forces are derived from

$$T_c = \frac{GK_{ij}}{H}\frac{d\omega'}{dx'} \quad\ldots\ldots\ldots\ldots\ldots\ldots\ldots\ldots\ldots\ldots\ldots\ldots\ldots\ldots (70)$$

and $\quad N_c = \dfrac{6EJ}{\lambda}\,P_{ij}\displaystyle\int_x^H \dfrac{dy}{dx}\,dx = \dfrac{6EJ}{\lambda}\,P_{ij}L\left(\displaystyle\int_{x'}^1 \dfrac{dy_1'}{dx'}\,dx' + \dfrac{z_j}{L}\displaystyle\int_{x'}^1 \dfrac{d\omega'}{dx'}\,dx'\right)$

$$= \frac{6EJ}{\lambda}\,P_{ij}L\,[y_1'(1) - y_1'(x')] + \frac{z_j}{L}\,[\omega'(1) - \omega'(x')] \quad\ldots\ldots\ldots\ldots (71)$$

in which $\quad P_{ij} = \dfrac{\beta_{i-1,j}'}{(L_{i-1,j})^2} + \dfrac{\beta_{i,j}}{(L_{i-1,j})^2} - \dfrac{\beta_{i,j}'}{(L_{i,j})^2} - \dfrac{\beta_{i+1,j}}{(L_{i,j})^2} \quad\ldots\ldots\ldots\ldots (72)$

A summary of the solution algorithm, which can be translated into a computer code, follows.

1. Calculate the coefficients A, A', A'', B', B'' using Eq. 36.

2. Convert into dimensionless quantities a, a', a'', b, b', b'' using Eq. 38.

3. Calculate the auxiliary coefficients: r_1 (Eq. 43); r_2 (Eq. 45); d_1 (Eq. 41); d_2 (Eq. 42); d_3 (Eq. 48); and d_4 (Eq. 51). For a symmetric building $d_4 = 0$.

4. Using the coefficients determined in items 2 and 3 establish the coefficient matrix **A** and the column matrix **B** of the system $\mathbf{AK} = \mathbf{B}$ in the unknowns K_3, K_4, K_5, and K_6 (see Eqs. 60, 61, 63, 65).

5. After the solution of this system of equations the other coefficients are found: K_1 (Eq. 58); C_3 (Eq. 48); C_4 (Eq. 49); C_5 (Eq. 50); C_6 (Eq. 51); C_2 (Eq. 46); and C_1 (Eq. 47).

6. The functions y_1' and ω' are now computed from Eqs. 40, 43, 44, and 45. The derivatives can also be calculated: $(dy_1')/(dx')$, $(d^2y_1')/dx'^2$, $(d\omega')/(dx')$, $(d^2\omega')/dx'^2$.

7. From the data calculated under item 6, all internal actions can be determined from Eqs. 66, 67, 68, 69, 70, 71, and 72.

Check

The accuracy of the approximate calculation was checked by means of a computer assisted calculation, based upon the displacement method (6,7), adapted to the specific character of deformation of longitudinal multistory buildings.
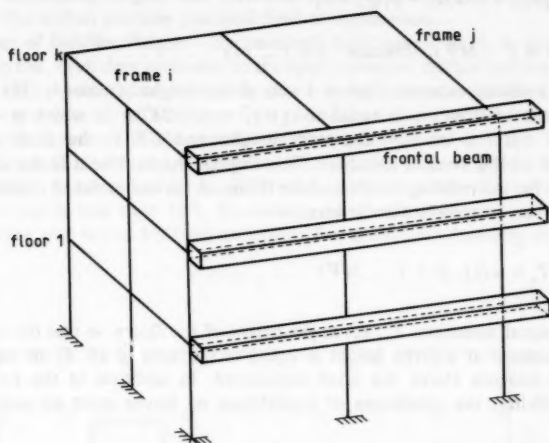
FIG. 10.—Idealizing of Structure
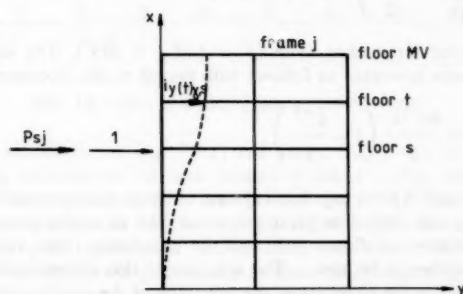
FIG. 11.—Definition of Influence Coefficient i_y

The floors were assumed rigid in plane. This was simulated in the program by connecting the successive plane frames with rigid frontal beams (Fig. 10).

As the first step the y displacements were calculated for each frame ($1-m$) under the influence of a unit load acting at the height of each floor (Fig. 11).

This calculation was carried out by means of the displacement method. The y displacements of the floors are the influence coefficients $i_y(t)_{j,s}$ for the

displacement y on floor t, when the force acts on floor s, if the frame j is isolated from the rest of the building. The real interaction forces $P_{s,j}$ between the frames and the front beams provide the satisfaction of the compatibility conditions:

$$\sum_{s=1}^{MV} i_y(t)_{j,s} P_{s,j} - \omega(t) z_j - y_1(t) = 0;$$

(floors: $t = 1 \ldots MV$), (frames: $j = 1 \ldots m$) . . . . (73)

When a twisting moment $T(s) = 1$ acts at the height of floor, s, the angular displacement of floor, t, is equal to $i_\omega(t)_s = \lambda/(GK)a$ in which $a = t$ if $t \leq s$; $a = s$ if $t > s$; λ = the story height; and GK = the total torsional stiffness of all the vertical members. This angular displacement is the influence coefficient for the twisting rotation of the floors. A second series of compatibility conditions can be written for the torsion

$$\sum_{s=1}^{MV} i_\omega(t)_s T_s = \omega(t), \ (t = 1, \ldots MV)$$ . . . . (74)

The torsional moments, T_s, act at the height of the floors so that the resulting twisting moment at a given height is equal to the sum of all T_s on the floors which are situated above the level considered. In addition to the conditions of compatibility, the conditions of equilibrium of forces must be satisfied as well.

The horizontal equilibrium is expressed as

$$\sum_{j=1}^{m} P_{t,j} = hL\lambda \left(1 - \frac{\delta_t^{MV}}{2} \right) \ (t = 1 \ldots MV)$$ . . . . (75)

in which δ = the Kronecker delta ($\delta = 1$ if $t = MV$). The equilibrium of torsional moments is written as follows with regard to the reference point:

$$\sum_{j=1}^{m} P_{t,j} z_j + T_t = \frac{hL^2\lambda}{2} \left(1 - \frac{\delta_t^{MV}}{2} \right).$$ . . . . (76)

Eqs. 73, 74, 75, and 76 form together a system of linear equations in the unknowns $y_1(t)$, $\omega(t)$, $P_{t,j}$, and $T(t)$. The parameter t can take all values included between one and the number of floors MV and the parameter j the values between one and the number of frames s. The solution of this system provides all the data which serve for the checking of the accuracy of the approximation method.

EXAMPLES

The approximation method was applied to a high-rise building whose plan is shown in Fig. 12. The framework always consists of nine frames, in the third of which the elevator shaft is included. All columns have as dimensions 0.70 m × 0.28 m and the horizontal beams 0.2 m × 0.4 m. The lift shaft measures 6.5 m × 4 m and has a wall thickness of 0.18 m. The story height is 3 m. In the calculations the elasticity modulus $E = 25,000$ N/mm², and

the G modulus $= 10,417$ N/mm^2. The distribution of forces in the framework was calculated under a wind load $h = 1$ kN/m^2.

The accuracy of the approximation method (AM) was derived through a comparison with the displacement method explained in the "check" section. For this purpose several structures were constructed on the groundplan (Fig. 12) with decreasing heights and different relative stiffnesses, with a view to checking the widest possible practical field of application.

Influence of Building Height.—Successively buildings of 10, 8, 6, and 4 floors were analyzed, each time according to the approximation method and the stiffness method (SM). As described previously, the calculation starts with the determination of the translation y_1 of reference frame 1 and the rotation ω. The displacements y_1 and ω as functions of the number of floors are plotted in Figs. 13(a) and 13(b). The small circles are AM results, the solid line indicates SM results.

From eight floors upwards the difference is 1%–2% while for low buildings the difference is less than 10%. In addition to the displacements, the internal actions were also tested for their accuracy. For a ten story building the bending
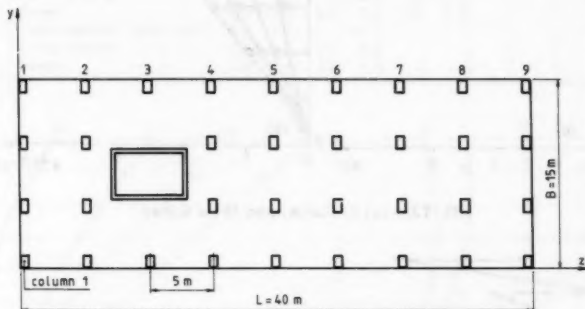
FIG. 12.—Plan of Building under Consideration

moments are plotted in the Fig. 14(a) and 14(b). Fig. 14(a) shows the curve of the bending moments in the wall column of frame 1. Fig. 14(b) shows the curve of the bending moments in the elevator shaft. The small circles give, as before, AM results and the full line gives SM results. Here also appears to exist a very good agreement. This is made still clearer by the values in Table 1, in which the bending moments in the wall column (Fig. 12) of frame 9 are recorded in the case of a decreasing number of floors. At the greatest moments, those at the foundation, the difference is small (5%–7%) even with low buildings.

Influence of Internal Stiffness Proportions.—As shown in Fig. 12, the elevator shaft provides an important contribution both to the bending and the torsional stiffness of the building. Due to crack formation these stiffnesses can change significantly (7). A good approximation for the change of bending rigidity as a result of cracking is a reduction to nearly one third of the original value, and for the torsional rigidity a reduction to one tenth. In Fig. 15 the displacements y_1 and ω are shown for a ten-story building, with a plan according to Fig.

12, in which the bending rigidity EI and the torsional rigidity GK have been changed. The accuracy of the approximation method is again shown to be good.
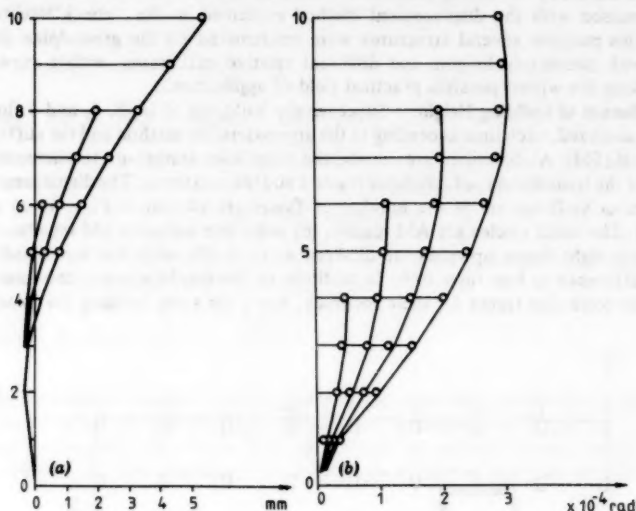
FIG. 13.—(a) y_1 Curve; and (b) ω Curve
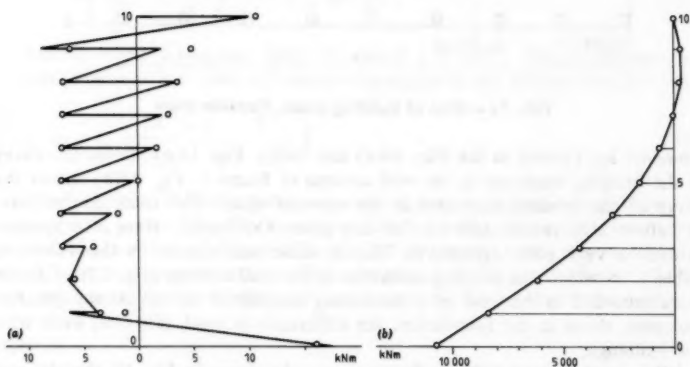
FIG. 14.—(a) Bending Moments in Frame 1; and (b) Bending Moments in Elevator Shaft

When the bending moment of inertia I of the elevator shaft decreases (cases II and IV in Fig. 15), the error in the translation increases slightly, because in this case the influence of the normal force deformation becomes greater,

which is not taken into account in the approximation method.

As in the case of cracking, the torsional rigidity of the elevator shaft can decrease to one tenth of the original value. It is interesting to check the course

TABLE 1.—Bending Moments in Column 1 of Frame 9

Frame 9	Column 1	FLOOR NUMBER											
Number of stories (1)	Moment, in kilo-newton-meters (2)	0		2		4		6		8		10	
		AM (3)	SM (4)	AM (5)	SM (6)	AM (7)	SM (8)	AM (9)	SM (10)	AM (11)	SM (12)	AM (13)	SM (14)
10	Upper column	−82.8	−87.2	−15.4	−15.3	−7.1	−6.3	−3.2	−2.1	−0.7	1.3	—	—
	Lower column	—	—	−10.7	−10.5	−16.7	−16.8	−15.3	−15.4	−11.9	−12.6	−10.9	−6.0
	Beams	—	—	26.1	25.5	23.8	23.8	18.5	17.5	12.6	11.4	10.9	6.0
8	Upper column	−64.5	−68.0	−9.7	−9.5	−2.4	−1.6	0.7	1.9	—	—		
	Lower column	—	—	−9.5	−9.3	−13.3	−13.6	−10.8	−11.3	−6.7	−4.5		
	Beams	—	—	19.2	18.8	15.7	15.2	10.1	9.4	6.7	4.5		
6	Upper column	−46.3	−49.0	−4.3	−3.9	1.7	2.3	—	—				
	Lower column	—	—	−8.1	−8.2	−9.7	−10.1	−3.3	−3.2				
	Beams	—	—	12.4	12.2	8.0	7.8	3.3	3.2				
4	Upper column	−28.3	−30.3	0.7	0.7	—	—						
	Lower column	—	—	−6.6	−6.6	−1.1	−2.3						
	Beams	—	—	5.9	5.9	1.1	1.3						

I   (I , K)
II   (I/3, K)
III   (I , K/10)
IV   (I/3, K/10)
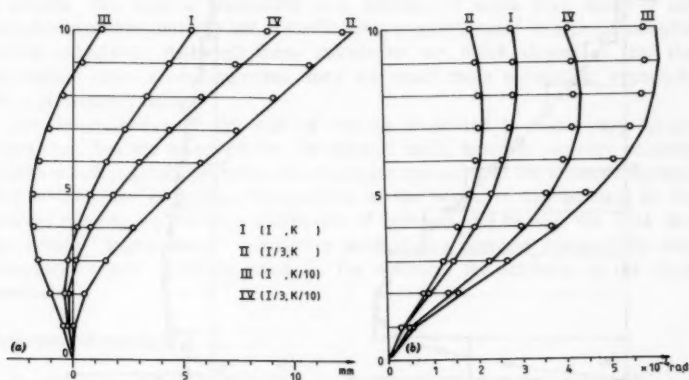
FIG. 15.—(a) y_1 Displacement; and (b) ω Displacement

of the bending and torsional moments in this shaft. In Table 2 these bending moments are represented, whereas the twisting moments for the stiffness combinations (K, I) and $(K/10, I)$ have been indicated in Figs. 16(a) and 16(b). The stepped course of the torsional moments, calculated with the stiffness method (SM), is due to the fact that in this method we make concentrated torsional moments act at the level of the floors (see the "check" section). The accuracy of the approximation method for the shaft is somewhat better than for the columns.

TABLE 2.—Bending Moments

Frame 9	Box				
	Moment, in	0		2	
Case (1)	kilonewton-meters (2)	AM (3)	SM (4)	AM (5)	SM (6)
Box K, I	Upper column	−10,717	−10,773	−6,185	−6,236
	Lower column	—	—	6,176	6,227
	Beams	—	—	9.0	9.3
Box $K, I/3$	Upper column	−7,778	−7,801	−3,710	−3,756
	Lower column	—	—	3,691	3,737
	Beams	—	—	18.3	18.3
Box $K/10, I$	Upper column	−9,238	−9,256	−5,307	−5,348
	Lower column	—	—	5,299	5,341
	Beams	—	—	7.7	7.6
Box $K/10, I/3$	Upper column	−6,925	−6,937	−3,336	−3,395
	Lower column	—	—	3,320	3,379
	Beams	—	—	16.2	16.0
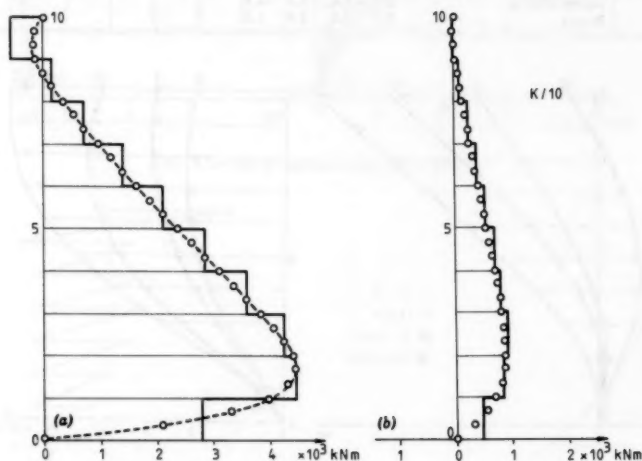
FIG. 16.—(a) Curve of Torsional Moments in Elevator Shaft (K, I); and (b) Curve of Torsional Moments in Elevator Shaft $(K/10, I)$

CONCLUSIONS

An approximation method for the calculation of long, high-rise buildings under horizontal wind loading has been described. The calculation of the displacements and the internal actions is reduced to the solution of the linear system of Eqs. 60, 61, 63, and 65. This can be done by means of a simple pocket calculator.

| FLOOR NUMBER | | | | | | | |
| 4 | | 6 | | 8 | | 10 | |
AM (7)	SM (8)	AM (9)	SM (10)	AM (11)	SM (12)	AM (13)	SM (14)
−2,730	−2,750	−608	−591	284	331	—	—
2,716	2,736	593	581	−299	−346	−15.1	−12.5
13.7	13.4	15.4	15.0	15.4	15.3	15.1	12.5
−999	−1,011	404	425	728	789	—	—
973	986	−430	−451	−752	−813	−22.3	−18.7
25.4	25.0	26.0	25.6	23.9	23.7	22.3	18.7
−2,457	−2,477	−661	−658	153	182	—	—
2,445	2,465	647	645	−167	−195	−13.4	−11.3
11.8	11.6	13.4	13.1	13.6	13.4	13.4	11.3
−1,025	−1,065	230	207	595	589	—	—
1,003	1,042	−254	−230	−617	−612	−20.8	−18.4
22.9	22.7	23.8	23.8	22.2	22.5	20.8	18.4

The stiffness method, on the contrary, always requires the solution of a system with dozens and mostly hundreds of equations. For this purpose a large computer is needed. The manual calculation can, besides, be made even easier if the calculation of the great number of coefficients is programmed on a programmable pocket calculator. Although these calculators are much slower so that the calculation takes several minutes, they are much more accessible, especially for a preliminary design.

The determination of the internal actions is limited to some very simple operations. Despite its simplicity, the method leads, however, to very accurate results which is amply proved in the examples appearing in the example section. The method can be applied irrespective of the height of the building or the relative bending and twisting stiffnesses of columns and beams. We think that the simple "approximate" calculation method can compete successfully with so-called "exact" methods, such as, for instance, the stiffness or the force method.

APPENDIX.—REFERENCES

1. De Roeck, G., "Combined Torsion and Bending in Prestressed Concrete," *Cement*, 1977, The Netherlands (in Dutch).
2. Haris, A., "Approximate Stiffness Analysis of High-Rise Buildings," *Journal of the Structural Division*, ASCE, Vol. 104, No. ST4, Proc. Paper 13700, Apr., 1978, pp. 681–696.
3. Mortelmans, F., "Analysis of High-Rise Buildings under Wind Loading," Revue C, 1969, Belgium (in Dutch).
4. Mortelmans, F., "Analysis of High-Rise Buildings under Wind Loading," Revue C, 1972, Belgium (in Dutch).
5. Mortelmans, F., De Roeck, G., Van Gemert, D., discussion of "Approximate Stiffness Analysis of High-Rise Buildings," by Ali A. K. Haris, *Journal of the Structural Division*, ASCE, Vol. 105, No. ST5, Proc. Paper 14551, May, 1979, pp. 967–969.
6. Van Gemert, D., "Numerical Analysis of Structures," Lecture notes, Katholieke Universiteit Leuven, Belgium, 1973 (in Dutch).

7. Zienkiewicz, O. C., *The Finite Element Method in Engineering Science,* McGraw-Hill
Book Co., Inc., New York, N.Y., 1971.

Lap Splices in Reinforced Concrete under Impact

By Telvin Rezansoff,[1] James O. Jirsa,[2] M. ASCE,
and John E. Breen,[3] F. ASCE

Introduction

Nineteen beams containing lapped splices in a constant moment region were tested under dynamic (impact) loading and the behavior was compared with that under static loading. The purpose of the tests was to determine whether splices subjected to impact loading could be designed using established procedures for splices under static loading. Loading rates that were used can occur under explosion or vehicular impact.

The main variable was the loading applied. Failure was achieved by either a single impact load, incrementally increasing impact loads to failure, repeated unidirectional impact loads at fixed levels, and repeated reversed impact loads at fixed levels. The load-time curve was a ramp function, with the peak at less than 4 msec. Beam cross sections and tensile reinforcement were not varied. Three different splice lengths were investigated. Transverse reinforcement was provided in the splice region in some specimens.

Splice performance was evaluated according to the strength and toughness exhibited. Toughness was examined in terms of number of cycles of loading and the deflection sustained prior to failure.

Experimental Program

Test Specimens.—Details and notation of all specimens are summarized in Fig. 1 and Table 1. All beams were 15 in. (380 mm) deep by 17 in. (430 mm) wide reinforced with two No. 8 bars. Splice lengths investigated were 18 in., 30 in., and 42 in. (460 mm, 760 mm, and 1,070 mm). Beam dimensions, tensile reinforcing, and splice details duplicated four beams tested statically by Ferguson and Breen (4). The four beams denoted as the RS series (reference static) with

one additional beam tested statically in this program provide the tests against which the beams subjected to impact loads are compared.

With concrete strength of 3,500 psi (24 MPa) and steel yield stress of 60 ksi (410 MPa), the American Concrete Institute (ACI) (1) specifications require a splice length of 44 in. (1,120 mm) for a class C splice (all bars spliced, stress greater than half the yield stress) meeting the requirements of ACI section 12.5(d) for static loading. For the same conditions, the approach suggested by
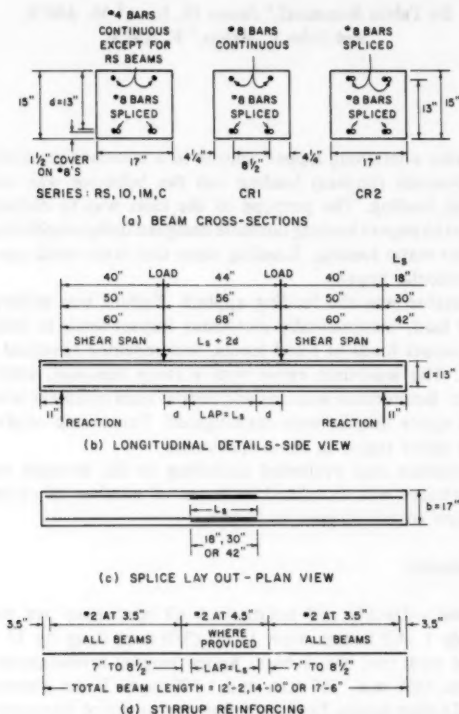
FIG. 1.—Specimen Details (1 in. = 25.4 mm)

Ferguson and Krishnaswamy (5) results in a splice length of 43 in. (1,090 mm). Most specimens tested under impact had splice lengths of 30 in. (760 mm). It was expected that a 30-in. (760-mm) splice would develop yield under static loading but not under impact and would not allow large deflections before failure.

Loading System and Instrumentation.—The dynamic loading system shown in Fig. 2 consisted of a structural steel frame which supported a 2,600 lb (1,180 kg) weight which was dropped on the test specimen. Vermiculite concrete cushions (Fig. 3) were placed at the two symmetrically positioned load points to receive

the direct impact of the weight. With cushioning the impact approximates ramp shaped forcing functions with rise times of about 4 msec. A typical force-time curve from impact on a similar but stationary vermiculite concrete cushion is reproduced in Fig. 4 from work by Bufkin (2). Levelling of the 2,600 lb (1,180 kg) weight prior to loading resulted in near simultaneous impact of the two load points. Elastic analyses (10) indicated that the moment remained nearly

TABLE 1.—Details of Test Specimens

Series (1)	Splice length, in inches[a] (2)	Steel yield strength, in kips per square inch (3)	Concrete strength, in pounds per square inch (4)	Age at testing, in days (5)	Notes (6)
RS	18	75.0	3,470		Reference static tests (from
RS	30	75.0	3,030		Ref. 4)
RS	30T	75.0	2,610		
RS	42	75.0	2,660		
S	18	60.0	3,330	95	
IM	18	63.3	3,180	43	Incremental loading (impact)
IO	18	63.3	3,180	47	O: one loading to failure
IM	30	63.3	3,160	43	M: multiple loads increasing
IO	30	63.3	3,160	43	incrementally
IM	30T	63.3	3,610	28	
IO	30T	63.3	3,610	29	
IM	42	63.3	3,260	21	
IO	42	63.3	3,260	21	
C	18-1	60.0	3,330	100	Cyclic loads (impact)
C	18-2	60.0	3,400	30	C: repeated loading
C	18-3	60.0	3,400	31	CR1: reversed load-splice one
C	30-1	60.0	4,060	68	face only
C	30-2	60.0	4,060	69	CR2: reversed load-splice
C	30-1T	60.0	3,820	64	both faces
C	30-2T	60.0	3,820	67	
CR1	30	60.0	4,320	88	
CR2	30	60.0	4,320	95	
CR1	30T	60.0	3,340	56	
CR2	30T	60.0	3,340	57	

[a]Notation following splice length indicates several tests with same details; S = static test for reference in C series; and T denotes transverse reinforcement in splice region, No. 2 @ 4.5 in.
Note: 1 in. = 25.4 mm; 1 ksi = 6.895 MPa; and 1 psi = 0.006895 MPa.

constant between the load points under the impact loads imposed. Inertia effects varied the moment by less than 3% along the splice.

Instrumentation consisted of strain gages along the splice (generally at the splice ends and center), load cells at the reactions, and DCDT deflection gages positioned at the load points. Mechanical dial gages were used to measure residual deflection after each impact load.

Impact forces applied through the vermiculite cushions at the load points were not monitored because the instrumentation necessary to do so was not available to the study. The moment on the lap splice under impact loading
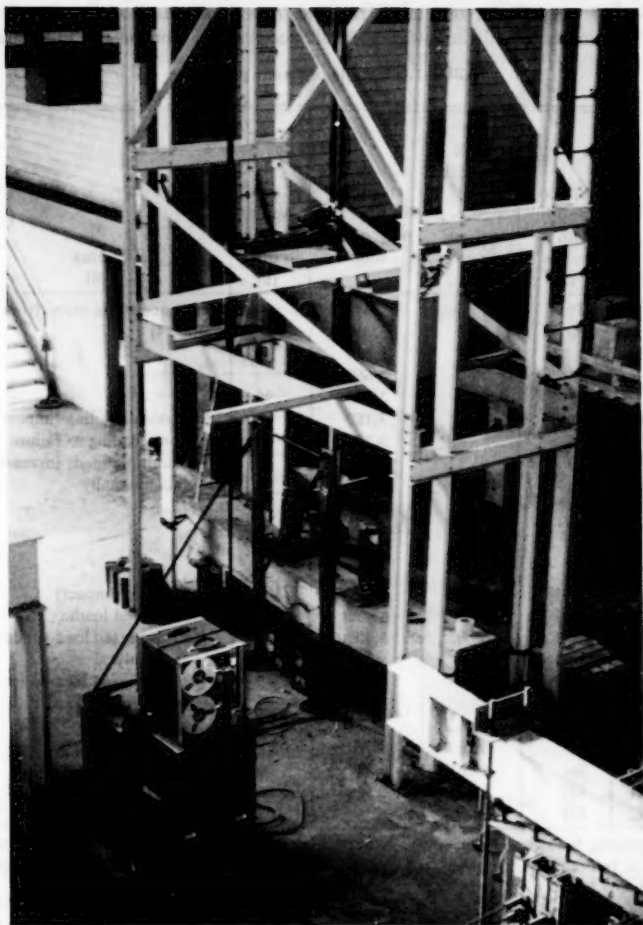
FIG. 2.—Dynamic Loading System

was obtained from the strains recorded in the reinforcing bars along the splice. In addition, it was found that the reaction forces (which were measured) could be used to estimate the moment existing along the splice. The beam was supported by pin and roller assemblies which rested on large load cells.

Test Results.—Strains, reactions, and deflections were recorded on magnetic tape and reproduced using a light-beam oscillograph. Typical results for selected responses are shown in Fig. 5. Each channel was calibrated prior to each test. A vertical line gives magnitudes of all responses at the time instant selected.

Reactions.—The reactions showed an overall sinusoidal shaped response (fundamental vibration mode) on which higher mode vibrations were superimposed. Analytical studies (10) shown in Fig. 6 indicated that the higher mode vibrations could have been caused by a combination of effects including rapid
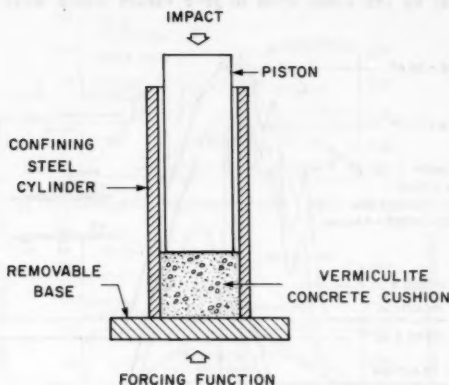
FIG. 3.—Cushioning Detail
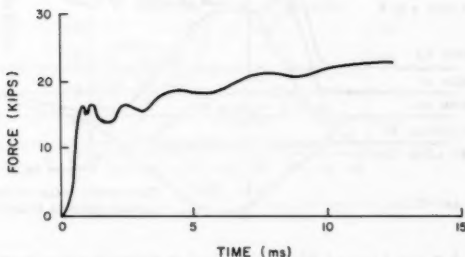
FIG. 4.—Force-Time Curve of Cushioned Impact Load (2) (1 kip = 4.45 kN)

application of load which excited higher modes, minor misalignment during loading which caused nonsimultaneous impact at the two load points, and inelastic effects such as concrete cracking and steel yielding which affected symmetry of the specimen. The analytical results in Fig. 6 are for the same beam geometry (modelling test beams with 30-in. splices) and three different loading cases. In Fig. 6(a), the loading rise time (TR) of 10 msec is slow with respect to the natural period of the beam (52 msec) and higher mode vibrations are not excited. For Fig. 6(b), with a faster rise time (TR = 2 msec) the third vibration

mode is visible. With different magnitude load functions at different starting times (nonsimultaneous impact simulation) in Fig. 6(c), a strong second mode vibration is apparent in the reactions. Note that even though the reactions were influenced by variations in the load function, little change was noted in the moments or deflections.

From the elastic analysis, it was concluded that smooth reaction curves could be drawn to eliminate the higher mode vibrations and moments in the splice region can then be obtained by multiplying the maximum reaction (from the smoothed curve) by the shear span to give values which were within 5% of
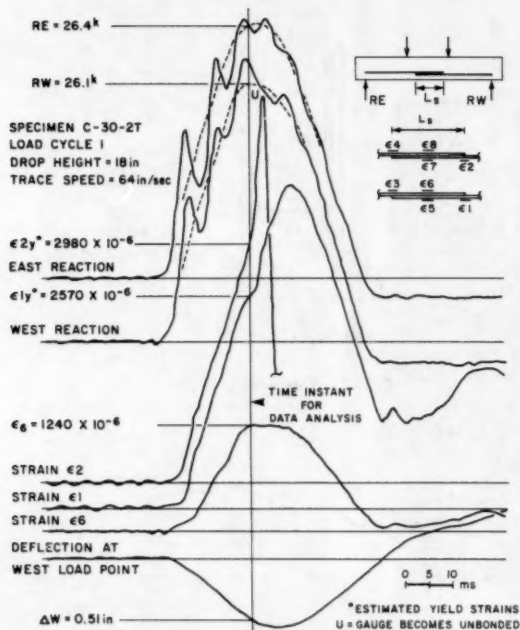
FIG. 5.—Typical Dynamic Data (1 in. = 25.4 mm, 1 kip = 4.45 kN)

the moments using exact analysis. It should be noted that the close approximation of maximum moment would not be applicable under different loading arrangement (load points or load functions).

For the model beam used in the analyses shown in Fig. 6(c) with a shear span of 50 in. (1,270 mm) and a maximum reaction (from the smoothed curve) of about 27 kips (120 kN), the approximate center line moment of 1,350 in.-kips (150 kN-m) compares favorably with the theoretical maximum center line moment. The reaction traces shown in Fig. 5 have been approximated by dashed lines to illustrate the approach.

The typical data shown in Fig. 5 starts just before impact and about 40 msec after impact, the beam bounced off the reaction load cell supports. The reaction exhibited negative magnitude at this point since the weight of the beam was not carried by the reaction load cells.

Strains.—Strain $\epsilon6$ shown in Fig. 5 is typical of a bar which does not yield at the gage location. Strains $\epsilon1$ and $\epsilon2$ are complicated due to yielding which occurred during the loading. The magnitude of the dynamic yield strain (where
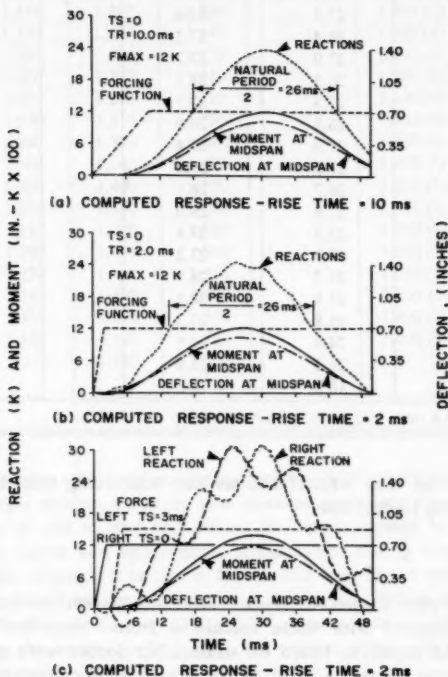
FIG. 6.—Typical Analytical Data (1 in. = 25.4 mm, 1 kip = 4.45 kN)

bars first yielded) can only be estimated. The large dynamic yield strains (well above the static yield strain of about $2,050 \times 10^{-6}$) estimated for strains $\epsilon1$ and $\epsilon2$ (Fig. 5) were reasonable based on the strain rates and measured reactions which were larger than those measured under static loading. A large residual tensile strain is shown in strain $\epsilon1$ indicating yielding of the reinforcing steel. The gage measuring strain $\epsilon2$ became unbonded (point U in Fig. 5).

Deflections.—The deflection response shown in Fig. 5 is typical for load cycles during which the steel yielded. The load point deflection continued to

TABLE 2.—Typical Test

Load cycle (1)	Drop height, in inches (2)	East reaction, RE, in kips (3)	West reaction, RW, in kips (4)	Steel Strains in micro-inches		
				$\epsilon1$ (5)	$\epsilon2$ (6)	$\epsilon3$ (7)
1	18	26.4	26.1	2,370	2,780	2,670
2	18	26.1	26.9	2,560		2,780
3	18	27.3	26.6			
4	18	26.4	27.2			
5	18	27.0	27.7			
6	18	26.5	28.5			
7	18	27.3	27.7			
8	18	28.8	26.9			
9	18	27.9	27.4			
10	18	28.6	27.9			
11	18	26.7	28.1			
12	18	27.9	28.0			
13	18	27.3	27.9			
14	18	27.3	27.2			
15	18	25.7	28.8			
16	18	27.5	28.5			
17	18	25.8	27.3			
18	18	24.8	26.5			
19	18	24.2	23.8			
20	18	18.2	19.2			

Note: 1 in. = 25.4 mm; 1 kip = 4.448 kN; 1 in.-kip = 113 N·m.

increase beyond the time when reactions and reinforcing steel loads peaked and were beginning to decrease.

ANALYSIS OF DATA

Calculation of Splice Region Moments.—Moments determined from measured strains were compared with those calculated from "smoothed" maximum reactions. For the moments based on strains, bar forces were multiplied by an effective internal moment arm which was taken as 0.9 of the effective depth (d). A complete tabulation of the test results may be found in Ref. 9. Averaged maximum reactions, strains, and moments based on reactions and strains are given in Table 2 for specimen C-30-2T. The average reaction was multiplied by the shear span to give the moment M_{ave}. Strain readings at the ends of the splice and at the center line were used to calculate the moments $M\epsilon E$, $M\epsilon W$, and $M\epsilon C$. The percent variation of the moments calculated from strains as compared to the moment calculated from the reaction is given in parenthesis.

In specimen C-30-2T the bars yielded in the first cycle and the gages at the ends of the splice did not operate beyond the second cycle. Gages $\epsilon7$ and $\epsilon8$ (Fig. 5) at the center of the splice were not functioning but gages $\epsilon5$ and $\epsilon6$ gave consistent readings and were used to calculate moment at the center of the splice. The strains recorded during the first load cycle were adjusted

Data (Specimen C-30-2T)

Along Splice, per inch			Moments Along Splice, in inch-kips			
$\epsilon 4$ (8)	$\epsilon 5$ (9)	$\epsilon 6$ (10)	M_{ave} (11)	$M\epsilon E$ (12)	$M\epsilon C$ (13)	$M\epsilon W$ (14)
2,350	1,100	1,090	1,310	1,360 (4)	1,190 (9)	1,390 (6)
2,510	1,240	1,150	1,330	1,430 (8)	1,290 (3)	1,380 (4)
	1,310	1,200	1,350		1,360 (1)	
	1,370	1,220	1,340		1,400 (4)	
	1,390	1,250	1,370		1,430 (4)	
	1,430	1,270	1,380		1,460 (6)	
	1,410	1,260	1,380		1,440 (4)	
	1,370	1,310	1,390		1,450 (4)	
	1,390	1,300	1,380		1,460 (6)	
	1,380	1,360	1,410		1,480 (5)	
	1,400	1,400	1,370		1,520 (11)	
	1,330	1,410	1,400		1,480 (6)	
	1,340	1,380	1,380		1,470 (7)	
	1,390	1,470	1,360		1,550 (14)	
	1,430	1,450	1,360		1,560 (15)	
	1,380	1,490	1,400		1,550 (11)	
	1,330	1,430	1,330		1,490 (12)	
	1,190	1,390	1,280		1,400 (9)	
		1,180	1,200			
			935			

to account for two effects of concrete cracking. After cracking the beam weight produced larger strains. Cracking also released shrinkage strains in the beams. Adjustments of 150×10^{-6} and 200×10^{-6} were applied to strains recorded at the splice center and splice ends, respectively, during the first load cycle. A typical gage response is shown in Fig. 7. The base line A which approximates the strain recorded by the gage prior to impact has shifted upward from zero in the first load cycle to over 200×10^{-6} in subsequent load cycles. The line B represents the strain reading after the impact when vibration has stopped and the drop weight is resting on the specimen.

In most cases the moments calculated from strains and from reactions varied by 10% or less with a maximum variation of 15% (Table 2). It was observed that the two sets of spliced bars usually carried unequal forces at a given section which resulted in greater variation in moments if strains in some of the bars at the cross section were unknown. In general, the moments calculated when all strains at a given cross section were available, were within 10% of those calculated from reactions.

Impact Strength of Lap Splices

Static strength is given in Table 3 (column 5 and 6) for the reference tests. Since the static moment capacities were governed by anchorage splitting failures,

the moments were adjusted for nominal concrete strength of $f'_c = 3,000$ psi. It was assumed the bond (splitting tensile) resistance of the concrete varied as the square root of the concrete compressive strength ($f_t \propto \sqrt{f'_c}$). For the 18-in. (460-mm) splices the variation in the two static test results can be attributed to the large scatter which occurs in bond and anchorage tests. Scatter is especially large with short embedment lengths.

The measured static beam strengths, adjusted to a concrete strength $f'_c = 3,000$ psi (20 MPa), in column 6 of Table 3, exceed the predicted strengths based on work by Orangun, Jirsa, and Breen (8) given in column 7. Differences are to be expected, since the predicted strengths are based on average test data from all sources. The measured strengths are from 8%–13% above the predicted, except for specimens utilizing the very short 18-in. (460-mm) splice length, where the developed reinforcement stresses are below the range for which the equations for predicting strength apply. Comparisons with impact
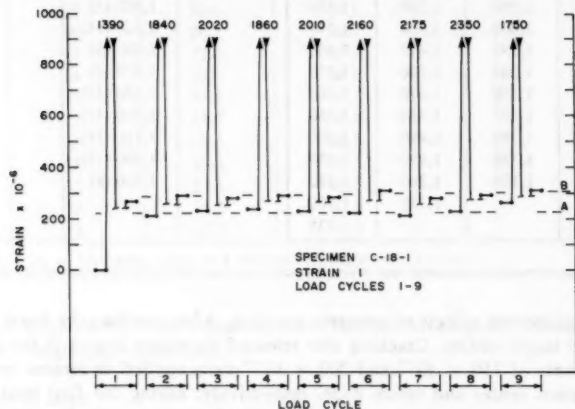
FIG. 7.—Shrinkage and Self Weight Strain Correction for First Load Cycle

strengths are made later using the measured static beam strengths given in column 6.

Precluding a splice failure, static yield moments based on an internal moment arm of $jd = 0.9d$ are $M_y = 1,170$ in.-kips (130 kN·m) for I series beams [$f_y = 63.3$ ksi (436 MPa)] and $M_y = 1,110$ in.-kips (125 kN·m) for all C series beams [$f_y = 60.0$ ksi (414 MPa)]. Static moment capacities based on splice failure (Table 4, column 2) and adjusted for concrete strength exceeded the static yield moment in twelve specimens [M_s greater than 1,100 in.-kips (130 kN·m)]. Under static loading, yielding of the steel would occur and prevent a splice failure unless the steel strength is increased by strain hardening or very large deformations are imposed. Under rapid load rates, steel yield strength may increase and moment capacity based on splice failure with concrete controlling the strength provides a useful reference.

Comparison of Impact and Static Splice Strength.—The strength of specimens

tested under impact is compared with static strength in Table 4. The static moment capacity in column 2 (M_s) was obtained from values in Table 3, column 6 and adjusted for the concrete strength of the specimens under impact ($M_s\sqrt{f'_c/3,000}$). The expected static moment capacity is based on failure governed by splitting (splice failure) and assumes the moment is not limited by yielding in the steel.

The dynamic load was varied by changing the drop height of the impacting weight, the loading piston diameter, and the cushioning vermiculite cylinder height. In most of the tests 6-in. (150-mm) pistons and 6-in. (150-mm) vermiculite cylinder heights were used. Drop height varied from 8 in.–84 in. (200 mm–2,130 mm). Full details are available in Ref. 10.

The ratio of impact moment to static moment capacity based on splice strength (tensile splitting dependent on concrete tensile strength) is shown in column

TABLE 3.—Splice Strength: Static Loading

Specimen (1)	Concrete compressive strength, in pounds per square inch (2)	Steel yield strength, in kips per square inch (3)	Maximum measured steel stress, in kips per square inch (4)	Maximum moment, in inch-kips (5)	Maximum moment,[a] in inch-kips (6)	Predicted moment,[b] in inch-kips (7)
RS-18	3,470	75	42.4	784	728 (776)	609
S-18	3,330	60	47.0	868	824 (776)	609
RS-30	3,030	75	52.5	970	965	892
RS-30T	2,610	75	57.3	1,060	1,135	1,002
RS-42	2,660	75	66.2	1,224	1,300	1,175

[a] Adjusted for nominal $f'_c = 3,000$ psi.
[b] As per Ref. 8 for nominal $f'_c = 3,000$ psi.
Note: 1 ksi = 6.895 MPa; 1 psi = 0.006895 MPa; 1 in.-kip = 113 N·m; 1 in. = 25.4 mm.

4 of Table 4. The maximum impact moment carried by the beam always exceeded the static capacity. Impact moment magnitudes increased with increasing drop heights.

In the reversed loading studies, the beam was turned 180° after each impact. For similar drop heights it was found that the moments were generally lower for reversed loading compared to unidirectional loading. It is likely that more impact energy was absorbed because the beams deflected more under reversed loading. The beam had to be displaced through the residual deflection from the previous load application before net deflection in the reversed direction occurred.

Comparison of Impact and Static Yield Strength.—The ratios in Table 4, column 5, impact moment/static yield moment, show that in all but one case (specimen C-18-2), peak impact moments exceeded the static yield moments. For 18-in.

(460-mm) splices the impact moment was up to 19% greater than the static yield moment for the large drop heights. For smaller drop heights, a larger number of impact loads producing smaller moments were sustained before collapse.

For 30-in. (760-mm) splices the highest dynamic to static yield moment ratio was 1.67 for the third load cycle on specimen C-30-1T. Specimen C-30-1T had stirrups along the splice, and was subjected to a large impact [drop height

TABLE 4.—Comparison of Impact and Static Capacities

Speci-men (1)	Static moment, M_s, in inch-kips[a] (2)	Number of cycles (3)	Ratio of impact to static moment, M_i/M_s, (splice failure) (4)	Ratio of impact to static yield moment, M_i/M_y, (steel yielding) (5)
1M-18	800	4	0.58, 0.85, 1.74, 1.69	0.39, 0.58, 1.19, 1.15
1O-18	800	1	1.68	1.15
C-18-1	820	3	1.24, 1.39, 1.41	0.92, 1.03, 1.05
C-18-2	830	11	1.01, 3 @ 1.20,[c] 6 @ 1.28, 0.58	0.76, 3 @ 0.90,[c] 6 @ 0.96, 0.43
C-18-3	830	5	1.11, 1.20, 1.25, 1.35, 0.65	0.83, 0.90, 0.94, 1.01, 0.49
1M-30	990	4	0.47, 1.02, 1.39, 1.48	0.40, 0.86, 1.18, 1.26
1O-30	990	1	1.43	1.21
C-30-1	1,130	3	0.99, 1.44, 1.43	1.01, 1.47, 1.46
C-30-2	1,130	6	1.22, 4 @ 1.29, 1.17	1.24, 4 @ 1.31, 1.19
1M-30T	1,245	6[b]	0.39, 0.76, 1.10, 1.21, 2 @ 1.30	0.42, 0.80, 1.17, 1.29, 2 @ 1.38
1O-30T	1,245	1[b]	1.24	1.32
C-30-1T	1,280	5	0.98, 1.23, 1.45, 1.30, 1.02	1.14, 1.41, 1.67, 1.50, 1.18
C-30-2T	1,280	20	17 @ 1.12, 1.05, 0.98, 0.78	17 @ 1.28, 1.22, 1.14, 0.90
1M-42	1,360	4[b]	0.43, 0.84, 1.11, 1.13	0.50, 0.97, 1.29, 1.31
1O-42	1,360	1[b]	1.10	1.28
CR1-30	1,160	27	0.81, 2 @ 0.91, 15 @ 1.02, 6 @ 1.08, 2 @ 1.18, 1.43	0.85, 2 @ 0.95, 15 @ 1.07, 6 @ 1.13, 2 @ 1.23, 1.50
CR2-30	1,160	8	4 @ 1.16, 3 @ 1.11, 0.74	4 @ 1.21, 3 @ 1.16, 0.77
CR1-30T	1,200	32[b]	1.09, 1.18, 30 @ 1.10	1.18, 1.27, 30 @ 1.19
CR2-30T	1,200	13	12 @ 1.10, 0.92	12 @ 1.19, 0.99

[a] Static moment is adjusted for the concrete strength of specimen.
[b] No splice failure.
[c] Multiload values have range of ±0.05.
Note: 1 in.-kip = 113 N·m.

= 72 in. (1,830 mm)]. For specimens without stirrups, the highest ratio of 1.50 was found in specimen CR1-30 using a large drop height of 84 in. (2,130 mm). Prior impact loads on specimen CR1-30 at loads near the static capacity (column 4) did not appear to weaken the splice. Two impacts using larger 24-in. (610-mm) drop heights were subsequently carried successfully (2 @ 1.18 in

column 4) before failure under the large final impact using the 84-in. (2,130-mm) drop height.

Influence of Transverse Reinforcement.—The data in Table 4 indicates specimens with stirrups through the splice region fared better, as expected. In several instances (specimens CR1-30T, IM-30T and IO-30T) a bond failure was not achieved under the impact loadings imposed even though similar specimens without stirups failed in the splice. Specimens with stirrups which failed in the splice sustained more severe loading in terms of impact level or cycles of loading prior to failure, or both, compared with specimens containing no stirrups through the splice.

Specimens subjected to loading reversals (excluding top face splices) appeared to perform as well as unidirectionally loaded specimens. The results from specimens with both top and bottom face splices (CR2-30 and CR2-30T) reflected the poorer bond characteristics associated with top cast bars. Considering that the ACI code (1) requires an increase of 40% in the length of top cast splices, the observed behavior of the top cast splices under impact was very good. For static loading the splice length required for top bars by the ACI code for a concrete strength of 3,500 psi (24 MPa) is 62 in. (1,600 mm). The static yield strength was exceeded with only 30-in. (760-mm) splice lengths.

Influence of Loading Rates.—The impact strengths (Table 4) exceeded both the static yield strength (controlled by f_y) and the static splice strength (controlled by the tensile splitting strength of the concrete). High strain rates increase the yield stress of steel (3,6,9). Measured strain rates (obtained from the slope of the strain-time curves in the reinforcing steel of the test specimens) reached 0.4–0.5 in./in./sec prior to yielding. For example, in Fig. 5 the estimated dynamic yield strain $\epsilon l_y = 2,570 \times 10^{-6}$ was reached in about 16 msec resulting in a strain rate of $2,570 \times 10^{-6}/(16 \times 10^{-3}) = 0.16$ in./in./sec for this relatively low impact cycle with a drop height of 18 in. (460 mm).

For a strain rate of 0.4 in./in./sec, Nadai (9) reports an increase of dynamic over static yield stresses of about 45% for mild steel with a static yield stress of 28 ksi (190 MPa), while Feldman, Keenan, and Siess (3) found increases of about 40% for intermediate grade reinforcing bars [static yield = 40 ksi–49 ksi (280 MPa–340 MPa)]. For steel with a static yield stress of 70 ksi (480 MPa), Flathau (6) reports an average increase of some 10%–15% over static. For the reinforcing steel of the dynamically tested specimens (static yield stresses of 60 ksi and 63.3 ksi (410 MPa and 440 MPa), dynamic yield stress increases in the order of 20%–30% could be anticipated for a strain rate of 0.4 in./in./sec. These increases are sufficient to explain the M_i/M_y ratios in Table 4. The largest ratios of M_i/M_y occurred under large impact loads (high drop height) where strain rates could not be determined because gages had been destroyed in previous load cycles. In those cases strain rates much larger than 0.4 in./in./sec would be expected.

The measured impact strengths exceeded the static strength based on anchorage (tensile splitting) failure (Col. 4, Table 4). The high tensile stress rates in the concrete increased the concrete strength over static values. Rates of stress may be estimated by taking the static tensile concrete strength, say $7.5 \sqrt{f'_c} = 7.5 \sqrt{4000} = 474$ psi (3.27 MPa) for 4,000 psi (28 MPa) concrete and dividing by the impact rise time to failure recorded in the reactions of the test data. A rise time of 20 msec represents an average value from the data and gives

a tensile stress rate of $474/(20 \times 10^{-3}) = 23,700$ psi/sec (163 MPa/s).

A study by Galloway and Raithby (7) evaluated the effect of high stress rates on the modulus of rupture of 20 in. $\times$ 4 in. $\times$ 4 in. (510 mm $\times$ 100 mm $\times$ 100 mm) plain concrete beams loaded at the third points. Results of tests using two concretes with cube strengths of 6,500 psi (45 MPa) and 4,830 psi (33 MPa) showed that a stress rate of 25,000 psi/sec (172 MPa/s) increased the modulus of rupture by 65% over that observed using a very slow rate. The aforementioned stress rate is comparable to the 23,700 psi/sec (160 MPa/s) which was estimated for the splice tests. More precision in estimating stress rates during testing is not warranted since the study showed that a much lower stress rate of 10,000 psi/sec (70 MPa/s) still produced large (35%–50%) increases over static modulus of rupture.

The high impact to static moment ratios (M_i/M_s) for specimens with 18-in. and 30-in. (460-mm and 760-mm) splices subjected to large impact loads compare favorably with values expected if the tensile concrete strengths were adjusted for the high stress rates. The ratios were higher for the 18-in. (460-mm) splices than for the 30-in. (760-mm) splices. Since material strengths under similar impact loads increased the concrete tensile capacity more than the steel yield strength, yielding limited the increase in the impact resistance of the 30-in. (760-mm) splices while concrete strength limited the resistance of the 18-in. (460-mm) splices.

TOUGHNESS OF LAP SPLICES UNDER IMPACT LOADING

Definition of Toughness.—The measurement of toughness of a splice under rapid loading is complicated because of the increases in dynamic strength of the steel and concrete over static strengths. Simple criteria used with static
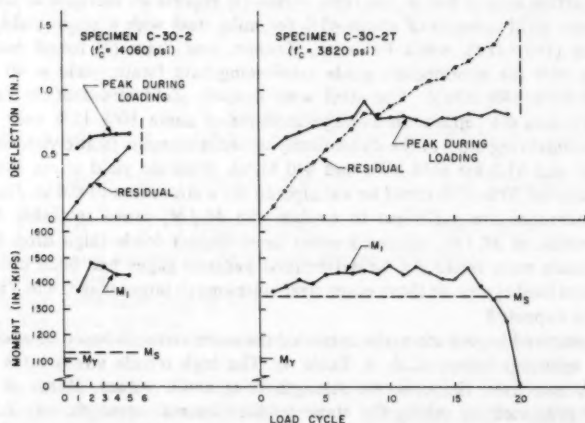

FIG. 8.—Deflections at Load Points: Unidirectional Loading (1 in. = 25.4 mm, 1 in.-kip = 113 N·m, 1 psi = 0.0069 MPa)

loading such as requiring the splice to carry at least 25% more capacity (5) than the yield strength of the steel are difficult to apply to impact loads since both the steel yield and the tensile splitting strength of the concrete depend on loading rates which cannot be easily defined. Therefore, measures of toughness must be related to peak strengths, number of impact loads, deflections, and energy absorbed before failure.

Though the test specimens performed well under the impact loads imposed and moments exceeded static capacities, strength is an inadequate measure of impact performance as seen from the data in Table 4. For specimens with
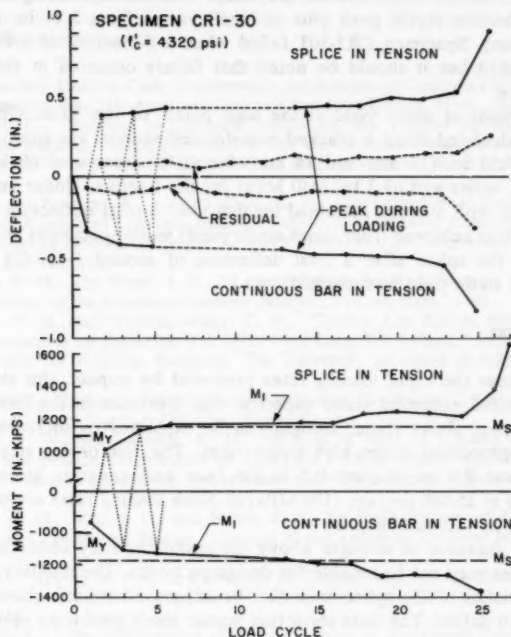
FIG. 9.—Deflections at Load Points: Reversal Loading (1 in. = 25.4 mm, 1 in.-kip = 113 N·m, 1 psi = 0.0069 MPa)

18-in. (460-mm) splices, impact moments varied from around 1.70 times the reference static moment when failure was achieved in one or two large impact loads (specimens IM-18 and IO-18) to 1.01-1.33 of static for failure under 10 cycles of smaller impact loads (specimen C-18-2). Specimens with 30-in. (760-mm) splices showed a similar increase in number of loads to failure with reductions in magnitude of impact loads.

Performance Related to Beam Deflections.—Peak deflections produced under each impact load and residual deflections after each impact (cumulative for all cycles) are shown in Fig. 8 and Fig. 9. In Fig. 8, unidirectional loading

on C-30-2 and C-30-2T resulted in a gradual accumulation of residual deflections. A larger buildup of residual deflection prior to failure was observed for a beam with stirrups (specimen C-30-2T). In Fig. 9, reversal loading on specimen CR1-30 prevented the buildup of residual deflections during the initial low magnitude impact loads.

The total load point deflections occurring in the beams with the 30-in. (760-mm) splices in the load cycle just prior to failure gave an indication of the difference in toughness between specimens with and without transverse splice reinforcement. Without stirrups along the splice, the total deflection prior to failure ranged from 0.85 in. (20 mm)–1.33 in. (35 mm). With stirrups along the splice, the total deflection (cycle peak plus residual) varied from 2.11 in. (55 mm)–2.39 in. (60 mm). Specimen CR2-30T failed when a deflection of 1.41 in. (35 mm) was reached but it should be noted that failure occurred in the weaker top cast splice.

Deflections at static yield at the load points of the 30-in. (760-mm) splice beams calculated using a cracked transformed section are approximately 0.50 in. and 0.53 in. (13 mm and 14 mm) for yield stresses of 60 ksi (410 MPa) for the C series and 63.3 ksi (440 MPa) for the I series. Under impact loading, specimens with stirrups sustained loading until a total deflection of over 2 in. (50 mm) was achieved (four times static yield) while specimens without stirrups failed in the splice after a total deflection of around 1 in. (25 mm) or two times the static yield was reached.

CONCLUSIONS

1. Under the rapid loading rates produced by impact, the strength of the splices tested exceeded static capacity. The increases in the flexural strength under impact above static strength can be explained by increases in material strength properties under high strain rates. The reinforcing steel strain rates were about 0.4 in./in./sec–0.5 in./in./sec and concrete stress rates were estimated at 25,000 psi/sec (170 MPa/s). Such loading rates are possible under explosion or vehicular impact.

2. The increase in strength above the static capacity observed under high strain rates may not be reliable for design purposes. The ductility or toughness characteristics of the splice must also be adequate but such characteristics are difficult to define. The tests show that impact loads producing moments slightly above the static capacity can be sustained for many cycles while large impact loads (30% or more above static capacity) fail the splice after relatively few applications.

3. Splice performance under reversal loading appears to be no worse than that under unidirectional loading. With reversal, smaller reactions and splice moments are induced under the same impact (drop height) because more energy is absorbed in inelastic deformation (residual deflection and cracking) as the beam is deflected in opposite directions.

4. Light stirrups along the splice greatly enhance toughness and durability characteristics of the splice. For the 30-in. (760-mm) splices, impact loads were sustained with total deflections at least twice the magnitude of deflections at failure of similar specimens without stirrups. With stirrups, approximately four times the static yield deflection was sustained. Where impact loads are anticipated

it is recommended that stirrups be placed along the splice length.

5. Reduction in the anchorage strength of top cast bars due to bleeding and entrapment of air beneath the bars for dynamic loading appears no more severe than the 40% reduction factor used in design for static loading.

6. Impact loading which produces moments equal to the static strength of the splice can be safely sustained for strain rates in the steel as high as 0.4 in./in./sec. It appears that higher strain rates could be carried satisfactorily, provided the static capacity of the splice is not exceeded. Further study is needed to ensure that impact loads producing moments exceeding static splice strength will not result in a sudden (nonductile) failure.

APPENDIX I.—REFERENCES

1. "*ACI Standard Building Code Requirements for Reinforced Concrete* (ACI 318-77)," ACI Committee, No. 318, American Concrete Institute, Detroit, Mich., Oct., 1977.
2. Bufkin, M. P., "Behavior of Concrete Reinforcing Bar Lapped Splices Subjected to Dynamic Loading," thesis presented to The University of Texas, at Austin, Tex., in January, 1974, in partial fulfillment of the requirements for the degree of Master of Science.
3. Feldman, A., Keenan, W. A., and Seiss, C. P., "Investigation of Resistance and Behavior of Reinforced Concrete Members Subjected to Dynamic Loading, Part III," *Civil Engineering Studies, Structural Research Series*, No. 243, University of Illinois, Urbana, Ill., Feb., 1962.
4. Ferguson, P. M., and Breen, J. E., "Lapped Splices for High Strength Reinforcing Bars," *Journal of the American Concrete Institute*, Vol. 62, Sept., 1965.
5. Ferguson, P. M., and Krishnaswamy, C. N., "Tensile Lap Splices Part 2: Design Recommendations for Retaining Wall Splices and Large Bar Splices," *Research Report 113-3*, Center for Highway Research, The University of Texas at Austin, Austin, Tex., Apr., 1971.
6. Flathau, W. J., "Dynamic Tests of Large Reinforcing Bar Splices," *Technical Report N-71-2*, U.S. Army Engineer Division, Huntsville, Ala., Apr., 1971.
7. Galloway, J. W., and Raithby, K. D., "Effects of Rate of Loading on Flexural Strength and Fatigue Performance of Concrete," *TRRL Report LR547*, Transport and Road Research Laboratory, Department of the Environment, Crowthorne, Berkshire, 1973.
8. Orangun, C. O., Jirsa, J. O., and Breen, J. E., "A Re-evaluation of Test Data on Development Length and Splices," *Journal of the American Concrete Institute*, Vol. 73, Mar., 1977.
9. Nadia, A., "Theory of Flow and Fracture of Solids," *Engineering Societies Nomographs*, Volume I, 2nd ed., McGraw-Hill Book Co., Inc., New York, N.Y., 1950, pp. 309–316.
10. Rezansoff, T., "The Performance of Lapped Splices in Reinforced Concrete Under Rapid Loading," thesis presented to the University of Texas, at Austin, Tex., in May, 1976, in partial fulfillment of the requirements for the degree of Doctor of Philosophy.

APPENDIX II.—NOTATION

The following symbols are used in this paper:

A_s = reinforcing steel area of two bars;
d = distance from center of tension steel to extreme fiber of compression face;
E_s = modulus of elasticity for reinforcing steel;
f'_c = ultimate compressive concrete strength;

FMAX = peak load applied by forcing function;
f_s = reinforcing steel stress;
f_t = splitting tensile concrete strength;
M_{ave} = moment calculated from average of two end reactions;
M_i = impact moment = M_{ave} + dead weight moment;
M_s = static moment capacity;
M_y = static yield moment;
$M\epsilon C$ = moment calculated from strains measured at center of splice;
$M\epsilon E$ = moment calculated from strains measured at east end of splice;
$M\epsilon W$ = moment calculated from strains measured at west end of splice;
n = number of gages operating at section under consideration;
RE = reaction at east end of beam;
RW = reaction at west end of beam;
TR = forcing function rise time;
TS = forcing function start time;
ϵ_s = reinforcing steel strain; and
ϵ_x = strain reading at gage position X.

LOGICAL ANALYSIS OF TENTATIVE
SEISMIC PROVISIONS

By James Robert Harris,[1] Steven J. Fenves,[2] Members, ASCE,
and Richard N. Wright,[3] F. ASCE

INTRODUCTION

The "Tentative Provisions for the Development of Seismic Regulations for Buildings" (1) (hereafter denoted Provisions) were prepared by the Applied Technology Council (ATC) to "present, in one comprehensive document, current state-of-knowledge in the fields of engineering seismology and engineering practice as it pertains to seismic design and construction of buildings" (1). The Provisions are intended to be used in the development of national standards, model codes, and building regulations in order to reduce hazards due to earthquakes. This paper is based on a report, "Analysis of Tentative Seismic Design Provisions for Buildings" (4) (hereafter denoted Analysis) prepared in parallel with the ATC project. The Analysis is intended to assist those responsible for the assessment and implementation of the Provisions by providing a formal representation and a consistent documentation of their content and a constructive critique of possible clarifications and improvements. This paper summarizes the findings and methods of the Analysis for potential users of the Provisions. In addition, readers may find the methods of analysis valuable for use in other efforts in the formulation, assessment, and implementation of new or revised design standards and other normative documents.

The development of the Provisions by ATC was a major undertaking which involved broadening the scope beyond previous seismic design and construction provisions as well as introducing new technical approaches. The Provisions cut across the existing family of national standards for the structural design of buildings. For instance, loading standards consider earthquake effects as one of many design loadings, while resistance standards normally concentrate on one specific material and usually treat earthquake resistance as one of many requirements for that material. Therefore, a large number of standards developing

organizations need to study and adapt the ATC Provisions. To assist in this process of implementation, the National Science Foundation sponsored an analysis study to use previously developed (2) technical aids for the analysis, formulation and expression of standards. The objectives of the study were to: (1) Assist ATC in the preparation of the Provisions; (2) provide a formal representation of the Provisions to assist their potential users, particularly the standards and codes organizations that would draw upon portions of the Provisions; and (3) to explore alternative arrangements of these Provisions that would make them more readily usable by various categories of users.

This paper focuses on the second objective. The accomplishments towards all objectives are cited in the longer report (4).

Approach to Logical Analysis

The techniques of analysis have been adapted and developed from concepts of logic, taxonomy and computer science to provide technical aids for the formulation, expression, and use of standards. Provided here is a concise overview of the techniques; more detailed exposition is available elsewhere (2).

A standard can be analyzed to determine if it is clear, complete, consistent, and to some extent, correct. The analysis techniques do not correct any deficiencies identified. This is the responsibility of the standard-writing team.

The basic unit of a standard is a provision. Two kinds of provisions are recognized, based on a functional distinction:

1. Requirements.—Those provisions that are directly indicative of compliance with some portion of a standard; such provisions can normally be characterized by the fact that their evaluation yields a value of "satisfied" or "violated."

2. Determinations.—All provisions that are not requirements; such provisions are normally characterized by the fact that their evaluation results in either numerical or logical values, even by two-state values (like true and false), but the results are not amenable to characterization as "satisfied" or "violated."

The basic unit used in the analysis is a datum. The status of each requirement is a datum. Each result or variable produced by a determination is also a datum. In addition, every other variable referred to in a standard but not explicitly assigned a result by some provision is a datum.

A list of datums is used in the analysis to provide a systematic reference system for the provisions and to uncover possible ambiguities such as using two (or more) names for the same datum, or using the same (or similar), names for different datums.

The set of datums plus the systems that are used to express rules for evaluating and relating the datums contain all the information necessary to evaluate compliance with a standard. An additional set of information, a classification of the provisions, is used to provide quick and reliable access to the provisions pertinent to any given situation. Three principal tools are used in the analysis of the relations among datums and classifiers:

1. Decision tables are used to represent the meaning of individual provisions. They are easily analyzed to assure that the reasoning always leads to a unique result and that no possibility exists for encountering an unanticipated situation.

Decision tables are convenient for representing parallel thought processes, whereas the written text, and to some extent flowcharts, both describe a sequential thought pattern. The analysis of a decision table for clarity and completeness is performed by constructing a decision tree from the table.

2. Information networks are used to represent the precedence relations among provisions. Each datum corresponds to one node in the network. The nodes are connected by branches that represent the flow of information through a set of related provisions.

3. Families of classifiers for provisions are developed to cover pertinent physical elements of buildings, building processes, and the qualities required for these elements and processes. Relationships among classifiers and between classifiers and provisions guide the construction of the index, guide in outlining the text, and provide appropriate headings for the text. Alternative outlines can be generated and those best suited to the given use selected.

TABLE 1.—Decision Table and Table of Ingredients

Decision table (1)	Rules				
	1 (2)	2 (3)	3 (4)	4 (5)	E (6)
Conditions					
1. Seismic performance category = D	N	Y	Y	Y	
2. Building stage = new		Y	—	N	
3. Proposed work on existing building = change of use *and* seismic performance category before proposed work ≠ D		—	Y	N	
4. Potential exists for ground rupture from active fault = true		N	N		
Actions					
1. CDSLR = satisfied	X	X	X	X	
2. CDSLR = violated					X

Note: Ingredients (by datum name) are seismic performance category, building stage, proposed work on existing building, seismic performance category before proposed work, and potential exists for ground rupture from active fault.

The following examples illustrate the approach to the logical analysis. A representative requirement is as follows (1):

> 1.4.4 Site Limitation for Seismic Design Performance Category D: No new building or existing building which is, because of changing use, assigned to Category D shall be sited where there is a potential for an active fault to cause rupture of the ground surface at the building.

The corresponding decision table is shown in Table 1. The four parts of the decision table are separated by the row and column of asterisks. The "condition stub" in the upper left defines all logical conditions that affect the provision,

for instance "seismic performance category = D." The lower left portion of the decision table is the "action stub" that defines all possible values for the datum. Here, action 1 states CDSLR = satisfied (i.e., the category D site limitation requirement is satisfied) and action 2 states that it is violated. The "condition entry" in the upper right is divided into a set of rules. Each column contains one combination of condition values that defines rule. For instance, rule 1, read columnwise, states that condition 1 is N (No), and the other three conditions are immaterial (.). Rule 2 states that condition 1 is Y (Yes), condition 2 is Y, condition 3 is false [it need not be checked because it is predetermined to be false (−) by the outcome for condition 2], and condition 4 is N. Rule 5, labelled E (for ELSE), corresponds to any possible combination of condition values not included explicitly in the preceding rules. The lower right-hand portion, the "Action Entry," shows by each X the action appropriate to each rule.
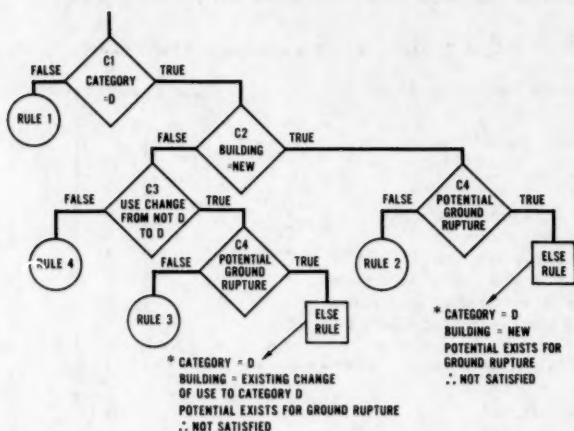

FIG. 1.—Decision Tree

The decision tree generated from the decision table of Table 1 is shown in Fig. 1. The figure repeats the logic of the decision table in detail giving exactly the same information for rules 1–4, but shows explicitly, in place of the fifth rule labelled E in Table 1, the two combinations of values for the four conditions for which the provision is violated.

The occurrence of the ELSE in the decision tree is a major tool in the analysis of provisions for completeness. Each such situation is checked to see whether one single action such as "CDSLR = violated" is appropriate or whether additional rules need be defined to cover the scope of the provision completely.

The "ingredients" tabulated below the decision table in Table 1 are those datums that need to be known in order to evaluate to the datum CDSLR. Similarly, CDSLR is termed a "dependent" of each of its ingredients.

The individual provisions, and their corresponding decision tables, are interrelated by the fact that the ingredients of one provision may be the output or

results of other provisions. The "information network" represents graphically the flow of information through the datums in the set of provisions. Fig. 2 shows the portion of such a network. The figure shows that the determination of the "required level of seismic analysis" depends on the datums "seismic performance category," "building configuration," "plan configuration," and "vertical configuration," which, in turn depend on other datums.

The entire information network can be assembled once each of the datums and its direct ingredients are known. The assembly is easily performed with a computer program. The complete information network can then be used for
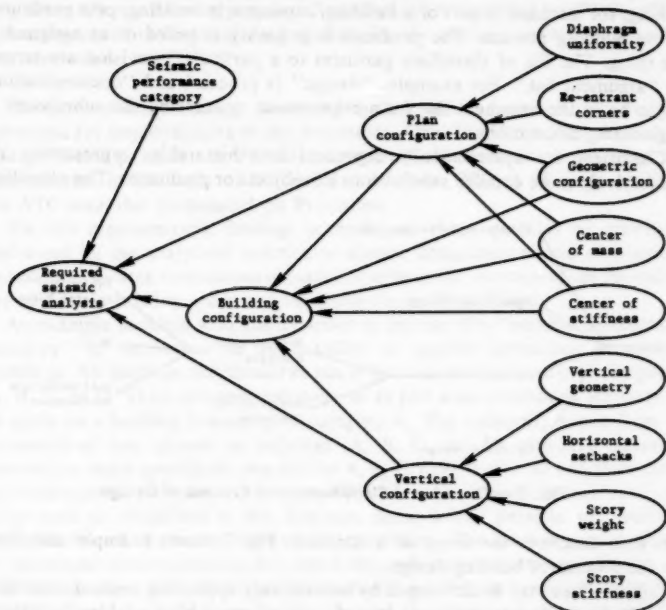
FIG. 2.—Information Network: Branch is Directed from Ingredient Datum to Dependent Datum

three general operations: (1) To determine the dependents of each datum; (2) to trace the global ingredience of a particular datum (i.e., all the datums that have any possible influence on the datum in question); and (3) to trace the global dependence of a particular datum (i.e., all the datums that might be influenced by the datum in question).

The information network is used to detect loops in the precedence relations among provisions, that is, when a datum appears in its own global ingredience. The information network also detects detached (unreferenced) sets of provisions. Examination of how a datum is used in the evaluation of its various dependents

is a check on the consistency of these dependent provisions.

The information network assists users of a standard by supplying cross references to the places where each datum is defined and used. The information network also guides the organization and expression of a standard. Generally a high level requirement is the topic of a chapter or section. Provisions along the requirement's ingredient branches are incorporated in the text until all pertinent provisions are incorporated or cited by cross references.

The overall organization of a standard is based on a basic structure of a provision and a classification of each provision according to that structure (4). Each provision consists of two parts, subject and predicate. The subject is a thing, for instance, a part of a building, a process in building, or a participant in the building process. The predicate is a quality required of or assigned to the thing. The list of classifiers pertinent to a particular provision are termed its "argument list." For example, "design" (a process) and "documentation" might be in the argument list for a requirement concerning the submission of engineering calculations.

Classifiers are systematically organized into hierarchies representing the successively more detailed subdivisions of subjects or predicates. The classifica-
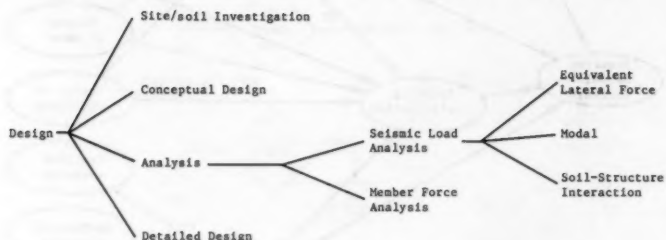

FIG. 3.—Three Level Classification of Process of Design

tion thus describes the scope of a standard. Fig. 3 shows example classifiers for the process of building design.

Trial outlines may be developed by successively appending trees of classifiers from the hierarchies to produce a tree of headings resembling a table of contents. Different outlines are obtained by varying the order in which the trees are appended. Thus the classification is also used to work with the arrangement of a standard. Note that the existence of a provision corresponding to each significant combination of subject and predicate classifiers is an important check on the completeness of a standard. Thus, study of the organization is useful during the early stages of developing a standard.

The provisions classified by a particular classifier are called its "scopelist." The scopelist is generated by transposing the argument lists for all the provisions. An index is generated from the classifiers and their scopelists.

REPRESENTATIVE FINDINGS

The magnitude of the effort of synthesis involved in the development of

the Provisions is well defined by the magnitude of the formal representation developed by the analysis:

1. The Provisions contain over 1,200 discrete items of data, including individual provisions and definitions.

2. There are over 340 provisions involving logical choices and expressed by decision tables.

3. Information networks, showing the path of the logic from input to evaluation that the building satisfies the provisions, show that as many as 51 provisions need be evaluated in series sequence.

4. Over 400 provisions appropriate for indexing are classified by 170 classifiers that are grouped in five major categories. On the average, each provision has five arguments.

The representative findings illustrated in this section focus on opportunities perceived for improvements in the Provisions. One should not infer from them that problems pervade the Provisions. Overall, the analysis shows very few uncertainties in the logic of individual provisions. This is of great credit to the ATC team that formulated the Provisions.

We cite representative findings according to three qualities of provisions addressed by the analytical techniques: clarity, completeness and consistency. In addition, we note some issues expected to arise as the contents of the Provisions are applied to existing codes and standards for building design.

An example problem with clarity arises in the use of a "seismic performance category" to determine the applicability of specific provisions to specific buildings. All buildings are classed as one of four seismic performance categories: A, B, C, or D. There is some ambiguity as to just what provisions are intended to apply to a building belonging to category A. The ambiguity stems from the mismatch of four classes of buildings (A, B, C, and D) with five classes of provisions, those specifically marked for A, B, C, or D, and those undifferentiated as to the seismic performance category. The four seismic performance categories were used as classifiers in the Analysis; thus, it was possible to produce a complete list of all the undifferentiated provisions. The list was then examined to determine those provisions for which the ambiguity may be significant.

It is not clear that all the undifferentiated provisions apply to category A buildings, and in fact, it is directly implied that some of them do not. For example, section 3.6.1 of the Provisions requires that category A buildings ". . . need only comply with the minimum seismic force requirements of Sec. 3.7.5 and 3.7.6, and to the requirements of Sec. 3.7.7 and 7.4." This implies rather strongly that sections 3.7.1 through 3.7.4 and 3.7.8 through 3.7.11, which do deal with seismic force requirements, should not apply to category A, even though they are not specifically identified as applying to categories B, C, or D.

A second example of a problem with clarity arises with the response modification factor R used in the Provisions to relate the seismic force effect to the energy absorbing capacity of the structural system. It was the intention of the ATC team to provide a direct design procedure, without the need for backtracking on previous design steps as a result of later decision. For such a procedure, the building type would be defined, the appropriate value selected for R, the

seismic force effects computed, the total force resultant effects calculated and the components checked (or designed and detailed in the design phase) for these forces. Table 2 is a reproduction of Table 3-B of the Provisions dealing with the determination of R. A problem occurs for buildings using moment

TABLE 2.—Table for R from Provisions

RESPONSE MODIFICATION COEFFICIENTS

Type of Structural System (1)	Vertical Seismic Resisting System (2)	Coefficients R (3)	C_d (4)
BEARING WALL SYSTEM: A structural system with bearing walls providing support for all, or major portions of, the vertical loads.	Light framed walls with shear panels	6 1/2	4
Seismic force resistance is provided by shear walls or braced frames.	Shear walls Reinforced concrete Reinforced masonry	4 1/2 3 1/2	4 3
	Braced frames	4	3 1/2
	Unreinforced and partially reinforced masonry shear walls	1 1/4	1 1/4
BUILDING FRAME SYSTEM: A structural system with an essentially complete Space Frame providing support for vertical loads.	Light framed walls with Shear panels	7	4 1/2
Seismic force resistance is provided by shear walls or braced frames.	Shear walls Reinforced concrete Reinforced masonry	5 1/2 4 1/2	5 4
	Braced frames	5	4 1/2
	Unreinforced and partially reinforced masonry shear walls	1 1/2	1 1/2
MOMENT RESISTING FRAME SYSTEM: A structural system with an essentially complete Space Frame providing support for vertical loads.	Special Moment frames Steel Reinforced concrete	8 7	5 1/2 6
Seismic force resistance is provided by Ordinary or Special Moment Frames capable of resisting the total prescribed forces.	Ordinary moment frames Steel Reinforced concrete	4 1/2 2	4 2
DUAL SYSTEM: A structural system with an essentially complete Space Frame providing support for vertical loads.	Shear walls Reinforced concrete Reinforced masonry	8 6 1/2	6 1/2 5 1/2
A Special Moment Frame shall be provided which shall be capable of resisting at least 25 percent of the prescribed seismic forces.	Wood sheathed shear panels	8	5
The total seismic force resistance is provided by the combination of the Special Moment Frame and shear walls or braced frames in proportion to their relative rigidities.	Braced Frames	6	5
INVERTED PENDULUM STRUCTURES: Structures where the framing resisting the total prescribed seismic forces acts essentially as isolated cantilevers and provides support for vertical load.	Special Moment Frames Structural steel Reinforced concrete	2 1/2 2 1/2	2 1/2 2 1/2
	Ordinary Moment Frames Structral Steel	1 1/4	1 1/4

frames or "dual systems" to resist seismic forces because the wording (". . . capable of resisting the total prescribed forces.") states that R depends on the prescribed seismic forces (the load effect). Two complete loops occur in the evaluation process as shown in Figs. 4 and 5. For the first: R depends

on the total prescribed force resultants, which depend on the seismic force, which, in turn, depends on R. This same R cannot be determined before determining the total prescribed force which cannot be determined without knowing R. The second arises because the strength of certain concrete components is given in terms of the level of seismic force. That loop goes thus: R depends on the strength of the moment frame, which depends on the seismic force, which in turn, depends on R.

This problem was revealed by constructing the information network for the global ingredience of the strength provisions. The loops can be eliminated by
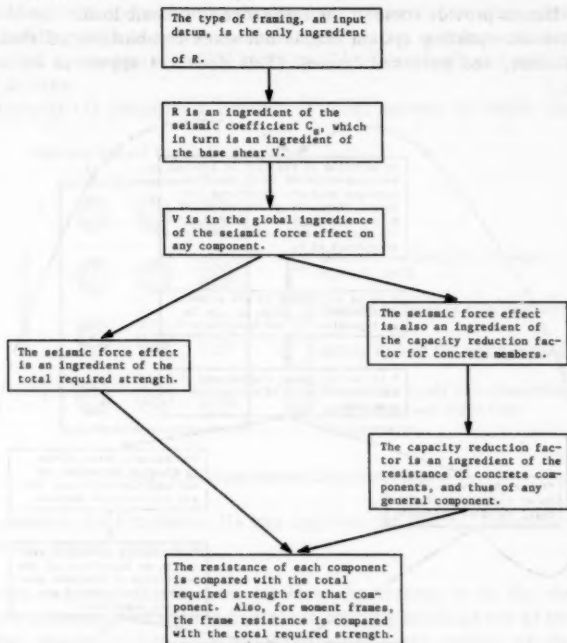
FIG. 4.—Probable Intent for Evaluation of Response Modification Factor R

relating R to the resistance rather than the prescribed force.

Analysis of completeness of individual provisions is accomplished using the decision tree analyses such as that represented by Fig. 1. One example of incompleteness occurs in Table 2 (Table 3-B of the Provisions) because some types of structural systems are not included. These systems, as were identified by decision table and decision tree analyses of Table 2:

1. Bearing wall and building frame systems that have a shear wall other than concrete, masonry, light framed, or wood sheathed (e.g., steel plate).

2. Moment frame systems that are not composed of either steel or reinforced concrete or that do not satisfy the special strength requirements for such systems.

3. Inverted pendulum structures that use shear walls or braced frames for seismic resistance, that use bearing walls for vertical support, or that use ordinary moment frames of reinforced concrete. (Consider an airport control tower with concrete walls.)

4. A dual system using an ordinary moment frame or using a shear wall other than reinforced concrete, reinforced masonry, or wood sheathing on light framing.

5. A structure in which bearing walls support some of the vertical load and moment frames provide some of the resistance to seismic load.

6. A seismic resisting system that is not some combination of shear walls, braced frames, and unbraced frames. (This does not appear to be a serious omission.)

In addition to the type of framing, the comparison of total required strength with the resistance for moment frames is an ingredient of R, yet its ingredients (shown with the dashed lines) are in the global dependence of R.

R is an ingredient of the seismic coefficient C_s, which in turn is an ingredient of the base shear V.

V is in the global ingredience of the seismic force effect on any component.

The seismic force effect is an ingredient of the total required strength.

The seismic force effect is also an ingredient of the capacity reduction factor for concrete members.

The capacity reduction factor is an ingredient of the resistance of concrete components, and thus of any general component.

The resistance of each component is compared with the total required strength for that component.
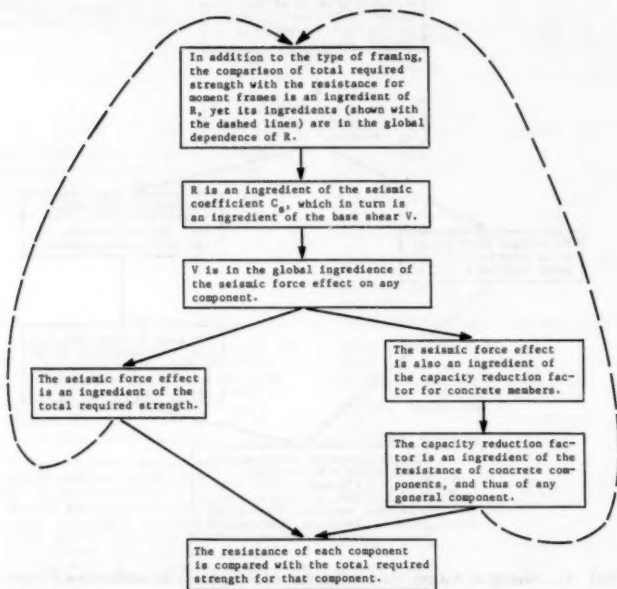
FIG. 5.—Apparent Loops in Evaluation of Response Modification Factor R

Although the intent may be that these structural systems do not qualify for any reduction factor R, it would be more clear to say so explicitly or to make reference to the general provision for alternate methods and materials of construction.

The use of the seismic performance category provides an example for the analysis of consistency. The seismic performance category depends on the seismity index, a measure of the geographically varying seismic hazard, and

the seismic hazard exposure group, a measure of the consequences of the building failure, and is used throughout the Provisions as the primary decision point for defining discontinuous requirements on framing systems, materials, construction, etc. However, certain provisions (e.g., for quality assurance planning, for the applicability of the architectural, mechanical and electrical provisions, and for defining when mechanical and electrical utilities shall be provided with shutoff devices) used different combinations of seismicity index and seismic hazard exposure group, as shown in Fig. 6. Conversion of all of the foregoing separate classifications to the most appropriate seismic performance category would avoid a large number of multiple groupings such as: (1) Category B and C buildings with and without quality assurance plan requirements; (2) category A and B buildings with and without anchorage of certain architectural, mechanical and electrical components; and (3) category C buildings with and without utility shut-off devices.

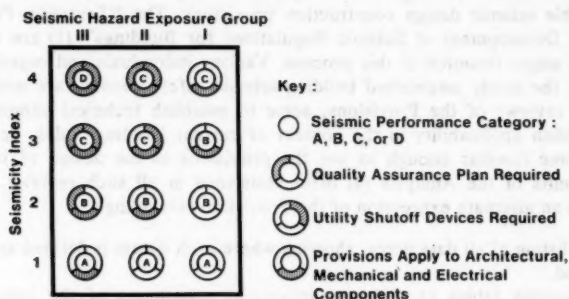The Analysis (4) identifies a number of other aspects in which those who

FIG. 6.—Inconsistent Decision Points

further develop the Provisions (1) can improve the clarity, completeness and consistency. Among these are:

1. Points requiring clarification: (a) How the references to the chapter on systematic abatement of seismic hazards in existing buildings are to be handled when that chapter is not adopted; (b) whether some aspects of the quality assurance provisions should be imposed when a quality assurance plan is not required; (c) whether the increased allowable stresses provided in the chapters amending the reference standards for structural materials apply for category A; and (d) whether all seismic hazard exposure group III buildings shall have the capacity to function during an earthquake.

2. Points appearing incomplete: (a) Lack of specification of capacity reduction factors for significant components; (b) the admissible design approaches for wood frame buildings; (d) the types of attachment for mechanical and electrical equipment for which amplification factors are specified; and (e) cross references concerning plan configuration, modifications to hazardous existing buildings, and unspecified seismic forces.

3. Points appearing inconsistent: (a) Potentially conflicting height limitations

for moment frames; (b) citations of reference standards ranging from none to specific citations to implicit incorporations; and (c) variations from performance to prescriptive provisions, with some performance requirements lacking objective measures of compliance, and some prescriptive requirements without a rationale given in the commentary.

The formal representation of the Provisions, further elaboration of the foregoing points, and other comments and suggestions noted in the Analysis (4) may also be of interest to designers using the Provisions (1) as a guide to design.

CONCLUSIONS AND RECOMMENDATIONS

The National Earthquake Hazards Reduction Program announced by the President in June 1978 calls for a strong cooperative effort involving the design professions, building code organizations, standards organizations, and other elements of the building community to develop and implement nationally applicable seismic design construction provisions. The "Tentative Provisions for the Development of Seismic Regulations for Buildings" (1) are expected to be a major resource in this process. Various individuals and organizations, such as the newly established building seismic safety council, are undertaking careful reviews of the Provisions, some to establish technical validity, some to establish applicability in the context of current building codes, and others to become familiar enough to use the provisions in the design of buildings. The results of the Analysis (4) offer assistance in all such reviews, as they provide an alternate expression of the Provisions, including:

1. A listing of all data items, showing where each datum is defined and where it is used.
2. Decision tables providing unambiguous statements of the logic of the provisions.
3. Information networks representing the precedence among provisions and thereby allowing the tracing of implications of changes.
4. An index and a classification of the provisions that, together with the information network, may facilitate the adaption and organization of a subset of the provisions to fit within the scope of one or another national standard.

As the process of assessment of the Provisions and the implementation of the improved provisions in national standards and model codes proceeds, we recommend that this formal representation of the Provisions be concurrently updated and maintained. Portions of the representation are stored in a computer-processible form, with potential for access by remote terminal. Plans exist to make a continually updated formal representation of the Provisions readily available to all concerned users.

The work reported herein has served not only the specific aim of improving provisions for seismic resistant building design construction, but also has resulted in improvement of the methodology for analyzing and representing standards and other normative documents. The large report (4) contains a review of the lessons learned during interactions with the ATC team in the development of the Provisions. This experience may be useful to others undertaking similar technical support of major efforts in the formulation and expression of standards.

APPENDIX.—REFERENCES

1. "Tentative Provisions for the Development of Seismic Regulations for Buildings," *Special Publication 510,* Applied Technology Council, National Bureau of Standards, Washington, D.C., June, 1978.
2. Fenves, S. J., and Wright, R. N., "The Representation and Use of Design Specifications," *Technical Note 940,* National Bureau of Standards, Washington, D.C., June, 1977.
3. Fenves, S. J., Rankin, K., and Tejuja, H., "The Structure of Building Specifications," *Building Science Series 90,* National Bureau of Standards, Washington, D.C., Sept., 1976.
4. Harris, J. R., Fenves, S. J., and Wright, R. N., "Analysis of Tentative Seismic Design Provisions for Buildings," *Technical Note 1100,* National Bureau of Standards, Washington, D.C., July, 1979.

Warping Restraint in Three-Dimensional Frames

By Mohammed M. Ettouney,[1] M. ASCE and Jeffrey B. Kirby,[2] A. M. ASCE

Introduction

Evaluation of the effects of warping restraint on the behavior of different systems has always been of importance to analysts and designers. Finite difference and finite element techniques have been used to solve the static (3,5,6,7), and dynamic (8) problems of continuous planar curved beams. The finite element method (13) was used to evaluate the warping functions of circular girders subjected to torsional loadings. Analytical (14,15), semi-analytical (10), and approximate (12) solutions of beam problems with different end conditions, different loading conditions and different cross-sectional shapes have been presented. These solution techniques for restrained warping problems have always assumed that the loading and the beam cross section are such that there is no coupling between biaxial bending and warping terms, an assumption which is not true for unsymmetrical cross sections subjected to general loading conditions. It has also been assumed that the system under consideration is a planar curved, or straight, beam supported by two or more supports. The effects of the three-dimensional intersections of beams have not been considered.

The purpose of this paper is to present a solution of the beam problem, accounting for the restraining of warping. The solution is based on the finite element technique, which considers all coupling terms in the general three-dimensional beam strain-displacement relationships. The warping effects are considered by adding a seventh degree of freedom to the conventional six degree-of-freedom beam nodes. In order to account for any general three-dimensional framing arrangement, the concepts of continuous warping and partially restrained warping are introduced. The new beam element is utilized for a simple case of restrained warping, where the analytical solution is known. The agreement between the two solutions is very good. Since the major application of this approach is in such three-dimensional massive framed structures as machine foundations, where the warping effects are important, a practical example of a turbine generator

pedestal is presented and the effects of warping constraints are computed. It is found that consideration of warping restraints in this class of structure could have a large effect on the predicted design displacements and stresses.

THEORETICAL BACKGROUND

Strain Expansions.—Consider the prismatic beam shown in Fig. 1. The strain vector of the cross section can be expressed as

$$\xi^T = [\epsilon_1 \gamma_{12} \gamma_{13}] \quad \dots \dots \dots \dots \dots \dots \dots \dots (1)$$

The strain expansions ϵ_2, ϵ_3 and γ_{23} are assumed to be zero, in accordance with the conventional beam theory (2).

Connor (2), showed that the strain expansions are

$$\epsilon_1 = \frac{dU_1}{dx_1} + x_3 \frac{d\chi_2}{dx_1} - x_2 \frac{d\chi_3}{dx_1} + \phi \frac{df}{dx_1} \quad \dots \dots \dots \dots \dots (2a)$$

$$\gamma_{12} = \frac{dU_2}{dx_1} - \chi_3 - (x_3 - \bar{x}_3) \frac{d\chi_1}{dx_1} + f \frac{d\phi}{dx_2} \quad \dots \dots \dots (2b)$$

$$\gamma_{13} = \frac{dU_3}{dx_1} + \chi_2 + (x_2 - \bar{x}_2) \frac{d\chi_1}{dx_1} + f \frac{d\phi}{dx_3} \quad \dots \dots \dots (2c)$$

in which ϵ_1 = normal strain in the x_1 direction; γ_{12}, γ_{13} = shear strains in the $x_1 x_2$ and $x_1 x_3$ planes, respectively; U_1, U_2, U_3 = rigid body translation
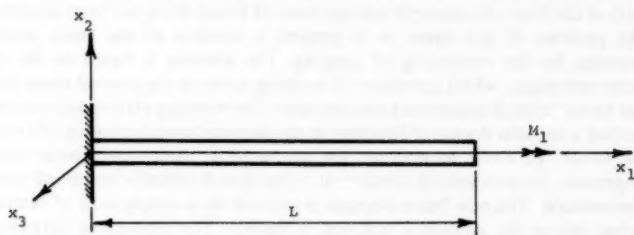

FIG. 1.—Local Coordinate System

of the shear center; χ_1, χ_2, χ_3 = rigid body rotations of the cross section; $f = f(x_1)$ = warping parameter of the cross section; $\phi = \phi(x_2, x_3)$ = warping function of the cross section; and $\bar{x}_2$, $\bar{x}_3$ = coordinates of the shear center of the cross section.

Eq. 2 can be expressed as

$$\xi = \bar{D}U \quad \dots \dots \dots \dots \dots \dots \dots \dots \dots \dots \dots \dots (3)$$

in which $\bar{D}$ = differential operator matrix and

$$U^T = [U_1 U_2 U_3 \chi_1 \chi_2 \chi_3 f] \quad \dots \dots \dots \dots \dots \dots \dots (4)$$

Stress-Strain Relations.—The stress-strain relation of the prismatic beam in Fig. 1 is

$$\sigma = D\xi \quad \dots\dots\dots\dots\dots\dots\dots\dots\dots\dots\dots\dots\dots\dots\dots\dots \quad (5)$$

in which $\quad D = \begin{bmatrix} E & & \\ & G & \\ & & G \end{bmatrix} \dots\dots\dots\dots\dots\dots\dots\dots\dots\dots\dots \quad (6)$

and $\quad \sigma^T = [\sigma_{11}\tau_{12}\tau_{13}] \dots\dots\dots\dots\dots\dots\dots\dots\dots\dots\dots\dots \quad (7)$

E = modulus of elasticity; G = shear modulus; σ_{11} = normal stress on the cross section; and τ_{12}, τ_{13} = shear stress on the cross section in the x_2 and x_3 directions, respectively.

Element Matrices.—The principle of virtual displacements (1,2,16) states that

$$\iiint\limits_V \xi^T\sigma d(V) = \iint\limits_S \delta U^T P d(S) \dots\dots\dots\dots\dots\dots\dots\dots \quad (8)$$

in which P = the surface forces vector; δU = arbitrary displacement vector; Substituting Eqs. 3 and 4 into Eq. 5 results in

$$\iiint\limits_V \delta U^T \bar{D}^T D\bar{D}U d(V) = \delta \bar{U}^{n,T} \bar{F}^n \dots\dots\dots\dots\dots\dots\dots \quad (9)$$

in which $\quad \bar{U}^{n,T} = n$th element nodal displacements vector

$$= [U_A^{n,T} : U_B^{n,T} : U_D^{n,T}] \dots\dots\dots\dots\dots\dots\dots\dots\dots\dots\dots \quad (10)$$

$$U_A^{n,T} = [U_1^A U_2^A U_3^A \chi_1^A \chi_2^A \chi_3^A f^A] = \text{displacement vector at node } A \quad\dots\dots \quad (11)$$

$U_B^{n,T}$ = displacement vector at node B; $U_D^{n,T}$ = intermediate nodes displacements vector and

$$\bar{F}^{n,T} = [F_A^{n,T} : F_B^{n,T} : 0] \dots\dots\dots\dots\dots\dots\dots\dots\dots\dots\dots\dots \quad (12)$$

$$F_A^{n,T} = \text{force vector at node } A = [F_1^A F_2^A F_3^A M_1^A M_2^A M_3^A M_\phi^A];$$

$$F_B^{n,T} = \text{force vector at node } B \dots\dots\dots\dots\dots\dots\dots\dots\dots\dots\dots \quad (13)$$

The forces F_1, F_2, F_3, M_1, M_2, and M_3 are defined according to the engineering theory of beams (2). The force parameter M_ϕ is called the bimoment (2,6) and is expressed as

$$M_\phi = \iint\limits_A \sigma_{11}\phi d(A) \dots\dots\dots\dots\dots\dots\dots\dots\dots\dots\dots\dots \quad (14)$$

The critical step in evaluating the beam stiffness matrix is the choice of the displacement expansions. The displacement expansions chosen for this problem are (1) Cubic expansions for U_2 and U_3; (2) quadratic expansions for χ_2, χ_3 and f; and (3) linear expansions for U_1 and χ_1.

These expansions were chosen so as to reproduce the results of the conventional engineering theory of beams, neglecting the warping restraints. Note that this choice of displacement expansions will require the use of 21 undetermined

coefficients. These displacement expansions can be expressed as

$$U = B\bar{U}^n \quad \dots \dots \dots \dots \dots \dots \dots \dots \dots \dots \dots \dots \quad (15)$$

The displacement vector U_D^n is introduced in order to account for the differences between the required 21 undetermined coefficients in the displacement expansions and the 14 available displacement parameters at nodes A and B. Matrix B can be evaluated using the conventional finite elements techniques (1,16).

Eq. 6 can be expressed as

$$\delta\bar{U}^{n,T}\bar{K}^n\bar{U}^n = \delta\bar{U}^{n,T}\bar{F}^n \quad \dots \dots \dots \dots \dots \dots \dots \dots \dots \dots \quad (16)$$

in which $\bar{K}^n = \iiint\limits_V C^T DC\, d(V) \quad \dots \dots \dots \dots \dots \dots \dots \quad (17a)$

$$C = \bar{D}B \quad \dots \dots \dots \dots \dots \dots \dots \dots \dots \dots \dots \dots \quad (17b)$$

The element equilibrium equation can be written as

$$\bar{K}^n\bar{U}^n = \bar{F}^n \quad \dots \dots \dots \dots \dots \dots \dots \dots \dots \dots \dots \quad (18)$$

It is desired to eliminate the intermediate nodal displacement in order to have a two-node beam element which is consistent with the conventional beam element. The method of static condensation (1) can be used to obtain

$$K^n U^n = F^n \quad \dots \dots \dots \dots \dots \dots \dots \dots \dots \dots \dots \dots \quad (19a)$$

in which $U^{n,T} = [U_A^{n,T} : U_B^{n,T}] \quad \dots \dots \dots \dots \dots \dots \dots \dots \quad (19b)$

$$F^{n,T} = [F_A^{n,T} : F_B^{n,T}] \quad \dots \dots \dots \dots \dots \dots \dots \dots \dots \quad (19c)$$

and K^n = Condensed beam element matrix, with two nodes.

Boundary Conditions.—The presence of the seventh degree of freedom, f, in the new beam element requires special attention to its end conditions. Two possible end conditions will be considered; the continuous end, and the end partially restrained against warping.

Continuous End.—This boundary condition was reviewed in many references (2,6,16). It can be enforced by setting $f^l = f^r$ or $M_\phi^l = M_\phi^r$ in which the superscripts l and r indicate to the left and right of the joint, respectively.

End Partially Restrained against Warping.—Eq. 9 can be rewritten as

$$K_{11}^n U_1^n + K_{12}^n U_2^n = F_1^n \quad \dots \dots \dots \dots \dots \dots \dots \dots \dots \quad (20a)$$

$$K_{21}^n U_1^n + K_{22}^n U_2^n = F_2^n \quad \dots \dots \dots \dots \dots \dots \dots \dots \dots \quad (20b)$$

in which subscript "1" refers to the continuous degrees of freedom in the beam element and subscript "2" refers to the degrees of freedom partially restrained against warping.

It can be shown (2) that the bimoments at the end(s) of the beam elements due to *total* warping restraint is

$$M_\phi^l = K_{21}^n U_1^n \quad \dots \dots \dots \dots \dots \dots \dots \dots \dots \dots \dots \quad (21)$$

In order to specify the partial warping restraint, a warping condition matrix A will be introduced. It is expressed as

$$\mathbf{A} = \begin{bmatrix} a_1 & 0 \\ 0 & a_2 \end{bmatrix} \quad \dots \dots \dots \dots \dots \dots \dots \dots \dots \dots \dots \quad (22)$$

if the two ends are partially restrained, or

$$\mathbf{A} = [a_i]; \quad i = 1 \quad \text{or} \quad 2, \dots \dots \dots \dots \dots \dots \dots \dots \dots \quad (23)$$

if one end (i) is partially restrained and the other is continuous.

The factors a_i specify the degree of partial restraint in which

$$0 \le a_i \le 1.0 \dots \dots \dots \dots \dots \dots \dots \dots \dots \dots \dots \dots \dots \quad (23a)$$

where $a_i = 0$, free to warp; and $a_i = 1.0$, total warping restraint.

The end bimoment(s) can be expressed as

$$\bar{\mathbf{M}}_\phi = \mathbf{A} \mathbf{M}'_\phi = \mathbf{A} \mathbf{K}^n_{21} \mathbf{U}^n_1 \dots \dots \dots \dots \dots \dots \dots \dots \dots \quad (24)$$

From Eqs. 10b and 13

$$\mathbf{U}^n_2 = \mathbf{G} \mathbf{U}^n_1 \dots \dots \dots \dots \dots \dots \dots \dots \dots \dots \dots \dots \quad (25)$$

$$\mathbf{G} = (\mathbf{K}^n_{22})^{-1}(\mathbf{A} - \mathbf{i})\mathbf{K}^n_{21} \dots \dots \dots \dots \dots \dots \dots \dots \dots \quad (26)$$

in which $\mathbf{i}$ = identity matrix.

Eq. 25 shows the relation between the partially restrained degrees of freedom $\mathbf{U}^n_2$ and the rest of the degrees of freedom of the beam element $\mathbf{U}^n_1$. Eq. 20a can be modified so as to account for this condition, such that

$$\mathbf{K}^{n^*} \mathbf{U}^n_1 = \mathbf{F}^{n^*} \dots \dots \dots \dots \dots \dots \dots \dots \dots \dots \dots \dots \quad (27)$$

in which $\quad \mathbf{K}^{n^*} = \mathbf{K}^n_{11} + \mathbf{K}_{12}\mathbf{G} + \mathbf{G}^T\mathbf{K}_{21} + \mathbf{G}^T\mathbf{K}_{22}\mathbf{G} \quad \dots \dots \dots \dots \quad (28)$

$$\mathbf{F}^{n^*} = \mathbf{F}^n_1 + \mathbf{G}^T\mathbf{F}^n_2 \dots \dots \dots \dots \dots \dots \dots \dots \dots \dots \dots \quad (29)$$

Eqs. 26 and 27 can be used to specify any desired partial warping restraint at either of the two ends of the beam element, by controlling the coefficients of matrix $\mathbf{A}$.

Solution of the Total Problem.—The element stiffness matrix $\mathbf{K}^{n^*}$ is formulated in the local element coordinates. Either of its two nodes may have (1) Seven degrees of freedom for continuous warping; or (2) six degrees of freedom, for partially restrained warping.

The solution of the total structural system will be in the

1. Global coordinate system for all six of the conventional degrees of freedom. The conventional transformation matrices (1,2) can be used to make the necessary transformations.

2. Local coordinate system only for the seventh degree of freedom, f, for the continuous warping case.

The global element stiffness matrix can be expressed as

$$\mathbf{K}^n_g = \mathbf{T}^T \mathbf{K}^{n^*} \mathbf{T} \dots \dots \dots \dots \dots \dots \dots \dots \dots \dots \dots \dots \quad (30)$$

in which the transformation matrix $\mathbf{T}$ is formulated according to the previous notes.

The global element stiffness matrices can be assembled to form the system

stiffness matrix **K**, using the conventional finite elements approach (1,16). The system equilibrium equation is

$$\mathbf{K}\mathbf{U}_g = \mathbf{F}_g \quad \dots\dots\dots\dots\dots\dots\dots\dots\dots\dots\dots\dots\dots\dots\dots \quad (31)$$

in which $\mathbf{U}_g$ = displacements vector of the system; and $\mathbf{F}_g$ = force vector of the system.

Eq. 31 can be solved for the unknown displacements. The element forces can be obtained by back-substitution into the element equilibrium equation (20).

CASE STUDIES

The beam element presented here will be compared to the known analytical solution of a simple cantilever beam with restrained warping. The beam elements will then be used to evaluate the structural behavior of a massive structure, where the effect of warping restraints are believed to be important.
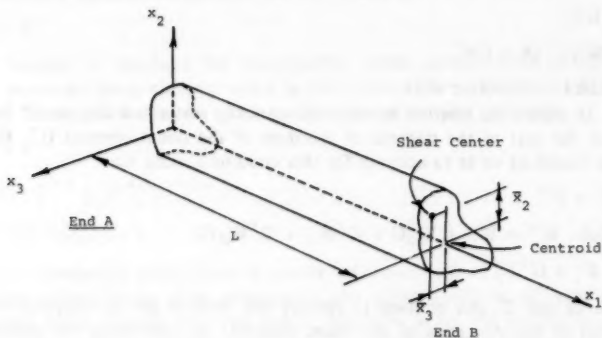
FIG. 2.—Simple Cantilever Beam

Cantilever Beam.—Consider the cantilever beam shown in Fig. 2. The beam is assumed to be totally fixed at one end and is subjected to a torsional moment (M_1) at the free end. The beam is represented by several models with different numbers of the beam elements described earlier. Fig. 3 shows a comparison between the rotation at the free end as obtained by the analytical solution (6) and as obtained from the different finite element models. Figs. 4 and 5 show similar comparisons between the analytical solution and the finite element solution for the warping of the free end, and the bimoment at the fixed end, respectively. The finite element solution predicted an accurate result when five refined elements were used. It is concluded that a five element beam is capable of predicting the required displacements and forces with an acceptable degree of accuracy.

Practical Case of Massive Structure.—Connor (2) presented the geometric properties of prismatic members where the restraint against warping significantly affects the member's displacements and forces. Many three-dimensional framed structures have individual elements with geometric properties such that the

restrained warping effect should be large. However, these effects were always neglected since the analytical tools to account for restrained warping effects in three-dimensional frames were not available.

The beam element presented earlier can be used to solve this class of structural problem. Consider, e.g., the reinforced concrete turbine generator pedestal shown
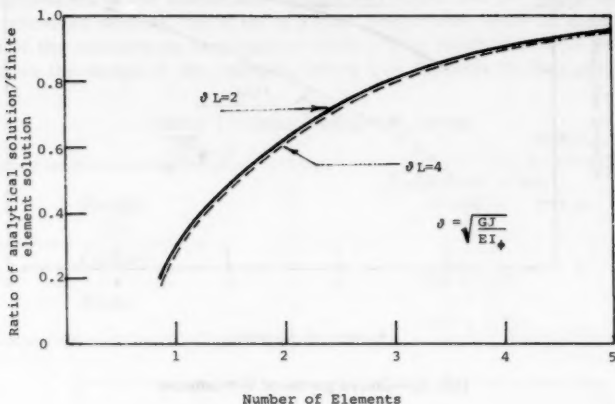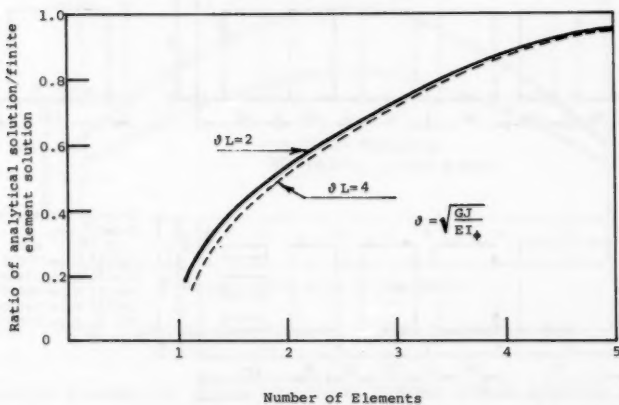

FIG. 3.—Convergence of Free End Rotations

FIG. 4.—Convergence of Warping Parameter

in Fig. 6 and Table 1. The pedestal has to be massive in order to reduce the static and dynamic responses to the machine loads. This results in a very small span-to-depth ratio of the members of the structure, as shown in the figure. This small ratio indicates the importance of including the restrained warping

effects in the analysis. The columns are assumed to be fixed at the bottom. The joints of the structure are so massive that all the structural members will
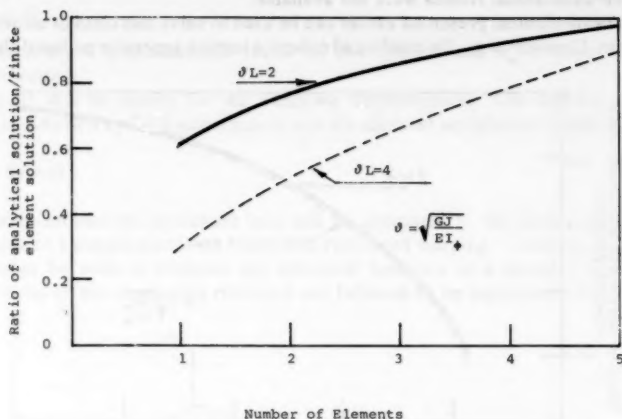
FIG. 5.—Convergence of Bimoments

Elevation
(Dimensions are in feet)

Side View

Plan
(Dimensions are in feet)

Poisson's ratio =0.16
$E=3\times10^6$ psi
$=(2.07\times10^7$ kPa)
P1=157 Kips(71000 Kg)
P2=252 Kips(114000 Kg)
P3=213 Kips(96000 Kg)
P4=128 Kips(58000 Kg)
P5= 81 Kips(37000 Kg)
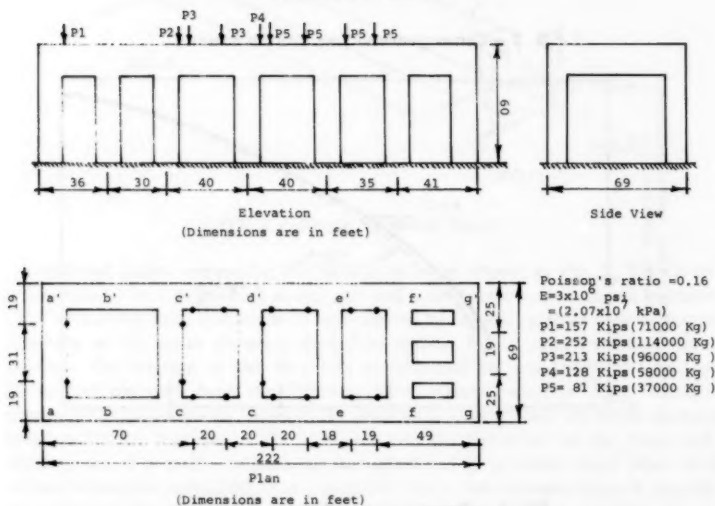
FIG. 6.—Typical Turbine Generator Pedestal (1 ft = 0.305 m)

be assumed to be totally restrained against warping at these joints. This structural system will be analyzed for the weight of the turbine generator as shown in Fig. 6.

Fig. 7 shows the rotation of member (cc') about its longitudinal axis. It shows that the differences between the predicted rotations by the conventional beam analysis and the present method can be as large as 40%. This result is of importance since the rotations of the members results in additional displacements of the bearings of the turbine which, in turn, could affect its alignment and operability. The differences in the calculated rotations also means that the actual system, with restrained warping, has a set of natural frequencies which is higher than those of the approximate conventional system. This result also could have an effect on the design of the pedestal, where it is desirable to have maximum

TABLE 1.—Cross-Sectional Properties

Variable (1)	Dimensions, in feet (meters) (2)
Columns	12×12 (3.66×3.66)
Beams	16×12 (4.88×3.66)
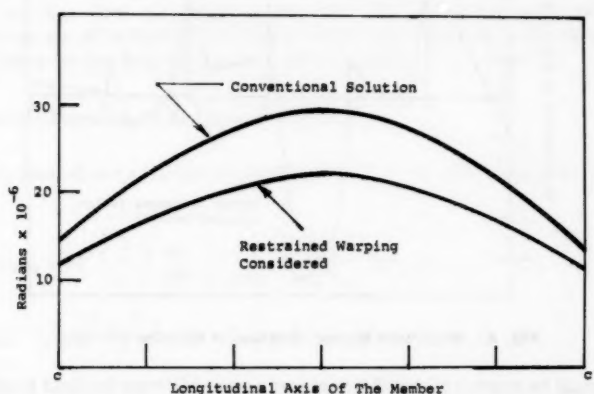
FIG. 7.—Rotations of Member (c-c) about Longitudinal Axis

separation between the system frequencies and the turbine operating speed. Therefore, an accurate prediction of the system's natural frequencies is of extreme importance (9).

Fig. 8 shows the maximum normal stress (σ_{11}) due to warping restraint in member ($abcdefg$), using the equation

$$(\sigma_{11})_{max} = \frac{M_\phi}{I_\phi} (\phi)_{max} \dots\dots\dots\dots\dots\dots\dots\dots\dots\dots\dots\dots (32)$$

in which $I_\phi = \iint\limits_A \phi^2 dA$ . . . . (33)

The parameter I_γ, known as the warping constant (9), and the warping function ϕ can be evaluated for thin walled open and closed cross sections following the approaches in Refs. 2 and 6. Appendix I shows the expressions of ϕ and I_ϕ for the rectangular solid cross sections of this example.

The maximum normal stresses in the same member due to biaxial bending moments are shown in the same figure. It may be seen that the warping normal stresses are as much as 10%–40% of the conventional bending normal stresses at the structural joints. This is a further demonstration of the importance of including the effects of the warping restraints for this class of problem.
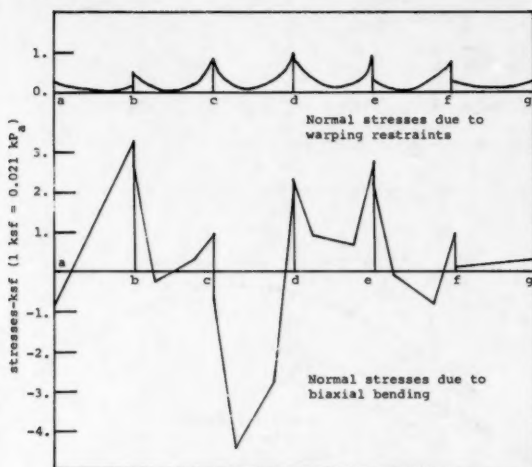
FIG. 8.—Maximum Normal Stresses in Member (*abcdefg*)

It should be mentioned that there are many cases of design loadings in addition to the turbine self weight (4,9). All of these cases of loadings should be considered in order to obtain the maximum displacements and stresses. The purpose of this example was only to show the practicality of the new beam element and the importance of considering the warping restraints in this class of structures.

SUMMARY AND CONCLUSIONS

The finite element formulation of beams accounting for warping restraint is presented. The formulation is general enough to account for any cross section shape of the beams and any applied loading conditions. The concepts of partial warping restraint and continuous warping were introduced and were used in

the solution of problems of three-dimensional framed structures where the restrained warping at the joints could have a large effect on the computed displacements and stresses. The new beam element was used to solve a simple case and the results were compared against a known analytical solution. The beam element was also used to solve a practical case of a turbine generator pedestal where the individual members were stocky.

The results of these case studies indicate that:

1. The new beam element predicts displacement and stress results which compare well with the analytical predictions of the restrained warping problem.

2. The concepts of partial warping restraint and continuous warping provide a method of accounting for restrained warping in three-dimensional framed structures.

3. Accounting for warping restraints in three-dimensional framed structures with short members could be of extreme importance for proper calculations of displacements and stresses.

APPENDIX I.—PROPERTIES OF RECTANGULAR SECTIONS

It has been shown (11) that the warping function, ϕ, of a rectangular section is:

$$\phi = -x_2 x_3 + 4b^2 \left(\frac{2}{\pi}\right)^2 \sum_{i=0} \frac{(-1)^i}{(2i+1)^3} \frac{\sinh \eta \, x_2}{\cosh \eta \, z} \sin \eta \, x_3 \quad \ldots \ldots \ldots \quad (34)$$

in which $\quad \eta = \dfrac{(2i+1)\pi}{2b}$ $\ldots \ldots \ldots \ldots \ldots \ldots \ldots \ldots \ldots$ (35)

and $2a$, $2b$ = longer and shorter dimensions of the rectangle, respectively.

The warping constant, I_ϕ, defined in Eq. 19, can be expressed as:

$$I_\phi = \frac{I_2 I_3}{4ab} - b^2 \sum_{i=0} \frac{8\psi}{\eta^4} (\eta a - \tanh \eta a)$$

$$+ ab^5 \sum_{i=0} \psi^2 \left(\frac{\tanh \eta \, a}{\eta \, a} - \frac{1}{\cosh^2 \eta \, a}\right) \ldots \ldots \ldots \ldots \ldots \ldots \quad (36)$$

in which $\quad \psi = \dfrac{4}{(b\eta)^3}$ $\ldots \ldots \ldots \ldots \ldots \ldots \ldots \ldots$ (37)
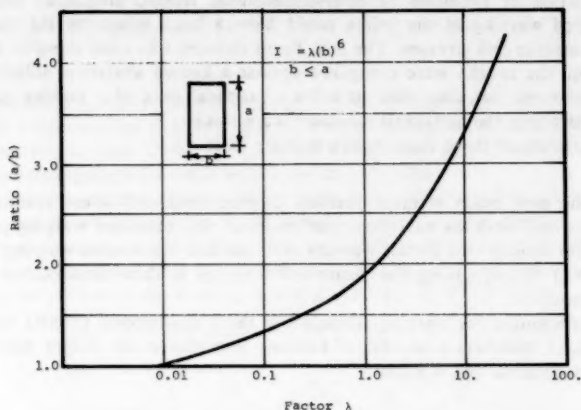
FIG. 9.—Warping Constant for Rectangular Sections

The expression for I_ϕ can be rewritten as

$$I_\phi = b^6 \lambda \quad \dots \dots \dots \dots \dots \dots \dots \dots \dots \dots \dots \dots \dots \dots (38)$$

in which λ = a function of the ratio (a/b) only. The function λ is shown in Fig. 9.

APPENDIX II.—REFERENCES

1. Bathe, K. J., and Wilson, E. L., *Numerical Methods in Finite Element Analysis*, Prentice-Hall Inc., Englewood Cliffs, N.J., 1976.
2. Connor, J. J., *Structural Member Systems*, Ronald Press Co., New York, N.Y., 1976.
3. Fam, A. R. M., "Static and Free Vibration Analysis of Curved Box Bridges," thesis presented to McGill University, at Montreal, Canada, in partial fulfillment of the requirements for the degree of Doctor of Philosophy.
4. "Turbine Generator Foundations," *GEK 63383*, General Electric Company Instruction Report, General Electric Co.
5. Evich, D. R., and Heins, Jr., C. P., "Torsion of Nonprismatic Beams of Open Section," *Journal of the Structural Division*, ASCE, Vol. 98, No. ST12, Proc. Paper 9453, Dec., 1972, pp. 2769–2784.
6. Heins, C. P., *Bending and Torsional Design in Structural Members*, Lexington Books, Lexington, Mass., 1975.
7. Heins, C. P., and Potocko, R. A., "Torsional Stiffness of I-Girder Webs," *Journal of the Structural Division*, ASCE, Vol. 105, No. ST8, Proc. Paper 14788, Aug., 1979, pp. 1689–1698.
8. Heins, C. P., and Sahin, M. A., "Natural Frequency of Curved Box Girder Bridges," *Journal of the Structural Division*, ASCE, Vol. 105, No. ST12, Proc. Paper 15064, Dec., 1979, pp. 2591–2600.
9. Jagadeesh, H. N., "Low-Tuned Concrete Turbine-Generator Foundations," presented at the March, 1979, ACI Annual Convention, held at Milwaukee, Wisc.
10. Just, D. J., and Walley, W. J., "Torsion of Solid and Hollow Rectangular Beams," *Journal of the Structural Division*, ASCE, Vol. 105, No. ST9, Proc. Paper 14845, Sept., 1979, pp. 1789–1804.

11. Love, A. E. H., *A Treatise on the Mathematical Theory of Elasticity*, Dover Publications, New York, N.Y., 1944.
12. Smith, E. A., "Restrained Warping in Free-Standing Staircases," *Journal of the Structural Division*, ASCE, Vol. 106, No. ST3, Proc. Paper 15231, Mar., 1980, pp. 734–738.
13. Thasanatorn, C., and Pilkey, W. D., "Torsional Stresses in Circularly Curved Bars," *Journal of the Structural Division*, ASCE, Vol. 105, No. ST11, Proc. Paper 14984, Nov., 1979, pp. 2327–2342.
14. Timoshenko, S. P., and Gere, J. M., *Theory of Elastic Stability*, McGraw-Hill Co., New York, N.Y., 1961.
15. Vlasov, V., "Thin-Walled Beam Theory," National Science Foundation, Washington, D.C., 1961.
16. Zienkiewicz, O. C., *The Finite Element Method in Engineering Science*, McGraw-Hill Co., New York, N.Y., 1971.

Appendix III.—Notation

The following symbols are used in this paper:

$$
\begin{aligned}
\mathbf{A} &= \text{warping condition matrix;}\\
a_1, a_2 &= \text{warping restraint factors;}\\
\mathbf{B} &= \text{strain-displacement relations matrix;}\\
\mathbf{D} &= \text{constitutive relations matrix;}\\
\bar{\mathbf{D}} &= \text{differential operator matrix;}\\
E &= \text{modulus of elasticity;}\\
\mathbf{F}_g &= \text{system nodal force vector;}\\
F_1, F_2, F_3 &= \text{element forces;}\\
\mathbf{F}_1^n, \mathbf{F}_2^n &= \text{element force subvectors;}\\
\mathbf{F}^n, \bar{\mathbf{F}}^n, \mathbf{F}^{n'} &= \text{element force vectors;}\\
\mathbf{F}_A^n, \mathbf{F}_B^n &= \text{nodal force vectors;}\\
f &= \text{warping parameter;}\\
G &= \text{shear modulus;}\\
I_\phi &= \text{warping constant;}\\
I_2, I_3 &= \text{moment of inertia;}\\
\mathbf{i} &= \text{identity matrix;}\\
\mathbf{K} &= \text{system stiffness matrix;}\\
\mathbf{K}^n, \bar{\mathbf{K}}^n, \mathbf{K}^{n'} &= \text{element stiffness matrix;}\\
\mathbf{K}_g^n &= \text{global element stiffness matrix;}\\
\mathbf{K}_{11}^n, \mathbf{K}_{12}^n, \mathbf{K}_{21}^n, \mathbf{K}_{22}^n &= \text{element stiffness submatrices;}\\
M_\phi &= \text{bimoment;}\\
\bar{M}_\phi &= \text{end bimoment;}\\
M_\phi^t &= \text{bimoments due to total warping restraint;}\\
M_1, M_2, M_3 &= \text{element forces (moments);}\\
\mathbf{P} &= \text{body force vector;}\\
\mathbf{T} &= \text{transformation matrix;}\\
\mathbf{U} &= \text{displacement vector;}\\
\mathbf{U}_g &= \text{system displacement vector;}\\
U_1, U_2, U_3 &= \text{displacements of shear center;}\\
\mathbf{U}^n, \bar{\mathbf{U}}^n &= \text{element displacement vectors;}\\
\mathbf{U}_A^n, \mathbf{U}_B^n, \mathbf{U}_D^n &= \text{nodal displacement vectors;}\\
\mathbf{U}_1^n, \mathbf{U}_2^n &= \text{element displacement subvectors;}
\end{aligned}
$$

$\bar{x}_2, \bar{x}_3$ = location of shear center in element coordinates;

$\gamma_{12}, \gamma_{13}, \gamma_{23}$ = shearing strains;

σ = stress vector;

$\epsilon_1, \epsilon_2, \epsilon_3$ = normal strains;

λ = shape parameter;

ξ = strain vector;

σ_{11} = normal stress;

τ_{12}, τ_{13} = shear stresses;

ϕ = warping function; and

χ_1, χ_2, χ_3 = rotations of cross section.

Superscripts

l = left;

r = right; and

T = transpose.

Sheet Steel Welding [a]

By Teoman Pekoz[1] and William McGuire[2]

Introduction

Light, cold formed steel sections have been arc welded without the benefit of a general guiding specification for many years. By the late nineteen sixties the structural use of this fastening method was sufficient to create a demand for a more systematic approach. Rational use of light steel panels as horizontal diaphragms and vertical shear walls, as well as other applications of light steel framing, panels, and decks, requires one. Accordingly, the American Iron and Steel Institute (AISI) initiated a project to develop welding procedures and to verify them through tests of welded connections. In a series of such tests at Cornell University, the behavior of the most common types of arc welds in sheet steel has been studied. This paper is a summary of the Cornell tests and an interpretation of the results.

The Cornell research has provided the basis for the current welding provisions in the AISI Specification for the Design of Cold-Formed Steel Structural Members (Ref. 1) and for a new specification, Welding Sheet Steel in Structures (AWS D1.3-80, Ref. 2).

Sufficient data are available to support the ultimate load prediction equations proposed in this paper and the design equations contained in the specifications previously referred to. Since they represent the first attempt to codify this type of structural fastening process, it is anticipated that desirable modifications will become apparent as research and practice advance.

Sheet steel may be as thick as 0.230 in. (5.80 mm). The thicknesses commonly used in cold-formed steel in building construction are generally not as large as this, however. The largest total sheet thickness used in the Cornell tests was approximately 0.150 in. (3.80 mm).

Although sheet-steel welds may be made with conventional equipment and electrodes, the fact that they are made on thin steel results in a special situation. Stress resisting areas are not as regular or as easy to define as they are in

the welding of structural steel and plate. Some welds, such as arc spot and arc seam welds (Ref. 3), are made through the welded sheet without any advance preparation. Galvanizing and paint are normally not removed prior to welding. Failure modes are complex and difficult to categorize. A relatively large amount of scatter in test results can be expected. Qualification of welders and welding procedures and the inspection of work, are of particular importance. The fact that a welder may have satisfactorily passed a test for structural steel welding does not necessarily mean that he can produce sound welds on sheet steel. Welders may require considerable instruction and practice before mastering the technique.

WELD TYPES

The types of arc welds used to connect a light steel sheet to another plate, either light or heavy, are shown in Fig. 1. Most of the terms used follow standard

Square Groove Weld   Arc Spot Weld
                            (round puddle weld)

Arc Seam Weld   Fillet Welds
(oblong puddle weld)

Flare Bevel Welds   Flare Vee Welds
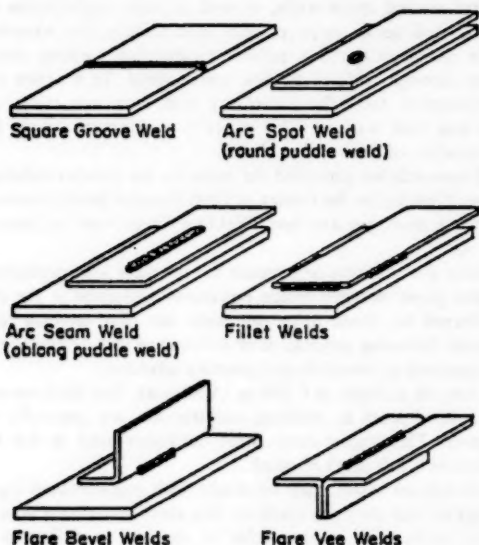
FIG. 1.—Sheet Steel Weld Types

nomenclature. Arc spot welds (commonly called puddle welds) are welds in which coalescence proceeds from the surface of one member into the other. As mentioned previously, the weld is made without preparing a hole in either member. Arc seam welds (oblong puddle welds) are the same in that neither member is slotted. Arc spot and seam welds are commonly used to attach cold formed steel decks and panels to their supporting frames. Arc seam welds find particular application in the narrow troughs of such elements. Flare bevel

and flare vee welds are used on the outside of the curved edges that are typical of cold formed members. Square groove welds are rarely used in thin steel.

As in conventional structural welding, it is general practice to require that the deposited filler metal have a tensile strength at least equal to that of the members being joined. For members of unequal strength, the weld materials should be matched at least to the strength level of the weaker member.

FAILURE MODES

Failures in welded sheet steel connections are generally quite complicated. They often occur as a combination of basic modes, accompanied by a large amount of out-of-plane inelastic deformation. The primary features of the basic modes encountered in the Cornell tests are shown in Fig. 2. While these are simplified pictures of true failures, they have been found, nevertheless, to provide reasonable categories for the assessment of strength and the development of

(a) Sheet Tear Transverse Fillet   (b) Sheet Tear Longitudinal Fillet   Transverse Sheet Tear   Longitudinal Sheet Tear

(c) Flare Bevel Weld

Weld Shear   Sheet Tear   Sheet Tear and Buckling

(d) Round Puddle Welds
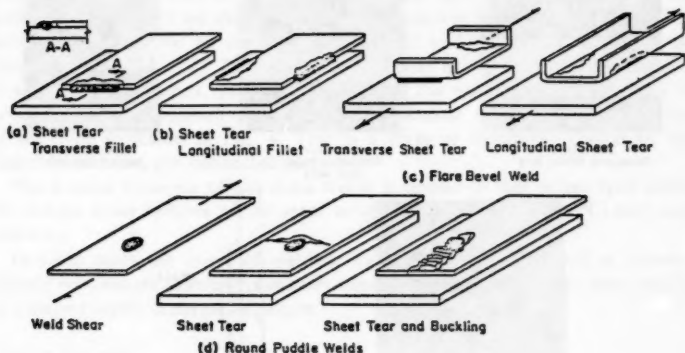
FIG. 2.—Typical Failure Modes

design equations. Photographs of some of the typical failed specimens are given in Fig. 3. For simplicity, groove weld failures are not shown. Properly matched groove welds can be expected to develop the full strength of the sheet.

For fillet welds on the sheet sizes tested, the dimension of the leg on the sheet edge is generally equal to the sheet thickness and the other leg is often two or three times longer. The actual throat is commonly larger than the throat of a conventional fillet weld of the same size [see Section A-A, Fig. 2(a)]. Ultimate failure of fillet welded joints is usually found to occur by tearing of the plate adjacent to the weld. Tearing is the result of applied shearing or tensile forces, depending upon whether the weld is longitudinal or transverse. These conditions are illustrated in Fig. 2(a) and 2(b). Also, in a number of the longitudinally welded specimens tested at Cornell, the welds were long enough to result in tensile failure of the narrow connected sheets. Some conventional weld shear was also observed in a few of the longitudinally welded specimens.

These and other failure conditions will be described further in later sections of this report.

The chief mode of failure in cold-formed channels welded by flare bevel welds, and loaded transversely, was also sheet tearing along the contour of the weld. Fig. 2(c) shows these conditions.
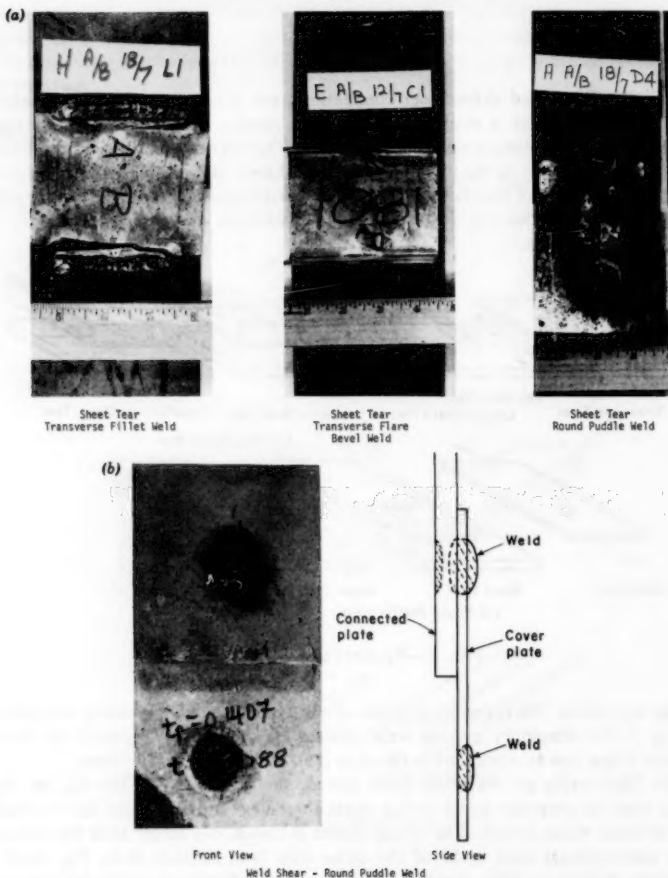
Sheet Tear
Transverse Fillet Weld

Sheet Tear
Transverse Flare
Bevel Weld

Sheet Tear
Round Puddle Weld

Front View   Side View
Weld Shear - Round Puddle Weld

FIG. 3.—Typical Failure Modes, Specimens after Failure: (a) Sheet Tear; and (b) Weld Shear

Only in a few cases was weld shear a primary factor in the failure of either fillet or flare bevel welds. Most failures were accompanied by inelastic out-of-plane deformation of the connected plates.
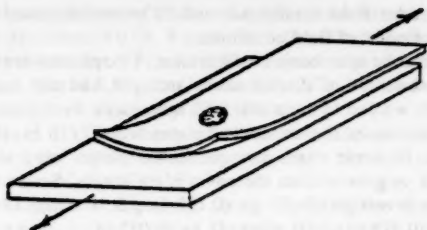
FIG. 4.—Out-of-Plane Distortion

Three modes of ultimate failure of arc spot welds were observed in the Cornell tests [see Fig. 2(d)]. The first is simple shear failure of the weld metal in the plane of the faying surface. The second is plate tearing on the loaded side of the sheet. Failure of this sort starts by tearing along the contour of the weld; it then progresses across the sheet. In the third mode, tearing along the contour of the weld on the tension side is followed by plowing of the weld into the end material as that material buckles and shears, as shown in the third sketch of Fig. 2(d). This type of failure may occur when the end distance is small. Many failures, particularly those of the plate tearing type, may be preceded or accompanied by considerable inelastic out-of-plane deformation of the type indicated in Fig. 4. This is a form of instability similar to that observed in wide, pin-connected plates.

The general behavior of arc seam welds is similar to that of arc-spot welds. No simple shear failures of arc seam welds were observed in the Cornell tests however.

In most cases the onset of yielding was either poorly defined or followed closely by ultimate failure. As in most connections, rupture rather than yielding is a more reliable criterion of failure.

TESTING PROGRAM

Tests were conducted at Cornell for the American Iron and Steel Institute on 342 symmetric fillet, flare bevel, arc spot, and arc seam welded connections subjected to monotonically increasing static loading. A breakdown of the program is as follows:

Type	Number of specimens
Transverse fillet welds	55
Longitudinal fillet welds	64
Transverse flare bevel welds	42
Longitudinal flare bevel welds	32
Arc spot welds	126
Arc seam welds	23
Total	342

One hundred and thirty connections were made in steel fabricating shops,

122 were made under field conditions, and 90 were fabricated in the Cornell laboratory under simulated field conditions.

All specimens had the same basic configuration. Two plates were butted together with one or, in the case of double sheet arc spot and arc seam welds, two cover plate sheets welded to each side. All specimens were welded with E6010 electrodes. In most cases the connected plates were 7/16 in. thick hot rolled A36 steel plates. In some cases the connected plates were sheets having a thickness equal to or greater than the cover plate sheets. Seven different cover plate gages were investigated: 10 ga (0.138 in., 3.51 mm); 12 ga (0.108 in., 2.74 mm); 14 ga (0.079 in., 2.01 mm); 18 ga (0.052 in., 1.32 mm); 22 ga (0.034 in., 0.86 mm); 24 ga (0.028 in., 0.71 mm); and 28 ga (0.019 in., 0.48 mm). All of the 10 gage, 12 gage, and 22 gage steel, most of the 18 gage material, and some of the 14 gage cover plate sheets, were made from A446, Grade A steel [minimum σ_y = 33 ksi (227,700 kN/m^2) and σ_u = 45 ksi (310,500 kN/m^2)]. The remainder of the cover plate sheets were A446, Grade E steel [minimum σ_y = 80 ksi (552,000 kN/m^2) and σ_u = 82 ksi (565,800 kN/m^2)]. Tension coupon tests were made of all cover plate steel used. The measured ultimate strengths are used in the strength prediction equations cited as follows.

Arc spot and arc seam welded specimens with single and double sheet cover plate were tested. The double sheet condition is encountered in practice when overlapping sheets are fastened to the supporting frame by welds that penetrate both plies of material.

Complete details of the test program and the results are contained in Refs. 4 through 8. A summary of the specimen and test data needed to interpret the results is given in Ref. 10.

Test Results and Strength Predictions

In the following sections, the performance of each of the types of weld investigated is summarized. Equations for predicting the ultimate resistance of each type of connection are presented and compared with the test results. The predicted ultimate loads, P_u, are given for a single weld. The predicted ultimate loads for each specimen, P_{up}, is to be found by multiplying P_u by the number of welds that must fail in order to cause the failure of the specimen.

Transverse Fillet Welds.—A total of 55 transverse weld specimens were tested. The cover plate material was either 12 gage or 18 gage A446, Grade A steel. Complete details are contained in Refs. 4 and 5. In all but eight of the tests, primary failure was by tearing of the connected sheets along, or close to, the contour of two of the welds. In the remainder, there was secondary weld shear. In seven of the tests, ultimate failure was preceded by substantial out-of-plane plastic deformation.

Fig. 5 presents a comparison of the experimental ultimate load P_{uo} with the failure load P_{up} predicted from the equation

$$P_u = tL\sigma_u \qquad \ldots \ldots \ldots \ldots \ldots \ldots \ldots \ldots \ldots \ldots \ldots \ldots \ldots \ldots \ldots (1)$$

in which t = the cover plate thickness; L = the length of the weld; σ_u = the measured ultimate strength of the cover plate material; and P_u = the ultimate load per weld. The ultimate load for the specimen P_{up} is twice P_u since the specimen failure involves the failure of two welds. For the 24 shop welded

connections the average ratio of observed to predicted ultimate strength is 1.04, with a standard deviation of 0.09. For the 31 field welded specimens the average and standard deviation are 0.97 and 0.11, respectively, and for all specimens these values are 1.00 and 0.11. It is believed that Eq. 1 is an excellent predictor of the failure strength of transverse fillet welds.

The basic reason for the ability of transverse fillet welds to develop the tensile strength of the adjacent sheet appears to be the one referred to earlier in the consideration of Fig. 2(a). For welds on thin sheets, the dimension of the weld leg on the sheet edge is generally equal to the sheet thickness and the weld throat is commonly larger than the throat of a conventional fillet weld of the same size. Under these circumstances, if the deposited filler metal has a tensile strength greater than that of the sheets being joined, as should be the case with conventionally matched materials and properly made welds, it can be expected that the sheet is the critical element.

Longitudinal Fillet Welds.—A total of 64 longitudinal fillet weld specimens were tested. Again, all of these tests were on 12 gage or 18 gage A446, Grade A material. Complete details are contained in Refs. 4 and 5. In 33 of the tests, tensile tearing across the connected sheets was either the sole cause of failure or a major contributing factor. In the remainder of the tests, failure was the result of weld shear, weld peeling, tearing of the sheet along or roughly parallel to the contour of the weld, or a combination of these effects. In many of the longitudinally welded specimens there was also a substantial amount of out-of-plane deformation.
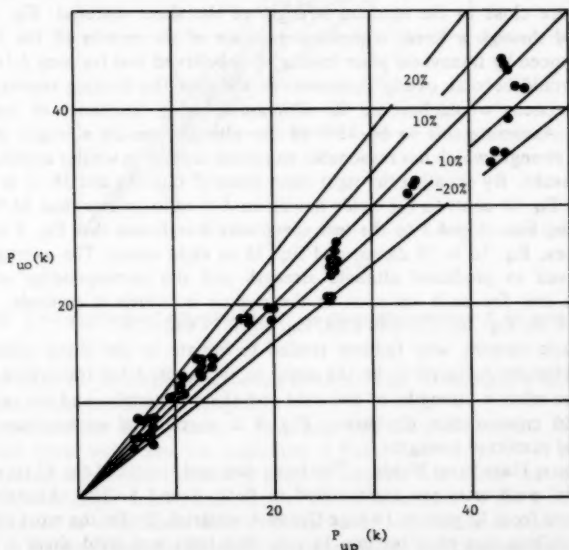
FIG. 5.—Transverse Fillet Welds (P_{up} is According to Eq. 1)

The following equation was found satisfactory to predict failure by tensile tearing across the cover plate:

$$P_u = 0.4tS\sigma_u \quad\dots\dots\dots\dots\dots\dots\dots\dots\dots\dots\dots\dots\dots\dots \quad (2)$$

in which S and t = the width and thickness of each cover plate, respectively. However, failures involving tearing along the weld contour, weld shear, and combinations of the two were predicted satisfactorily by the larger value obtained from

$$P_u = tL\left(1 - 0.011\frac{L}{t}\right)\sigma_u \quad\dots\dots\dots\dots\dots\dots\dots\dots\dots\dots \quad (3a)$$

or $\quad P_u = 0.75tL\sigma_u \quad\dots\dots\dots\dots\dots\dots\dots\dots\dots\dots\dots\dots \quad (3b)$

in which L = the average weld length. The ultimate load for the specimens, P_{up} is four times P_u.

In the 33 tests in which tensile tearing across the sheet was a primary factor, it was observed that it occurred at an average stress on the cross section of the connected plates equal to about 80% of the ultimate strength of the sheet material. That is the reason for Eq. 2.

It was also observed that for all other failures there appeared to be some correlation between the ultimate resistance of the connection and the length of the welds. Indeed, for very short welds, average stresses obtained by dividing the actual ultimate load by the product of the sheet thickness and total weld length were close to the ultimate strength of the sheet material. Eq. 3a was developed through a linear regression analysis of the results of the 31 tests not influenced by transverse plate tearing. It is believed that for long L/t ratios, Eq. 3a would become overly conservative and that the limiting resistance for such specimens would become the ultimate shearing resistance of the sheet material. Assuming this to be 75% of the ultimate tensile strength (a value for shear strength which has reasonable empirical support in similar applications), Eq. 3b results. By equating the right hand sides of Eqs. 3a and 3b, it is readily seen that Eq. 3b controls for welds having an L/t ratio greater than 22.7.

Applying Eqs. 2 and 3 to the test specimens it is found that Eq. 2 controls in 38 cases, Eq. 3a in 18 cases, and Eq. 3b in eight cases. The average ratio of observed to predicted ultimate strength and the corresponding standard deviation are, for each equation in the regime in which it controls: Eq. 2, 1.00 and 0.10; Eq. 3a, 1.05 and 0.08; Eq. 3b, 0.89 and 0.09.

The basic reasons why failures tended to initiate in the sheet rather than in the welds are believed to be the same as those cited for transverse welds; mainly the relative strengths of the weld and sheet materials, and the relatively large weld cross-section dimension. Fig. 6 is a graphical comparison of the actual and predicted strengths.

Transverse Flare Bevel Welds.—The basic data and results of the 42 transverse flare bevel weld tests are summarized in Refs. 4 and 5. The channels were cold formed from 12 gage or 18 gage Grade A material. By far the most common mode of failure was plate tearing. In only five tests was weld shear a factor. Significant out-of-plane distortion was experienced in twelve tests. The experimental failure loads predicted satisfactorily by the equation

$$P_u = 0.8 \, tL\sigma_u \dots \dots \dots \dots \dots \dots \dots \dots \dots \dots \dots \dots \dots \dots \dots (4)$$

in which each quantity is as previously defined. The ultimate load of the specimens P_{up} is two times P_u. For the 26 shop welded connections the average rate of observed to predicted ultimate strength is 0.97, with a standard deviation of 0.15. For the sixteen field welded specimens the average and standard deviation are 1.16 and 0.14, respectively, and for all specimens these values are 1.04 and 0.17.

The basic reasons why failures tended to originate in the connected sheet rather than the weld appear to be the relative strength of the two materials and the weld dimensions. With one exception the effective weld throat dimension was greater than the sheet thickness. It is believed that this will also be the
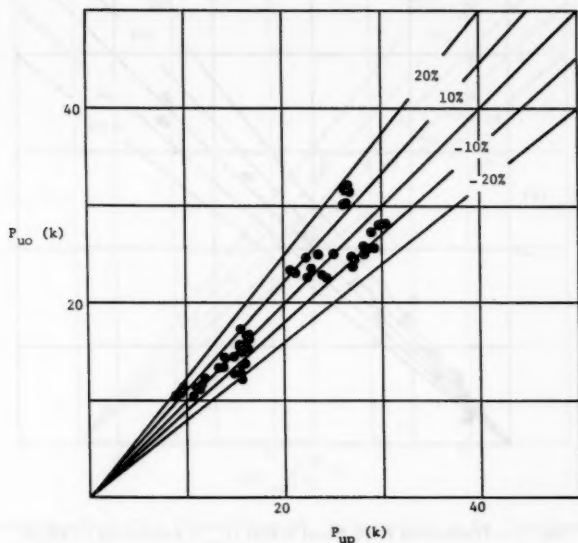
FIG. 6.—Longitudinal Fillet Welds (P_{up} is According to Eqs. 2, 3a, and 3b)

case in practice for welds made according to Ref. 2. Fig. 7 is a graphical comparison of the actual and predicted strengths.

Longitudinal Flare Bevel Welds.—The basic data and results of the 32 longitudinal flare bevel weld tests are contained in Refs. 4 and 5. In 22 of the tests, tensile tearing across the connected channel sections was either the sole cause of failure or a major contributing factor. In the remainder of the tests, failure was the result of weld shear or a combination of weld shear and plate tearing parallel to the weld contour, generally accompanied by out-of-plane deformation. The experimental failure loads are predicted satisfactorily in this case by the smaller value obtained from

$$P_u = 0.4A\sigma_u \dots \dots \dots \dots \dots \dots \dots \dots \dots \dots \dots \dots \dots \dots \dots \dots (5)$$

in which A = the area of the channel cover plate, or two times the result calculated by Eq. 3b. The result obtained from Eq. 3b was multiplied by two in order to account for the fact that the shear force is resisted by the upstanding flange as well as the web of the channel. The ultimate load, P_{up}, for the specimens is four times P_u.

Applying Eqs. 5 and 3b to the test specimens it is found that Eq. 5 controls in 19 cases and Eq. 3b in 13 cases. The average ratio of observed to predicted ultimate strength and the corresponding standard deviation are, for each equation
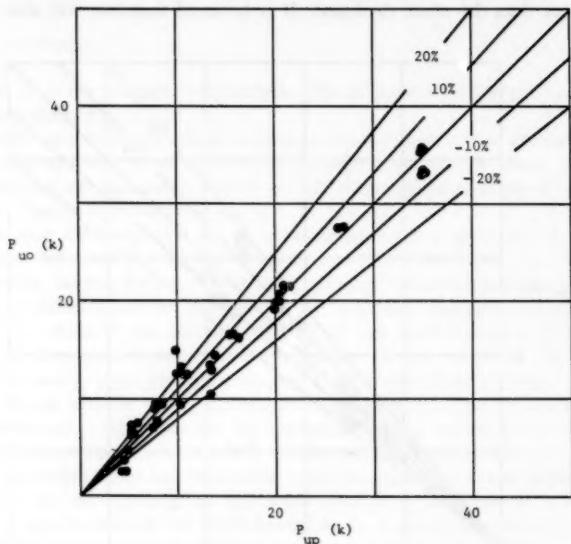
FIG. 7.—Transverse Flare Bevel Welds (P_{up} is According to Eq. 4)

in the regime in which it controls: Eq. 5, 1.03 and 0.10; and Eq. 3b, 1.01 and 0.14. Fig. 8 is a graphical comparison of the actual and predicted strengths.

Arc Spot Welds.—The basic data and results of the 126 arc spot weld tests are contained in Refs. 4, 5, 6, and 8.

In evaluating these tests, clarity requires that a distinction be made between those which failed in pure shear and those which failed in one of the other modes. In 31 shear failures, measurements were made of the net areas of the sheared welds which contained substantial pitting and porosity. These irregular surfaces were converted to circles of the same area, and the equivalent diameter, d_{en}, recorded. The linear equation found to provide the best fit to these diameters is

$$d_{en} = 0.70d - 1.5t \dots \dots \dots \dots \dots \dots \dots \dots \dots \dots \dots \dots \dots \dots \dots (6)$$

in which d = the visible diameter; and t = the net sheet thickness. The measured equivalent diameter in the specimens tested ranged from 0.39 in. (10 mm)–0.70 in. (17.90 mm). This equation is plotted in Fig. 9 for illustration. Weld shear failure loads were predicted satisfactorily by the equation

$$P_u = \frac{3\pi}{16} d_{en}^2 \sigma_{uw} \quad \dots \dots \dots \dots \dots \dots \dots \dots \dots \dots \dots \dots \dots \dots \dots \dots (7)$$

in which σ_{uw} = 60 ksi (414,000 kN/m^2), the nominal tensile strength of E60 filler metal. The ultimate load for the specimen, P_{up}, is two times P_u.
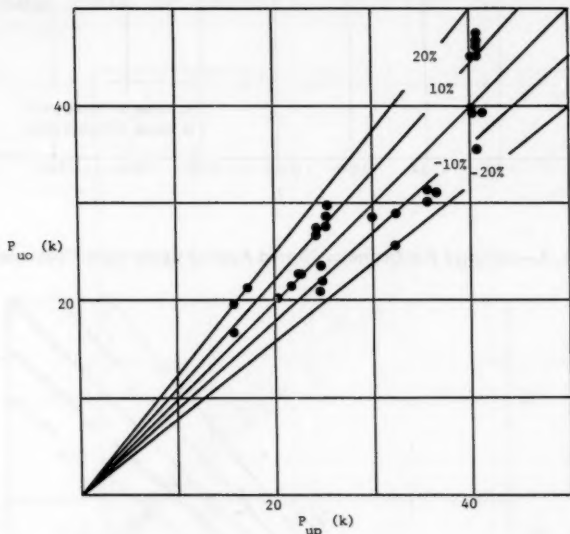
FIG. 8.—Longitudinal Flare Bevel Welds (P_{up} is According to Eq. 5 or Two Times Eq. 3b)

Based on an analysis of conditions in the cover sheets in the immediate region of the arc spot welds, Omer Blodgett of the Lincoln Electric Company proposed in unpublished correspondence two equations for the prediction of the strength of arc spot welded connections that fail by plate tearing. The Blodgett equations incorporate the observation that, for cases in which weld shear failure did not control, failure was generally by transverse tearing when d/t was less than $240/\sqrt{\sigma_u}$, and by longitudinal tearing and end zone buckling where d/t was greater than $240/\sqrt{\sigma_u}$, where σ_u is the ultimate strength of the sheet material, in kips per square inch. This limit can be expressed nondimensionally as $1.4\sqrt{E/\sigma_u}$. The best fit equations were found to be, for $d/t < 140/\sqrt{\sigma_u}$ (or nondimensionally $0.82\sqrt{E/\sigma_u}$)
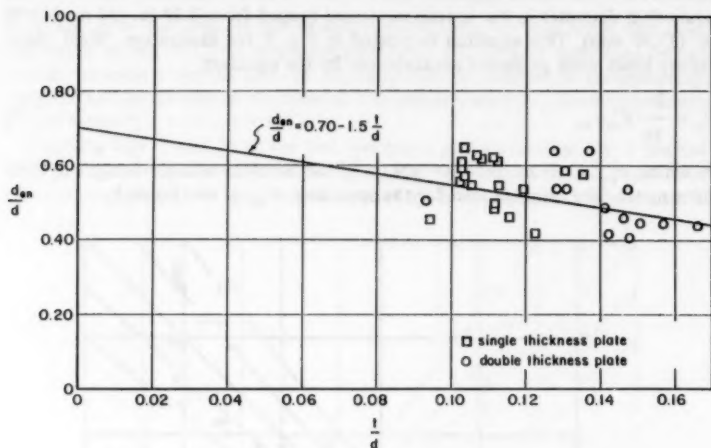
FIG. 9.—Effective Net Diameter Plotted Against Cover Plate Thickness

$$\frac{d_{en}}{d} = 0.70 - 1.5\frac{t}{d}$$

□ single thickness plate
○ double thickness plate
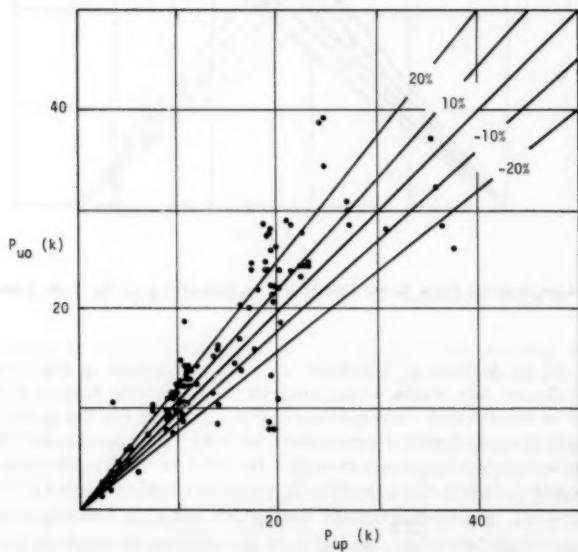
FIG. 10.—Arc Spot (Puddle) Welds (P_{up} is According to Eqs. 7, 8, or 9)

$$P_u = 2.2td\sigma_u \quad \ldots \ldots \ldots \ldots \ldots \ldots \ldots \ldots \ldots \ldots \ldots (8)$$

and, for $d/t \geq 240/\sqrt{\sigma_u}$ (or nondimensionally $1.4\sqrt{E/\sigma_u}$)

$$P_u = 1.4td\sigma_u \quad \ldots \ldots \ldots \ldots \ldots \ldots \ldots \ldots \ldots \ldots (9a)$$

For the range $140/(\sqrt{\sigma_u}) \leq d/t \leq 240/(\sqrt{\sigma_u})$ the following transition equation seems reasonable:

$$P_u = 0.28\left(1 + \frac{960t}{d\sqrt{\sigma_u}}\right)td\sigma_u \quad \ldots \ldots \ldots \ldots \ldots \ldots \ldots (9b)$$

The second term in the brackets can be expressed nondimensionally as $5.59t/d\sqrt{\sigma_u/E}$.
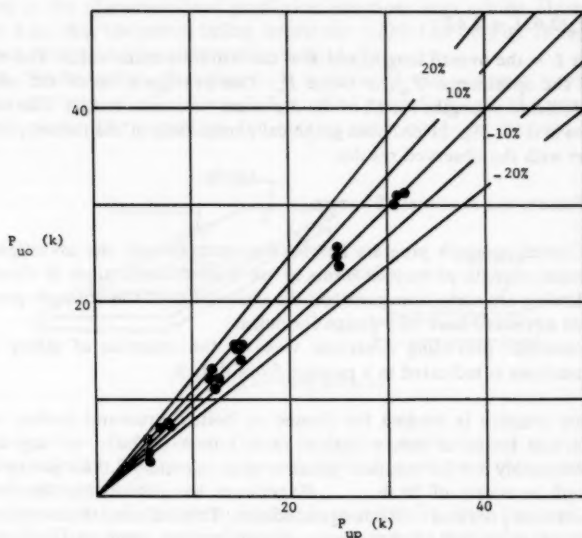
FIG. 11.—Arc Seam Welds (P_{up} is According to Eq. 10)

In the aforementioned equations, $d = d_v - t$, in which d_v = the visible diameter; and t = the net thickness of the single-ply or double-ply welded sheet. The limits of applicability of these equations are related to the ultimate strength rather than the yield strength of the steel. In each case, the ultimate load, P_{up}, is twice P_u.

The average ratio of the observed to the predicted strengths for the 78 tests in which Eq. 8, 9, or 10 controlled the predicted failure load is 1.07. The standard deviation is 0.26. The average ratio of the observed to the predicted strength for the 45 tests in which Eq. 7 governed is 1.22 and the corresponding standard deviation is 0.37. The conservative nature of Eq. 7 can be justified on the

basis of the variability of the weld quality and particularly on the amount of porosity encountered in practice. All of the field welded arc spot welds reported in Ref. 5 were poorly made. Fig. 10 provides a graphical comparison of the weld shear and plate failure equations with the observed results.

Arc Seam Welds.—The basic data and results of the 23 arc seam welds are contained in Ref. 8. Based on an analysis of conditions in the cover plates in the immediate region of the arc seam welds, Omer Blodgett proposed, in unpublished correspondence, an equation for the prediction of the strength of arc seam welds that fail by a combination of tensile tearing of the sheets along the forward edge of the weld contour plus shearing of the sheets along the sides of the welds. Linear regression analysis performed by the writers on the results of the tabulated tests has resulted in the following modified version of the Blodgett equation:

$$P_u = t\sigma_u(0.63L + 2.4B) \quad \ldots \ldots \ldots \ldots \ldots \ldots \ldots \ldots \ldots \ldots \ldots \ldots \quad (10)$$

in which L = the overall length; and B = the width of seam welds. The ultimate load of the specimens, P_{up}, is twice P_u. The average ratio of the observed to the predicted strengths for all of the arc seam weld tests is 1.01. The standard deviation is 0.10. Fig. 11 provides graphical comparison of the failure prediction formulas with the observed results.

SAFETY FACTORS AND ALLOWABLE STRESSES

The Cornell research program has been concerned with the investigation of the ultimate strength of various forms of arc welded connections in sheet steel. The following are some comments on the conversion of the strength prediction equations advanced here into design formulas.

The currently prevailing American view on the selection of safety factors for connections is indicated in a passage from Ref. 9:

> If past practice is studied for riveted or bolted structural carbon steel joints, the factor of safety against sheet failure is found to vary from approximately 3.3 for compact joints to approximately 2.0 for joints with a length in excess of 50 in. . . . Experience has shown that this factor of safety has provided a safe design condition. This indicates that a minimum factor of safety of 2.0 has been satisfactory; the same margin is also used for fasteners in tension.

Similarly, in the American Institute of Steel Construction Specification, the basic allowable tensile stress is $0.60 \ F_y$, but not more than one-half of the maximum tensile stress of the steel.

American practice in the design of statically loaded welded connections implies a basic *nominal* factor of safety of 2.5 with respect to failure. Thus, if as in Eqs. 3b and 7 it is assumed that the ultimate strength in pure shear is 75% of the ultimate tensile strength, it follows that the allowable shear stress obtained using a safety factor of 2.5 is $0.30\sigma_u$ or $0.30\sigma_{uw}$. The latter is the value prescribed for weld shear in buildings in Ref. 2. If one considers the uncertainties which are inevitable in the strength of connections, a *nominal* safety factor of 2.5 is consonant with the intention of having a *minimum* margin of safety of

approximately two. The writers believe that this is a reasonable minimum margin of safety for conventional applications of sheet steel in buildings. It follows that they believe that working stress equations obtained by applying a factor of safety of 2.5 to the ultimate resistance equations proposed will be reasonable design equations.

Welding Procedures

Although this is primarily a report on the results of experimental research on the strength of welded connections, it is appropriate to include brief summaries of some of the practical requirements for obtaining sound welds in sheet steel. Detailed criteria for proper workmanship, technique, qualification, and inspection are contained in Ref. 2. Unless these criteria are satisfied, welds of the quality presumed in the aforementioned prediction equations may not be obtained. It is noted, e.g., that the points falling below the −20% line on Fig. 10 represent tests conducted on substandard welds (Refs. 4, 5).

Details, Workmanship, Technique.—It is intended that arc spot welds have a fused zone (nugget) of at least 1/2 in. (12.5 mm) diam into the supporting structural piece. The capability for making such welds is assessed during
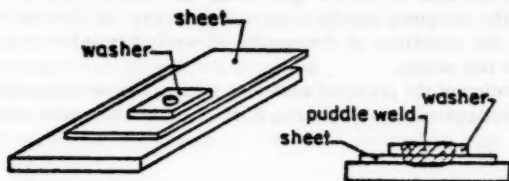
FIG. 12.—Weld Washer

qualification tests. Generally, a flat or horizontal weld position is preferred. It is also necessary that parts to be joined be brought into close contact to facilitate complete fusion.

Effective control of current is absolutely essential for obtaining consistently sound welds. The current required for arc spot or arc seam welding is considerably higher than for most conventional welds. In preparing specimens for the Cornell tests, E6010 electrodes were used, as noted earlier. In one weld qualification test using 5/32 in. (3.97 mm) electrodes to make 1 in. (25.4 mm) (visible diameter) arc spot welds in 0.108 in. (2.74 mm) galvanized sheet, the current was 275 amps and the welding time approximately 6 sec. The burn-off rate [called the melting rate by the American Welding Society (AWS)] of the electrode was 22 in./min (559 mm/min). Using 1/8 in. (3.18 mm) electrodes to make 3/4 in. (19.05 mm) arc spot welds in 0.052 in. (1.32 mm) galvanized sheet, 210 amps and 10 sec were required. The burn-off rate was 18 in./min (457.20 mm/min).

There is a considerable body of opinion among welding experts that the best practical way to maintain uniformity in sheet steel welding is through regulation of the electrode burn-off rate.

In making arc spot welds in sheet of 24 gage (0.028 in., 0.71 mm) and lighter, weld washers may be required. These are small tabs of 16 gage (0.064 in., 1.63 mm) or similar material with punched holes somewhat smaller in diameter than the visible weld diameter (see Fig. 12). They permit the weld to be made without burning the thin sheet.

Because of the relatively high currents used in arc spot and arc seam welding, the coating on some electrodes may break down and produce shallower penetration than that required. This may necessitate limiting the number of welds which may be made in rapid succession with one electrode.

Qualification, Inspection.—Both the procedure and the welder must be carefully qualified following rules prescribed in an appropriate specification such as Ref. 2. Such rules include simple but severe mechanical tests on sample welds.

Conclusions

The results of an extensive test program have been evaluated and strength prediction equations have been derived. The strength prediction equations can be converted into design equations through the use of appropriate safety factors as considered in this report.

Except for the case of the arc spot welds, the correlation between the test results and the computed results is quite satisfactory. In the case of the arc spot welds, the variability of the quality of welds has led to a rather large scatter in the test results.

The application of the proposed equations presupposes welds made according to the quality standards of the Welding Sheet Steel in Structures, AWS D1.3-80 (Ref. 2).

Acknowledgments

Appendix I.—References

1. "Specification for the Design of Cold-Formed Steel Structural Members," American Iron and Steel Institute, Washington, D.C., Sept. 3, 1980.
2. "Welding Sheet Steel in Structures," *AWS D1.3-80*, American Welding Society, Miami, Fla., 1980.
3. "Welding Terms and Definitions," *AWS A3.0-76*, American Welding Society, Miami, Fla.
4. Dhalla, A. K., and Peköz, T., "Tests on Puddle and Fillet Weld Connections," Department of Structural Engineering, Cornell University, Ithaca, N.Y., Oct., 1971.
5. Yarnell, R. S., and Peköz, T., "Tests on Field Welded Puddle and Fillet Weld Connections," Department of Structural Engineering, Cornell University, Ithaca, N.Y., Jan., 1973.

6. Fraczek, J., and Peköz, T., "Tests on Puddle Weld Connections," Department of Structural Engineering, Cornell University, Ithaca, N.Y., 1975.
7. Shephard, M., Peköz, T., and Winter, G., "Interpretation of Tests on Welded Light Gage Steel Connections," Department of Structural Engineering, Cornell University, Ithaca, N.Y., June, 1976.
8. Struble, J. W., Peköz, T., and McGuire, W., "Tests on Puddle Weld Connections," Department of Structural Engineering, Cornell University, Ithaca, N.Y., Apr., 1978.
9. Fisher, J. W., and Struik, J. H. A., "Guide to Design Criteria for Bolted and Riveted Joints," John Wiley and Sons, Inc., New York, N.Y., 1974.
10. Peköz, T., and McGuire, W., "Welding of Sheet Steel," SG 79-2, American Iron and Steel Institute, Washington, D.C., Jan., 1979.

Appendix II.—Notation

The following symbols are used in this paper:

A = area of channel cover plate, in square inches;
B = average width of arc seam welds, in inches;
d = $d_v - t$;
d_v = visible diameter of arc spot weld, in inches;
L = average length of welds of specimen, in inches;
P_u = ultimate strength of each weld, k;
P_{uo} = observed ultimate strength of connection, k;
P_{up} = predicted ultimate strength of connection, k;
S = average cover plate width, in inches;
t = average cover plate thickness, in inches;
σ_u = ultimate stress of cover plate material, in kips per square inch;
σ_{uw} = nominal tensile strength of E60 filler material, in kips per square inch; and
σ_y = yield stress of cover plate material, in kips per square inch.

Proposed Failure Criteria for Concrete Block Masonry under Biaxial Stresses

By Ahmad A. Hamid[1] and Robert G. Drysdale[2]

Introduction

The available failure hypotheses (2,12,13) for masonry are related to the failure theories for isotropic materials (11) such as Coulomb's theory of internal friction, the maximum stress theory, and Mohr's theory of failure. Although it is known that these theories are not applicable in a generalized form to masonry, they have been utilized (2,12,13) to predict failure of masonry assemblages under particular stress conditions. It has been shown (3,4) that masonry strength is highly sensitive to the orientation of the stress with respect to the critical-bed and head-joint directions. Therefore, as has been shown for layered materials (9), the failure theories for isotropic materials are not applicable for masonry because they were derived on the basis of the invariant state of stress concept where the stress orientation has no effect on the strength.

For block masonry, grouting the cores provides partial continuity which reduces the degree of anisotropy of the composite. Hegemier et al. (7) suggested a linear interaction failure envelope for the tension-compression state of stress. This assumption can be justified where the strength characteristics of the grout match those of the block. However this assumption does not provide a generalized solution applicable to other combinations of materials or to ungrouted blockwork.

In this paper, failure criteria are proposed as a generalized form for masonry under biaxial stresses taking into consideration its anisotropic nature as a composite material. These criteria are then compared with the results of tests (4) of grouted and ungrouted concrete block masonry prisms under combined stress conditions.

Failure Theories for Composite Materials Applied to Masonry

Because the mortar joints in masonry are relatively weak compared to the masonry units, the bed- and head-joint directions are the critical planes where

[1] Asst. Prof., School of Civ. Engrg. and Environmental Sci., Univ. of Oklahoma, Norman, Okla.

[2] Prof., Dept. of Civ. Engrg. and Engrg. Mechanics, McMaster Univ., 1280 Main Street West, Hamilton, Ontario, Canada L85 4L7.

failure is likely to be initiated. The mortar bed joints, because of their continuous nature, divide the media into layers of equal thickness and thus give masonry the appearance of a laminated composite material.

The bed- and head-joint directions are assumed to be the planes of strength symmetry (orthogonal principal material directions, x and y, see Fig. 1), where the strength characteristics have to be determined. The various strength characteristics are shown in Fig. 1. For masonry there is no transverse symmetry and therefore the strength characteristics of the assemblage should also be evaluated in the z direction to be able to fully express the behavior of the composite under biaxial states of stress (8).

To provide a basis of comparison, the applicabilities of existing failure theories for composite material such as the maximum stress theory (9), the Hill-Tasia
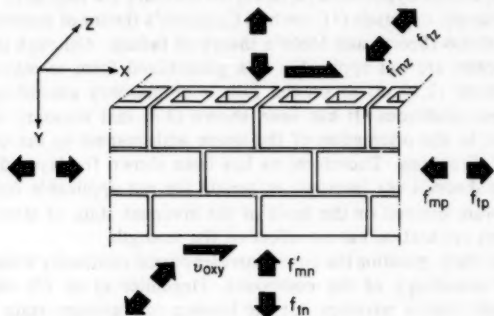
FIG. 1.—Illustration of Strength Characteristics for Masonry under Multiaxial States of Stress

theory (9), and the Hoffman theory (8) were examined. These will be compared with test results and the proposed criteria later in this paper.

PROPOSED FAILURE CRITERIA

To formulate a failure criterion for masonry, it is necessary to account for the possible modes of failure under biaxial stresses. The resulting failures may be by shear along the critical bed and head joints or tension failure of the block, mortar, and grout, or both. Shear failure should take into account the normal compression stress perpendicular to the slip plane since this parameter was shown (4,5,12) to have a significant influence on the shear capacity of the assemblage.

It is not logical to expect that a single failure criterion can describe the biaxial strength of masonry where more than one mode of failure controls. It has been shown (3,4,5,6) that two modes of failure occur for masonry under combined stresses. As described in the next two sections, these are: (1) Shear failure along either the bed joints or the head joints (the critical planes); and (2) tension failure incorporating the interaction of the block, mortar, and grout.

Shear Failure Criterion.—The shear strength of the mortar bed joint, (ungrouted

masonry), τ_{xyu}, under normal stress, σ_y, can be expressed, using Coulomb's theory of friction (5,9,12,13) as

$$\tau_{xyu} = v_{ob} + \mu\,\sigma_y \dots\dots\dots\dots\dots\dots\dots\dots\dots\dots\dots (1)$$

in which v_{ob} = the shear-bond strength of the bed joint when no normal stress is present; and μ = the coefficient of internal friction.

For grouted masonry, due to the external shear and precompression, the grout core will be under combined shear and compression stresses which create a biaxial state of tension and compression principal stresses as shown in Fig. 2. Using the octahedral shear-stress criterion, and adopting a linear expression
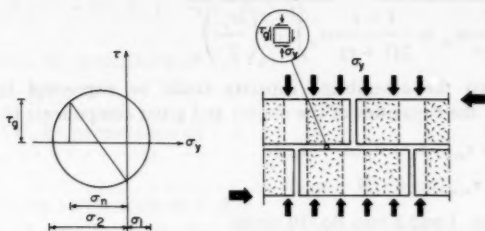
FIG. 2.—Stresses Acting on Element of Grout

to relate the octahedral shear stress, τ_{oct}, with the octahedral normal stress, σ_{oct}, in the form (10)

$$\tau_{oct} = a - b\,\sigma_{oct} \dots\dots\dots\dots\dots\dots\dots\dots\dots\dots\dots (2)$$

in which a and b = the material constants and

$$\tau_{oct} = \frac{1}{3}\sqrt{(\sigma_1 - \sigma_2)^2 + (\sigma_2 - \sigma_3)^2 + (\sigma_3 - \sigma_1)^2} \dots\dots\dots\dots (3)$$

and $$\sigma_{oct} = \frac{1}{3}(\sigma_1 + \sigma_2 + \sigma_3) \dots\dots\dots\dots\dots\dots\dots\dots (4)$$

the yielding surface (fracture surface in the case of brittle materials) can be expressed, for a biaxial state of stress ($\sigma_3 = 0$), in the form

$$(2\sigma_1^2 + 2\sigma_2^2 - 2\sigma_1\sigma_2)^{1/2} + \sqrt{2}\,\frac{1-r}{1+r}(\sigma_1 + \sigma_2)$$

$$- 2\sqrt{2}\,\frac{r}{1+r}\sigma_{cg} = 0 \quad (\text{for } \sigma_1 > 0 \text{ or } \sigma_2 > 0) \dots\dots\dots\dots (5)$$

in which σ_{cg} = the compressive strength of the grout; and r = the ratio of the tensile strength of the grout to its compressive strength, σ_{tg}/σ_{cg}. Eq. 5 may be simplified using Mohr's function for a biaxial state of stress (10) to be

$$\frac{1}{2}(\sigma_1 - \sigma_2) = \frac{r}{1+r}\sigma_{cg} - \frac{1}{2}\frac{1-r}{1+r}(\sigma_1 + \sigma_2) \dots \dots \dots \dots \dots \dots (6)$$

Obviously, the two principal stresses, σ_1 and σ_2, can be expressed as a function of the applied shear, τ_g, and the normal stress, σ_y, acting on an element of grout (Fig. 2) so that

$$\sigma_{1_2} = -\frac{\sigma_n}{2} \pm \sqrt{\left(\frac{\sigma_{y2}}{2}\right) + \tau_g^2} \dots \dots \dots \dots \dots \dots \dots \dots \dots \dots \dots (7)$$

substituting the σ_1 and σ_2 values from Eq. 7 into Eq. 6 yields

$$\tau_g = \sqrt{\left(\frac{r}{1+r}\sigma_{cg} + \frac{1-r}{2(1+r)}\sigma_y\right)^2 - \left(\frac{\sigma_y}{2}\right)^2} \dots \dots \dots \dots (8)$$

Considering that the assemblage capacity could be expressed by a linear combination of the capacities of the mortar and grout components (4), then

$$\text{then} \quad \tau_{xyg}A_g = \tau_{xyu}[A_n + \tau_g(A - A_n)] \dots \dots \dots \dots \dots \dots \dots (9)$$

$$\text{so that} \quad \tau_{xyg} = \tau_{xyu}[\eta_h + \tau_g(1 - \eta_h)] \dots \dots \dots \dots \dots \dots (10)$$

Substituting Eqs. 1 and 8 into Eq. 10 yields

$$\tau_{xyg} = \eta_h(v_{ob} + \mu\sigma_y)$$
$$+ (1 - \eta_h)\sqrt{\left(\frac{r}{1+r}\sigma_{cg} + \frac{1-r}{2(1+r)}\sigma_y\right)^2 - \left(\frac{\sigma_y}{2}\right)^2} \dots \dots \dots \dots (11)$$

in which for grouted masonry, τ_{xyg} = the average shear stress at failure along the bed joint, based on the gross area; η_h = the ratio of the net to gross area of the block at the critical failure plane; and v_{ob} = the mortar shear-bond strength of the bed joint when no normal stress is present.

Considering the lack of detailed information, it seems reasonable to describe the apparent shear capacity along the head joint for zero normal stress, v_{oyx}, as the average of the shear-bond strength of the head joint, v_{oh}, and the shear strength of the face shells of the block, τ_b. This can be expressed as

$$v_{oyx} = \frac{1}{2}(v_{oh} + \tau_b) \dots \dots \dots \dots \dots \dots \dots \dots \dots \dots \dots \dots \dots (12)$$

The shear capacity along the head joint, τ_{yx}, including the effect of the normal stress, σ_x, can be expressed, using Coulomb's theory of friction, as

$$\tau_{yx} = v_{oyx} + \mu\sigma_x \dots \dots \dots \dots \dots \dots \dots \dots \dots \dots \dots \dots \dots \dots \dots (13)$$

Tension Failure Criterion.—The phenomenological failure condition proposed by Hoffman (8) for brittle composite materials is used to provide the tension criterion. However, it will be modified to take into account the interaction between the shear strength of the mortar joints and the normal compression. In developing his fracture condition for triaxial stresses, Hoffman adopted a pattern of failure conditions for orthotropic material in which he accounted for various differing tensile and compressive strengths that characterize brittle behavior. He did this by introducing linear terms which are odd functions of

σ_x, σ_y, and σ_z. This led to the following fracture condition

$$c_1(\sigma_y - \sigma_z)^2 + c_2(\sigma_z - \sigma_x)^2 + c_3(\sigma_x - \sigma_y)^2 + c_4\sigma_x + c_5\sigma_y$$
$$+ c_6\sigma_z + c_7\tau_{yz}^2 + c_8\tau_{zx}^2 + c_9\tau_{xy}^2 = 1 \quad\dots\dots\dots\dots\dots (14)$$

in which the constants c_1–c_9 are nine material parameters which are uniquely determined from the basic strength characteristics, namely: (1) The three uniaxial tensile strengths—f_{tp}, f_{tn}, f_{tz}; (2) the three uniaxial compressive strengths—f'_{mp}, f'_{mn}, f'_{mz}; and (3) the three pure shear strengths—$v_{oxy}, v_{oyz}, v_{ozz}$.

The following expressions can be readily verified as follows:

$$C_1 = \frac{1}{2}((F_{ty}F_{cy})^{-1} + (F_{tz}F_{cz})^{-1} - (F_{tx}F_{cx})^{-1})^{-1} \quad\dots\dots\dots\dots (15)$$

Also, C_2 and C_3 by permutation of x, y, z

$$C_4 = (F_{tx})^{-1} - (F_{cx})^{-1} \quad\dots\dots\dots\dots\dots\dots (16)$$

Also, C_5 and C_6 by permutation of x, y, z

$$C_7 = (F_{syz})^{-1} \quad\dots\dots\dots\dots\dots\dots\dots\dots\dots (17)$$

and C_8 and C_9 by permutation of x, y, z.

However, for the case of in-plane loading (biaxial stress condition), σ_z, τ_{yz}, and τ_{zx} are equal to zero. Therefore, eliminating these terms and substituting the aforementioned constants into Eq. 14 yields the following expression for biaxial stress conditions:

$$\left(\frac{1}{2f_{tn}f'_{mn}} + \frac{1}{2f_{tz}f'_{mz}} + \frac{1}{2f_{tp}f'_{mp}}\right)\sigma_y^2 + \left(\frac{1}{2f_{tz}f'_{mz}} + \frac{1}{2f_{tp}f'_{mp}} + \frac{1}{2f_{tn}f'_{mn}}\right)\sigma_x^2$$
$$+ \left(\frac{1}{2f_{tp}f'_{mp}} + \frac{1}{2f_{ty}f'_{cy}} + \frac{1}{2f_{tz}f'_{mz}}\right)(\sigma_x - \sigma_y)^2 + \left(\frac{1}{f_{tp}} - \frac{1}{f'_{mp}}\right)\sigma_x$$
$$+ \left(\frac{1}{f_{tn}} - \frac{1}{f_{mn}}\right)\sigma_y + v_{oxy}\tau_{xy}^2 = 0 \quad\dots\dots\dots\dots\dots\dots (18)$$

The last term in Eq. 18 contains the value of the constant $c_9 = v_{oxy}$ which
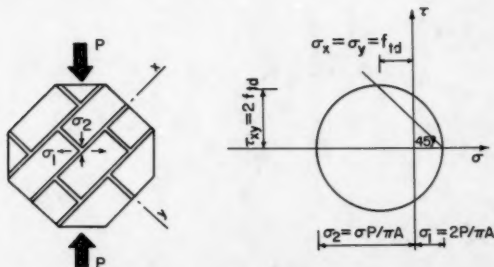
FIG. 3.—Stressed Developed at Center of Masonry Disk Loaded at 45° from Bed Joint

is not applicable where tension is the mode of failure under biaxial stresses. (It represents a local failure along the bed joint and has been considered for the shear mode of failure.) The value of the constant c_9 may be found using the results of tests of masonry disks under splitting loads oriented at 45° from the bed-joint direction (3). As shown in Fig. 3, at the center of the disk under this test condition, the state of normal stress along the bed and head joints can be expressed as

$$\sigma_x = \sigma_y = f_{td} \quad \dots \dots \dots \dots \dots \dots \dots \dots \dots \dots \dots \dots \dots \quad (19)$$

which was empirically found from the tests to be (4)

$$f_{td} = \frac{2}{3}(f_{tp} + f_{tn}) \quad \dots \dots \dots \dots \dots \dots \dots \dots \dots \dots \dots \quad (20)$$

and the shear stress along the bed joint can be expressed as

$$\tau_{xy} = 2f_{td} = \frac{4}{3}(f_{tx} + f_{ty}) \quad \dots \dots \dots \dots \dots \dots \dots \dots \dots \dots \quad (21)$$

Substituting the values of σ_x, σ_y, and τ_{xy} in Eq. 18, the shear constant c_9 can be determined in terms of the strength characteristics in the principal material directions.

EVALUATION OF FAILURE CRITERIA

Test Results.—To evaluate the proposed failure criteria, results (4) are used from concrete block masonry prisms tested under compressive or tensile loads for different orientations, θ, of the bed joint from the applied axial load. Fig. 4 shows the basic concept of the tests. If x and y are the principal material directions, then for a particular orientation, θ, of the applied stress, σ_c, with respect to the x-axis, the stress resultant can be expressed as

$$\sigma_x = \sigma_c \cos^2 \theta \quad \dots \dots \dots \dots \dots \dots \dots \dots \dots \dots \dots \dots \dots \quad (22)$$

$$\sigma_y = \sigma_c \sin^2 \theta \quad \dots \dots \dots \dots \dots \dots \dots \dots \dots \dots \dots \dots \dots \quad (23)$$
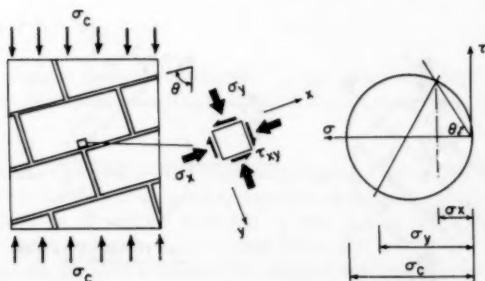
FIG. 4.—Masonry Assemblage Tested Using Different Orientations of Bed Joints (Off-Axis Compression)

$$\tau_{xy} = \sigma_c \sin \theta \cos \theta \quad \dots \dots \dots \dots \dots \dots \dots \dots \dots \dots \dots \dots \quad (24)$$

The normal weight concrete blocks used in these tests had an average compressive strength of 2,850 psi (20 MPa) based on the net area. The 2-core, 6-in. (150 mm) blocks had a minimum net to gross area ratio of 0.59. The splitting tensile strength of the blocks was 248 psi (170 MPa). Type S mortar composed of 1.0:0.5:4.0 parts of Portland Cement, lime, and sand was used which resulted in a cube compressive strength of 2,630 psi (18 MPa). A medium strength grout composed of 1.0:0.44:3.55:0.7 parts by weight of Portland Cement, lime, sand, and water was used. The water-cement ratio was established to give about a 10-in. (250 mm) slump. The compressive strength of block moulded
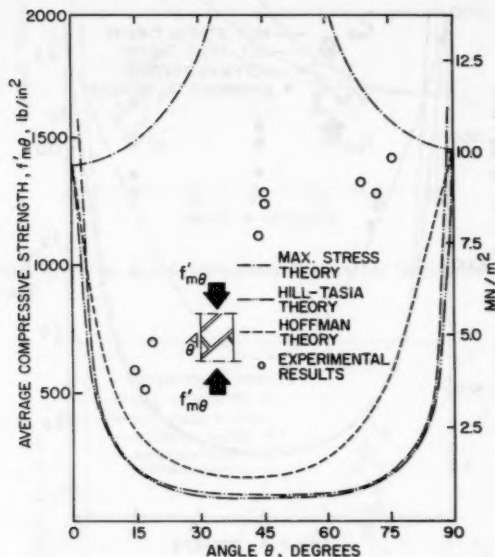
FIG. 5.—Failure Theories and Experimental Results for Ungrouted Masonry Prisms under Off-Axis Compression

grout prism was 3,800 psi (26 MPa) whereas using nonabsorbant 3-in. diam × 6-in. long (76 mm × 152 mm) moulds resulted in a cylinder strength of 2,800 psi (19 MPa).

Evaluation of Existing Failure Criteria.—In Figs. 5 and 6, the test results for off-axis compression are used to evaluate existing failure criteria [maximum stress theory (9), Hill-Tasia theory (9), and Hoffman theory (8)]. In these evaluations, the test results for the principal material directions (θ = 0 and θ = 90°) were used as the starting points. The poor agreement between the experimental results and the theoretical failure envelopes, particularly for cases of medium levels of shear and normal compressive stresses along the bed-

and head-joint directions, indicates the problem with existing failure criteria. The discrepancies could be attributed to the very low values of the shear strengths along the bed-joint direction (5), when it is remembered that these failure theories do not account for the interaction between the shear capacities of the joints and the normal compressive stresses perpendicular to them. Also, these failure theories do not take into consideration the possible shear failure along either the critical-bed or head-joints planes.

Figs. 7 and 8 show the failure envelopes for the existing failure criteria for off-axis tension loading. Aside from the experimental values for the principal material directions ($\theta = 0$ and $\theta = 90°$), only one set of tests were run for
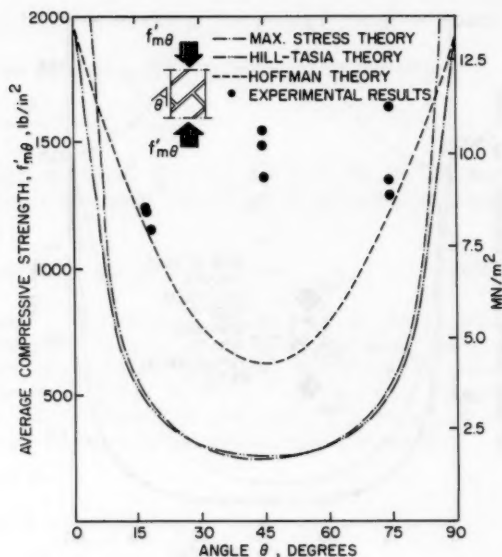
FIG. 6.—Failure Theories and Experimental Results for Grouted Masonry Prisms under Off-Axis Compression

each of the ungrouted and grouted series. Based on this limited number of tests, it appears that the Hoffman theory agrees better with the experimental results for both the ungrouted and grouted cases compared to the Hill-Tasia theory which only seems appropriate for the grouted case.

Evaluation of Proposed Failure Criteria.—The failure envelopes for the proposed failure criteria are shown in Figs. 9 and 10 for the ungrouted and grouted masonry, respectively. There are two curves in each figure to describe the shear-failure condition along either the bed or the head-joint planes and there is one curve describing the tension-failure condition. As shown in the figures, the minimum failure stress defines the governing failure condition for any stress combination.
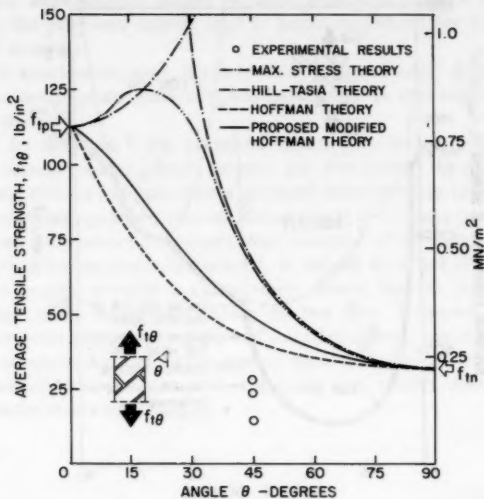
FIG. 7.—Failure Theories and Experimental Results for Ungrouted Prisms under Off-Axis Tension
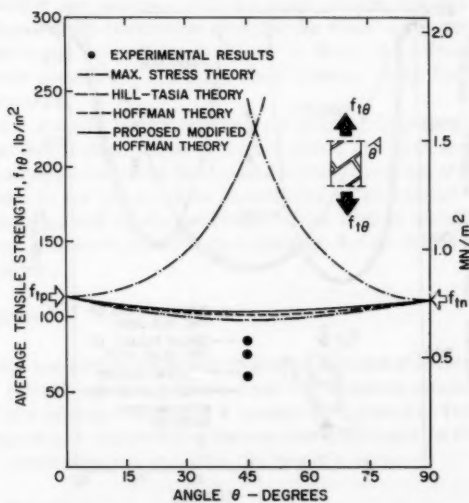
FIG. 8.—Failure Theories and Experimental Results for Grouted Prisms under Off-Axis Tension
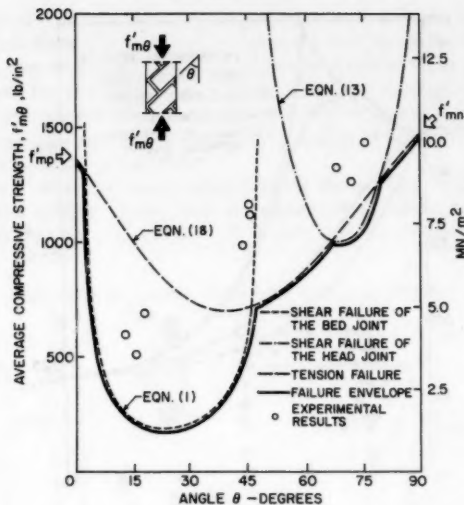
FIG. 9.—Proposed Failure Criteria for Ungrouted Masonry Under Off-Axis Compression
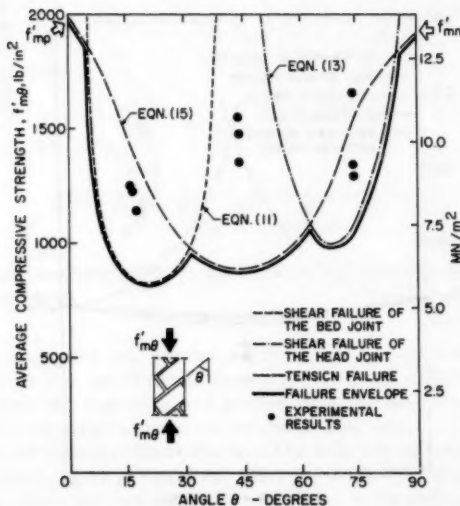
FIG. 10.—Proposed Failure Criterion for Grouted Masonry Prisms under Off-Axis Compression

For the same experimental results as were plotted in Figs. 5 and 6, it can be seen that the proposed criteria lead to better agreement for both ungrouted and grouted masonry.

For the off-axis tension tests, it can be seen in Figs. 7 and 8 that the proposed criteria does not provide quite as good agreement as the original version of Hoffman's theory.

It should be noted that the proposed failure criteria not only predict the capacity of masonry under biaxial stresses, but also predict the mode of failure. The proposed criteria are based on a physical interpretation rather than being strictly phenomenological and it is suggested that these criteria have a promising potential since the inherent anisotropic characteristics of masonry as a composite material have been rationally considered. It should be noted that as they now stand, these criteria provide a conservative (lower bound) prediction of the strength under shear compression along the bed joint. However, the predicted values under shear tension along the bed joint are slightly nonconservative.

It has to be stated that before the general applicability of the proposed criteria is recommended, comparisons with full-scale test results covering different material combinations are required.

Conclusions

The failure theories for isotropic materials are not applicable for masonry under biaxial stresses because they were derived on the basis of the invariant state of stress concept where the stress orientation has no effect on the strength. Also, the available failure theories for composite materials cannot be directly applied to predict the masonry strength under biaxial stresses because they do not account for the interaction between the shear capacities of the joints and the compressive stresses perpendicular to them. In addition, these failure theories do not consider the possible shear failures along the critical-bed or head-joint directions.

To provide a realistic failure criterion for in-plane loading of masonry, the possible shear and tension modes of failure should be taken into account. For the shear slip along the bed or the head joint direction, the effect of the compressive stresses normal to the failure plane should also be considered. These aspects have been incorporated in the proposed failure criteria which are presented as a contribution toward establishing a rational theory of failure for in-plane loading of masonry.

Acknowledgments

Appendix I.—References

1. Bresler, B., and Pister, K. S., "Strength of Concrete under Combined Stresses,"

American Concrete Institute Journal, Vol. 55, Sept., 1958, pp. 321–345.

2. Borchelt, J. G., "Analysis of Shear Walls Subject to Axial Compression and In-plane Shear," *Proceedings of the Second International Brick Masonry Conference*, Stoke-on-Trent, Apr., 1970, pp. 263–265.

3. Drysdale, R. G., Hamid, A. A., and Heidebrecht, A. C., "Tensile Strength of Concrete Masonry," *Journal of the Structural Division*, ASCE, Vol. 105, No. ST7, Proc. Paper 14669, July, 1979, pp. 1261–1276.

4. Hamid, A. A., "Behaviour Characteristics of Concrete Masonry," thesis presented to McMaster University at Hamilton, Ontario, Canada, in 1978, in partial fulfillment of the requirements for the degree of Doctor of Philosophy.

5. Hamid, A. A., Drysdale, R. G., and Heidelbrecht, A. C., "Shear Strength of Concrete Masonry Joints," *Journal of the Structural Division*, ASCE, Vol. 105, No. ST7, Proc. Paper 14670, July, 1979, pp. 1227–1240.

6. Hamid, A. A., Drysdale, R. G., and Heidelbrecht, A. C., "Effect of Grouting on the Strength Characteristics of Concrete Block Masonry," *Proceedings of the North American Masonry Conference*, Aug., 1978, Paper No. 11.

7. Hegemier, G. A., Nunn, R. O., and Arya, S. K., "Behaviour of Concrete Masonry Under Biaxial Stresses," *Proceeding of the North American Conference*, Aug., 1978, Paper No. 1.

8. Hoffman, O., "The Brittle Strength of Orthotropic Materials," *Journal of Composite Materials*, Vol. 1, No. 2, Apr., 1967, pp. 200–206.

9. Jones, R. M., "Mechanics of Composite Materials," 1st ed., McGraw-Hill Book Co., Inc., Washington, D.C., 1975.

10. Mikkola, M. J., and Schnohrich, W. C., "Material Behavior Characteristics for Reinforced Concrete Shells Stressed Beyond the Elastic Range," *Civil Engineering Studies*, Structural Research Series No. 347, University of Illinois, Urbana, Ill., 1970.

11. Nadai, A., "Theory of Flow and Fracture of Solids," Vol. 1, McGraw-Hill Book Co., Inc., New York, N.Y., 1950.

12. Sinha, B. P., and Hendry, A. W., "Racking Tests on Storey Height Shear Wall Structures with Openings Subject to Precompression," *Designing, Engineering and Construction with Masonry Products*, F. B. Johanson, ed., Gulf Publishing Co., Houston, Tex., May, 1969, pp. 192–199.

13. Yokel, F. and Fattal, G., "Failure Hypotheses for Masonry Shear Walls," *Journal of the Structural Division*, ASCE, Vol. 102, No. ST3, Proc. Paper 11992, Mar., 1976, pp. 515–532.

APPENDIX II.—NOTATION

The following symbols are used in this paper:

A = gross area of block in bed-joint plane;

A_g = area of grout in bed-joint plane;

A_n = net area of block in bed-joint plane;

a, b = material constants;

f'_{mn} = compressive strength of masonry normal to bed joint (y direction);

f'_{mp} = compressive strength of masonry parallel to bed joint (x direction);

f'_{mz} = compressive strength of masonry in z direction;

$f'_{m\theta}$ = compressive strength of masonry under load having orientation θ from bed joint;

f_{td} = diagonal tensile strength of masonry;

f_{tn} = tensile strength of masonry normal to bed joint (y direction);

f_{tp} = tensile strength of masonry parallel to bed joint (x direction);

f_{tz} = tensile strength of masonry in z direction;

$f_{t\theta}$ = tensile strength of masonry under load having orientation θ from bed joint;

r = ratio of tensile and compressive strengths of grout;

v_{ob} = shear-bond strength of mortar bed joint when no normal stress is present;

v_{oh} = shear-bond strength of mortar head joint;

v_{oxy} = shear strength of masonry along bed joint direction under zero precompression;

v_{oyx} = shear strength of masonry along head joint direction under zero precompression;

v_{oyz} = shear strength of masonry in y-z plane;

v_{ozx} = shear strength of masonry in z-x plane;

η_h = net to gross area ratio of block in bed-joint plane, A_n/A;

θ = angle of applied load (compression or tension) with respect to bed-joint direction;

μ = coefficient of friction;

$\sigma_1, \sigma_2, \sigma_3$ = principal stresses expressing invariant state of stress for isotropic materials;

σ_c = applied compression or tension stress at orientation θ from bed-joint direction;

σ_{cg} = compressive strength of grout;

σ_{oct} = octahedral normal stress;

σ_{tg} = tensile strength of grout;

$\sigma_x, \sigma_y, \sigma_z$ = applied stresses in x, y, and z directions, respectively;

τ_b = shear strength of face shells of block;

τ_g = shear strength of grout core in direction parallel to bed joint plane under biaxial stresses;

τ_{oct} = octahedral shear stress;

τ_{xy} = shear stress in x-y plane at failure;

τ_{xyu} = shear stress for ungrouted masonry in x-y plane at failure;

τ_{xyg} = shear stress for grouted masonry in x-y plane at failure;

τ_{yz} = shear stress in y-z plane at failure; and

τ_{zx} = shear stress in z-x plane at failure.

DISCUSSION

Discussions

Discussions may be submitted on any *Proceedings* paper or technical note published in any *Journal* or on any paper presented at any Specialty Conference or other meeting, the *Proceedings* of which have been published by ASCE. Discussion of a paper/technical note is open to anyone who has significant comments or questions regarding the content of the paper/technical note. Discussions are accepted for a period of 4 months following the date of publication of a paper/technical note and they should be sent to the Manager of Technical and Professional Publications, ASCE, 345 East 47th Street, New York, N.Y. 10017. The discussion period may be extended by a written request from a discusser.

The original and three copies of the Discussion should be submitted on 8-1/2-in. (220-mm) by 11-in. (280-mm) white bond paper, typed double-spaced with wide margins. The length of a Discussion is restricted to two *Journal* pages (about four typewritten double-spaced pages of manuscript including figures and tables); the editors will delete matter extraneous to the subject under discussion. If a Discussion is over two pages long it will be returned for shortening. All Discussions will be reviewed by the editors and the Division's or Council's Publications Committees. In some cases, Discussions will be returned to discussers for rewriting, or they may be encouraged to submit a paper or technical note rather than a Discussion.

Standards for Discussions are the same as those for Proceedings Papers. A Discussion is subject to rejection if it contains matter readily found elsewhere, advocates special interests, is carelessly prepared, controverts established fact, is purely speculative, introduces personalities, or is foreign to the purposes of the Society. All Discussions should be written in the third person, and the discusser should use the term "the writer" when referring to himself. The author of the original paper/technical note is referred to as "the author."

Discussions have a specific format. The title of the original paper/technical note appears at the top of the first page with a superscript that corresponds to a footnote indicating the month, year, author(s), and number of the original paper/technical note. The discusser's full name should be indicated below the title (see Discussions herein as an example) together with his ASCE membership grade (if applicable).

The discusser's title, company affiliation, and business address should appear on the first page of the manuscript, along with the *Proceedings* paper number of the original paper/technical note, the date and name of the *Journal* in which it appeared, and the original author's name.

Note that the discusser's identification footnote should follow consecutively from the original paper/technical note. If the paper/technical note under discussion contained footnote numbers 1 and 2, the first Discussion would begin with footnote 3, and subsequent Discussions would continue in sequence.

Figures supplied by the discusser should be designated by letters, starting with A. This also applies separately to tables and references. In referring to a figure, table, or reference that appeared in the original paper/technical note use the same number used in the original.

It is suggested that potential discussers request a copy of the *ASCE Authors' Guide to the Publications of ASCE* for more detailed information on preparation and submission of manuscripts.

STRONG AND TOUGH CONCRETE COLUMNS FOR SEISMIC FORCES [a]

Discussion by R. G. Oesterle,[5] A. E. Fiorato,[6] M. ASCE
and W. G. Corley,[7] F. ASCE

The authors have provided a practical summary of design and construction considerations for columns in earthquake-resistant structures. In the paper, several questions were raised about reinforcement details for boundary elements of structural walls ("pilaster columns"). The writers would like to present some relevant observations from an experimental investigation of structural walls conducted at the Construction Technology Laboratories of the Portland Cement Association. This investigation is sponsored by the National Science Foundation under Grant No. ENV 77-15333 and the Portland Cement Association.

In the investigation, isolated structural walls were tested as vertical cantilevers with reversing horizontal loads applied at the top of the wall (13,26). The walls had a height of 180 in. (4.6 m), a horizontal length of 75 in. (1.9 m), and web thickness of 4 in. (102 mm). One objective of the tests was to establish reinforcement details for earthquake-resistant walls.

As noted by the authors, it is important to distinguish between a column that is an integral part of a wall (a boundary element) and a column that is part of a frame. A boundary element is subjected to forces and deformations significantly different from those of a column in a frame. In particular, boundary elements act integrally with the wall when the wall responds to lateral forces by bending as a vertical cantilever beam. Unless the web of the wall is damaged significantly, the boundary element is not subjected to the same magnitude of local bending that would occur in a column of a moment-resisting frame. These differences in behavior are not reflected in current design practice. Rather, reinforcement details for wall boundary elements are based on those developed for columns of moment-resisting frames.

The following questions, related specifically to boundary elements of structural walls, are considered in this discussion:

1. What are design criteria for special transverse reinforcement in boundary elements?
2. Are alternating "candystick" crossties effective?
3. Are boundary elements susceptible to lateral instability?

---

4. How effective is special transverse reinforcement for maintaining the integrity of lap splices in vertical boundary element reinforcement?

Ref. 26 contains a detailed discussion of use of special transverse reinforcement in boundary elements of structural walls. Tests indicate that transverse reinforcement is effective in increasing inelastic deformation capacity of walls. It was significant, however, that beneficial effects of transverse reinforcement were not observed until lateral displacements corresponding to interstory drifts in excess of 1.5% were reached. Thus, the amount of transverse reinforcement that is required for wall boundary elements is related to the level of inelastic deformation capacity demanded of the wall.

Tests also indicate that special transverse reinforcement is required only within potential hinging regions. In cantilevered wall specimens, the zone of primary damage did not extend above the estimated hinging region. Strain gages on hoops and crossties indicated that this reinforcement was stressed significantly only in the first story of the walls. This corresponded to about one half of the height of the hinging region. In actual structures, potential hinging and damage is most critical at the wall base. However, hinging at discontinuities resulting from strength taper, changes in geometry, or higher mode inertial forces must also be considered.

As one variable in the test program, details used for special transverse reinforcement were evaluated. Initially, supplementary crossties used as confinement reinforcement in boundary elements were made with 180° bends at each end. This detail caused numerous construction problems. Subsequently, crossties were made with 90° bends at one end and 135° bends at the opposite end. These ties were alternated end for end over the height of the wall as the boundary element was constructed. Tests demonstrated that this type of "candystick" crosstie was effective. Consequently, it is recommended for use in boundary elements of structural walls.

The writers do not recommend use of spliced crossties within the hinging region of walls. Under severe load reversals, the effectiveness of these ties is questionable (26).

Isolated wall tests also provided some insight into the question of lateral stability of boundary elements. The authors correctly note that, under severe inelastic reversals, resistance of vertical boundary element reinforcement to out of plane displacements is reduced because of substantial reductions in effective moment of inertia.

Of the 23 isolated walls tested, five were rectangular sections without thickened boundary elements. Lateral instability was observed in only one of these specimens. However, this rectangular specimen had no lateral support. This condition would not exist in an actual structure because floor slabs would provide lateral restraint at each story level. Even without restraint, lateral instability was not observed in the specimen until interstory drifts in excess of 1.7% were reached. This indicated that while lateral instability must be considered in design, it is a function of deformation demands as well as slenderness of the wall.

The final question to be covered in this discussion relates to the need for special transverse reinforcement in regions of tensile lap splices of vertical bars. Tests reported in Ref. 25 were conducted to simulate conditions in wall boundary elements. These tests indicate that special transverse reinforcement,

designed in accordance with current code provisions, is effective for maintaining integrity of lap splices under severe reversals. Tests also indicate that transverse hoops located near ends of the splice are most effective for maintaining load transfer capacity. Hoops located at the interior region of the splice were not strained significantly. The implication of these results is that lap splices could be effectively confined by concentrating hoops near the ends of the lap. However, it may be more practical to maintain a uniform distribution of hoops. Another important finding of the lap splice tests is that transverse hoops must be in contact with vertical bars to be effective.

APPENDIX.—REFERENCES

25. Aristizabal-Ochoa, J. D., Fiorato, A. E., and Corely, W. G., "Tension Lap Splices Under Severe Load Reversals," *Proceedings of the Seventh World Conference on Earthquak. Engineering,* Vol. 7, Sept., 1980, pp. 55–62.
26. Oesterle, R. G., Fiorato, A. E., and Corley, W. G., "Reinforcement Details for Earthquake-Resistant Structural Walls," *Concrete International,* American Concrete Institute, Vol. 2, No. 12, Dec., 1980, pp. 55–66.

Discussion by Basile G. Rabbat,[8] and Norman W. Hanson,[9] Members, ASCE

This discussion addresses the authors' question of the value of 90° hooks in "candystick" crossties and confirms that experimental work is being done to establish the amount of confinement steel needed in columns.

The following observations are based on tests of specimens from an ongoing experimental investigation at the Construction Technology Laboratories of the Portland Cement Association. The project is funded by the National Science Foundation under Grant No. PFR-7902611 and the Portland Cement Association.

Tests are being conducted on full-size column specimens. The purpose is to establish reinforcement details for seismic resistant design of lightweight concrete columns. Each test specimen represents a portion of a building frame at the joint between column and beams. The column portion extends from midheights of stories above and below the joint. To ensure column hinging during repeated loads, beams and joint are overreinforced. A photograph of the test setup is shown in Fig. 9. Test procedure is similar to that used in earlier frame joint tests (27).

Details of column reinforcement are shown in Fig. 10. The "candystick" crossties have a 135° hook with a ten-diameter extension at one end and a 90° hook with a six-diameter extension at the other end. Crossties are alternated end-for-end along the column longitudinal reinforcement. Crossties are fitted tightly around column bars at the middle of each face without difficulty.

Incrementally increasing reversing loads are applied to the beam ends while the column load is maintained constant. Hysteretic loops showing column moment versus story height drift for two specimens are shown in Fig. 11. Specimens

[8] Sr. Structural Engr., Structural Development Dept., Portland Cement Association, 5420 Old Orchard Road, Skokie, Ill. 60077.
[9] Principal Structural Engr., Structural Development Dept., Portland Cement Association, 5420 Old Orchard Road, Skokie, Ill. 60077.

LC4 and LC1 had a hoop volumetric ratio, ρ_s, of 1.5 and 3.0%, respectively. These ratios are respectively lower and higher than the ratio $\rho_s = 2.0\%$ required by ACI 318-77 (4).

In the early part of the test, column axial load was equal to 10% of the
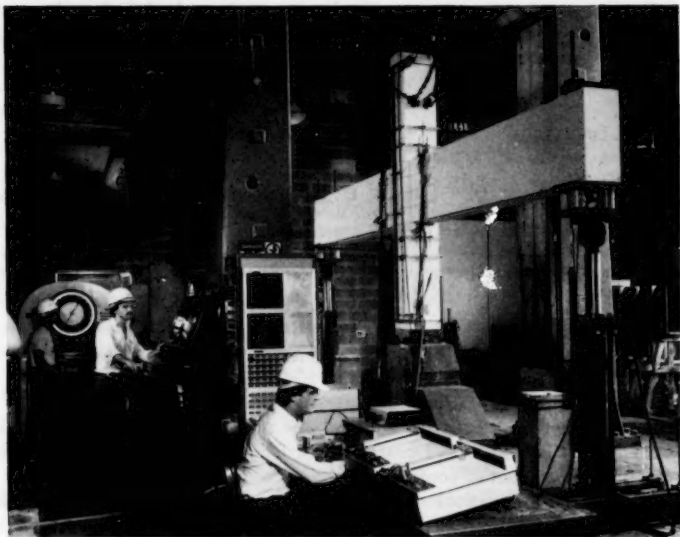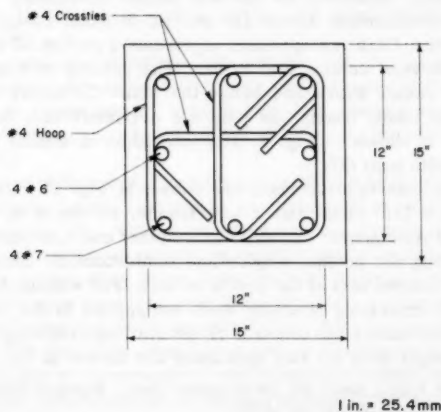

FIG. 9.—Test Setup

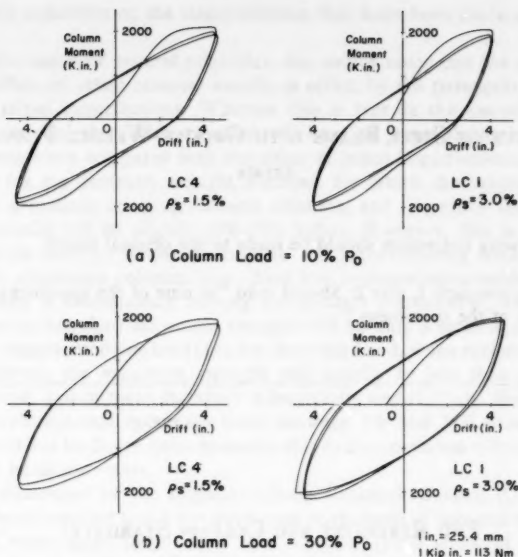
FIG. 10.—Column Reinforcing Steel

1 in. = 25.4mm

(a) Column Load = 10% P_O

(b) Column Load = 30% P_O

1 in. = 25.4 mm
1 Kip in. = 113 Nm

FIG. 11.—Repeated Load Cycles

design axial load strength, ΦP_o. In the latter part of test, the column axial load was increased to 30% of ΦP_o.

For each of these column axial loads, several cycles of inelastic deformations were applied up to a maximum column drift of eight times yield of the column steel. At a ratio of eight, the column concrete shell had spalled. There were no signs of unhooking of the 90° hooks of the crossties.

In Fig. 11, the column moment versus column drift at a ductility of eight is plotted for two different column loads. Based on these hysteretic loops as well as the observed behavior during the tests, it is concluded that the 90°, 135° "candystick" crosstie detailing used in these specimens was adequate.

APPENDIX.—REFERENCE

27. Hanson, N. W., and Conner, H. W., "Tests of Reinforced Concrete Beam-Column Joints Under Simulated Seismic Loading," *RD012.01D*, Portland Cement Association, Skokie, Ill., 1972.

FATIGUE OF STEEL BEAMS WITH GROOVE-WELDED FLANGES[a]

Errata

The following correction should be made to the original paper:

Page 1857, paragraph 1, line 2: Should read "in nine of the specimens." instead of "in none of the specimens."

END RESTRAINT AND COLUMN STABILITY[b]

Discussion by Reidar Bjorhovde,[2] M. ASCE

The author is to be complimented on providing a useful review of column design approaches, and how the effect of end restraint might be included in future solution methods. In particular, his description of research needs for end-restrained columns and how some of these are being met through ongoing projects focus on a parameter in column stability analysis that has not received sufficient attention in the past. However, the writer does not agree that the *basic* column problem is not well understood, nor that most design methods are based entirely on empirical formulas. Significant advances have been made over the past number of years, including in the area of limit states design, through explicit inclusion of realistic column strength factors. Thus the author himself acknowledges the extensive research that has dealt with residual stresses and initial crookedness. Accounting for the effects of end restraint will improve the column stability analysis in an important respect, but it is incorrect to imply that only by doing so will the elusive *practical* design approach be obtained. Rather, the practicality of the current methods will be enhanced, since one more strength contribution thus will have been quantified.

Since the publication of the paper, important column strength results have been obtained by the researchers at the University of Sheffield (10,20), with further input provided by the writer (17). It is the purpose of this discussion to expand on these results in the context of the author's presentation, as well

as to clarify a number of the interpretations that have been made of previous studies.

In his discussion of general principles, the author notes that the strength-increasing effect of strain reversal usually is offset by the (strength) decreasing effect of initial imperfections. Whereas this is true in the general sense, it must be observed that strain reversal will have an insignificant influence on real columns when compared with the effect of initial imperfections. It is more important for the perfectly straight member, for which the tangent modulus load gives a realistic buckling strength estimate, and for which the maximum strength usually will be slightly (2%–5%) higher. However, this is very much influenced by the type of column material and manufacturing method that has been used. Aluminum columns, e.g., have low to nonexistent residual stresses and normally a continuously curving stress-strain relationship. Research has indeed shown that their maximum strength will be only a small amount higher than their tangent modulus load (19). On the other hand, when real steel columns are considered, the maximum strength will usually be less than the tangent modulus load, and in many instances substantially less (1,2,3,9). Research (3,9) has demonstrated that maximum loads between 5% and 25% lower than the tangent modulus loads are quite common, due to the combined effect of residual stress and initial curvature.

In the discussion of the original Column Research Council (CRC) Curve, it should be pointed out that it was developed on the basis of light and medium-size hot-rolled wide-flange shapes in ASTM A7 steel [yield stress of 33 ksi (230 MPa)]. Although subsequent design curves that were based on the CRC Curve were applied to a variety of shapes, sizes, and materials, the background data should be kept in mind.

At this stage it is inappropriate to observe that "it is believed that the behavior and strength of columns will be significantly affected by the presence of unavoidable end restraints." The results of Chapuis and Galambos (4) and Zandonini (16) indicated effects much less than originally anticipated, and the data that now have become available through the work of Jones, et al. (20) confirm and expand these findings. Some additional observations will be given later in this discussion.

The author presents an extensive evaluation of the development of column curves for design specifications (pp. 2282–2288). However, a number of clarifications should be made, in order to prevent a misinterpretation of certain research results and how they relate to the current design codes. This will be done in enumerative form, to facilitate reader understanding of the most important points, as follows:

Analytical Results for Aluminum Columns.—Fig. 1 (p. 2283) shows analytical results for aluminum columns, for which the residual stresses are equal to zero. As will be demonstrated later, such stresses have a significant influence on the effect of the end restraint. It is therefore misleading to show Fig. 1 without at the same time pointing out the importance of the difference between steel and aluminum members. Furthermore, Fig. 1 shows another effect that is important for all end-restrained columns. The influence of the end restraint is strongly affected by the effective slenderness ratio of the member, or rather by the degree of end restraint relative to the column slenderness ratio. The percentage of strength increase as the effective length factor reduces from 1.0

to 0.9 therefore decreases along with the slenderness ratio. The approximate strength increases are, for some selected L/r values in Fig. 1 shown in Table 1. The strength increase is thus significantly reduced as the slenderness ratio goes from 120 to 40, and most noticeably as L/r drops below 80. The same effect has been found in steel columns, where the presence of residual stress further reduces the influence of end restraint (17).

Residual Stress in Hot-Rolled Members.—It is not correct to state that (p. 2284) "most hot-rolled wideflange sections exhibit the maximum residual stress of approx 0.3 times the yield stress." The statement is acceptable for small and medium-size hot-rolled wide-flange shapes in mild structural steel (ASTM A26, e.g.), but not for any of the larger W-shapes (unconservative), nor for a number of shapes in higher strength steel [0.3 σ_y is conservative for some of these (3,9)].

Welded Columns Are not always Weaker.—It is not correct to state generally that welded columns are weaker than their hot-rolled counterparts. Although it does apply to small and medium-size built-up shapes using universal mill plates in the flanges, the differences are not significant for heavy shapes of such manufacture. Furthermore, a shape that utilizes flame-cut plates will generally be *stronger* than a hot-rolled shape of similar appearance (18).

TABLE 1.—Approximate Strength Increases

L/r (1)	Increase, as a percentage (2)
120	25
100	21
80	20
60	14
40	4

Crookedness in Welded Members.—To the writer's knowledge, there are no out-of-straightness data available that substantiate the author's statement that welded built-up members exhibit more crookedness than rolled shapes. Secondly, welded shapes have to satisfy materials delivery standards to within the same or more stringent straightness requirements as do the rolled shapes.

Maximum Column Strength Analysis.—The writer's study of maximum column strength (3) was performed concurrently with the European work by Beer and Schultz (2). The projects developed sets of multiple column curves independently, but the results were compared and found to correlate satisfactorily, as was expected (3). However, the methods of analysis were significantly different, as were the input data (residual stress, initial out-of-straightness, steel grades, etc.).

Column Slenderness Ratio.—The importance of the column slenderness ratio for the effect of the end restraint has already been discussed to some extent. The recent work at the University of Sheffield (20) has confirmed and expanded on these findings, such that for steel columns the following conclusions can be made (17,20).

1. The strength-raising effect of end restraint depends on the relative stiffness

of the connection providing the end restraint and the column. For example, if a certain type of connection is used for end restraint on two columns with different slenderness ratios (but otherwise identical), then the connections at the ends of the more slender member will appear relatively stiffer, and therefore will have a more pronounced strength raising influence. This finding was demonstrated by Johnston (19) in his study of aluminum columns, as noted previously, but has now been extended to include steel columns with a variety of types of end connections (20). As an example of the results of Jones, et al. (17,20), the strength of a column with T-stub connections was 56% higher than an identical one with pinned ends, when the slenderness ratio was 100. However, the strength increase was only 10% when L/r was equal to 75. It is emphasized that these percentages apply to columns *without* residual stress, and also that the T-stub connection represents one of the most rigid of all beam-to-column connections.

2. Jones, et al. (20) did not present an extensive set of column strength data, and none for columns with slenderness ratios less than 75. Similarly, residual stress effects can only be discerned from some of their data. It is anticipated that this deficiency will be rectified through the continuation of their work. However, the results that are given (20) for a column with a slenderness ratio of 75, comparing the behavior and strength of members with T-stub connections to ones with pinned ends, and using residual stress-free wideflange shapes as well as sections with "Lehigh" type residual stress distributions (9,22) (maximum compressive residual stress at flange tips of 0.3 times the yield stress), show the following strength data: (a) No residual stress, T-stub connection versus pinned connection, slenderness ratio = 75, strength increase: 21%; and (b) with "Lehigh" type residual stress, T-stub connection versus pinned connection, slenderness ratio = 75, strength increase: 9%. It is therefore obvious that the presence of residual stress *significantly* reduces the impact of end restraint. When combined with the importance of the relative stiffness of the connection and the column, the effect of realistic end restraints on realistic columns is to raise the strength but a relatively minor amount.

The lack of column strength data (at this stage) for members with L/r less than 75 is particularly regrettable in view of North American design and construction practice, where column slenderness ratios normally are maintained well below 75, and in many cases as low as 30. In the absence of actual results, but based on the data that are available (19,20), it is likely that for a column with residual stress and a slenderness ratio of 50, the increase in strength from the pinned-end case to the T-stub case will be *at the most* 5%. Smaller strength increases should be anticipated for shorter members, as well as for members with markedly higher residual stress levels (e.g., heavy rolled shapes). The practical impact of including the effect of end restraint therefore would appear to be somewhat less than the author intimates.

3. Geometric imperfections in the column are also important. As expected, the British research (20) has shown that increasing the initial out-of-straightness will reduce the influence of end restraint, and also that this reduction will be smaller for members with more rigid end connections.
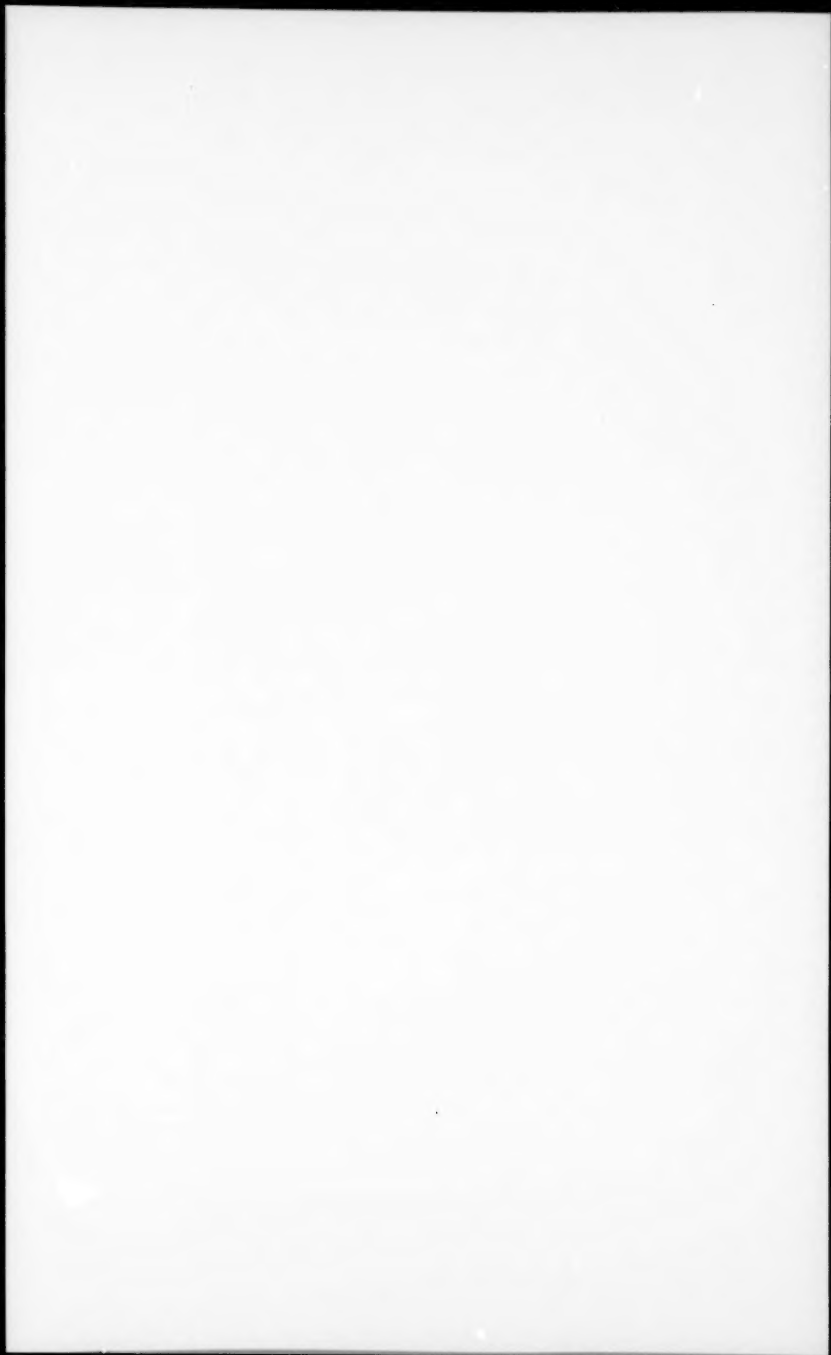
Although not analyzed, an eccentrically applied load would be of significant influence. This is especially important since it imposes an end moment that

will consume some of the moment capacity of the end connection, and also will accentuate the lateral deflection of the column. Future research activities should pay particular attention to this problem, not the least because of its relevance to beam-columns.

Summarizing, the efforts to quantify the effects of column end restraint are very important, and the author is to be commended for having taken the lead in this work. However, it is to be hoped that the results of the current and some future research work will be available before any final conclusions are made. Preconceived notions of causes and effects may lead to misinterpretation and incorrect applications of the data that are produced.

APPENDIX.—REFERENCES

17. Ackroyd, M. H., and Bjorhovde, R., discussion of "Effects of Semi-Rigid Connections on Steel Column Strength," by S. W. Jones, D. A. Kirby, and D. A. Nethercot, *Journal of Constructional Steel Research*, London, England, Vol. 1, No. 3, Apr., 1981.
18. Bjorhovde, R., Brozzetti, J., Alpsten, G. A., and Tall, L., "Residual Stresses in Thick Welded Plates," *Welding Journal*, Vol. 51, No. 8, Aug., 1972.
19. Johnston, B. G., "Buckling Behavior Above the Tangent Modulus Load," *Journal of the Engineering Mechanics Division*, ASCE, Vol. 87, No. EM6, Proc. Paper 3019, Dec., 1961, pp. 79–99.
20. Jones, S. W., Kirby, P. A., and Nethercot, D. A., "Effects of Semi-Rigid Connections on Steel Column Strength," *Journal of Constructional Steel Research*, London, England, Vol. 1, No. 1, Sept., 1980, pp. 38–46.

TECHNICAL PAPERS

Original papers should be submitted in triplicate to the Manager of Technical and Professional Publications, ASCE, 345 East 47th Street, New York, N.Y. 10017. Authors must indicate the Technical Division or Council, Technical Committee, Subcommittee, and Task Committee (if any) to which the paper should be referred. Those who are planning to submit material will expedite the review and publication procedures by complying with the following basic requirements:

1. Titles must have a length not exceeding 50 characters and spaces.

2. The manuscript (an original ribbon copy and two duplicate copies) should be double-spaced on one side of 8-1/2-in. (220-mm) by 11-in. (280-mm) paper. Three copies of all figures and tables must be included.

3. Generally, the maximum length of a paper is 10,000 word-equivalents. As an *approximation*, each full manuscript page of text, tables or figures is the equivalent of 300 words. If a particular subject cannot be adequately presented within the 10,000-word limit, the paper should be accompanied by a rationale for the overlength. This will permit rapid review and approval by the Division or Council Publications and Executive Committees and the Society's Committee on Publications. Valuable contributions to the Society's publications are not intended to be discouraged by this procedure.

4. The author's full name, Society membership grade, and a footnote stating present employment must appear on the first page of the paper. Authors need not be Society members.

5. All mathematics must be typewritten and special symbols must be identified properly. The letter symbols used should be defined where they first appear, in figures, tables, or text, and arranged alphabetically in an appendix at the end of the paper titled Appendix.—Notation.

6. Standard definitions and symbols should be used. Reference should be made to the lists published by the American National Standards Institute and to the *Authors' Guide to the Publications of ASCE*.

7. Figures should be drawn in black ink, at a size that, with a 50% reduction, would have a published width in the *Journals* of from 3 in. (76 mm) to 4-1/2 in. (110 mm). The lettering must be legible at the reduced size. Photographs should be submitted as glossy prints. Explanations and descriptions must be placed in text rather than within the figure.

8. Tables should be typed (an original ribbon copy and two duplicates) on one side of 8-1/2-in. (220-mm) by 11-in. (280-mm) paper. An explanation of each table must appear in the text.

9. References cited in text should be arranged in alphabetical order in an appendix at the end of the paper, or preceding the Appendix.—Notation, as an Appendix.—References.

10. A list of key words and an information retrieval abstract of 175 words should be provided with each paper.

11. A summary of approximately 40 words must accompany the paper.

12. A set of conclusions must end the paper.

13. Dual units, i.e., U.S. Customary followed by SI (International System) units in parentheses, should be used throughout the paper.

14. A practical applications section should be included also, if appropriate.